Wedge diffraction in planar microwave circuits

Marchetti, S.

Award date:
1992

Awarding institution:
University of Bath

WEDGE DIFFRACTION IN PLANAR MICROWAVE CIRCUITS

WEDGE DIFFRACTION
IN PLANAR MICROWAVE CIRCUITS

Submitted by **S. Marchetti**

for the degree of **PhD**

of the **University of Bath**

1992

COPYRIGHT

ProQuest LLC
789 East Eisenhower Parkway
P.O. Box 1346
Ann Arbor, MI 48106-1346

To my Parents

and their grand-daughter Virginia

PREFACE

This work is concerned with the field analysis of Microwave and Millimeter wave Circuits Components and Antennas where wide use is required of conducting plane sectors, cones and bidimensional wedges . A complete rigorous solution for the EM fields diffracted on these wedges is presented together with the simplified formulation of their main behaviour by the conductors, where singularities occur that are distribuited along the edges and localised on the tips .

There is a wide gap to cover between the more recent developments in Applied Mathematics on the solutions of Maxwell's equations in coordinate system like the Ellipsoidal, Conical and Spherical ones, and the more recent algorithms developed by the Microwave Community to analyse and/or synthesize circuitry in Printed Conductor Tecnology . The connection point of these two disciplines is represented by the "elementary brick" in printed circuits, that is a finite plane conductor, often shaped as a wedge or double-wedge, where an incident EM wave diffracts in a predictable way by knowing the three-dimensional vector solutions of Maxwell's equations for the ideal infinite sector or double- sector. In fact the two geometries fit each other by the tip, permitting, in particular, rigorous and easily formulated descriptions of the singularities along the conductor boundary, as required in circuit analysis.

Chapter 1 is dedicated to a unified formulation for the above geometries where we investigate the general physically meaningful solutions of the scalar wave Helmholtz equation, using Jacobian or Trigonometric forms according to

their usefulness at the various stages of the development .

In Chapter 2 physical boundary conditions are introduced such as those pertaining to the plane sector, double-sector and related geometries, recovering the complete spectra of eigenvalues and eigenfunctions that are straightforwardly related to the static E-field . From the latter, a "singularity vector" is deduced which describes just the singular or the main behaviour of the dynamic E-field so as required in circuit analysis.

In Chapter 3 we solve the complete vector Maxwell's equations for the EM fields diffracted by the same geometries where, among other things, Babinet's principle and the Image principle are implied. A " singularity vector " for the H-field, with the features above indicated for the E-field, is then formulated.

In Chapter 4 we recover classical, but sometimes more accurate results for the cone and bi-dimensional wedges using a quite novel specialization of the theoretical apparatus developed for conical geometry to the case of a spherical coordinate system . These wedges are met in the most widespread applications and their behaviour permits to point out differences between the scalar and vectorial nature respectively of the density of charge and of current on the tips.

In Chapter 5 the results obtained are applied in a new " Generalized Transverse Resonance Approach " as an attempt to quantify the reflection due to a corner in a waveguide taper and has resulted into a new analysis alghorithm for the design of an " Optimum Smooth Taper " in waveguide .

In Chapter 6 applications of the singularity vector on the plane of the conductor, normal to it and on the conductor itself are indicated in the implementation of classical algorithms like the " Transverse Resonance Approach ", the " Matching Mode Method " and the " Moment Method " respectively .

AKNOWLEDGEMENTS

The author would like to thank Prof. T. Rozzi for his expert supervision and reviewing of the work .

Many thanks are also directed to Prof. D.S. Jones, Prof. F.M. Arscott and Prof. R. Lupini for their suggestions in matters of Applied Mathematics .

The author would also like to thank Ir. F.C. De Ronde, Dr. S. Pennock and all the others from the Electrical Engineering of Bath's University who contributed, directly or indirectly, to discussions about experimental, computational and theoretical aspects of MIC circuit applications .

Thanks are also due to the EEC (Grant no. ST 200349) and to the Electrical Engineering Departement for their financial support .

Finally, thanks are due to the, " Dipartimento di Elettronica della Universita' di Ancona " and to the " INSA de l'Universite' de Rennes " for their kind technical support in preparing the typesetting of this thesis .

LIST OF PUBLICATIONS

S. Marchetti and T. Rozzi, " Electric Field Behavior Near Metallic Wedges", *IEEE Trans. on A&P*, vol. 38, no. 9, September 1990 .

S.Marchetti and T. Rozzi, " Electric Field Singularities at Sharp Edges of Planar Conductors ", *IEEE Trans. on A&P*, vol. 39, pp. 1312-1320, Sept. 1991.

S. Marchetti and T. Rozzi, " $\vec{H}$-field and $\vec{J}$-current Singularities at Sharp Edges in Printed Circuits ", *IEEE Trans. on A&P*, vol. 39, pp. 1321-1331, Sept. 1991 .

LIST OF CONFERENCES

S. Marchetti and T. Rozzi, " Edges Singularities of Discontinuities in Microwave Integrated Circuits (MIC) ", 7^{th} *National Meeting of Applied Electromagnetism*, pp. 189-192, September 1988, Rome .

S. Marchetti and T. Rozzi, " Electric Field Singularities in Microwave Integrated Circuits (MIC) ", *Proc.* 20^{th} *European Microwave Conference*, pp. 823-828, September 1990, Budapest .

S. Marchetti and T. Rozzi, " EM Field Singularities in Microwave Integrated Circuits (MIC) ", *Proc. International IEEE AP-S*, pp. 882-885, June 1991, London, Ontario .

S. Marchetti and T. Rozzi, " Generalized Transverse Resonance Method for Nonuniform Lines in Microwave integrated Circuits (MIC) ", *Proc.* 21^{st} *European Microwave Conference*, pp. 878-883, September 1991, Stuttgart .

ORIGINAL AND NOVEL CONTRIBUTIONS

The eigenvalues relative to the problem of the plane sector are determined with higher accuracy with respect to previous works because of the novel analytic approach to the problem .

In particular the evaluations of the first eigenvalue, which establishes the Electro-Magnetic singularities at the tip, has been obtained with an accuracy of say 7 decimal figures .

The complete spectrum of diffracted modes for the problem of the double-sector has been originally obtained with the accuracy used for the sector .

The complete spectra of diffracted modes for other five 3D-wedges conductor geometries of secondary applicativity in Microwave, have been recovered as sub-spectra of those relative to the sector and double-sector .

Original formulation of some "singularity vectors" for the Electro-Magnetic fields relative to the named 3D-wedges has permitted to express the singular behaviour of the fields in an easy-to-handle way for Microwave and Millimeter wave applications .

The theory of the 2D-wedge and Cone-wedge has been reduced to a particular case of that of the 3D-wedge permitting general conclusions and comparison for the Electric and Magnetic singularities relative to tips conductor of arbitrary cross section .

Original method of analysis for smooth taper in unilateral Fin-line has been ideated which has permitted evaluation of the complex distribuited impedance .

An original method of numerical synthesis has followed which also has permitted the synthesis of an approximate novel analytic expression for the taper profile .

Indication of the way in which the singularity vectors enter the usual algorithms for the analysis of Passive Circuit Components for Microwave has been finally reported .

List of Abbreviations

b.c. : boundary conditions

c.s. : coordinate system

EM : Electro-Magnetic

i.e. : id est, that is to say

e.g. : that is to say

List of symbols and functions in order of apparition

(**N.B.**: a very few symbols are used 2 times with different meanings)

x, y, z	right tern of rectangular coordinates for the rectangular c.s.
X, Y, Z	right tern of rectangular coordinates for the main rectangular c.s.
r, θ, ϕ	right tern of trigonometric coordinates for the spherical c.s.
r, θ, ϕ	right tern of trigonometric coordinates for the conical c.s.
r', θ, ϕ	right tern of trigonometric coordinates for the ellipsoidal c.s.
r, β, α	right tern of Jacobian coordinates for the conical c.s.
γ, β, α	right tern of Jacobian coordinates for the conical c.s.
sn, cn, dn	Jacobian functions of complex variable
ϵ	semi angular aperture of the sector
k	parameter of the conical and ellipsoidal c.s.

K	complete elliptic integral of parameter k
k'	related parameter of the conical and ellipsoidal c.s.
K'	complete elliptic integral of parameter k'
l	second parameter of the ellipsoidal c.s.
$w(z)$	Lamè's function versus complex variable z
$y(v)$	Lamè's function versus real variable v
u, φ, ϑ	useful real variables for Lamè's functions
$A(\alpha), \Xi(\varphi), \Phi(\phi)$	Lamè's functions versus the 3^{rd} coord. of the conical c.s.
$B(\beta), U(u), \Upsilon(\vartheta), \Theta(\theta)$	Lamè's functions versus the 2^{nd} coord. of the conical c.s.
$C(r), R(r;\omega), R(r)$	Bessel's functions versus the 1^{st} coord. of the conical c.s.
ν, h	order and degree of the Lamè's functions
μ, h'	useful variables function of ν, h
η	useful variables function of ν, h or μ, h'
X_i, A_i, B_i	series expansion coeff. for periodic Lamè's functions
κ	wave number
ω	angular frequency
f	frequency
μ, μ_0	magnetic permeability of generic medium and of vacuo
$\epsilon, \epsilon_0, \epsilon_r$	dielectric constant of generic medium, vacuo, relative
σ	angular aperture of the sector conductor
$\Psi, \Psi_0, \Psi_1, \Psi_2$	forms of the scalar Helmholtz potential
V	scalar electric potential
∇	vector operator
$\vec{E}, \vec{L}, \vec{N}, \vec{M}$	forms of the vector electric field
$\vec{H}, \vec{H}_N, \vec{H}_M$	forms of the vector magnetic field

$\vec{s}_E$	electric field singularity vector
$s_{E_x}, s_{E_y}, s_{E_z}$	scalar components of $\vec{s}_E$
$\vec{s}_H$	magnetic field singularity vector
s_{Hx}, s_{H_y}, s_{H_z}	scalar components of $\vec{s}_H$
τ	EM degree of singularity or zero at the tip
τ_e	electric degree of singularity or zero at the tip
τ_h	magnetic degree of singularity or zero at the tip
j_ν	spherical Bessel function of 1^{st} kind
$\hbar_\nu$	spherical Bessel function of 2^{st} kind
$h_\nu^{(2)}$	Henkel function of 2^{st} kind
η	characteristic impedance of the medium
ρ_s	surface density of charge
$\vec{J}$	vector density of current
T, P, S	useful functions of θ, of ϕ and of θ, ϕ
$S_\theta, S_{\theta_N}, S_{\theta_M}$	useful functions of r, θ, ϕ
$S_\phi, S_{\phi_N}, S_{\phi_M}$	useful functions of r, θ, ϕ
$\Delta, \Delta_1, \Delta_2$	useful functions of x, y, z or X, Y, Z
$\vec{\Pi}_e, \vec{\Pi}_h$	vector electric and magnetic Hertzian potentials
$f(z)$	correction function
Ψ_e, Ψ_h	functional components of $\vec{\Pi}_e, \vec{\Pi}_h$
χ_{e_n}, χ_{hn}	functional components of Ψ_e, Ψ_h
ϕ_{e_n}, ϕ_{hn}	functional components of Ψ_e, Ψ_h
U_{e_n}, U_{h_n}	series expansion coefficients for Ψ_e, Ψ_h
$\gamma, j\beta$	propagation constant along z
k_{mn}	propagation constant along y

$\hat{Y}_{ij}$	kernel of integral equation
y_{ij_n}	series expansion coefficients for $\hat{Y}_{ij}$
$\underline{\underline{Y}}_{ij}$	block of the matrix impedance
$(Y_{ij})_{mn}$	component of the matrix impedance
Q_{mn}, P_{mn}	series expansion coefficients for $(Y_{ij})_{mn}$
$\alpha_{1,2,3}, \beta_{1,2,3}, \gamma_{1,2,3}$	coefficients used in the recursive relations for Q_{mn}, P_{mn}
$w(z)$	fin-line aperture
$\theta(x), \theta(X), \theta_1(x), \theta_2(x)$	forms of mapping of x or X into θ
$F(z)$	useful functional for the mapping
$\ell, \ell_1, \ell_2, \ell_i$	line lengths
T	transition length
λ, λ_0	wavelength in the guide and in the vacuo
Z, Z_i	line impedances
V	electric tension
P	power
Γ	reflection coefficient
$\underline{\underline{S}}$	scattering matrix
S_{ij}	scattering matrix coefficients
$\underline{\underline{Z}}$	impedance matrix
Z_{ij}	impedance matrix coefficients
$\underline{\underline{G}}, \vec{G}_A, G_V$	dyadic,vector and scalar Green's functions
$\vec{A}$	vector potential
$\vec{\mathcal{E}}, \vec{\mathcal{H}}$	electric and magnetic trial fields
$\vec{e}_n, \vec{h}_n$	electric and magnetic modal fields
$\vec{E}_n, \vec{H}_n$	electric and magnetic waveguide modal fields

Contents

Chapter 1

SOLUTION OF THE SCALAR WAVE EQUATION

1.1 Introduction

From a general point of view, the diffraction by a conductor body, in particular with edges, can be completely quantified once the solution of the Maxwell's wave equations satisfying the boundary conditions (b.c.) pertaining to the conductor itself are known.

Actually, this problem can be solved in an analytical or quasi-analytical way only if there exists a geometry, that is to say a coordinate system (c.s.), where the solutions of the vectorial wave Maxwell's equations are obtainable from those of the scalar wave Helmholtz's equation and are expressible in separable form, allowing an easy implementation of the b.c. . In a more general sense, this problem could be solved in a complete numerical way in the space domain but the numerical algorithm involved requires in any case an approximate starting point

in order to converge fast and accurately, especially in the presence of singularities. Often, in fact, just the formulation of the main characteristics of the unknown EM fields, as, for instance, its singularities distributed along the edges or on tips as well as the zero distributions on regular surfaces, will suffice to increase speed and accuracy of the solution .

In this context we place the " coordinate matching procedure " (see [1]), according to which, locally fitting one or more equicoordinate surfaces of one of the 11 c.s. in which the scalar Helmholtz equation separates with just a part of the whole conducting structure, is sufficient to determine the main characteristics of the EM fields there .

When, in particular, these surfaces are plane degenerate ones, the solutions are among the easiest to be represented and to be computed in the given c.s. . Naturally, the considerable simplification involved is due to the Applied Mathematics work gone on mainly during these last 50 years, roughly speaking from Ince to Arscott (see [1, 2, 3, 5, 6, 7]) and some important questions in this matter are still waiting for an answer. Examples are the lack of a unique characteristic equation for Lamé's functions double-periodic with periods $4K$x$8K'$ (i.e. 2πx4π) met in the study of the plane sector, or the computation of the more general ellipsoidal waves (see [2]) .

Today's reduced interest in functional analysis is perhaps due to the fact that finding an analytical solution to a differential equation is considered by many workers a waste of time . Numerical solutions, however, give no real idea of its properties and their relations with the physical reality. This is why we decided to develop a simple procedure, closely connected to the physical meaning of the solution, which allows to operate successive selections in the whole space

of solutions for the Maxwell's equations in the given c.s. .

Once the final set of solutions for our problem has been singled out , there arises the problem of formulating it in such a way as to be put to use in further theoretical developments or to be physically interpreted or numerically computed, which purposes might require the use of different variable domains . In fact, we can state that the Jacobian form is by far the easier one to handle in the process of identification of the solution . On the other side, computation and application is far easier when the trigonometric form is used . Consequently, also remembering that various authors prefer to use just the first or second form according to whether their interests are purely theoretical or also applicative (see [8, 9, 10]), we make use of both forms according to the context .

Specifically, we will start with an overview on the equicoordinate surfaces for the spherical, conical and ellipsoidal c.s. with particular attention to the degenerate plane ones, among which are those involved in our " local fitting procedure " . Also noted is the specialization of geometrical parameters, permitting to derive from the ellipsoidal c.s. the conical c.s. and from the latter the spherical c.s. [1]. The solutions in separable form of the scalar wave equation in conical c.s. are then investigated, giving priority to those of the Lamé's differential equation in the complex plane . The Lamé's solutions of our interest are obtained by selecting firstly those physically acceptable, then satisfying the Hill's group properties and finally satisfying the physical b.c. . Thanks to the fact that the latter fit degenerate equicoordinate surfaces, the solutions can only be periodic Lamé's functions, whose evaluation can be reduced to solving a system of two continued fractions, to any prescribed accuracy .

1.2 Characterization of the coordinate systems

It is essential here to recall in brief the mathematical formulation of the three geometries involved in the work .

The transformation relations between the usual rectangular coordinates x, y, z, the spherical coordinates r, θ, ϕ, the conical coordinates r, β, α and the ellipsoidal coordinates γ, β, α are explicitely reported for the Spherical, Conical and Ellipsoidal coordinate systems .

An analytic procedure is also pointed out which permits to consider the conical geometry as a generalization of the spherical one and the ellipsoidal one as a generalization of the conical one . On this degeneracy procedure is based the possibility of a unified theory for the solution of the scalar wave equation in the three geometries .

Particular emphasis is given to the equation of the degenerate plane surfaces, always lying on the three cartesian planes, because the physical b.c. of our interest always will pertain one or more of them .

1.2.1 Spherical coordinate system

For this classic geometry the transformation relations and intervals for the variables are simply expressible like (see [11] pg. 24) :

$$x = rsin\theta cos\phi \qquad r \in [0, \infty) \tag{1.1}$$

$$y = rsin\theta sin\phi \qquad \theta \in [0, \pi] \tag{1.2}$$

$$z = rcos\theta \qquad \phi \in [0, 2\pi) \tag{1.3}$$

The equation of the equicoordinate surfaces shown in Fig. 1.1 are :

i) $(\frac{x}{r})^2 + (\frac{y}{r})^2 + (\frac{z}{r})^2 = 1$: spheres of radius r

ii) $(\frac{x}{sin\theta})^2 + (\frac{y}{sin\theta})^2 - (\frac{z}{cos\theta})^2 = 0$: cones with angular aperture θ

iii) $\frac{x}{cos\phi} - \frac{y}{sin\phi} = 0$: half planes forming an angle ϕ with the $x-$axis .

The degenerate surfaces in this geometry are shown in Figs. 1.2,3,4 and are :

i) on $x = 0$, the two half planes $y < 0, y \geq 0$

ii) on $y = 0$, the two half lines $x = 0 : z \geq 0, z < 0$

iii) on $z = 0$, the plane $z = 0$ without the origin and the origin $r = 0$

1.2.2 Conical coordinate system

In this geometry we will make use of either the transformation relations in terms of the Jacobian variables r, β, α or those in terms of the spherical ones r, θ, ϕ. As announced in the introduction, the first formalism will result by far more useful in handling the theoretical procedure aiming to identify the properties of the solution we will look for . On the other hand, the trigonometric formalism will simplify the physical interpretation and handling of the solutions.

The Jacobian form make use of the elliptic functions $sn(t;k), cn(t;k), dn(t;k)$ where the complex variable t can be either α or β while $k \in [0,1]$ is the parameter.

On the complex plane these functions are double periodic respectively with periods $4Kxj2K'$, $4Kxj4K'$, $2Kxj4K'$; $K = K(k)$ is known as the complete elliptical integral of the first kind while $K' = K'(k')$ is the same function of $k' = \sqrt{1-k^2}$ as K is of k (see for instance [1]) .

When $k = 0$, sn and cn degenerate into the common circular functions sin and cos while $dn \equiv 1$. On the other end when $k = 1$, sn becomes the $tanh$ while cn and dn becomes $\frac{1}{sinh}$.

Using these symbols the transformation relations may be written like :

$$x = krsn\alpha sn\beta = rcos\phi\sqrt{1-(k'cos\theta)^2} \tag{1.4}$$

$$y = j\frac{k}{k'}rcn\alpha cn\beta = rsin\phi sin\theta \tag{1.5}$$

$$z = \frac{1}{k'}rdn\alpha dn\beta = rcos\theta\sqrt{1-(kcos\phi)^2} \tag{1.6}$$

As far the relations between Jacobian and Trigonometric variables, as well as of their intervals of existence, is concerned, it is :

$$r \equiv r \qquad r \in [0,\infty) \tag{1.7}$$

$$\beta \in [K, K+2jK'] \qquad j\frac{k}{k'}cn\beta = sin\theta \qquad \theta \in [0,\pi] \tag{1.8}$$

$$\alpha \in [K, -3K) \qquad cn\alpha = sin\phi \qquad \phi \in [0,2\pi) \tag{1.9}$$

For the given classic intervals for θ, ϕ, those for β and α defined through-

out the previous relations are not univocally determinable because of the named periodicity properties of the elliptic functions . The choice of the intervals for α and β is made in such a way to let them concide at the extremity $\alpha = \beta = K$ but otherwise the first is always real and the second always complex . These properties will result of great importance in determining the double periodicity of the solutions in respect of these two variables .

The equations of the equicoordinate surfaces shown in Fig. 1.5 are :

i) $(\frac{x}{r})^2 + (\frac{y}{r})^2 + (\frac{z}{r})^2 = 1$: spheres of radius r

ii) $(\frac{x}{ksn\beta})^2 - (\frac{y}{kcn\beta})^2 - (\frac{z}{dn\beta})^2 = 0$: elliptic cones with angular aperture θ

iii) $(\frac{x}{ksn\alpha})^2 - (\frac{y}{kcn\alpha})^2 - (\frac{z}{dn\alpha})^2 = 0$: elliptic half cones with angular apert. ϕ

Besides, the degenerate surfaces are now obtainable as :

i) on $x = 0$, the two half planes $y < 0, y \geq 0$

ii) on $y = 0$, the sectors delimited by the straight lines $(\frac{x}{k})^2 - (\frac{z}{k'})^2 = 0$

iii) on $z = 0$, the plane $z = 0$ without the origin and the origin $r = 0$

These are shown in Figs. 1.6,7,8 respectively together with the Jacobian and Trigonometric variable values to them associated . Of great importance for our work is the relation between the geometric parameters k, k' and the semi-angular aperture ϵ of the sector $\theta = 0$ in Fig. 1.7:

$$k = sin\epsilon \qquad k' = cos\epsilon \qquad k^2 = 1 - k'^2 \in [0,1] \qquad (1.10)$$

Finally, we have to point out that the conical c.s. so characterized degenerates back into the spherical one previously considered when $k \rightarrow 0$, and naturally the same properties are verifiable for the degenerate surfaces .

1.2.3 Ellipsoidal coordinate system

For this geometry too we can formalize the transformation relations either in Jacobian γ, β, α or in some trigonometric r', θ, ϕ coordinates .

Nevertheless, to r', θ, ϕ we can no longer associate the familiar geometrical meanings because a new parameter $l \in [0, \infty)$ is introduced which generalizes the equicoordinate surfaces in the way shown here after .

In any case the transformation relations are :

$$x = k^2 l sn\alpha sn\beta sn\gamma = r' cos\phi \sqrt{1 - (k' cos\theta)^2} \tag{1.11}$$

$$y = (jk)^2 \tfrac{l}{k'} cn\alpha cn\beta cn\gamma = r' sin\phi sin\theta \sqrt{1 - (\tfrac{kl}{r'})^2} \tag{1.12}$$

$$z = j\tfrac{l}{k'} dn\alpha dn\beta dn\gamma = r' cos\theta \sqrt{1 - (k cos\phi)^2} \sqrt{1 - (\tfrac{l}{r'})^2} \tag{1.13}$$

The relations between the two sets of three variables and relative intervals of definitions are chosen consistently with the previous ones, i.e. :

$$\gamma \in [K + jK', jK') \qquad kl sn\gamma = r' \qquad r' \in [l, \infty) \tag{1.14}$$

$$\beta \in [K, K + 2jK'] \qquad j\tfrac{k}{k'} cn\beta = sin\theta \qquad \theta \in [0, \pi] \tag{1.15}$$

$$\alpha \in [K, -3K) \qquad cn\alpha = sin\phi \qquad \phi \in [0, 2\pi) \tag{1.16}$$

The equicoordinate surfaces equations can be now expressed together as :

$$(\frac{x}{kl sn t_0})^2 - (\frac{y}{kl cn t_0})^2 - (\frac{z}{l dn t_0})^2 = 1 \tag{1.17}$$

where $t_0 = \alpha_0, \beta_0$, or γ_0 and then, respectively, the surfaces are (see Fig. 1.9):

i) if $t_0 = \gamma_0$ then $sn\gamma_0$ is real, $cn\gamma_0, dn\gamma_0$ are imaginary : ellipsoids

ii) if $t_0 = \beta_0$ then $sn\beta_0, dn\beta_0$ are real,$cn\beta_0$ is imaginary: one sheet hyperb.

iii) if $t_0 = \alpha_0$ then $sn\alpha_0, cn\alpha_0, dn\alpha_0$ are all real: hyperboloids .

On the three cartesian planes, (1.17) degenerates into the equation for the degenerate surfaces :

i) on $x = 0$, the two half planes $y < 0, y \geq 0$

ii) on $y = 0$, the two branches of hyperbola $(\frac{x}{kl})^2 - (\frac{z}{k'l})^2 = 1$

iii) on $z = 0$, the ellipse of axes $k'l, l$, $(\frac{x}{l})^2 + (\frac{y}{k'l})^2 = 1$

These degenerate surfaces are drawn in Figs. 1.10,11,12 respectively together with both the Jacobian and Trigonometric associated variable values .

We will work in this geometry when dealing with conducting geometries like branch of hyperbolas or ellipses which will be a matter for future developments but their inclusion permits to observe how a unified theory is still possible with the previous geometries . This c.s. degenerates in fact into the conical one (see also [1]) when $l \rightarrow 0$, transmitting the same properties to the degenerate surfaces and then to the solution of the scalar wave equation we will deal with .

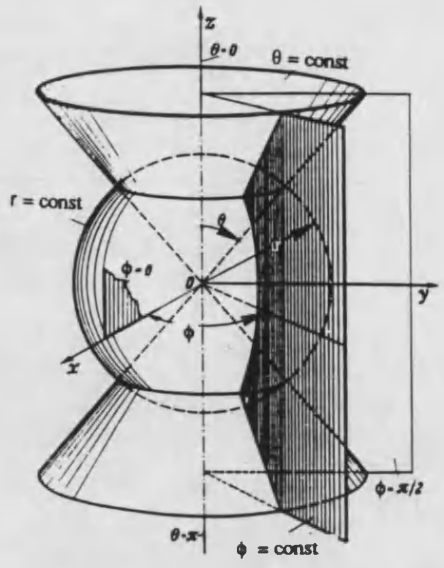

Fig. 1.1 : spherical coordinate system

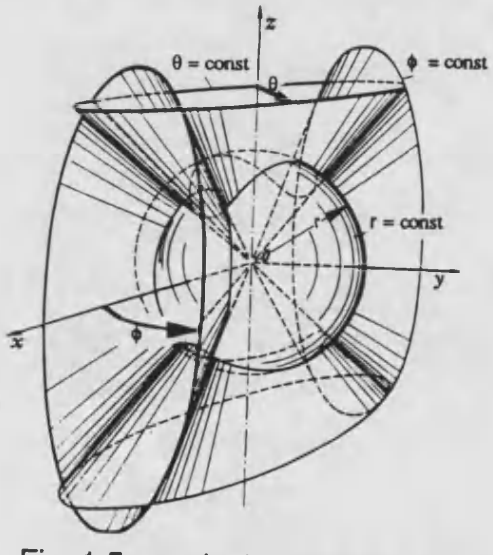

Fig. 1.5 : conical coordinate system

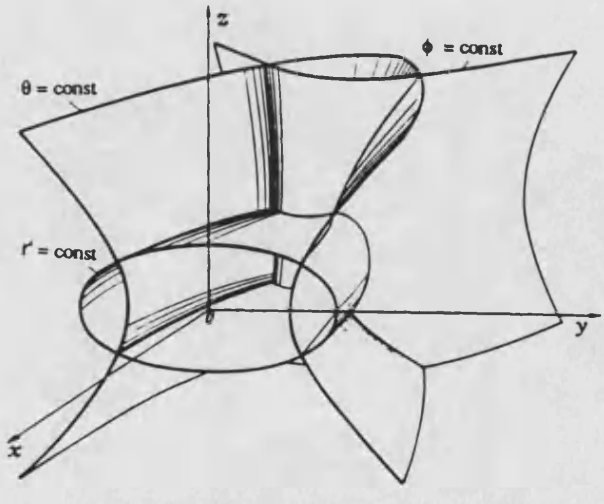

Fig. 1.9 : ellipsoidal coordinate system

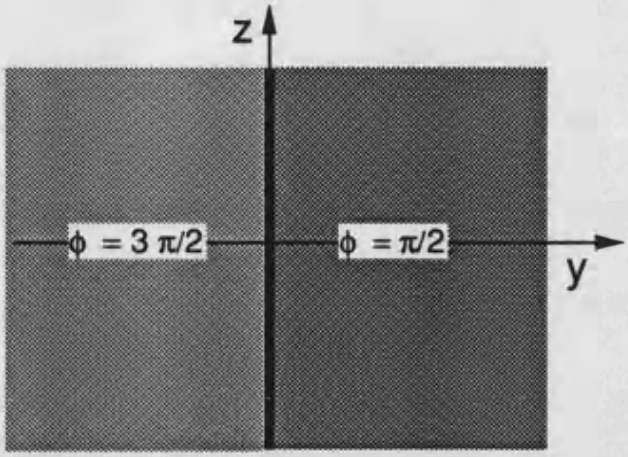

Fig. 1.2 : spherical degenerate surfaces on the plane x = 0

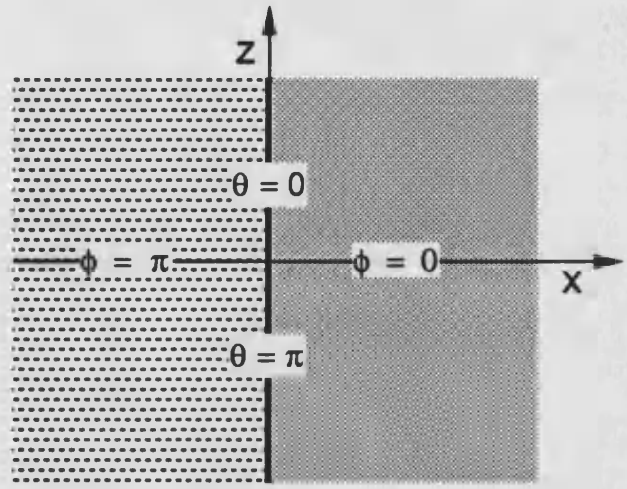

Fig. 1.3 : spherical degenerate surfaces on the plane y = 0

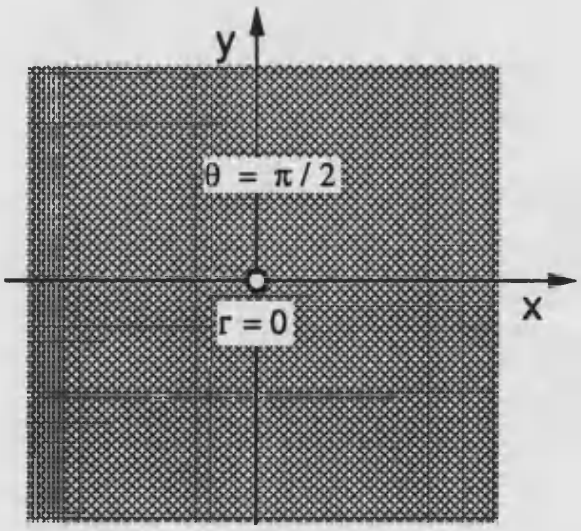

Fig. 1.4 : spherical degenerate surfaces on the plane z = 0

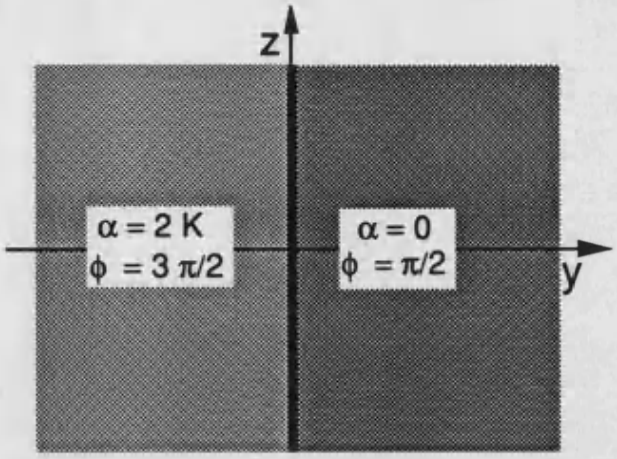

Fig. 1.6 : conical degenerate surfaces on the plane x= 0

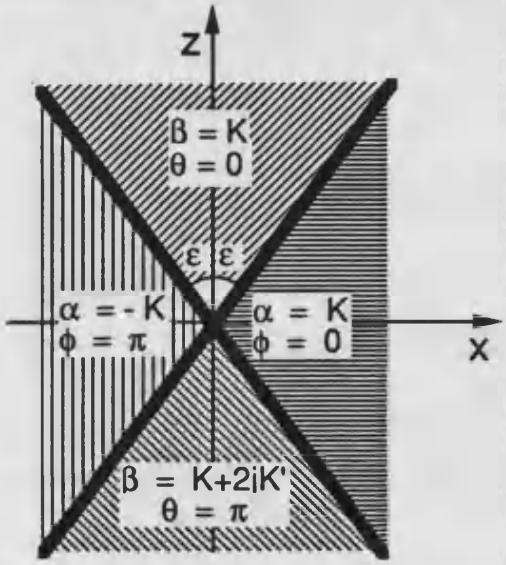

Fig. 1.7 : conical degenerate surfaces on the plane y= 0

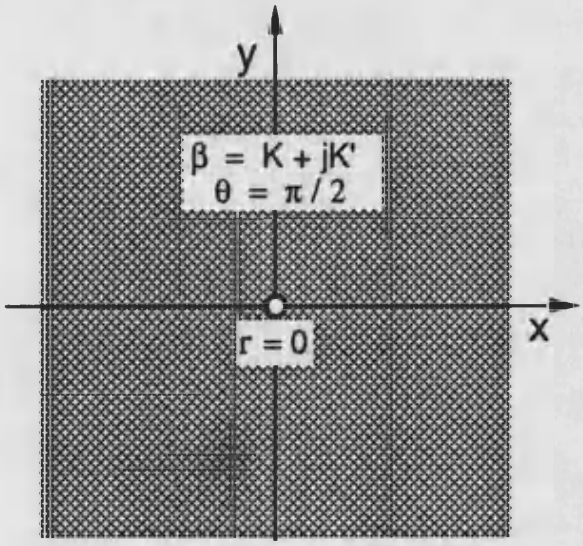

Fig. 1.8 : conical degenerate surfaces on the plane z= 0

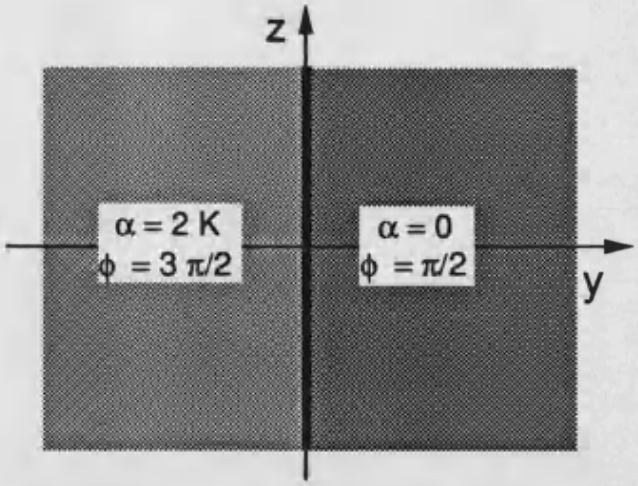

Fig. 1.10 : ellipsoidal degenerate surfaces on the plane x = 0

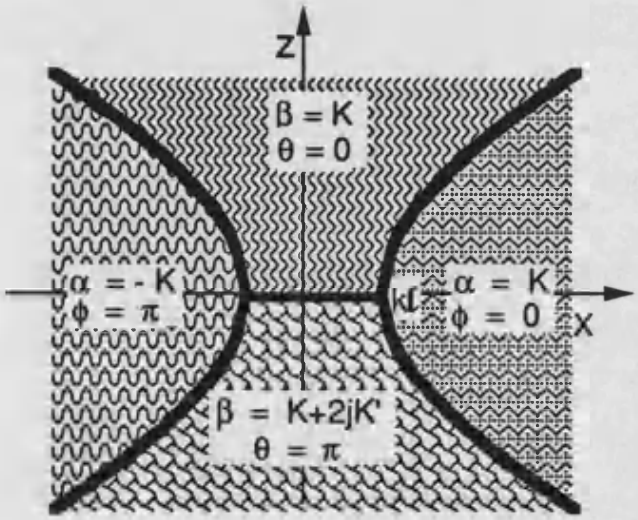

Fig. 1.11 : ellipsoidal degenerate surfaces on the plane y = 0

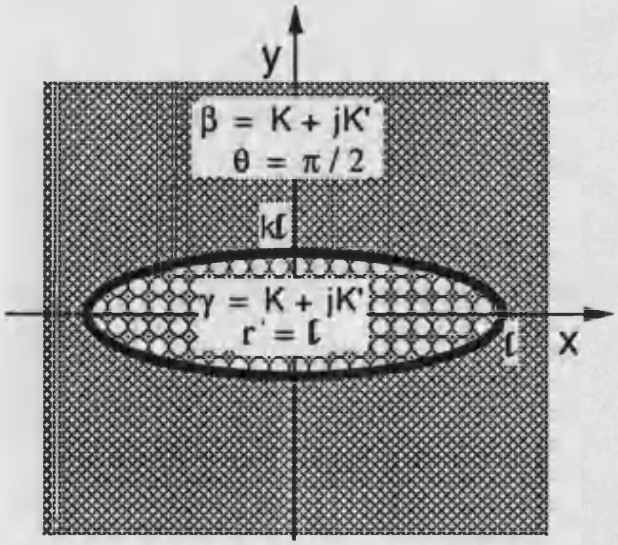

Fig. 1.12 : ellipsoidal degenerate surfaces on the plane z = 0

1.3 Characterization of the Solutions

The theory of " the solution " is developed in conical geometry as it permits an easy extension to the ellipsoidal c.s. and an easy particularization to the spherical c.s. . In this geometry, the three-dimensional EM fields solutions can be deduced from those of the scalar wave equation, which, in their turn, are separable along r as Bessel's, and along α, β as Lamé's differential equations (see [11, 12]) . Hence, from now on we denote by $F(r, \beta, \alpha)$ the solutions of the scalar Helmholtz equation.

The complete characterization of the Lamé's solutions is still in progress and they might present quite difficult forms to be classified and computed [7]. Nevertheless, a sequence of successive requirements to be satisfied by " the solution " make it at least periodic along α, β and consequently well classifiable, representable and easily computable .

The path of progressive specialization in the space of the totality of solutions passes through the following steps :

i) the geometrical properties of the coordinate system

ii) the smoothness properties of the solutions

iii) the mathematical properties of the Helmholtz equation

iiii) the physical boundary conditions

At this stage, the Jacobian formalism is simpler to use, even though we report sometimes the trigonometric one because of its familiarity to the reader .

1.3.1 The geometrical properties of the conical coordinate system

The choice of the intervals for the variables r, β, α made in 1.2.2 is such that they are as short as possible, compatibly with the necessity to associate to any point of the space at least one tern r_0, β_0, α_0 .

Nevertheless, with that choice, the one-to-one correspondence fails somewhere and in particular on the sectors shown in Fig. 1.7 where two sets of three variables are associated to the same point .

It is obvious to ask ourself if this fact implies that F assumes the same value on them and if this occurrence may be turned into a periodicity condition on F itself. In order to analytically demonstrate this possibility, we consider the sphere of radius r_0 of Fig. 1.13 which intersects the degenerate sectors $\beta = K, K + j2K'$ (i.e. $\theta = 0, \pi$) of Fig. 1.7 in the two arcs $\mathcal{C}^+, \mathcal{C}^-$. On these two arcs, the values $\alpha, 2K - \alpha$ (i.e. $\phi, \pi - \phi$) give the same point.

Any other value $\beta_0 \in (K, K + jK')$ (i.e. $\theta_0 \in (0, \frac{\pi}{2})$) gives a closed path surrounding $\mathcal{C}^+$ and a value $\beta_0 \in (K + jK', K + j2K')$ (i.e. $\theta_0 \in (\frac{\pi}{2}, \pi)$) gives an analogous path surrounding $\mathcal{C}^-$ while α varies over $[K, -3K)$, i.e. ϕ varies over $[0, 2\pi)$.

On the contrary, for a fixed $\alpha_0 \in [K, -3K)$ the point (r_0, β, α_0) moves following to an arc from a point on $\mathcal{C}^+$ to one on $\mathcal{C}^-$ while β varies through its domain $[K, K + j2K']$.

Summing up, a variation of α in $[K, -3K)$ brings the point (r_0, β_0, α) *back to its starting point* (for this we exclude $\alpha = -3K$ in the interval) while a variation of β in $[K, K + j2K']$ moves the point (r_0, β, α_0) along an half circuit

only .

Consequently, any physically meaningful solution $F(r, \beta, \alpha)$ must be periodic in α with period 4K or, equivalently, in ϕ with period 2π but not necessarily in β, i.e. :

$$F(r, \beta, \alpha) = F(r, \beta, \alpha + 4K) \tag{1.18}$$

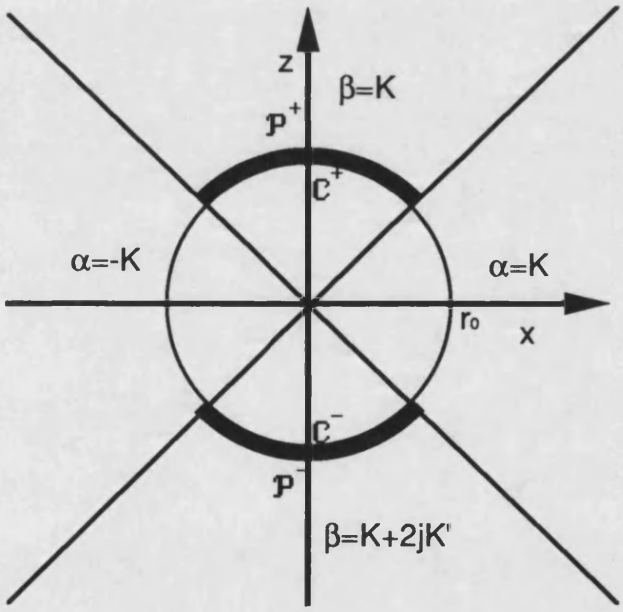

Fig. 1.13 : sphere of radius r_0 and degenerate arcs $C^- C^+$

1.3.2 The smoothness properties of the solutions

Similar arguments arise when we further require smoothness of any physically acceptable solution in conical c.s., i.e. it has to be continuous with continuous gradient in any homogeneous region .

Actually, new restrictions on F arise from the imposition of smoothness on the singular arcs $\mathcal{C}^+, \mathcal{C}^-$, at the singular origin point and on the sphere with infinite radius whenever no other physical b.c. are present .

Without loss of generality, we can limit attention to separable solutions of the general form :

$$F(r,\beta,\alpha) \;=\; C(r)B(\beta)A(\alpha) \tag{1.19}$$

The smoothness condition in F imposes some properties on the functions A, B, C which we can summarize, refering again to Fig. 1.13 and [1], as :

i) on the upper half of a sphere we must have :

$$\lim_{\alpha\to -3K} A(\alpha) = A(K), \quad \lim_{\alpha\to -3K} \dot{A}(\alpha) = \dot{A}(K) \quad \text{i.e. :}$$

either $A(\alpha)$ is even about K and, $\dot{B}(K) = 0$ (1.20)

or $A(\alpha)$ is odd about K and, $B(K) = 0$ (1.21)

ii) on the bottom half of a sphere we must have :

$$\lim_{\alpha\to -3K} A(\alpha) = A(K), \quad \lim_{\alpha\to -3K} \dot{A}(\alpha) = \dot{A}(K) \quad \text{i.e. :}$$

either $A(\alpha)$ is even about K and, $\dot{B}(K + j2K') = 0$ (1.22)

or $A(\alpha)$ is odd about K and, $B(K + j2K') = 0$ (1.23)

iii) at the origin $r = 0$ must be :

$$\lim_{r\to 0} C(r)B(\beta)A(\alpha) \quad \text{independent on} \quad \alpha \text{ and } \beta \tag{1.24}$$

iiii) at infinity $r \to \infty$:

$\lim_{r\to\infty} C(r)B(\beta)A(\alpha)$ must satisfy radiation conditions such as Sommerfield's (1.25)

The dot $\dot{}$ indicates the first total derivative with respect to the argument .

1.3.3 The mathematical properties of the Helmholtz equation

In third instance " the solution " has to satisfy the scalar wave equation :

$$\nabla^2 F + \kappa^2 F = 0 \tag{1.26}$$

which in conical c.s. separates into the following ordinary differential equations:

$$\ddot{w}(z) - [a + b(ksnz)^2 + q(ksnz)^4]w(z) = 0 \quad \text{Lamé's equation} \tag{1.27}$$

$$\ddot{C}(r) + \frac{2}{r}\dot{C}(r) + (\kappa^2 - \frac{d}{r^2})C(r) = 0 \quad \text{Bessel's spherical equation} \tag{1.28}$$

The solutions of Bessel's equation are well known for a long time (see [7]) and we remember here only the fact that one of its solutions of the 1^{st} kind satisfies the smoothness in the origin since $lim_{r\to 0}C(r) = 0$, while one of its solutions of the 3^{rd} kind satisfies the radiation conditions since $lim_{r\to\infty}C(r) \propto \frac{e^{-j\kappa r}}{r}$.

Equation (1.27) is satisfied by both $A(\alpha), B(\beta)$ on the two different but

contiguous intervals $\alpha \in [K, -3K)$ and $\beta \in [K, K + j2K']$.

In a complete general way it features the following properties :

i) it does not contain the term $\dot{w}(z)$ and the coefficient of w is even so that there is one solution which is even and one which is odd with respect to any ordinary point z_0 [2], in particular the points $z_0 = mK, z_0 = K + jnK'$ with m, n integers. Among them is the point $z_0 = K$ where the intervals for α and β meet .

ii) When z equals α, (1.27) is a Hill type equation with even coefficients and period $2K$, while when z equals β, it is a Hill type equation with even coefficients and period $2K'$; no singularities are present on or near the path in question . Thus the well known theory of Hill's equation [2] is suitable for our purposes .

According to the latter theory, conditions like (1.20,21) are turned into the properties that $A(\alpha)$ is either even or odd about $\alpha = 0, K$ and $2K$ is either a period or an anti-period, that is to say, it may only be one of 8 different forms .

Furthermore, for the property i), the condition (1.20) means $B(\beta)$ is even with respect to K, while (1.21) means $B(\beta)$ is odd with respect to K .

Thus, incidentally, $A(\alpha)$ and $B(\beta)$ are of the *same parity* with respect to $z_0 = K$ where, being z_0 a regular point, the Lamé's equation admits a *unique* even or odd solution .

Likewise, we can state the remarkable conclusion that the smoothness condition on the upper half of a sphere implies $A(\alpha), B(\beta)$ to be the *same solution*, i.e. :

$$F(r, \beta, \alpha) = C(r)w(\beta)w(\alpha) \tag{1.29}$$

Similar arguments arise when we apply i) in (1.22,23) so that $B(\beta)$ is either even or odd about $K + j2K'$ as well as about K. Hill's equation shows then that

$B(\beta)$ must be periodic with $j2K'$ either a period or an anti-period .

The 8 types of solutions so identified are the *Lamé's polynomials* and in Applied Mathematics they are often characterized by the combination of the three properties of (i) being odd or even in z, (ii) having real period $2K$ *or* $4K$ and (iii) having imaginary period $j2K'$ *or* $j4K'$. They can be expressed in a truncated Fourier-Jacobi series (see [6]) whose computation is easier and more accurate than any other Lamé's solution .

Nevertheless, the solutions we are searching for cannot be among these because the physical b.c., that are established by the conductor, will relax at least one of the set of hypotheses (1.20,23) .

However, the knowledge of the link and of the properties of the solutions along α and β will permit us to choice the position of the conductor, i.e. where smoothness is no longer required, in such a way to maintain the maximum simplicity for the solutions .

This way, it will be possible to maintain uniqueness and double-periodicity of the solution for the plane sector along α and β but with no longer fundamental periodicity along β which is now of $8K'$, whereas the second solution is completely aperiodic .

In the problem of the double-sector, both the two distinct solutions are involved but the first presents only real fundamental periodicity of $2K$ *or* $4K$ along α and the second only imaginary fundamental periodicity of $2K'$ *or* $4K'$ along β.

These are the *Transcendental Lamé's functions* .

In both cases the Fourier-Jacobi series representations of the solution do not terminate in general but, in spite of that, their computation is quite practicable.

1.3.4 The physical boundary conditions

At last, the conditions still to be satisfied by " the solution " are those established by the plane sector conductors fitting one or more degenerate surfaces $\alpha = -K, +K$, $\beta = K, K + j2K'$ showed in Fig. 1.7 .

We will show later that they are belong the Sturm-Liouville class and precisely of just the forms :

$$\dot{w}(z_0) = 0 \qquad w(z_0) = 0 \tag{1.30}$$

When w is A then $z_0 = \pm K$ while when w is B then $z_0 = K, K + j2K'$.

In order to reduce the number of different forms (1.30) for the b.c. we may change the variable β into u along a real interval according to :

$$\beta \in [K, K + j2K'] \qquad \beta = K + jK' - ju \qquad u \in [-K', K'] \tag{1.31}$$

This way, it will only prove necessary to consider the following three groups of b.c. in our applications :

$$w(-K) = 0, \; w(K) = 0 \tag{1.32}$$

$$\dot{w}(-K) = 0, \; w(K) = 0 \quad \text{or} \quad w(-K) = 0, \; \dot{w}(K) = 0 \tag{1.33}$$

$$\dot{w}(-K) = 0, \; \dot{w}(K) = 0 \tag{1.34}$$

and the analogous with K' in the place of K.

It is now obvious to ask ourself whether these conditions, as well as the previous ones, can be reduced to conditions of parity and periodicity for $w(z)$.

A rigorous demonstration based on the general properties of the Hill's equation is given in Appendix A whose conclusions can be summarized as in the following .

The b.c. $w(-K) = 0, w(K) = 0$ **imply :**

$$\text{either } w(z) \text{ even with period } 4K \tag{1.35}$$

$$\text{or } w(z) \text{ odd with period } 2K \tag{1.36}$$

The b.c. $\dot{w}(-K) = 0, w(K) = 0$ **imply :**

$$w(z) = w_1(z) + w_2(z) \text{ with period } 8K \tag{1.37}$$

The b.c. $w(-K) = 0, \dot{w}(K) = 0$ **imply :**

$$w(z) = w_1(z) - w_2(z) \text{ with period } 8K \tag{1.38}$$

The b.c. $\dot{w}(-K) = 0, \dot{w}(K) = 0$ **imply :**

$$\text{either } w(z) \text{ even with period } 2K \tag{1.39}$$

$$\text{or } w(z) \text{ odd with period } 4K \tag{1.40}$$

This is a very remarkable result because in the following *we will be allowed to translate straightforwardly the physical b.c. into the previous simple parity and periodicity conditions for " the solution " .*

1.4 The Solutions

Once the possible solutions have been identified as those with the properties just discussed, we have to express them in a form easy to compute and to handle theoretically .

Unfortunately, the up to date literature on this matter, see [1, 5, 6, 19, 10, 9], makes use of the more disparate forms either because of different symbolism and conventions or because the characteristics of the solutions (i.e. parity, periodicity, finiteness or fast convergence series representation, etc ...) are more understandable in one than in another form .

1.4.1 The analytic forms of the Lamé's equation

In the attempt to achieve goals like simplicity, rigour and accordance with the main literature, we shall present three main forms of the Lamé's equation . This way, we can start making the form (1.27) explicit as it will appear later in Jacobian form versus α .

$$\ddot{A} + [h - \nu(\nu+1)(ksn\alpha)^2]A = 0 \qquad \alpha \in [K, -3K) \tag{1.41}$$

whose trigonometric form (see [5]) and associated change of variable are given by :

$$[1 - (ksin\varphi)^2]\ddot{\Xi} - k^2 sin\varphi cos\varphi \dot{\Xi} + [h - \nu(\nu+1)(ksin\varphi)^2]\Xi = 0 \tag{1.42}$$

$$\alpha \in [K, -3K) \qquad \varphi = am(\alpha) \qquad \varphi \in [\tfrac{\pi}{2}, -3\tfrac{\pi}{2}) \tag{1.43}$$

where am is the amplitude function (see also [1]) whose property $am(nK) = n\frac{\pi}{2}$, permits a straightforward translation of the periodicities in Jacobian variables to those in trigonometric variables making use of the correspondence $K \to \frac{\pi}{2}$.

As function of trigonometric variables in the conical c.s., (1.41) becomes :

$$[1 - (kcos\phi)^2]\ddot{\Phi} + k^2 sin\phi cos\phi \dot{\Phi} + [\mu^2 + \nu(\nu+1)(ksin\phi)^2]\Phi = 0 \tag{1.44}$$

$$sin\phi = cn\alpha \quad \text{that is} \quad \phi = \tfrac{\pi}{2} - \varphi \qquad \phi \in [0, 2\pi) \tag{1.45}$$

The Lamé's equation versus β assumes the same form (1.41) :

$$\ddot{B} + [h - \nu(\nu+1)(ksn\beta)^2]B = 0 \qquad \beta \in [K, K + j2K'] \tag{1.46}$$

but since β belongs to a complex interval is preferable to turn it into a real variable according to :

$$\ddot{U} + [h' - \nu(\nu+1)(k'snu)^2]U = 0 \tag{1.47}$$

$$\beta = K + jK' - ju \qquad u \in [K', -K'] \tag{1.48}$$

Thus, following previous lines, we recover the trigonometric form and related change of variable :

$$[1 - (k'sin\vartheta)^2]\ddot{\Upsilon} - k'^2 sin\vartheta cos\vartheta\dot{\Upsilon} + [h' - \nu(\nu+1)(k'sin\vartheta)^2]\Upsilon = 0 \tag{1.49}$$

$$u \in [K', -K'] \qquad \vartheta = am(u) \qquad \vartheta \in [\tfrac{\pi}{2}, -\tfrac{\pi}{2}) \tag{1.50}$$

and using the trigonometric variables in the conical c.s. (1.46) becomes :

$$[1 - (k'cos\theta)^2]\ddot{\Theta} + k'^2 sin\theta cos\theta\dot{\Theta} + [-\mu^2 + \nu(\nu+1)(k'sin\theta)^2]\Theta = 0 \tag{1.51}$$

$$sin\theta = cnu \quad \text{that is} \quad \theta = \tfrac{\pi}{2} - \vartheta \quad \text{that is} \quad sin\theta = j\tfrac{k}{k'}cn\beta \qquad \theta \in [0, \pi] \tag{1.52}$$

The symbols h, ν will be obtained as separation constants while h', μ are related to them by the :

$$h' = -h + \nu(\nu+1) \tag{1.53}$$

$$\mu^2 = h - \nu(\nu+1)k^2 \tag{1.54}$$

1.4.2 The analytical form of the solutions

The representation problem of the Lamé's solutions with given parity and periodicity was successfully treated by Ince in 1940 [5, 6] .

His conclusion was that all the solutions we are interested in can be expressed as series whose coefficients are given by a three-terms recursive formulae.

Moreover when the series are not finite, their convergence can be greatly enhanced when trigonometric form is used and, especially as $k^2 \to 1$.

Precisely, if we indicate by X_i the i^{th} coefficient of the Jacobi or Fourier series, we have, respectively :

$$\lim_{i\to\infty} |\frac{X_i}{X_{i-1}}| = k^2 \qquad \lim_{i\to\infty} |\frac{X_i}{X_{i-1}}| = (\frac{1-k'}{k})^2 < k^2 \in (0,1) \tag{1.55}$$

The Fourier form presents two more advantages consisting in the orthogonal properties, of great utility in the applications, and in the easier computability of the circular functions in respect of the Jacobian ones (see Appendix in [1]) . In addition, during the study of the singularities we need only the first fundamental term of the series, which is easy to turn into Jacobian form, if necessary .

Furthermore, when an accurate complete solution is needed, we can express it straightforwardly in terms of the conical trigonometric coordinates θ and ϕ by simply shifting by $\frac{\pi}{2}$ those relative to ϑ and φ as indicated in (1.44,51) .

The continued fraction properties

The Fourier series representation, and then the function it represents, is uniquely identified by the succession of its coefficients $\{X_i\}$.

They obey a three-terms recursive formula associable to a continued fraction

whose main properties we now recall (see [7] pg.60) .

In the case of unilateral coefficients, that are those different from 0 only for $i \geq 0$, the recursivity relations can be expressed using the elements a_i, b_i, c_i as :

$$b_0 X_0 + c_1 X_1 = 0 \qquad i = 0 \qquad (1.56)$$

$$a_{i-1} X_{i-1} + b_i X_i + c_{i+1} X_{i+1} = 0 \qquad i \geq 1 \qquad (1.57)$$

whose associated i^{th} approximants are :

$$q_i = -\cfrac{a_i}{b_i - \cfrac{a_{i+1}c_{i+1}}{b_{i+1} - \cfrac{a_{i+2}c_{i+2}}{-\ldots}}} \qquad (1.58)$$

The convergence of the continued fraction are characterized by the two solutions t_1, t_2 of the equation :

$$a + bt + ct^2 = 0 \qquad (1.59)$$

where : $\quad a = \lim_{i\to\infty} a_i \qquad b = \lim_{i\to\infty} b_i \qquad c = \lim_{i\to\infty} c_i$

If $|t_1| < |t_2|$ to ensure convergence, it must be :

$$b_0 = q_1 c_1 \qquad \lim_{i\to\infty} \frac{X_i}{X_{i-1}} = t_1 \qquad (1.60)$$

The first equation represents the vanishing conditions for the coefficients with negative index and the second their asymptotic behaviour; together they ensure the uniqueness of the succession $\{X_i\}$ and then of the solution .

We will also meet more general solutions with bilateral coefficients in which to the first condition is substituted an asymptotic behaviour at $-\infty$.

1.4.3 The analytical expression of the solutions

We can now proceed by writing down the Fourier forms of the 6 kinds of solution we need consider and which we can characterize by the combinations of the two properties (i) of being even or odd and (ii) having periods $\pi, 2\pi, 4\pi$.

For simplicity, we indicate by $y(v)$ the generic solution along φ or ϑ .

Moreover, for each kind there exists (see [6]) a numerable infinity of solutions for each ν-value and given k^2 . Hence each individual solution should be labeled like (see [7, 6]) :

$$y_{even}(v) = E^m_{c_\nu}(v; k^2) \qquad h = a^\mu_\nu(k^2) \tag{1.61}$$

$$y_{odd}(v) = E^m_{s_\nu}(v; k^2) \qquad h = b^\mu_\nu(k^2) \tag{1.62}$$

where m is any integer, for example, with the meaning of :

$$pm = \text{ number of zeros in } v \in [0, p\pi) \tag{1.63}$$

and $p\pi$ is the periodicity of the solution .

For each one of the 6 kinds of solutions we report in Appendix B the three-terms recursive formula and associated continued fraction where we always have: $t_{1,2} = (\frac{1 \mp k'}{k})^2$. Besides, we show in the same Appendix B the tail-to-head computational implementation of the characteristic equation which permits to satisfy the conditions of convergence and uniqueness (1.60), so as to compute at once the eigenvalues $\nu(k^2), h(k^2)$ and associated succession $\{X_i\}$.

1.4.4 The degenerate cases $k^2 = 0, k^2 = 1$

There is still something important to say about the characteristic equations which can be seen as a transcendental equation in the unknowns $\nu(k^2), h(k^2)$, and precisely how they degenerate into a simple algebraic equation when k^2 reaches the limit values of its interval of definition.

Geometrically speaking, the conical c.s. degenerates into spherical c.s. and the Lamé's equations degenerate one into a harmonic equation and the other into a Legendre's equation (see [1]) .

This way, relatively for example to the Lamé's equation along α we get :

$$\ddot{A} + hA = 0 \qquad \text{when } k^2 = 0 \tag{1.64}$$

In this situation h becomes independent of ν and the solution degenerates into a circular function as :

per $2K$ or π even and odd :

$$h = (2m_0)^2, \qquad E_{c_\nu}^{2m_0} = cos(2m_0)\alpha \tag{1.65}$$

per $4K$ or 2π even and odd :

$$h = (2m_0 + 1)^2, \qquad E_{c_\nu}^{2m_0+1} = cos(2m_0 + 1)\alpha \tag{1.66}$$

per $8K$ or 4π even and odd :

$$h = (m_0 + \tfrac{1}{2})^2, \qquad E_{c_\nu}^{m_0} = cos(m_0 + \tfrac{1}{2})\alpha \tag{1.67}$$

where $m_0 = 0, 1, 2, ...$

The odd solutions are obtainable from these by simply changing *cos* with *sin* .

In a similar way, the same Lamé's equation degenerates into a form of Legendre' s equation (see also [5]) :

$$\ddot{A} + [h - \nu(\nu+1)tanh\alpha]A = 0 \qquad \text{when } k^2 = 1 \tag{1.68}$$

In this condition the simple algebraic relations between h and ν and relative Legendre's functions are (see also [5, 7]) :

per $2K, 4K$ or $\pi, 2\pi$ even :

$$h = (4m_1+1)\nu - (2m_1)^2, \qquad E_{c_\nu}^{2m_1} = P_\nu^{\nu-2m_1}(tanh\alpha) \tag{1.69}$$

per $2K, 4K$ or $\pi, 2\pi$ odd :

$$h = (4m_1+3)\nu - (2m_1+1)^2, \qquad E_{c_\nu}^{2m_1+1} = P_\nu^{\nu-(2m_1+1)}(tanh\alpha) \tag{1.70}$$

per $8K$ or 4π even and odd :

$$h = (2m_1+1)\nu - (m_1)^2, \qquad E_{c_\nu}^{m_1} = P_\nu^{\nu-m_1}(tanh\alpha) \tag{1.71}$$

where $m_1 = 0, 1, 2, \ldots$.

Moreover, in our applications Lamé's equations along α and β have to be valid simultaneously, the first with parameter k^2 and the second with parameter k'^2 . Hence, when the degeneracy $k^2 = 0, k'^2 = 1$ occurs, one h-value (1.65,66,67) has to coexist with one algebraic equation (1.69,70,71) written with h' in place of h .

By the system of these two equations we determine the indefinite numerable possible values of $h_{m_0,m_1}(0), \nu_{m_0,m_1}(0)$.

Analogously, when the degeneracy $k^2 = 1, k'^2 = 0$ is considered, we deter-

mine the values $h_{m_0,m1}(1), \nu_{m_0,m_1}(1)$.

The knowledge of these exact values are not just a scientific curiosity because they provide the important starting and ending points in the implementation of the algorithm determining ν, h versus k^2 .

In particular in our applications the $\nu(0)$-values will always be integers while, correspondently, $\nu(1) = \nu(0) + 1$ or $\nu(1) = \nu(0) \pm \frac{1}{2}$.

Under the same conditions, $h(0)$ will always be the square of an integer, while $h(1)$ will be integer or an odd half of an integer .

Chapter 2

THE E-FIELD SINGULARITY VECTOR

2.1 Introduction

This Chapter begins by dealing with the exact solutions of the scalar wave Helmholtz's equation satisfying the b.c. pertaining to the sector and double sector perfect plane conductor.

The problem is a three dimensional scalar one which, in the more appropriate geometry of a conical c.s., is reduced, in fact, to finding the solutions of a Bessel's equation and two Lamé's equations . As the first are well known, the problem is led again to determining for every sector aperture $\sigma \in [0, 2\pi]$ or double-sector aperture $\sigma \in [0, \pi]$ the eigenvalues spectrum $\{\nu, h\}$ and eigenfunction spectrum $\{B(\beta), A(\alpha)\}$ for a two-dimensional Sturm-Liouville problem.

The theory just developed in Chapter 1 permits the determination of these spectra with an accuracy which has never been reached before for the plane sector

(see [10, 9, 17, 14]) and, as far as we know, for the first time for the double-sector.

Furthermore, from these spectra are recovered those relative to other five novel derived wedges geometries by, say, simple identification of sub-spectra. This is possible because the conductor relative to these wedges fit, beside the sectors, some others degenerate surfaces, that are planes of symmetry, so as to realize those geometries that are met especially in boxed waveguide discontinuities or antennas .

In microwave ($3-30\ GHz$) and millimeter waves ($30-300\ GHz$) integrated circuits, only the tip wedges of these ideal structures are involved and only the knowledge of the main EM characteristics might suffice there when the frequencies are not too high and dimensions sufficiently small .

For this purpose, the Chapter will end by presenting the more accurate static E-field solutions subjected to successive approximations till a final E-field singularity vector is recovered that maintains just the correct satisfaction of the regular and singular b.c. .

The whole topic finds its location in the general context of diffraction by objects with edges, corners, tips etc... that has occupied the attention of several authors (see [23, 13, 12] and literature quoted there) since Sommerfeld solved the classic case of a half plane .

Analytically speaking, the plane sector and double-sector are " double discontinuities ", for the straight edges represent a discontinuity in the scattering surface since a normal cannot be defined univocally there . On the tip, however, also the tangent to the edge is undetermined .

Several authors like Kraus [21], Radlow [22], Jones [24] have made conjectures, centred particularly on the unicity of the singular solution, based on

approximations and physical reasoning .

Moreover, if we consider the aims of this work, the present approach seems to be redundantly rigorous, but a few theoretical and applicative motivations indicate the contrary . For instance the Green's function for the sector can be determined from the spectrum as indicated in [10] and it should be possible to identify a " scattering coefficient " for the tip using the procedure given in [23] .

Closer to our applications is the problem of representing an unknown diffracted field by means of an orthogonal, complete set of functions satisfying the b.c. . As a whole, these conditions cannot be satisfied by the EM field spectra. Hence in common microwave and millimeter waves applications it would be helpful to be able to express the unknown field on a finite plane surface according to a simple set of orthogonal and complete functions times a simple function satisfying exactly the b.c. pertaining to one or more wedges linked together .

Specifically to this b.c.-satisfying function, which we name singularity functions, is entrusted the task of describing exactly the distribution of zeros and singularities over all the conductor surfaces, edges and vertices of the components of the EM fields .

From this point of view, the work of this Chapter can be summarized as a procedure starting with the determination of the complete spectrum of solutions for the static E-field with the purpose of formulating the easiest possible E-field singularity vector still satisfying exactly the b.c. on the conductor and featuring its main behaviour on its vicinity . The singularity vector so defined is independent of frequency (see [13]), in accordance with a classic result which states that approaching a conducting surface by a quantity much smaller than the wavelength, the dynamic solution converges to the static one .

2.2 Solution of the scalar Helmholtz's equation

It has been proved (see for instance [12] pp.1762 – 1767) that in the geometry of a conical c.s. the solutions of the general vector wave equation for the EM fields, as well as those of the Laplace's equation for the static E-field, are obtainable by simply applying vector operators to the solutions of the scalar wave Helmholtz's equation for a potential function Ψ :

$$\nabla^2 \Psi(r,\beta,\alpha;\omega) + \kappa^2 \Psi(r,\beta,\alpha;\omega) = 0 \qquad (2.1)$$

A sinusoidal excitation will be always considered so that the time dependence is included in the wave number $\kappa = \omega\sqrt{\mu\epsilon}$, where $\omega = 2\pi f$ is the angular frequency , f is the frequency and, finally, μ and ϵ are respectively the magnetic permeability and dielectric constants of the medium which, in first approximation, we regard as homogeneous.

In the conical c.s. described in 1.2.2 and shown in Fig. 1.5, $\hat{r},\hat{\beta},\hat{\alpha}$ (or $\hat{r},\hat{\theta},\hat{\phi}$) constitute a proper set of three unit vectors and the metric coefficients (see also [11] pp. 1 – 3) are given by :

$$g_{11} = 1 \quad g_{22} = (kr)^2(sn^2\alpha - sn^2\beta) \quad g_{33} = (kr)^2(sn^2\beta - sn^2\alpha) \qquad (2.2)$$

$$g^{\frac{1}{2}} = (g_{11}g_{22}g_{33})^{\frac{1}{2}} = j(kr)^2(sn^2\alpha - sn^2\beta) \qquad (2.3)$$

Hence the scalar operator ∇^2 in (2.1) can be written explicitely as :

$$\frac{\partial}{\partial r}\left(\frac{g^{\frac{1}{2}}}{g_{11}}\frac{\partial\Psi}{\partial r}\right) + \frac{\partial}{\partial\beta}\left(\frac{g^{\frac{1}{2}}}{g_{22}}\frac{\partial\Psi}{\partial\beta}\right) + \frac{\partial}{\partial\alpha}\left(\frac{g^{\frac{1}{2}}}{g_{33}}\frac{\partial\Psi}{\partial\alpha}\right) + \kappa^2 g^{\frac{1}{2}}\Psi = 0 \qquad (2.4)$$

Without invalidating the generality of the solution, we can limit the attention to just the separable forms :

$$\Psi(r,\beta,\alpha;\omega) = R(r;\omega)B(\beta)A(\alpha) \tag{2.5}$$

where the space and frequency dependence are separated by ; .

With this position, (2.1) separates into the three following ordinary differential equations :

$$\ddot{R} + \frac{2}{r}\dot{R} + \left[\kappa^2 - \nu(\nu+1)\frac{1}{r^2}\right] R = 0 \tag{2.6}$$

$$\ddot{B} + \left[h - \nu(\nu+1)(ksn\beta)^2\right] B = 0 \tag{2.7}$$

$$\ddot{A} + \left[h - \nu(\nu+1)(ksn\alpha)^2\right] A = 0 \tag{2.8}$$

where ν and h are two generic separation constants .

The general solution of the spherical Bessel's equation (2.6) is chosen for a reason which will appear in Chapter 3, in the form :

$$R(r;\omega) = Cj_\nu^{(1)}(\kappa r) + Dh_\nu^{(2)}(\kappa r) = C\sqrt{\frac{\frac{\pi}{2}}{\kappa r}}J_{\nu+\frac{1}{2}}(\kappa r) + D\sqrt{\frac{\frac{\pi}{2}}{\kappa r}}H_{\nu+\frac{1}{2}}(\kappa r) \tag{2.9}$$

where the first solution $j_\nu^{(1)}$ is the spherical Bessel function of 1^{st} kind, the second solution $h_\nu^{(2)}$ is an Hankel function of 2^{nd} kind while ν is their oder and C, D are the linear combination constants .

Incidentally, R is the only part of Ψ that is dependent on ω through the factor κr, so that frequency, medium and radius act on it in the same way, that is, as a change of scale .

The differential equations (2.7,8), together with the b.c. along α, β of the

kinds considered in 1.3.4, constitute a two-dimensional Sturm-Liouville problem with general solution :

$$B(\beta) = \mathrm{E}\mathcal{E}_\nu^h(\beta) + \mathrm{F}\mathcal{F}_\nu^h(\beta) \tag{2.10}$$

$$A(\alpha) = \mathrm{G}\mathcal{E}_\nu^h(\alpha) + \mathrm{H}\mathcal{F}_\nu^h(\alpha) \tag{2.11}$$

where $\mathcal{E}_\nu^h, \mathcal{F}_\nu^h$ are the 1^{st} and 2^{nd} solutions of 1^{st} kind of order ν and degree h of the Lamé's equations, while E,F,G,H are the linear combination constants .

Some preliminary properties of these solutions can be obtained also considering the associated 2-dimensional Sturm-Liouville operator defined as in [10].

First of all, the b.c. require the solutions or their derivatives to vanish, but not simultaneously, thus for the linear independence of $\mathcal{E}, \mathcal{F}$ the solutions B, A are reduced to just $\mathcal{E}$ or $\mathcal{F}$, but not to any of their linear combinations .

The operator associable to the system (2.7,8) and specified in [10] is self-adjoint and positive definite and it can be easily proved looking at (2.6,7,8) that for any possible $\nu \geq -\frac{1}{2}$ there is one $\nu \leq -\frac{1}{2}$ which gives the same solution . Furthermore no solution occurs in $\nu \in (0, -\frac{1}{2}]$, for, without loss of generality, we can choose :

$$\nu \geq 0 \tag{2.12}$$

and for every ν there exist at most a finite number of h-values ≥ 0 (see (1.4.4)) and hence of eigenfunctions .

As a whole, for any couple of b.c. along α and β and for any geometry, i.e. given k, a spectrum of eigenvalues $\{\nu, h\}$ and eigenfunctions $\{B(\beta), A(\alpha)\}$ are identified .

From another point of view, because of the usual properties of the spectrum

of solutions of a differential equation, the individual equations and relative b.c. can be satisfied for each given ν by a numerable infinity of h values and pair of relative eigenfunctions . The spectrum of solutions so obtained constitutes a complete orthogonal set in the intervals $\beta \in [K, K + j2K']$ or $\alpha \in (-3K, K]$ respectively, which in particular, are arcs of circle on the plane $y = 0$
(see Fig. 1.7) .

The spectrum of the whole system presents instead bi-orthogonal properties on the sphere with weight function $(sn^2\alpha - sn^2\beta)$, i.e. (see [9]) :

$$\int_{\alpha=-3K}^{K} \int_{\beta=K}^{K+j2K'} A_{\nu_1}^{h_1}(\alpha) B_{\nu_1}^{h_1}(\beta) A_{\nu_2}^{h_2}(\alpha) B_{\nu_2}^{h_2}(\beta)(sn^2\alpha - sn^2\beta) d\alpha d\beta = 0 \qquad (2.13)$$

2.3 Static E-field spectrum for the sector and double-sector

In order to obtain maximum simplicity of the solutions in the sense specified in 1.3.3, the sector and double-sector are disposed in a conical c.s. as in Figs. 2.1,2. There we highlight the degenerate coordinate surfaces on the plane $y = 0$ and associated values of the variables α, β and of the real variable u defined in (1.48).

For any given ϵ, and hence $k = sin\epsilon$, we obtain the acute sector and double-sector of angular aperture $\sigma = 2\epsilon$ of Fig. 2.1a,b as well as the obtuse sector of angular aperture $\sigma = 2(\pi - \epsilon)$ of Fig. 2.1b .

The static E-field generated by a static charge induced on these conductors, can be derived from a potential V :

$$V(r,\beta,\alpha) = \lim_{\omega \to 0} \Psi(r,\beta,\alpha;\omega) = \Psi(r,\beta,\alpha;0) = R(r;0)B(\beta)A(\alpha) \qquad (2.14)$$

according to the gradient expression in conical c.s. :

$$\vec{E} = - \bigtriangledown \cdot V = - \left[\dot{R}BA \, \hat{r} + \frac{R\dot{B}A}{kr\sqrt{sn^2\alpha - sn^2\beta}} \, \hat{\beta} + \frac{RB\dot{A}}{kr\sqrt{sn^2\beta - sn^2\alpha}} \, \hat{\alpha} \right] \qquad (2.15)$$

The Bessel's R solution degenerates now into the exponential one :

$$R(r) = Cr^{\nu} + Dr^{-(\nu+1)} \qquad (2.16)$$

The solutions for A and B instead can be recovered by applying the b.c. . These are relative to the sector surfaces $\beta = K, K + j2K'$ and $\alpha = -K, K$ and can be obtained by means of physical considerations and using (2.14,15) .

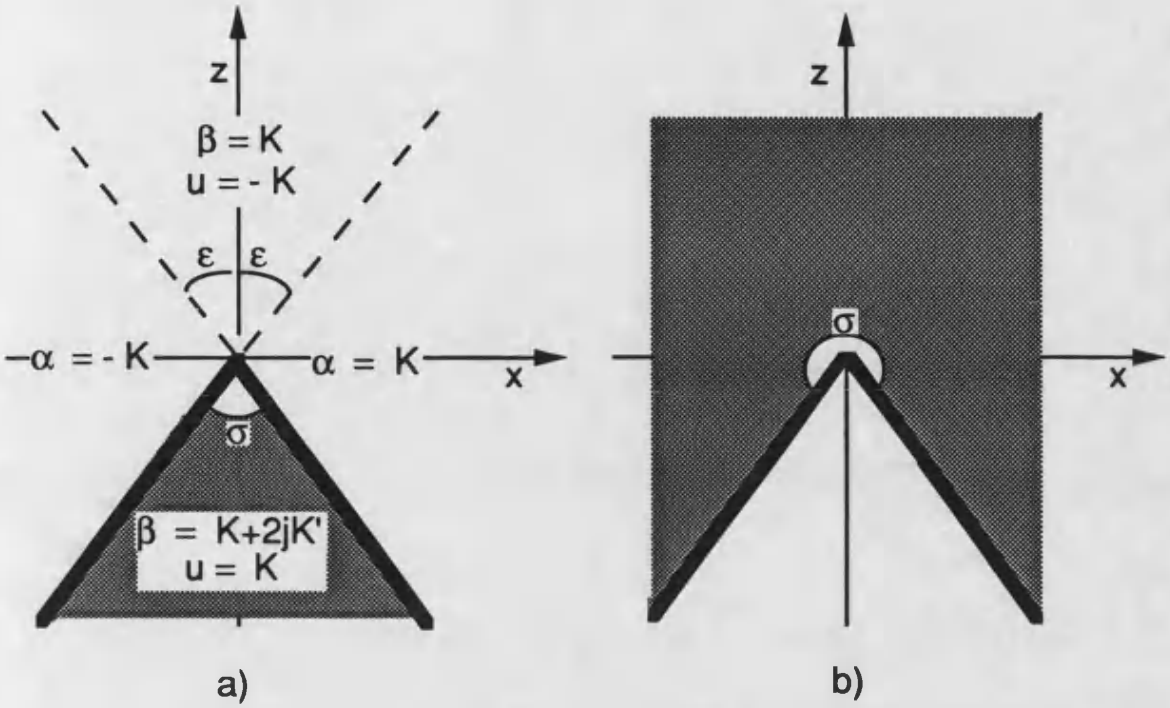

Fig. 2.1: plane acute a) and obtuse b) sector

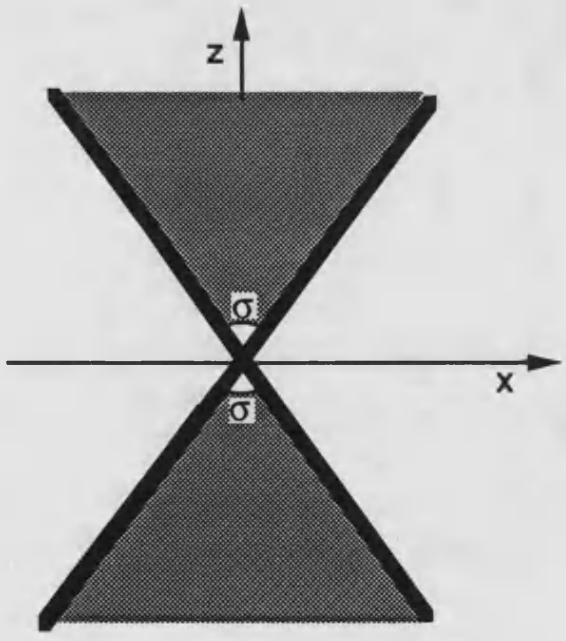

Fig. 2.2 : plane double sector

This way, we note that the conductor is an equipotential surface where, without loss of generality, we may set $V = 0$. From (2.14) it follows that if the conductor lies on a surface $\alpha = K$ or $-K$ then $A(\alpha) = 0$ there and analogously for $B(\beta)$, when the conductor fits the sectors $\beta = K$ or $K + j2K'$.

In second instance, since the static charge lies completely on the plane $y = 0$, the field component E_y must vanish on the portion of this plane that is adjacent to the conductor . Introducing this symmetry property in (2.15), we get the further conditions $\dot{A} = 0$ for a surface $\alpha = constant$, whereas $\dot{B} = 0$ on a surface $\beta = constant$.

Consequently, considering $U(u)$ in the place of $B(\beta)$ (see (1.47)), the full conditions to be satisfied in the three situations of Figs. 2.1a-b,2 are :

$$\text{acute sector} \quad \begin{cases} U(K') = \dot{U}(-K') = 0 \rightarrow \text{ period } {}^*8K' \\ \dot{A}(K) = \dot{A}(-K) = 0 \rightarrow \text{ period } {}^*2K \text{ even}, 4K \text{ odd} \end{cases} \tag{2.17}$$

$$\text{obtuse sector} \quad \begin{cases} U(K') = \dot{U}(-K') = 0 \rightarrow \text{ period } {}^*8K' \\ A(K) = A(-K) = 0 \rightarrow \text{period } 2K \text{ odd}, {}^*4K \text{ even} \end{cases} \tag{2.18}$$

$$\text{double-sector} \quad \begin{cases} U(K') = U(-K') = 0 \rightarrow \text{period } 2K' \text{ odd}, {}^*4K' \text{ even} \\ \dot{A}(K) = \dot{A}(-K) = 0 \rightarrow \text{ period } {}^*2K \text{ even}, 4K \text{ odd} \end{cases} \tag{2.19}$$

In the above, the use of real variable u permits to recover the sole forms of b.c. studied in 1.3.4; also indicated there by a $\rightarrow$ are their straightforward reductions to parity and periodicity conditions according to the discussion of 1.3.4 .

It appears now evident that the choice of the position of the acute and obtuse sectors is such that $A(\alpha)$ and $B(\beta)$ assume the same value at the meeting

point $z = K$ of the intervals for the variables . Hence, they are effectively part of the same double-periodic solution whose imaginary period $8K'$ is no longer the fundamental one, as announced in 1.3.3 .

Analogous properties cannot be obtained for the double-sector for which, however, the position of the conductor on the surfaces $\beta = K, K + j2K'$ ensure that both $A(\alpha)$ and $B(\beta)$ are periodic of fundamental period, one being the first and the other the second solution of the Lamé's equation, as anticipated in 1.3.3.

With these premises, the solution can be finally computed in Fourier series form in the manner discussed in 1.4.3 and indicated in Appendix B .

For example, relatively to the acute sector and because of the (2.17), (B.20,21) hold with the indicated change of sign; (B.28) holds with k and h changed into k' and h' respectively according to (1.47,48) .

By implementing the two correspondent continued fractions (B.23,24,25) and (B.29,30,31,32,33) in the more stable tail-to-head sequence and simultaneously solving them, we compute the eigenvalues ν, h versus $k^2 \in (0,1)$ with an accuracy that is only dependent on the maximum truncation index I and on the zero-finding procedure used.

For instance, in order to maintain an accuracy of, say, 6 decimal figures, I has to increase from a few tens when $k^2 \to 0$ up to a few hundreds when $k^2 \to 1$ according to (1.55), as the speed of convergence of the fraction slows down .

The ν, h-values assumed in the limit situations $k^2 = 0, 1$ can instead be determined analytically, as indicated in 1.4.4, thus providing, at the same time, the essential start and end points for determining the complete curves $\nu(k^2), h(k^2)$, as just described .

Explicitly, for the same acute sector, when $k^2 = 0, k'^2 = 1$, using the

(1.65,66,71) it must be :

$$h' = (2m_1 + 1)\nu - m_1^2 \qquad h = (2m_0)^2 \text{ or } (2m_0 + 1)^2 \tag{2.20}$$

that is to say :

$$\nu(0) = m_1 + \sqrt{h(0)} = n \qquad \text{period } 8K' \tag{2.21}$$

$$h(0) = (2m_0)^2 = m \qquad \text{period } 2K \tag{2.22}$$

$$h(0) = (2m_0 + 1)^2 = m \qquad \text{period } 4K \tag{2.23}$$

where $m_0, m_1 = 0, 1, 2, ...$, and m, n are the two integer values of $\nu(0), h(0)$.

It can be easily proved that the same values hold for the obtuse sector but with the exclusion of $m_1 = 0$.

For the double sector, we get instead in a similar way :

$$\nu(0) = 2m_1 + 1 + \sqrt{h(0)} = n \qquad \text{period } 2K' \tag{2.24}$$

$$\nu(0) = 2m_1 + \sqrt{h(0)} = n \qquad \text{period } 4K' \tag{2.25}$$

$$h(0) = (2m_0)^2 = m \qquad \text{period } 2K \tag{2.26}$$

$$h(0) = (2m_0 + 1)^2 = m \qquad \text{period } 4K \tag{2.27}$$

So that for the single couple of curves $\nu(k^2), h(k^2)$ we choose the ν, h-values corresponding to the given periodicities .

On the other hand, when $k^2 = 1, k'^2 = 0$ we get for the sector :

$$\text{periods } 2K, 4K \text{ (even)} , 8K' \quad \begin{cases} \nu(1) = 2m_1 + m_0 + \frac{1}{2} = n + \frac{1}{2} \\ h(1) = 4m_1(m_1 + m_0 + 1) + m_0 + \frac{1}{2} \end{cases} \tag{2.28}$$

$$\text{periods } 2K, 4K \text{ (odd)} , 8K' \quad \begin{cases} \nu(1) = 2m_1 + m_0 + \frac{3}{2} = n + \frac{1}{2} \\ h(1) = 4m_1(m_1 + m_0 + 2) + 3m_0 + \frac{7}{2} \end{cases} \tag{2.29}$$

And, finally, for the double-sector we obtain :

$$\nu(1) = 2m_1 + \sqrt{h'(1)} = n \qquad \text{period } 2K \tag{2.30}$$

$$\nu(1) = 2m_1 + 1 + \sqrt{h'(1)} = n \qquad \text{period } 4K \tag{2.31}$$

$$h'(1) = (2m_0)^2 = m \qquad \text{period } 2K' \tag{2.32}$$

$$h'(1) = (2m_0 + 1)^2 = m \qquad \text{period } 4K' \tag{2.33}$$

These simple formulae can be interpreted by saying that for the acute sector the ν-values start from any integer n for the terminating wire (see also Fig.4.7), corresponding to $k^2 = 0$, and increase monotonically up to $n + \frac{1}{2}$ for the half plane, corresponding to $k^2 = 1$, continuing to increase for obtuse sectors up to $n + 1$ for the plane conductor associated again with $k^2 = 0$ (see also Fig. 2.3) .

The h-curves follow similar rules starting from the square of any integer number and ending at the square of the successive, however, in general, they no longer increase monotonically (see also Fig. 2.3) .

The $\nu(k^2), h(k^2)$-curves for the double-sector are easier, as ν starts from any integer for the wire ($k^2 = 0$) and increases monotonically up to the successive

integer for the plane conductor ($k^2 = 1$), whereas the h-curves start from any square of an integer for the indefinite wire ($k^2 = 0$) and increase monotonically up to the integer recoverable from (2.32,33) for the plane conductor ($k^2 = 1$) as also indicated in Fig. 2.4 .

These repetitive properties of the spectrum $\{\nu, h\}$ permit to limit the attention, for instance, to just the first 15 of their numerable double infinity . As a way of example, relatively to the acute sector, we report in Appendix C the numerical evaluations of $\nu(k^2), h(k^2)$ for steps of 0.02 of k^2 and with an accuracy of 6 decimal figures .

More visually, the above reported properties of the curves $\nu(k^2), h(k^2)$ can be singled out from the plot in Fig. 2.3 for the sector and in Fig. 2.4 for the double sector .

When the zero-searching-procedure ends successfully, just by looking at the ratio of the successive series expansion coefficients $\frac{X_{i+1}}{X_i}$ in the continued fraction, we recover without any further operation the succession $\{X_i\}$ within an arbitrary multiplicative constant, and, then, the solution itself .

In Figs. 2.5-6 we draw the first 5 eigenfunctions normalized with respect to the maximum value relative to the particular $90^0, 270^0$ sectors corresponding to $k^2 = \frac{1}{2}$. They show explicitly all the different variables previously introduced for various reasons in the symmetric intervals $\theta, \phi \in [-2\pi, 2\pi]$, where all their periodicity and parity properties are identified . Similar graphs are reported in Fig. 2.7 for the right double-sector with $k^2 = \frac{1}{2}$.

In order to make these eigenvalue and eigenfunctions spectra readable, we present now a enumeration that is slightly different from that presented in 1.4.3, but closer to those used in waveguide theory . In fact, we label the single eigen-

value with two integer (i_1, i_2) defined so that $\nu(0) = i_1 + i_2$ while $h(0) = i_1^2$. Relatively to the eigenfunctions instead, for the same reason of better readability, we produce artificially a cusp in the point correspondent to the conductor simply by changing the sign of the functions after it . In these drawings i_1 indicates the number of zeros in $\theta \in (0, \pi)$ while i_2 indicates the number of zeros in $\phi \in (0, \pi)$, that is to say, the zeros other than those possibly present on the conductor along θ and halve of those along ϕ . This permits to retrieve the waveguide convention (see [25]) where the single modes were labeled by $(i_1, 2i_2)$ and the fundamental one by $(0, 0)$.

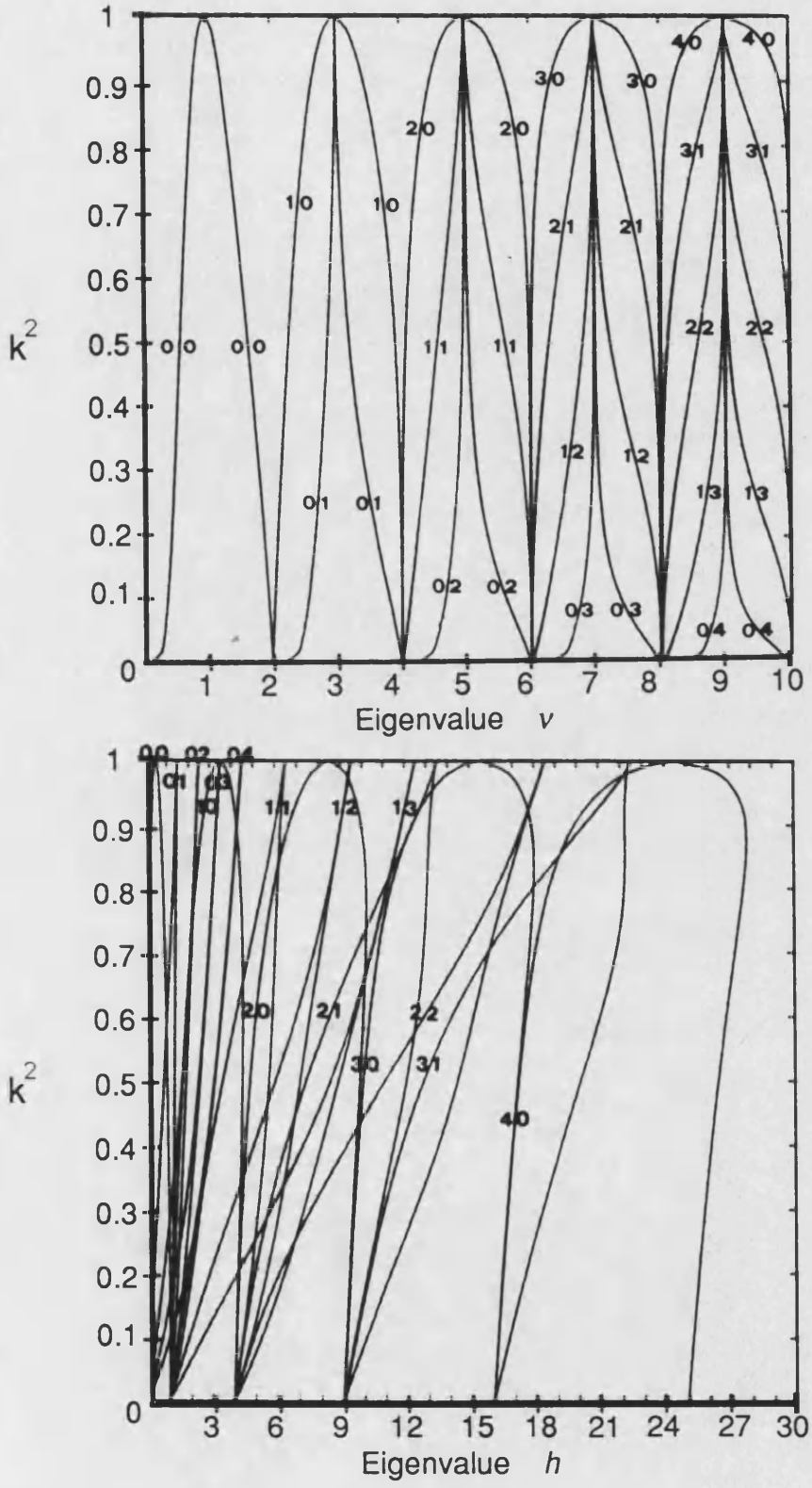

Fig. 2.3 : first 15 eigenvalues $\{\nu(k^2), h(k^2)\}$ for the sector

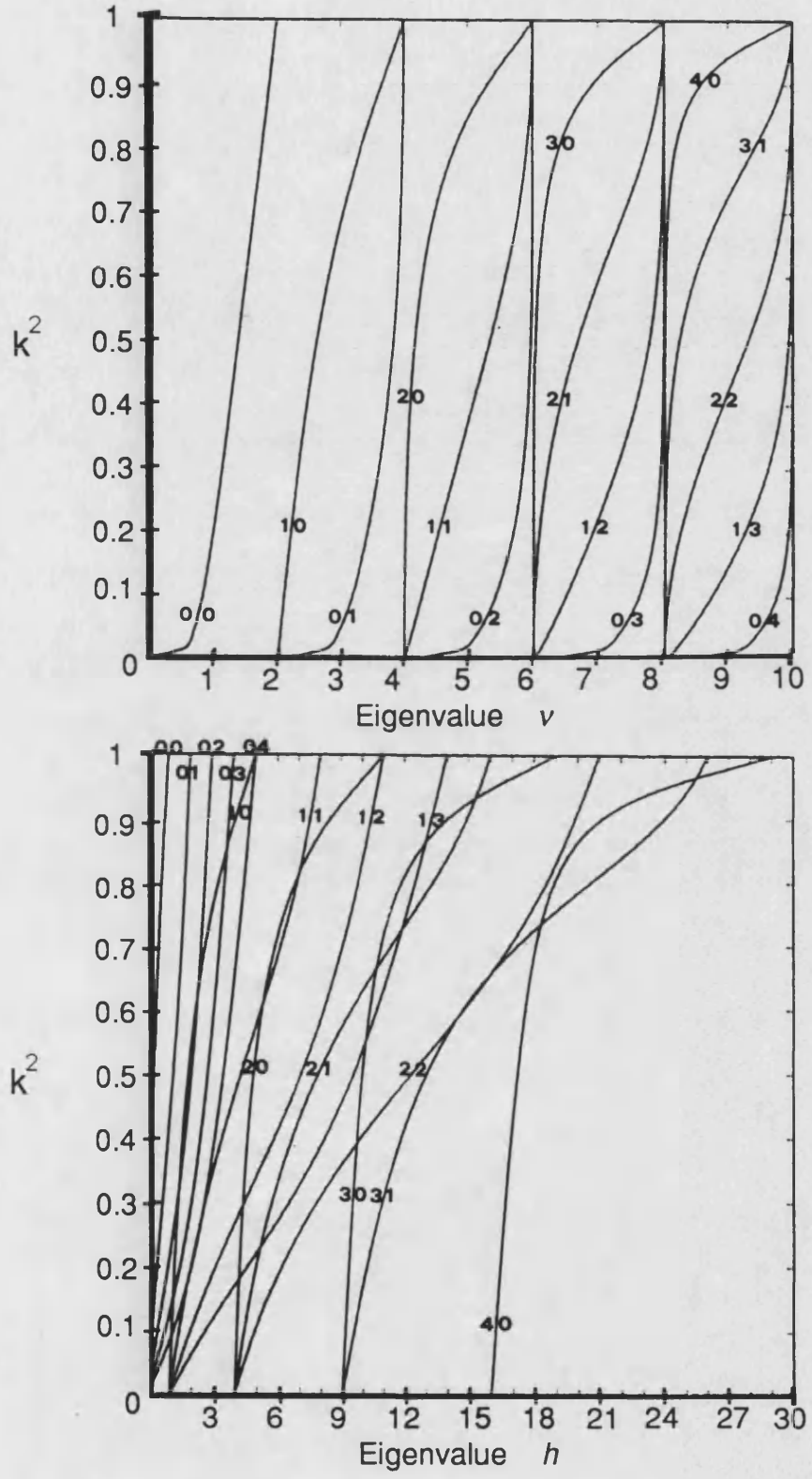

Fig. 2.4 : first 15 eigenvalues $\{\nu(k^2), h(k^2)\}$ for the double sector

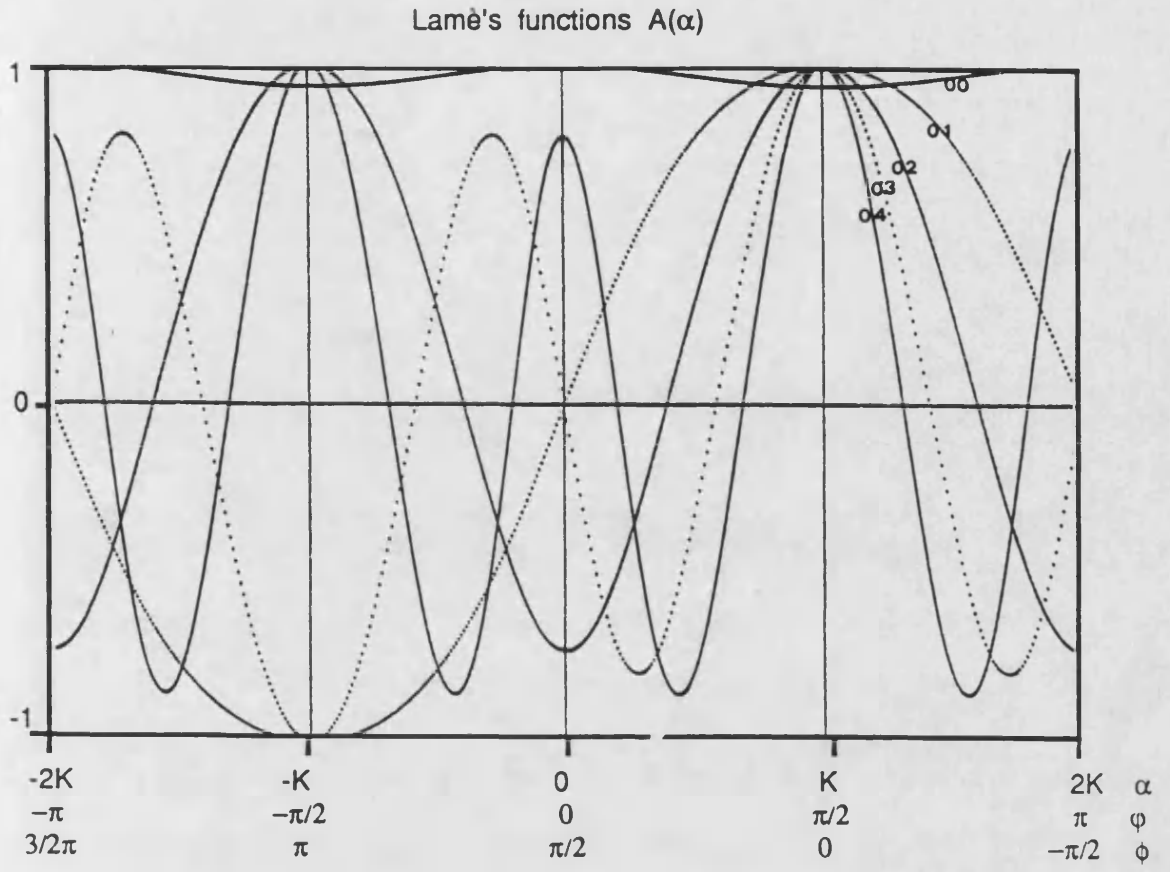

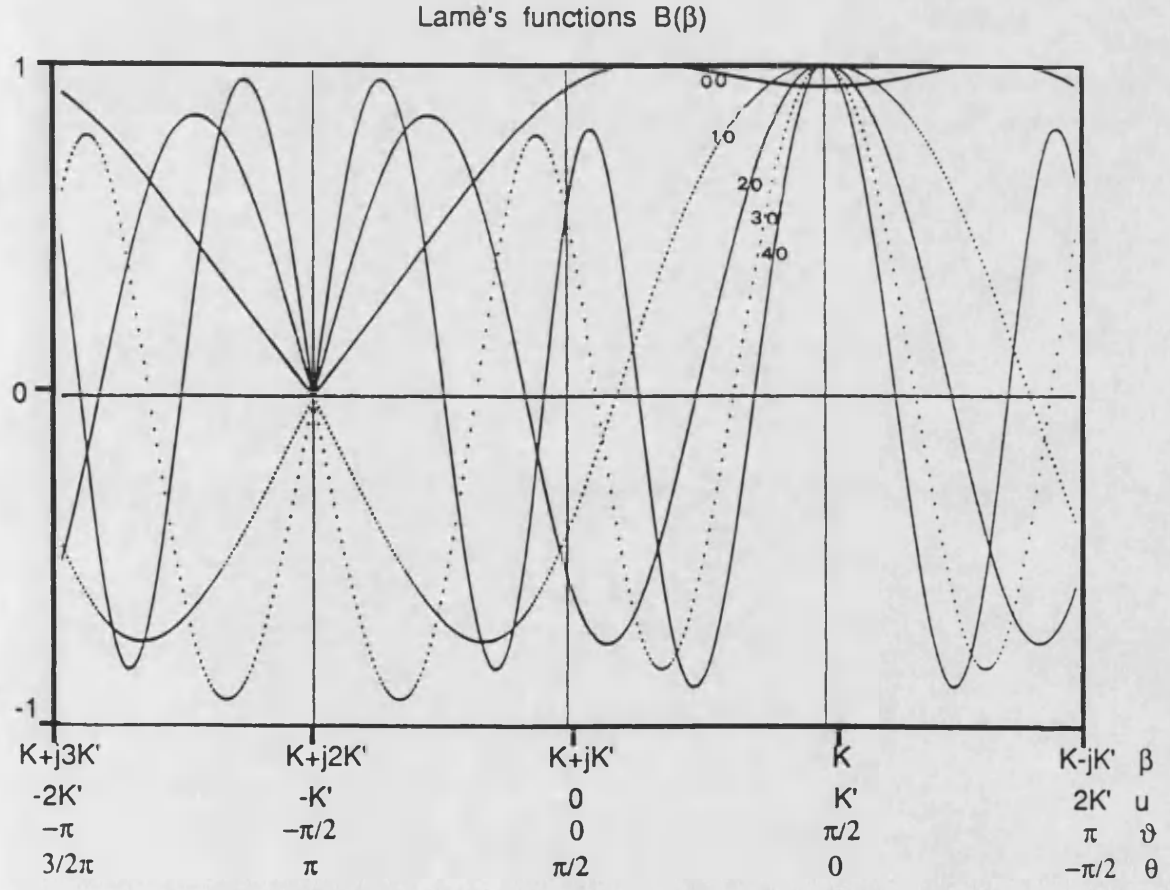

Fig. 2.5 : first 5 eigenvalues {B(β),A(α)} for the acute sector

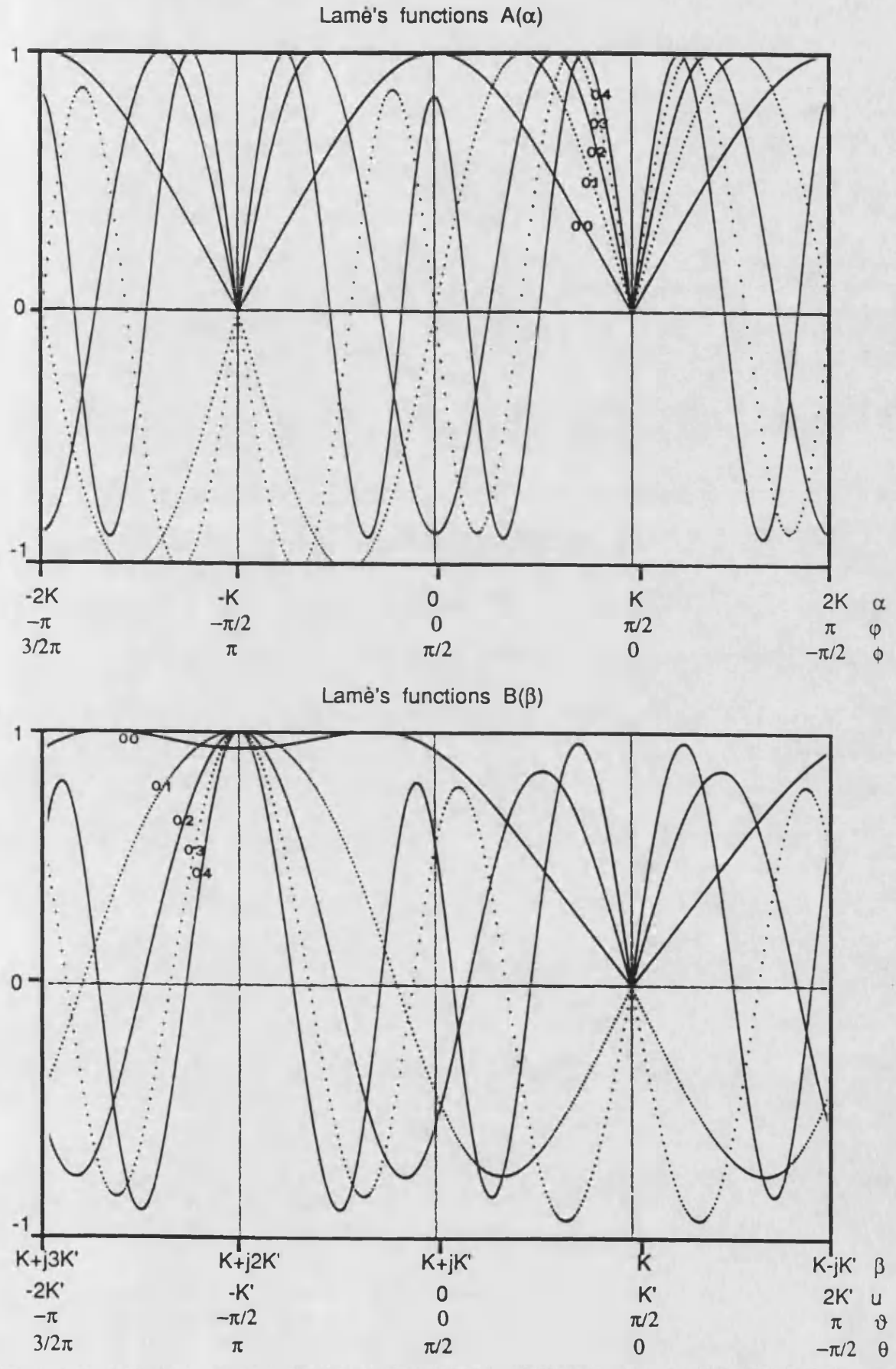

Fig. 2.6 : first 5 eigenvalues {B(β),A(α)} for the obtuse sector

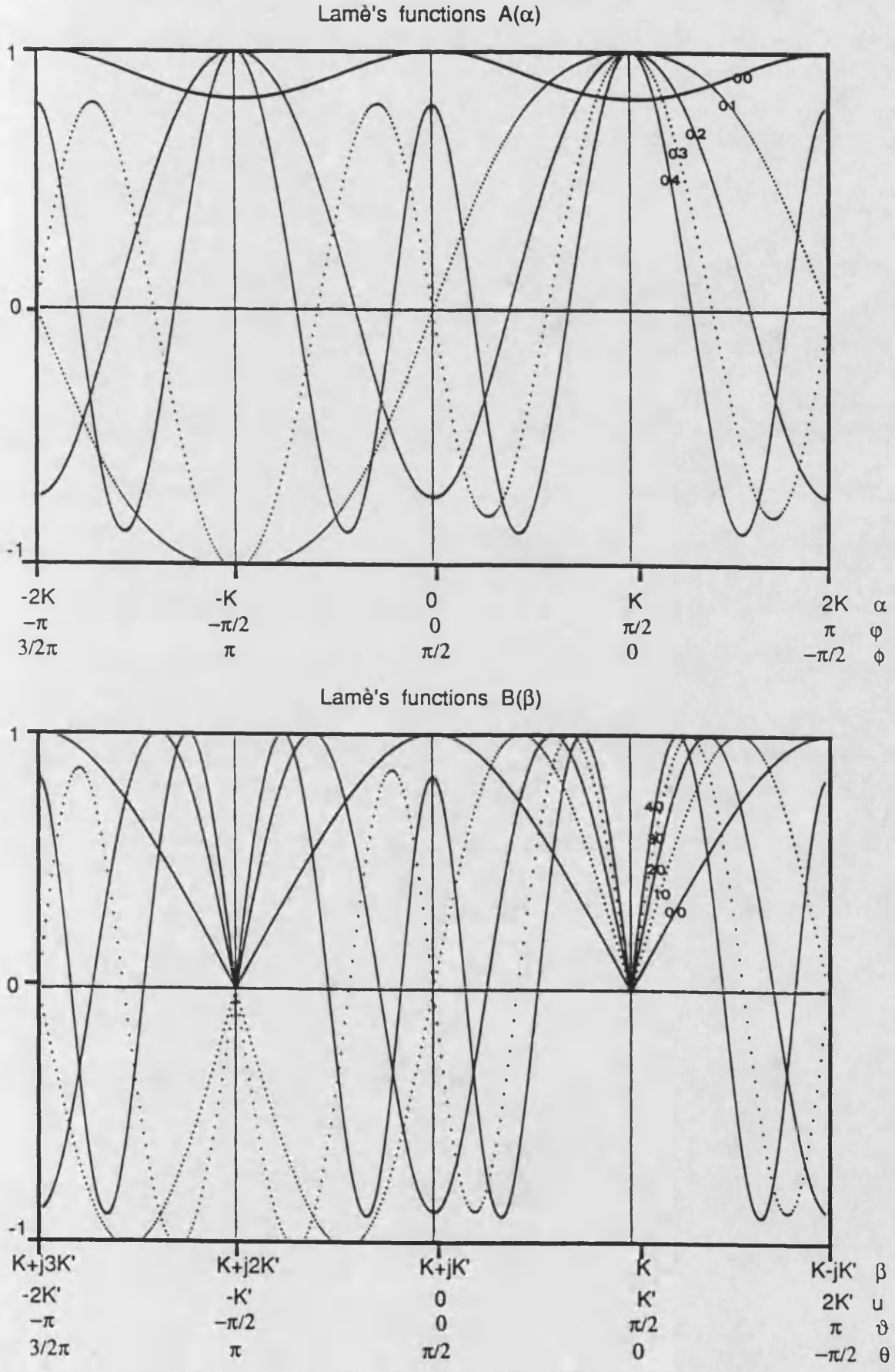

Fig. 2.7 : first 5 eigenvalues {B(β),A(α)} for the double sector

2.3.1 Static E-field spectra for composite sectors

There are five more conductor wedges geometries that we can easily analyze making use of the results just obtained for the sector and double sector . These wedges are mostly enclosed in metallic waveguides, or antennas making use of the image principle in order to reduce the burden .

They can be named the half acute and obtuse sector, the half double-sector the sector on a plane and the half sector on a plane, and can be drawn respectively as in Figs. 2.8a-b,9,10,11 .

Geometrically speaking, they can be obtained by inserting some plane conductors on the symmetry planes of the conductor for Figs. 2.8a-b and of the double-sector for Figs. 2.10,11,12 . These planes fit the other degenerate surfaces of the conical c.s., i.e. $\alpha = 0, 2K$ and $\beta = K + jK'$, that is $u = 0$ (see Figs. 1.6,8).

Analytically speaking, all these new b.c. can be reduced to periodicity conditions (see [7] p.64) with a procedure completely similar to that reported in 1.3.4. Incidentally, the latter indicate that the spectra for these new structures are a selection of the spectra relative to the fundamental sector and double-sector . To be precise, the condition $V = 0$ on the inserted plane select among the conditions (2.17,18,19) the following ones :

$$\text{half acute sector} \quad \begin{cases} U(K') = \dot{U}(-K') = 0 \rightarrow \text{ p. } {}^*8K', (0,1) \\ \dot{A}(K) = \dot{A}(0) = A(2K) = 0 \rightarrow \text{ p. } {}^*4K(o.), (0,1) \end{cases} \tag{2.34}$$

$$\text{half obtuse sector} \quad \begin{cases} U(K') = \dot{U}(-K') = 0 \rightarrow \text{ p. } {}^*8K', (0,1) \\ A(K) = A(0) = A(2K) = 0 \rightarrow \text{p. } {}^*2K(o.), (0,1) \end{cases} \tag{2.35}$$

$$\text{half double-sector} \quad \begin{cases} U(K') = U(-K') = 0 \rightarrow \text{p. } {}^*2K'(o.), 4K'(e.), (0,1) \\ \dot{A}(K) = A(0) = A(2K) = 0 \rightarrow \text{ p. } {}^*4K(o.), (0,1) \end{cases} \tag{2.36}$$

$$\text{sector on a plane} \quad \begin{cases} U(K') = U(0) = 0 \rightarrow \text{p. } {}^*2K'(o.), (1,0) \\ \dot{A}(K) = \dot{A}(-K) = 0 \rightarrow \text{ p. } 2K(e.), {}^*4K(o.), (1,0) \end{cases} \tag{2.37}$$

$$\text{half sector on a plane} \quad \begin{cases} U(K') = U(0) = 0 \rightarrow \text{p. } {}^*4K'(e.), (1,1) \\ \dot{A}(K) = A(0) = A(2K) = 0 \rightarrow \text{ p. } {}^*4K(o.), (1,1) \end{cases} \tag{2.38}$$

Where "p." stands for "period", $(e.), (o.)$ stand for even, odd respectively and the two integers between ( ) are the labels characterizing the fundamental mode for these geometries. The periodicities related to them are those indicated with *, as recoverable by remembering the meaning of the two integers and looking at Figs. 2.5,6,7; from the latter, it also appears that ν is always ≥ 1 .

2.3.2 Comparison of the approaches and results

It is perhaps appropriate to spend a few words about the various approaches used and degrees of accuracy reached over the years in determining the spectrum of eigenvalues and, in particular, the fundamental one that is responsible for the main EM fields behaviour by the conductor .

One of the most complete works was that already mentioned by Satterwhite [10], who used the present approach, but focused the attention on the quarter plane, for which he determined the first 192 eigenvalues and eigenfunctions so as to produce a very complete Green's function for it . He reached an accuracy of 4 decimals aided by a graphic method in order to identify the intersections in the locus of possible ν and h-values, for a given k^2, with a view to determining the approximate starting solutions.

Our approach, instead, starts from the exact ν, h limit values for $k^2 = 0, 1$ and uses them as first approximations to the values relative to a small variation of k^2. By successive steps, the whole curves $\nu(k^2), h(k^2)$ are recovered with an accuracy up to 6 decimals and more .

Authors like De Smedt [14] see the sector as a particular cone with arbitrary cross-section and solve numerically the eigenvalue problem by an application of the variational principle reaching, with some difficulty, the accuracy of 5 decimals.

One of the more recent works by Boersma [17] analyses the general problem of a cone with elliptic section whose b.c. provide a periodic and an aperiodic Lamé's function. No continued fraction exists for the aperiodic solution and consequently the accuracy of 5 decimals is reached somewhat laboriously .

Several other works have dealt with this problem, but the ones quoted are sufficient to let us conclude that the present approach, even at the price of an higher theoretical effort, produces the most accurate results available today and indicates that the ultimate goal in this direction would possibly be a further simplification due to the property of double periodicity of the solution .

In fact, we have to consider that this property simplifies considerably the problem when fundamental periodicity occurs, as in the Lamé's polynomials .

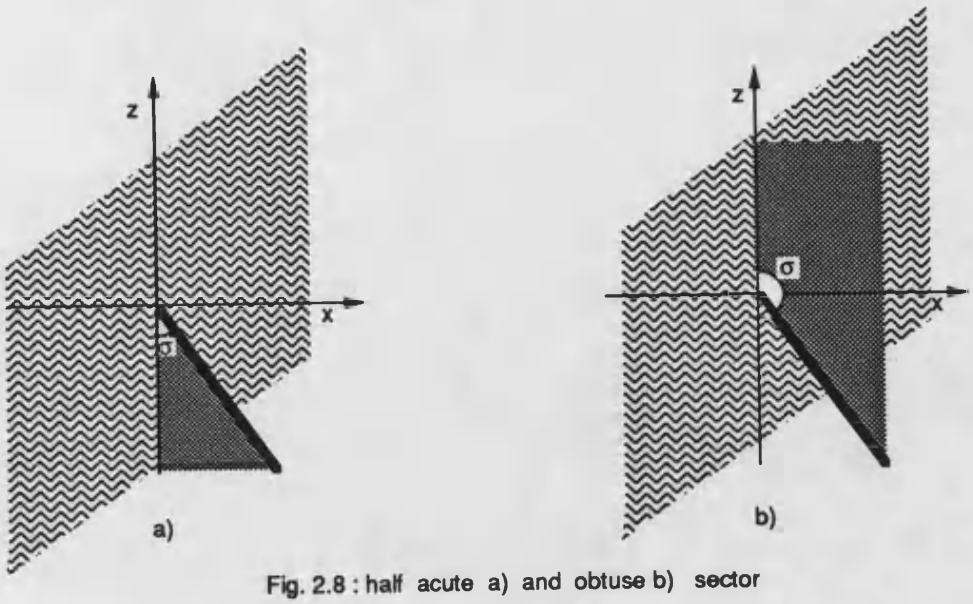

Fig. 2.8 : half acute a) and obtuse b) sector

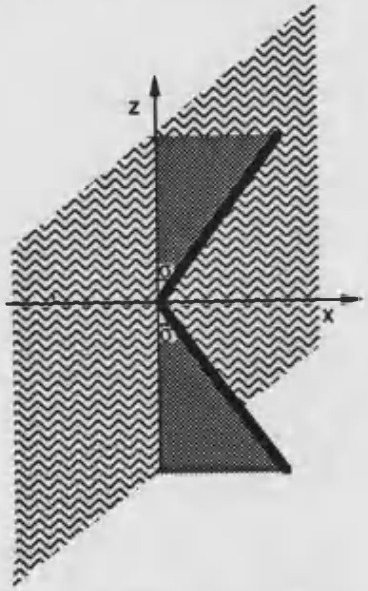

Fig. 2.9 : half double sector

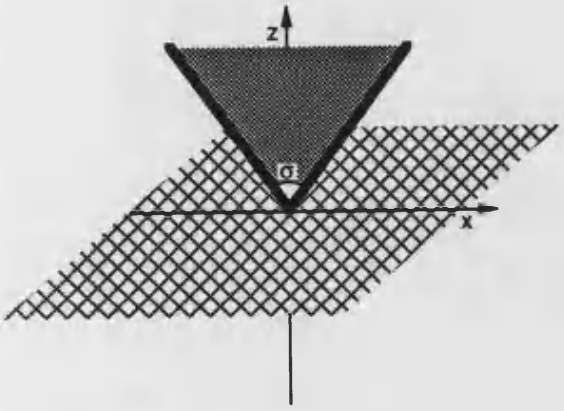

Fig. 2.10 : sector on a plane conductor

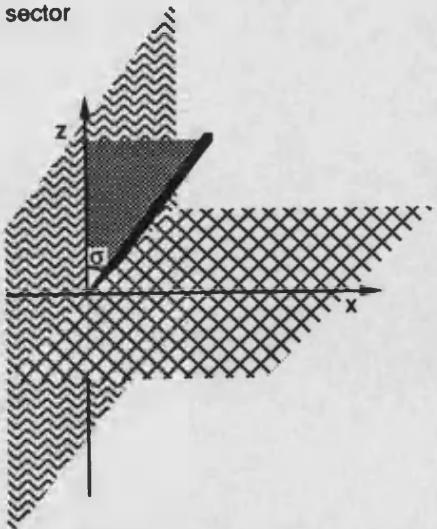

Fig. 2.11: half sector on a plane conductor

2.4 The main behaviour and singularity vector of the E-field in trigonometric variables

There is still a couple of physical conditions to be satisfied by (2.14,15), as stated in 1.3.2, and, precisely, that of smoothness at the origin and another condition at infinity .

Smoothness at the origin requires $V(0,\beta,\alpha)$ to be independent on β and α, but, as V vanishes identically on the conductor, it must also vanish at the origin, that is to say :

$$R(r) = r^{\nu} \tag{2.39}$$

On the other side, a physical condition at infinity can be the finiteness of the energy ($\propto \int |E|^2 dv$) stored in the space around the conductor, so that necessarily, $\lim_{r\to\infty} E = 0$, which can be satisfied by an R-solution of the form :

$$R(r) = r^{-(\nu+1)} \tag{2.40}$$

In practical applications, we are asked to analyze wedges making part of a printed circuit, so that whenever we are interested in the E-field behaviour in a limited region containing the tip, we use (2.39), while, if the region is the indefinite space we use (2.40) and, finally, if the region is limited and does not contain the tip, we can use the complete (2.16) .

Naturally, we limit our attention to the region around the tip, where, together with (2.39), we express $A(\alpha), B(\beta)$ preferably in trigonometric variables like $\Phi(\phi), \Theta(\theta)$ respectively .

For this purpose, the metric coefficients become :

$$g_{11} = 1 \quad g_{22} = r^2 \frac{(k^2 sin^2\phi + k'^2 sin^2\theta)}{1 - k'^2 cos^2\theta} \quad g_{33} = r^2 \frac{(k^2 sin^2\phi + k'^2 sin^2\theta)}{1 - k^2 cos^2\phi} \quad (2.41)$$

Hence, the static E-field can be explicited as :

$$\vec{E} = - \left[\nu \Theta \Phi \, \hat{r} + \sqrt{\frac{1 - k'^2 cos^2\theta}{k^2 sin^2\phi + k'^2 sin^2\theta}} \dot{\Theta} \Phi \, \hat{\theta} + \sqrt{\frac{1 - k^2 cos^2\phi}{k^2 sin^2\phi + k'^2 sin^2\theta}} \Theta \dot{\Phi} \, \hat{\phi} \right] r^{\nu - 1} \quad (2.42)$$

The above shows clearly the presence of the tip singularity whenever $\nu \leq 1$. This is matched to a $-\frac{1}{2}$ degree singularity of E_θ, E_ϕ along the conductor edges, where two among the values $\theta = 0, \pi$ and $\phi = 0, \pi$ occur simultaneously in the term $\sqrt{\frac{1}{k^2 sin^2\phi + k'^2 sin^2\theta}}$.

In conclusion, the E-field fundamental modes for the sector and double-sector assume primary theoretical importance because their singularities on the tip represent there the main behaviour of any diffracted E-field while the distributed singularities along the edges, are common to all the modes .

Nevertheless, applicatively speaking, the rigorous expression of the fundamental mode in the form (2.42) is not particularly helpful, if we except the special case in which the E-field is conveniently expressible in terms of the spectrum itself.

More often, only its main behaviour is sufficient . Hence, we have to formulate it as a simple function which still satisfies exactly the b.c. inclusive of edge and vertex conditions .

Ideally, this could be used as a " weight function " for a complete and orthogonal set of functions used to represent the E-field on some convenient surfaces along the circuit and ensuring exact satisfaction of the b.c., locally pertaining to

one of the 8 ideal structures in question .

The main behaviour is due to the fundamental mode, which is identifiable by means of its periodicity and parity as indicated by * in (2.17,18,19) for the fundamental sectors and by (2.34,35,36,37,38) for the composite wedges .

As a way of example, we determine explicitly the functions $R(r), \Theta(\theta), \Phi(\phi)$ for the particular, more useful situation, of $k^2 = 0.5$. The ν-value and the series coefficients $\{X_i\}$ characterizing these functions are reported in Table 2.1 .

The coefficients show a clear dominance of the term with fundamental period so as to justify the pseudo-harmonic form of $\Theta(\theta), \Phi(\phi)$ shown in the Figs. 2.5-6-7. The number of oscillations and parity are of fact maintained for any k^2 value, including the case $k^2 = 0$, when only the first coefficient is present, and $k^2 = 1$ when the function degenerates into one of Legendre's .

In view of simplifications, we can note that in proximity of a zero of Θ, Φ on a conductor surface, the terms of their series representations, for instance that in (B.2), go singularly to 0 because the conductor surface always fits some of the particular coordinate values $\bar{\theta} = 0, \frac{\pi}{2}, \pi$ or $\bar{\phi} = 0, \frac{\pi}{2}, \pi, 3\frac{\pi}{2}$.

What is more, the asymptotic behaviour of these terms on these zeros differ from each other by a multiplicative constant, so that the asymptotic behaviour of $\Theta(\bar{\theta})$ and $\Phi(\bar{\phi})$ is correctly represented by the whole series as well as by its fundamental term . The latter, depending on the parity and periodicity, can be written as:

$$even \left\{ \begin{array}{cccc} 1 & period & \pi & sin2\delta \\ cos\delta & period & 2\pi & sin\delta \\ cos\frac{\delta}{2} & period & 4\pi & sin\frac{\delta}{2} \end{array} \right\} odd \qquad (2.43)$$

where δ stands for θ or ϕ according to the context .

Then, if we consider, for instance, the acute sector, a simplified trigonometric expression of the E-field (2.42) which still satisfies exactly the b.c. is :

$$\vec{s}_E = \left[-\nu cos\frac{\theta}{2}\,\hat{r} + \frac{1}{2}\sqrt{\frac{1-k'^2cos^2\theta}{k^2sin^2\phi + k'^2sin^2\theta}}\,sin\frac{\theta}{2}\,\hat{\theta} \right] r^{\nu-1} \qquad (2.44)$$

This equation describes in quite an easy analytical way the map of singularities and zeros on the conductor as a product of the singularity on the tip, formulated by the term $r^{\nu-1}$, *with that along the edges, formulated by the term* $\sqrt{\frac{1}{k^2sin^2\phi+k'^2sin^2\theta}}$, *and with the zeros on the conductor surface, formulated by the eigenfunctions* $cos\frac{\theta}{2}, sin\frac{\theta}{2}$.

Remarkably, these simplified forms are valid for every sector or double-sector aperture only changing the ν-values . For this purpose, we collect in Table 2.2 the values of $\tau_e = \nu(\sigma) - 1$, namely, the degree of electric singularity, for σ-steps of 5^0 or 10^0 accurate up to 7 decimal figures for all the 8 geometries; values relative to apertures not reported in the Table can be obtained by means of interpolation .

This is why we name the expression (2.44) E-field *singularity vector* in trigonometric form, which, together with its easier expression in rectangular coordinates, constitutes one of the main goals of the work .

2.4.1 The main behaviour of the density of charge

A dual way of implementing field analysis algorithms makes use of the density of charge on the conductor which presents the advantage of being a bi-dimensional function .

The surface density of charge is related to the diffracted fields as :

$$\rho_s = \epsilon \vec{E} \cdot \hat{n} = \pm \epsilon E_n \tag{2.45}$$

where $\hat{n}$ is the outward pointing unit vector normal to the conducting surface, ϵ is the dielectric constant of the media in contact with it, while the $\pm$ signs refer to $\vec{E}_n$ going into or out of the conductor surface respectively . According to this definition, ρ_s assumes the forms :

$$|\rho_s| = \epsilon |E_\phi| = \epsilon |\frac{\Phi}{sin\phi}| r^{\nu-1} \qquad \text{in } \theta = 0, \pi \tag{2.46}$$

$$|\rho_s| = \epsilon |E_\theta| = \epsilon |\frac{\Theta}{sin\theta}| r^{\nu-1} \qquad \text{in } \phi = 0, \pi \tag{2.47}$$

The validity of the above equations could be queried at the two edges and at the tip, where the normal to the conductor can no longer be univocally defined and the expressions become singular . However, we can anticipate a result proved for the general dynamic situation which asserts that there can not exist an isolated charge on the conductor, that is to say, the density of charge changes continuously on it and assumes the limit value (2.46,47) when $\theta, \phi \rightarrow 0, \pi$.

CHARACTERISTIC COEFFICIENTS OF THE FUNCTIONS R(r),Θ(θ),Φ(ϕ)
Fundamental mode - $k^2 = 0.5$

	Fig. 2.1a	ν=0.296584	Fig. 2.8a	ν =1.131248
i	θ-per 4π even	ϕ-per π even	θ-per 4π even	ϕ-per 2π even
-5	0.000001		-0.000003	
-4	0.000009		-0.000025	
-3	0.000075		-0.000229	
-2	0.000752		-0.002524	
-1	0.010468		-0.046684	
0	1.000000	1.000000	1.000000	1.000000
1	-0.054644	-0.033084	-0.218468	-0.009271
2	-0.002632	-0.001594	-0.004143	-0.000646
3	-0.000231	-0.000186	-0.000315	-0.000064
4	-0.000025	-0.000021	-0.000032	-0.000007
5	-0.000003	-0.000003	-0.000003	-0.000001
	Fig. 2.1b	ν=0.814655	Fig. 2.8b	ν=1.955326
i	θ-per 4π even	ϕ-per 2π odd	θ-per 4π even	ϕ-per π odd
-5	-0.000002		-0.000003	
-4	-0.000014		-0.000025	
-3	-0.000122		-0.000249	
-2	-0.001289		-0.003264	
-1	-0.020708		-0.131919	
0	1.000000	1.000000	1.000000	
1	-0.146171	0.010835	-0.417261	1.000000
2	-0.004733	0.000806	0.011547	0.003154
3	-0.000386	0.000082	0.000645	0.000240
4	-0.000040	0.000010	0.000059	-0.000025
5	-0.000005	0.000001	0.000006	0.000003
	Fig. 2.2	ν =0.704321	Fig. 2.9	ν =1.311863
i	θ-per 2π odd	ϕ-per π even	θ-per 2π odd	ϕ-per 2π even
0	1.000000	1.000000	1.000000	1.000000
1	0.016714	-0.102762	-0.023588	-0.023588
2	0.001279	-0.005284	-0.001543	-0.001543
3	0.000131	-0.000473	-0.000150	-0.000150
4	0.000015	-0.000052	-0.000017	-0.000017
5	0.000002	-0.000006	-0.000002	-0.000002
	Fig. 2.10	ν = 1.918023	Fig. 2.11	ν = 2.688000
i	θ-per π odd	ϕ-per π even	θ-per π odd	ϕ-per 2π even
0		1.000000		1.000000
1	1.000000	-0.438126	1.000000	-0.200660
2	0.005747	-0.001841	-0.053492	-0.003350
3	0.000443	-0.000125	-0.002912	-0.000248
4	0.000046	-0.000012	-0.000267	-0.000025
5	0.000005	-0.000001	-0.000030	-0.000003

Table 2.1: characterization of the eigenfunctions $R(r), \Theta(\theta), \Phi(\phi)$ for the acute sector, half acute sector, obtuse sector, half obtuse sector, double sector, half double sector, sector on a plane and half sector on a plane respectively indicated by their Fig. number .

3D-WEDGES Degree of electric singularity τ_e							
$\frac{2\pi-\sigma}{2}$ °	Fig.2.1a,b	Fig.2.8a,b	$\frac{\pi-\sigma}{2}$ °	Fig. 2.10	Fig. 2.11	Fig. 2.2	Fig. 2.9
0.00	0.0000000	1.0000000	0.00	0.0000000	1.0000000	-1.0000000	0.0000000
5.00	-0.0019269	0.9999945	2.50	0.2789616	1.0028342	-0.7719023	0.0009497
10.00	-0.0079077	0.9999121	5.00	0.3434077	1.0111690	-0.7278994	0.0037824
15.00	-0.0183830	0.9995488	7.50	0.3960998	1.0246795	-0.6931375	0.0084681
20.00	-0.0338525	0.9985454	10.00	0.4435835	1.0430298	-0.6624549	0.0149799
25.00	-0.0546955	0.9963541	12.50	0.4881265	1.0659169	-0.6340656	0.0233004
30.00	-0.0809612	0.9921894	15.00	0.5307534	1.0930816	-0.6068899	0.0334242
35.00	-0.1121971	0.9849673	17.50	0.5719618	1.1243052	-0.5805848	0.0453591
40.00	-0.1474300	0.9732592	20.00	0.6119693	1.1594002	-0.5547600	0.0591268
45.00	-0.1853447	0.9553263	22.50	0.6508186	1.1981970	-0.5291900	0.0747630
50.00	-0.2245699	0.9293612	25.00	0.6884303	1.2405277	-0.5037155	0.0923175
55.00	-0.2639208	0.8940430	27.50	0.7246354	1.2862073	-0.4782217	0.1118536
60.00	-0.3025154	0.8492627	30.00	0.7592010	1.3350107	-0.4526276	0.1334477
65.00	-0.3397789	0.7964791	32.50	0.7918567	1.3866444	-0.4268797	0.1571889
70.00	-0.3753875	0.7382866	35.00	0.8223226	1.4407145	-0.4009492	0.1831778
75.00	-0.4092000	0.6775165	37.50	0.8503404	1.4966899	-0.3748310	0.2115239
80.00	-0.4411957	0.6165389	40.00	0.8757026	1.5538665	-0.3485447	0.2423432
85.00	-0.4714297	0.5570221	42.50	0.8982774	1.6113393	-0.3221360	0.2757527
90.00	-0.5000000	0.5000000	45.00	0.9180227	1.6680001	-0.2956786	0.3118631
95.00	-0.5270279	0.4460391	47.50	0.9349886	1.7225767	-0.2692759	0.3507670
100.00	-0.5526446	0.3953982	50.00	0.9493082	1.7737333	-0.2430628	0.3925218
105.00	-0.5769839	0.3481468	52.50	0.9611799	1.8202266	-0.2172050	0.4371258
110.00	-0.6001782	0.3042465	55.00	0.9708463	1.8610865	-0.1918973	0.4844843
115.00	-0.6223566	0.2636024	57.50	0.9785726	1.8957597	-0.1673581	0.5343655
120.00	-0.6436452	0.2260961	60.00	0.9846294	1.9241631	-0.1438215	0.5863474
125.00	-0.6641679	0.1916060	62.50	0.9892784	1.9466328	-0.1215263	0.6397625
130.00	-0.6840488	0.1600209	65.00	0.9927634	1.9638027	-0.1007028	0.6936545
135.00	-0.7034156	0.1312484	67.50	0.9953053	1.9764651	-0.0815593	0.7467763
140.00	-0.7224051	0.1052212	70.00	0.9970996	1.9854520	-0.0642704	0.7976561
145.00	-0.7411714	0.0819025	72.50	0.9983159	1.9915554	-0.0489683	0.8447508
150.00	-0.7598998	0.0612908	75.00	0.9990985	1.9954829	-0.0357391	0.8866607
155.00	-0.7788320	0.0434251	77.50	0.9995683	1.9978387	-0.0246241	0.9223365
160.00	-0.7983164	0.0283903	80.00	0.9998242	1.9991204	-0.0156253	0.9511953
165.00	-0.8189236	0.0163220	82.50	0.9999446	1.9997231	-0.0087142	0.9731090
170.00	-0.8417794	0.0074089	85.00	0.9999891	1.9999455	-0.0038427	0.9882884
175.00	-0.8699635	0.0018859	87.50	0.9999993	1.9999966	-0.0009547	0.9971206
180.00	-1.0000000	0.0000000	90.00	1.0000000	2.0000000	0.0000000	1.0000000

Table 2.2: degree of electric singularity or zero versus the angular aperture σ for the sector, half sector, sector on a plane, half sector on a plane, double sector and half double sector respectively indicated by their Fig. number .

2.5 E-field singularity vectors for the main sectors relatively to the main axes

Commonly, in EM fields analysis one make use of the more usual rectangular space domain (see Chapters 5,6) .

A complete formulation for the change of variables is given in Appendix D together with the analogous formulation in respect of a main rectangular c.s. X,Y,Z. This is obtained rotating clockwise by $\pi - \epsilon$ the axes $x - z$ so as to fit the positive semi z-axes with a conductor edge; x will fit the other edge in the particular cases of $90^0, 270^0$ sector and 90^0 double sector, which, for this reason, we indicate as *main sectors* .

Any E-field component along the main axes can be obtained from (D.7,8,9) using the unit vector relations recoverable from (D.16,17,18) and the functions P, T, S_θ, S_ϕ defined in the same Appendix D .

$$E_X = \nu(kPcos\theta + k'Tcos\phi)r^{\nu-1}\Theta\Phi + T\left[k'^3cos\theta cos\phi - kTP\right]S_\theta\dot{\Theta}\Phi + P\left[k^3cos\theta cos\phi - k'PT\right]S_\phi\Theta\dot{\Phi} \tag{2.48}$$

$$E_Y = \nu sin\theta sin\phi\Theta\Phi + T^2cos\theta S_\phi\dot{\Theta}\Phi + P^2cos\phi S_\theta\Theta\dot{\Phi} \tag{2.49}$$

$$E_Z = \nu(k'Pcos\theta - kTcos\phi)r^{\nu-1}\Theta\Phi - T\left[kk'^2cos\theta cos\phi - kTP\right]S_\theta\dot{\Theta}\Phi + P\left[k^2k'cos\theta cos\phi - kPT\right]S_\phi\Theta\dot{\Phi} \tag{2.50}$$

As far the esplicit formulation of the singularity vector is concerned, we limit the attention instead to the main sectors both because of their applicative importance and their simpler analytic formulation, proposing a generalization in the next section .

The quarter plane

Starting with the quarter plane of Fig. 2.12 and the half quarter plane, from (2.17-34) and Table 2.1 we recover respectively the approximate eigenfunctions :

$$\Theta \simeq cos\frac{\theta}{2} \qquad \Phi \simeq 1 \tag{2.51}$$

$$\Theta \simeq cos\frac{\theta}{2} \qquad \Phi \simeq cos\phi \tag{2.52}$$

By substituting these into (2.48,49,50) and simplifying so as to maintain unaltered the distribution of zeros and singularities all over the conductor surface and boundary, we obtain the singularity vector in rectangular components :

$$s_{E_X} = r^{\nu-1}cos\tfrac{\theta}{2} + (1 - cos\theta cos\phi)sin\tfrac{\theta}{2}S_\theta \tag{2.53}$$

$$s_{E_Y} = sin\tfrac{\theta}{2}\Phi(\phi)S_\phi \tag{2.54}$$

$$s_{E_Z} = r^{\nu-1}cos\tfrac{\theta}{2} + (1 + cos\theta cos\phi)sin\tfrac{\theta}{2}S_\theta \tag{2.55}$$

These forms in the system r, θ, ϕ are transformed in that X, Y, Z by using (D.21,22) but, in view of application requirements, we will explicit them only on the *three main cartesian planes* . On these planes, the following simple relations between θ, ϕ occur :

$$X = 0 \rightarrow \phi = \pi \pm \theta \tag{2.56}$$

$$Y = 0 \rightarrow \phi = 0, \pi; \theta = 0, \pi \tag{2.57}$$

$$Z = 0 \rightarrow \phi = \theta \tag{2.58}$$

After inserting the latter into (2.53,54,55), we obtain a first substantial

simplification that also deals with the indeterminate forms $\frac{0}{0}$ in the space r, θ, ϕ .

Leaving aside in the formulae so reduced multiplicative constants and/or additive functions vanishing on the conductor to higher degrees, we can isolate the simpler functions which still exactly satisfy the b.c. on the conductor.

Expressing the latter by means of the variables X, Y, Z we recover just the six simple expressions reported in Table 2.3 :

$$0 \quad r^{\nu-1} \quad \sqrt{|XZ|}r^{\nu-2} \quad \frac{r^{\nu}}{\sqrt{|XZ|}} \quad \sqrt{|Y|}r^{\nu-\frac{3}{2}} \quad \frac{r^{\nu-\frac{1}{2}}}{\sqrt{|Y|}} \tag{2.59}$$

In Table 2.3 the ; stands for intersection while in the last section are reported between brackets the forms on the plane $Z = 0$ whenever they are distinct from the correspondent ones on the plane $X = 0$.

Incidentally, the forms relative to the half quarter sector are exactly those in Table 2.3 and for the sole half space $x < 0$ or $x \geq 0$ and with the $\nu = 1.131248 > 1$ reported in Table 2.1 which indicates the presence of a zero rather than a singularity on the tip .

In particular, by consulting this Table we recover all the classic results regarding the half plane, i.e. the presence of a zero of degree $\frac{1}{2}$ for the tangential components and a singularity of the same degree for the normal components .

On the conducting surfaces only the normal components is different from 0 and proportional to the density of charge according to what said in 2.4.1 .

On the tip, instead, all the components behave like $\frac{r^{\nu}}{\sqrt{|XZ|}}$ or simply like $r^{\nu-1}$, which denotes an asymptotic behaviour dependent on the direction but whose limit value on the tip is always a singularity or a zero of degree never greater than $\nu - 1$.

These behaviours can be easily recognized as the traces on the cartesian planes of the three-dimensional matching between the cylindrical and polar singularities that appear exactly like those noted in S_θ, S_ϕ while studying (D.23,24).

In order to show the physical continuity of the field of different nature and degree of singularity along the conducting boundary we draw in Fig. 2.15 the magnitude of E_t in the plane of the conductor . Moreover, the E_n component is the continuation of this function on the sector where it is also proportional to the density of charge .

For the same purpose in Fig. 2.14 is drawn the magnitude of E on the plane $Z = 0$, which again shows the continuous passage between a singularity of degree $-\frac{1}{2}$ along the edge to one of degree $\nu - 1 \simeq -0.703116$ on the tip .

The three-quarter plane

Following the same lines, the three-quarter plane drawn in Fig. 2.15 and the half-three-quarter plane are characterized by, respectively, the eigenfunctions and singularity functions :

$$\Theta(\theta) \simeq sin\tfrac{\theta}{2} \qquad \Phi(\phi) \simeq sin\phi \tag{2.60}$$

$$\Theta(\theta) \simeq sin\tfrac{\theta}{2} \qquad \Phi(\phi) \simeq sin2\phi \tag{2.61}$$

$$s_{E_X} = (1 - cos\theta cos\phi) sin\tfrac{\theta}{2} S_\phi \tag{2.62}$$

$$s_{E_Y} = cos\tfrac{\theta}{2}\Phi(\phi) S_\phi + sin\tfrac{\theta}{2} cos\phi S_\theta \tag{2.63}$$

$$s_{E_Z} = (1 + cos\theta cos\phi) sin\tfrac{\theta}{2} S_\phi \tag{2.64}$$

Using the formalism and reasons argued for the quarter plane, the projections of these forms on the main planes are those collected in Table 2.4 .

The ones corresponding to Figs. 2.13,14 are now drawn in Figs. 2.16,17 which clearly show a singularity of degree $\nu - 1 \simeq -0.185345$ on the tip that is weaker than that of degree $-\frac{1}{2}$ along the two edges .

The double quarter plane

The discussion relative to the double-quarter plane drawn in Fig. 2.18 is substantially similar . Hence, we may start collecting, in the order, its simplified eigenfunctions, those of its half, of a quarter plane on a plane and of a half-quarter plane on a plane.

$$\Theta(\theta) \simeq sin\theta \qquad \Phi(\phi) \simeq 1 \tag{2.65}$$

$$\Theta(\theta) \simeq sin\theta \qquad \Phi(\phi) \simeq sin\phi \tag{2.66}$$

$$\Theta(\theta) \simeq sin\tfrac{\theta}{2} \qquad \Phi(\phi) \simeq 1 \tag{2.67}$$

$$\Theta(\theta) \simeq sin\tfrac{\theta}{2} \qquad \Phi(\phi) \simeq cos\phi \tag{2.68}$$

In spite of 4 distinct geometries the singularity vectors can be brought back to just the forms :

$$s_{E_X} = (1 - cos\theta cos\phi)S_\theta \tag{2.69}$$

$$s_{E_Y} = cos\theta\Phi(\phi)S_\phi \tag{2.70}$$

$$s_{E_Z} = (1 + cos\theta cos\phi)S_\theta \tag{2.71}$$

The projections of these formulae relatively to the double-quarter plane on the main planes are collected in Table 2.5, while the graphic evidence of the distributed singularities are shown in Figs. 2.19,20 . In this case also, the singularity on the tip of degree $\nu - 1 \simeq -0.295679$ is weaker than $-\frac{1}{2}$, which corresponds instead to an angular aperture of $\simeq 26^0$, as can be deduced from Appendix C .

The forms relative to the other three wedges are those reported in Table 2.5, relative to just the parts of the three main planes belonging to the wedges themselves as illustrated in Figs. 2.9,10,11 . Obviously, also according to the ν-values reported in Table 2.1 a zero is always present on the tip .

E-field singularity vector components for a quarter plane			
s_{E_X}	s_{E_Y}(and ρ_s)	s_{E_Z}	Sector
on the plane $Y = 0$			
$\frac{r^\nu}{\sqrt{\lvert XZ\rvert}}$	0	$\sqrt{\lvert XZ\rvert}r^{\nu-2}$	$z < 0; \phi = 0$
$r^{\nu-1}$	0	$r^{\nu-1}$	$z \geq 0; \phi = 0, \pi, \theta = 0$
$\sqrt{\lvert XZ\rvert}r^{\nu-2}$	0	$\frac{r^\nu}{\sqrt{\lvert XZ\rvert}}$	$z < 0; \phi = \pi$
0	$\frac{r^\nu}{\sqrt{\lvert XZ\rvert}}$	0	$z < 0; \theta = \pi$
on the plane $X = 0$ *(or* $Z = 0$*)*			
$\frac{r^{\nu-\frac{1}{2}}}{\sqrt{\lvert Y\rvert}}\left(\sqrt{\lvert Y\rvert}r^{\nu-\frac{3}{2}}\right)$	$\frac{r^{\nu-\frac{1}{2}}}{\sqrt{\lvert Y\rvert}}$	$\sqrt{\lvert Y\rvert}r^{\nu-\frac{3}{2}}\left(\frac{r^{\nu-\frac{1}{2}}}{\sqrt{\lvert Y\rvert}}\right)$	$Z > 0$ (or $X > 0$)
$r^{\nu-1}$	$r^{\nu-1}$	$r^{\nu-1}$	$Z \leq 0$ (or $X \leq 0$)

Table 2.3: E-field singularity vector projections on the main planes relative to the conductor and geometry indicated in Fig. 2.12; $\nu \simeq 0.296884$ for the quarter plane and $\nu \simeq 1.131248$ for the half-quarter plane .

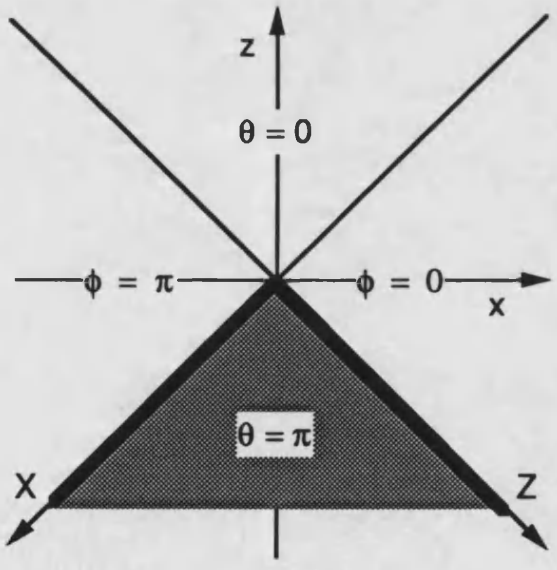

Fig. 2.12 : quarter plane

E-field singularity vector components for a three-quarter plane			
s_{E_X}	s_{E_Y}(and ρ_s)	s_{E_Z}	Sector
on the plane $Y = 0$			
0	$\frac{r^\nu}{\sqrt{\lvert XZ\rvert}}$	0	$z < 0; \phi = 0$
0	$r^{\nu-1}$	0	$z \geq 0; \phi = 0, \pi, \theta = 0$
0	$\frac{r^\nu}{\sqrt{\lvert XZ\rvert}}$	0	$z < 0; \phi = \pi$
$\frac{r^\nu}{\sqrt{\lvert XZ\rvert}}$	0	$\sqrt{\lvert XZ\rvert} r^{\nu-2}$	$x \geq 0; \theta = \pi$
$\sqrt{\lvert XZ\rvert} r^{\nu-2}$	0	$\frac{r^\nu}{\sqrt{\lvert XZ\rvert}}$	$x < 0; \theta = \pi$
on the plane $X = 0$ *(or* $Z = 0$*)*			
$\frac{r^{\nu-\frac{1}{2}}}{\sqrt{\lvert Y\rvert}} \left(\sqrt{\lvert Y\rvert} r^{\nu-\frac{3}{2}}\right)$	$\frac{r^{\nu-\frac{1}{2}}}{\sqrt{\lvert Y\rvert}}$	$\sqrt{\lvert Y\rvert} r^{\nu-\frac{3}{2}} \left(\frac{r^{\nu-\frac{1}{2}}}{\sqrt{\lvert Y\rvert}}\right)$	$Z > 0$ (or $X > 0$)
$\lvert Y\rvert r^{\nu-2}$	$r^{\nu-1}$	$\lvert Y\rvert r^{\nu-2}$	$Z \leq 0$ (or $X \leq 0$)

Table 2.4: E-field singularity vector projection on the main planes relative to the conductor and geometry indicated in Fig. 2.15; $\nu \simeq 0.814655$ for the three-quarter plane and $\nu \simeq 1.955326$ for the half three-quarter plane .

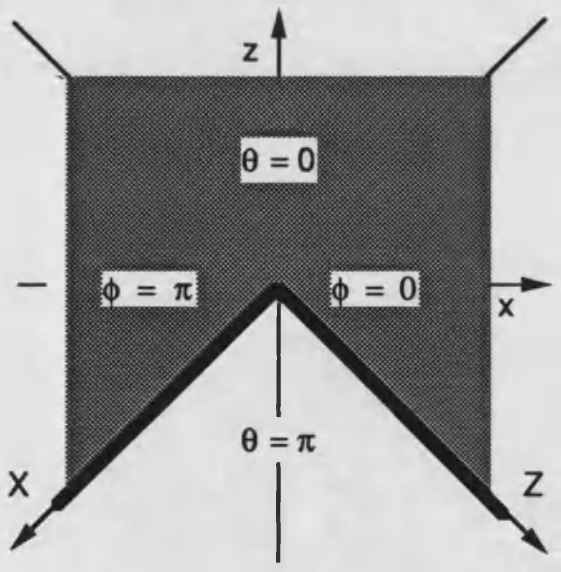

Fig. 2.15 : three-quarter plane

E-field singularity vector components for a double-quarter plane			
s_{E_X}	s_{E_Y}(and ρ_s)	s_{E_Z}	Sector
on the plane $Y = 0$			
$\frac{r^\nu}{\sqrt{\lvert XZ\rvert}}$	0	$\sqrt{\lvert XZ\rvert}r^{\nu-2}$	$z < 0; \phi = 0$
$\sqrt{\lvert XZ\rvert}r^{\nu-2}$	0	$\frac{r^\nu}{\sqrt{\lvert XZ\rvert}}$	$z \geq 0; \phi = 0$
0	$\frac{r^\nu}{\sqrt{\lvert XZ\rvert}}$	0	$\theta = 0$
$\frac{r^\nu}{\sqrt{\lvert XZ\rvert}}$	0	$\sqrt{\lvert XZ\rvert}r^{\nu-2}$	$z \geq 0; \phi = \pi$
$\sqrt{\lvert XZ\rvert}r^{\nu-2}$	0	$\frac{r^\nu}{\sqrt{\lvert XZ\rvert}}$	$z < 0; \phi = \pi$
0	$\frac{r^\nu}{\sqrt{\lvert XZ\rvert}}$	0	$\theta = \pi$
on the plane $X = 0$ *(or* $Z = 0$*)*			
$\frac{r^{\nu-\frac{1}{2}}}{\sqrt{\lvert Y\rvert}}\left(\sqrt{\lvert Y\rvert}r^{\nu-\frac{3}{2}}\right)$	$\frac{r^{\nu-\frac{1}{2}}}{\sqrt{\lvert Y\rvert}}$	$\sqrt{\lvert Y\rvert}r^{\nu-\frac{3}{2}}\left(\frac{r^{\nu-\frac{1}{2}}}{\sqrt{\lvert Y\rvert}}\right)$	any Z (or X)

Table 2.5: E-field singularity vector projections on the main planes relative to the conductor and geometry indicated in Fig. 2.18; $\nu \simeq 0.704321$ for the double-quarter plane, $\nu \simeq 1.311863$ for the half double-quarter plane, $\nu \simeq 1.918027$ for the quarter plane on a plane and $\nu \simeq 2.68800$ for the half quarter plane on a plane .

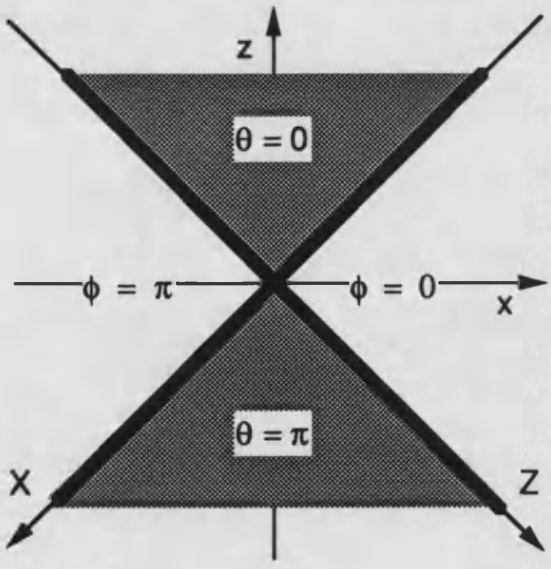

Fig. 2.18 : double-quarter plane

Magnitude of the electric field on the planes	
Y = 0	Z = 0
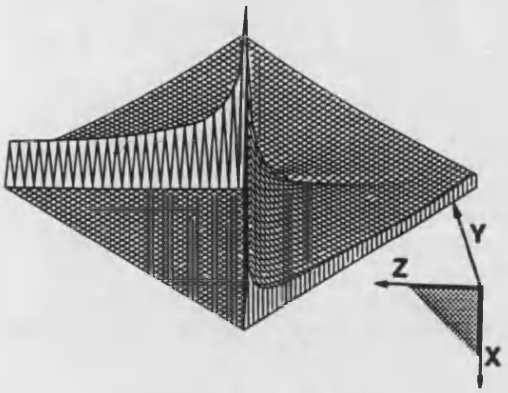 Fig. 2.13	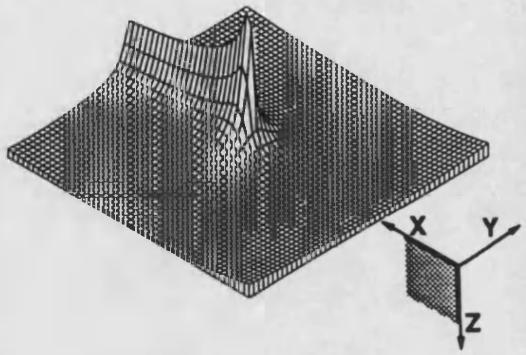 Fig. 2.14
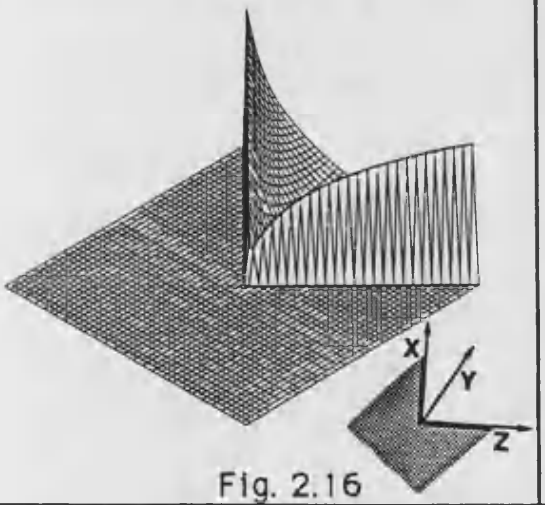 Fig. 2.16	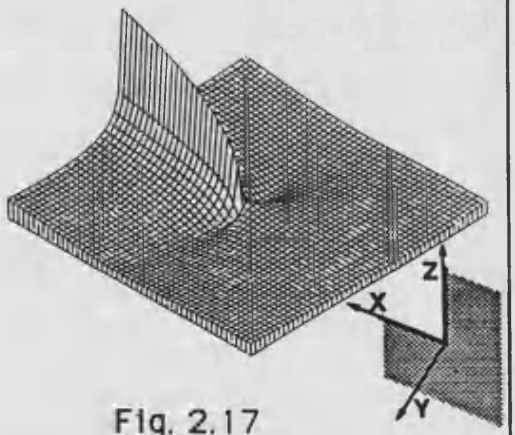 Fig. 2.17
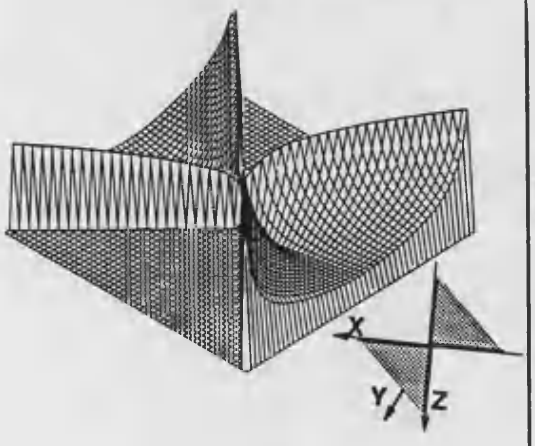 Fig. 2.19	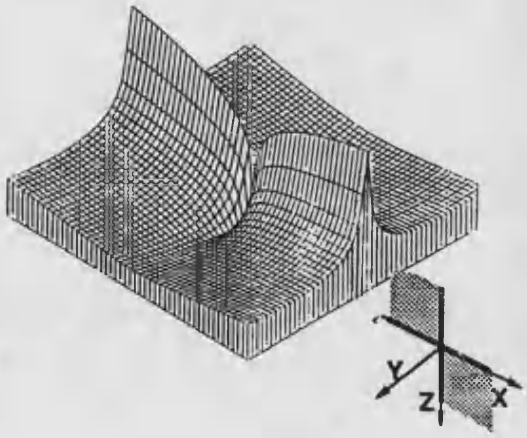 Fig. 2.20

2.6 E-field singularity vectors for sectors of any angular aperture

Although the singularity function forms reported in the Tables 2.3,4,5 would be those of most common application, it is also true that because of the evolution of fabrication techniques for planar circuits it becomes increasingly important to avail the analogous forms for sectors of arbitrary aperture σ (see the taper in Chapter 5) .

Fortunately, from an inspection of the general formulas (2.48,49,50) and of the singularity vectors components for the special cases of $k^2 = 0.5$, we deduce the singularity vectors for a sector of any aperture, i.e. $k^2 \in (0,1)$.

In fact, just by using the (D.12,13) for S_θ, S_ϕ and using the terms between [ ] of (2.48,50) for $(1 \pm cos\theta cos\phi)$ in the expressions relative to the quarter, three-quarter and double-quarter sectors, we obtain the singularity functions relative to arbitrary acute, obtuse and double-sectors respectively .

Also, their projection on the main axes can be extended directly considering that while the first edge still fits the Z axis, the other edge is no longer coincident with the X axis (see also Figs. D.1a,1b,2) but rather with the line $k'x + kz = 0$, i.e. $(k^2 - k'^2)X + 2kk'Z = 0$.

A simple inspection of the zeros and singularities in Tables 2.3,4,5 permits then to generalize those forms simply by operating the following substitutions:

$$Z \rightarrow (k^2 - k'^2)X + 2kk'Z \tag{2.72}$$

Some care has to be taken when dealing with composite sectors and in the

limit cases $k^2 = 0, 1$ because some new zeros are introduced which do not appear in the Tables . For example, in the case of the 90^0 sector, the median plane conductor imposes $E_X + E_Z = E_z = 0$ on its surface even though E_X, E_Z do not vanish there, as shown in Table 2.3, except in the limit cases .

For this reason, we postpone the treatment of composit sectors to Chapter 4 when dealing with wedges in spherical c.s. .

Chapter 3

THE H-FIELD SINGULARITY VECTOR

3.1 The dynamic E-field

Following the introductory notes and in the context of the results presented in Chapter 2, we are now aware of all the physical, theoretical, computational and graphical means necessary to approach the general dynamic problem of diffraction by a sector or double-sector with the main purpose of determining the singularity vector for the H-field .

We may start by recalling that in the linear, isotropic and homogeneous medium surrounding the conductor, the diffracted E-field is a solution of the Helmholtz wave equation :

$$\nabla \times \nabla \times \vec{E} - \kappa^2 \vec{E} = 0 \tag{3.1}$$

which satisfies the b.c. on the conductor :

$$\hat{n} \times \vec{E} = 0 \tag{3.2}$$

As already observed for the static case, the normal $\hat{n}$ to the conductor is not uniquely defined along the edges and on the tip, even though uniqueness of the singular solution will be proved without adding further conditions to (3.2) . The already stated conditions at the origin and at infinity will be easily satisfied simply by choosing particular forms of the solutions so determined.

It is likely to be found (see [12]) that the general solution of (3.1) in the geometry of a conical c.s. can be derived simply by applying vector operators on a scalar potential Ψ satisfying again the scalar wave equation (2.1) . This allows us the use of all the results obtained in Chapter 1-2 about its solutions .

Actually, three different families of E-field solutions are possible; in terms of vector operators and in explicit Jacobian form they look like :

$$\vec{L} = \nabla\Psi_0 = \frac{\partial\Psi_0}{\partial r}\,\hat{r} + \frac{G}{r}\left(j\frac{\partial\Psi_0}{\partial\beta}\,\hat{\beta} + \frac{\partial\Psi_0}{\partial\alpha}\,\hat{\alpha}\right) \tag{3.3}$$

$$\vec{M} = \nabla \times \Psi_1\vec{r} = -jG\left(j\frac{\partial\Psi_1}{\partial\alpha}\,\hat{\beta} + \frac{\partial\Psi_1}{\partial\beta}\,\hat{\alpha}\right) \tag{3.4}$$

$$\vec{N} = \frac{1}{\kappa}\nabla \times \nabla \times \Psi_2\vec{r} = \frac{\nu(\nu+1)}{\kappa r}\Psi_2\,\hat{r} + \frac{G}{\kappa r}\left[j\frac{\partial}{\partial\beta}\left(\frac{\partial(\Psi_2 r)}{\partial r}\right)\hat{\beta} + \frac{\partial}{\partial\alpha}\left(\frac{\partial(\Psi_2 r)}{\partial r}\right)\hat{\alpha}\right] \tag{3.5}$$

where we use the function and relations obtained from (2.5,6,7,8) :

$$G(\alpha,\beta) = \frac{1}{k\sqrt{sn^2\beta - sn^2\alpha}} \tag{3.6}$$

$$\frac{\partial^2\Psi}{\partial\beta^2} - \frac{\partial^2\Psi}{\partial\alpha^2} = \frac{\nu(\nu+1)}{G^2}\Psi \qquad \frac{\partial^2(\Psi r)}{\partial r^2} = \left(\frac{\nu(\nu+1)}{r^2} - \kappa^2\right)\Psi r \tag{3.7}$$

3.1.1 Solutions of the scalar wave equation for Ψ_0, Ψ_1, Ψ_2

We can immediately see that the source of the diffracted field is virtually localized on the conductor . Thus, in the space around it, it must be $\nabla \cdot \vec{E} = \nabla \cdot \nabla \Psi_0 = 0$, that is to say $\Psi_0 \equiv 0$.

Thus, limiting the attention to the vectors $\vec{M}, \vec{N}$, we can proceed by translating the vectorial b.c. (3.2) into simple scalar conditions on Ψ_1, Ψ_2, or better on their individual factors $A(\alpha), B(\beta)$.

In order to do this, we can note that whenever the conductor fits a surface $\bar{\beta} = constant$ or $\bar{\alpha} = constant$, (3.2) imposes there the conditions $M_\beta(r, \bar{\beta}, \alpha) = N_\beta(r, \bar{\beta}, \alpha) = 0$ or $M_\alpha(r, \beta, \bar{\alpha}) = N_\alpha(r, \beta, \bar{\alpha}) = 0$ respectively. In accordance to (3.4,5) and (2.5), these conditions become on $A(\alpha), B(\beta)$ respectively :

$$\frac{\partial \Psi_1}{\partial \beta} = R(r)\dot{B}(\beta)A(\alpha) = 0 \qquad \beta = \bar{\beta}, \forall r, \alpha \quad \Rightarrow \quad \dot{B}(\bar{\beta}) = 0 \tag{3.8}$$

$$\frac{\partial}{\partial \alpha}\left(\frac{\partial(\Psi_2 r)}{\partial r}\right) = \frac{d(rR(r))}{dr}B(\beta)\dot{A}(\alpha) = 0 \quad \beta = \bar{\beta}, \forall r, \alpha \quad \Rightarrow \quad B(\bar{\beta}) = 0 \tag{3.9}$$

or

$$\frac{\partial \Psi_1}{\partial \alpha} = R(r)B(\beta)\dot{A}(\alpha) = 0 \qquad \alpha = \bar{\alpha}, \forall r, \beta \quad \Rightarrow \quad \dot{A}(\bar{\alpha}) = 0 \tag{3.10}$$

$$\frac{\partial}{\partial \beta}\left(\frac{\partial(\Psi_2 r)}{\partial r}\right) = \frac{d(rR(r))}{dr}\dot{B}(\beta)A(\alpha) = 0 \quad \alpha = \bar{\alpha}, \forall r, \beta \quad \Rightarrow \quad A(\bar{\alpha}) = 0 \tag{3.11}$$

Further important conditions on $A(\alpha), B(\beta)$ can be identified by considering symmetry conditions pertaining to the " adjacent sectors " in respect to the conducting ones above (see Fig. 1.7) . In fact, because of the coplanarity of the latter with the source, that is to say the charge on the conductor, the normal

normal component of the E-field must vanish there . Using again (3.4,5), these conditions pertaining to " adjacent sectors " $\bar{\beta} = constant$ or $\bar{\alpha} = constant$ can be explicited respectively as :

$$\frac{\partial \Psi_1}{\partial \alpha} = R(r)B(\beta)\dot{A}(\alpha) \qquad \beta = \bar{\beta}, \forall r, \alpha \;\Rightarrow\; B(\bar{\beta}) = 0 \quad (3.12)$$

$$\frac{\partial}{\partial \beta}\left(\frac{\partial(\Psi_2 r)}{\partial r}\right) = \frac{d(rR(r))}{dr}\dot{B}(\beta)A(\alpha) \qquad \beta = \bar{\beta}, \forall r, \alpha \;\Rightarrow\; \dot{B}(\bar{\beta}) = 0 \quad (3.13)$$

or

$$\frac{\partial \Psi_1}{\partial \beta} = R(r)\dot{B}(\beta)A(\alpha) = 0 \qquad \alpha = \bar{\alpha}, \forall r, \beta \;\Rightarrow\; A(\bar{\alpha}) = 0 \quad (3.14)$$

$$\frac{\partial}{\partial \alpha}\left(\frac{\partial(\Psi_2 r)}{\partial r}\right) = \frac{d(rR(r))}{dr}B(\beta)\dot{A}(\alpha) = 0 \quad \alpha = \bar{\alpha}, \forall r, \beta \;\Rightarrow\; \dot{A}(\bar{\alpha}) = 0 \quad (3.15)$$

Summing up we can write :

	on the sector conductor		on the sector adjacent to the conductor	
for $\vec{M}$:	$\dot{A}$ and/or $\dot{B} = 0$	Neumann b.c.	A and/or $B = 0$	(3.16)
for $\vec{N}$:	A and/or $B = 0$	Dirichlet b.c.	$\dot{A}$ and/or $\dot{B} = 0$	(3.17)

The latter are sufficient, according to the modalities exposed in 1.3.4, to single out periodicity and parity of the solution from which the spectra of eigenvalues $\{\nu, h\}$ and eigenfunctions $\{A(\alpha), B(\beta)\}$ are recovered .

For this purpose, it is important to note that Dirichlet b.c. are the same as in electrostatics, so that Ψ_2 and its relative spectra are identical to Ψ and its spectra respectively as determined in Chapter 2 .

Equally important is the fact that Neumann b.c. are the same as in the static case but with a conductor complementary to the given one . This is expressed analytically by saying that the Ψ_1-spectra relative to an acute sector are

those in electrostatics for the complementary obtuse sector and vice-versa .

This simple and remarkable result permits to obtain all the $\vec{M}$ and $\vec{N}$ solutions with no further computational effort nor further consideration about spectral properties with respect to the static .

The same property naturally occurs for the double-sector in the sense that Ψ_2 is the static Ψ determined in Chapter 2 while Ψ_1 is determined like Ψ but relatively to the complementary double-sector so that it is recoverable from Ψ_2 itself by operating the substitutions :

$$\alpha \to \beta, \qquad k \to k', \qquad h(k^2) \to h'(k'^2), \qquad \nu(k^2) \to \nu(k'^2) \quad (3.18)$$

Taking into account these last relations, in fact, also the plots of the first 15 eigenvalues $\{\nu(k^2), h(k^2)\}$ and first 5 eigenfunctions $\{B(\beta), A(\alpha)\}$ relative to the Neumann problem are directly recoverable from Figs. 2.4,7 respectively, relative to the static Ψ or Ψ_2 .

For what concerns composite wedges, instead, the Ψ_2-spectra are selected from those relative to the sector or double-sector of origin exactly as indicated in the static case .

The Ψ_1-spectra are selected instead in the complementary sector or double-sector spectra with the criterion that $A(\alpha), B(\beta)$ also present vanishing derivative (see (3.16)) in correspondence of the plane conductors .

Finally, we ought to state that for all the wedges considered the R-solution is given by (2.9), where the explicit expression of the spherical Bessel function of the 1^{st} kind is :

$$j_\nu(\kappa r) = \sqrt{\frac{\pi}{4}}(\frac{\kappa r}{2})^\nu \sum_{i=0}^{\infty} \frac{(-\frac{\kappa^2 r^2}{4})^i}{i!\Gamma(\nu + i + \frac{3}{2})} \tag{3.19}$$

As $\nu > 0$ (see (2.12)), this is the only solution which satisfies the conditions of smoothness at the origin (1.24) as it vanishes there: the limit value $\nu = 0$ will be considered in Chapter 4 .

On the other hand, the Hankel function is the linear combination of the 1^{st} and 2^{nd} kind of spherical Bessel functions so defined :

$$h_\nu^{(2)} = j_\nu + \jmath \hbar_\nu \tag{3.20}$$

Its behaviour at infinity is of the type :

$$\lim_{r \to \infty} h_\nu^{(2)}(\kappa r) = \jmath^{(\nu+1)} \frac{e^{-\jmath \kappa r}}{\kappa r} \tag{3.21}$$

That is to say, the fields $\vec{N}, \vec{M}$ present an out-going wave nature satisfying the Sommerfeld radiation conditions (see also [13]) .

This said, we limit our attention to the solution (3.19) valid on the tip and its neighbourhood .

3.1.2 Physical considerations on $\vec{N}$ and $\vec{M}$

The above observations on the Ψ_1, Ψ_2-spectra permit now to draw some important physical considerations about the fields $\vec{M}, \vec{N}$ related to them trough (3.4,5) .

Firstly, we note that the "tie-up" between the above spectra finds its more rigourous justification in the classic Babinet's principle (see also [13, 23]) which allows replacement of the acute sector problem with the equivalent complementary obtuse sector problem .

Nevertheless, only very recently it has been explicitely formulated for the plane sector and its complementary ([18]) in term of fields $\vec{N}, \vec{M}$ and related magnetic field $\vec{H}_N, \vec{H}_M$ we define in the next section .

No analogous explicit formulation is available as yet for the double sector even though an extension of the previous ones would be quite staightforward .

Secondly, we ought to express analytically the fact $\vec{N}$ is the dynamic generalization of the static E-field . This can be proved by noting that as $r \to 0$, we have :

$$\frac{d(rR)}{dr} = (\nu+1)j_\nu(\kappa r) - \frac{j_{\nu+1}(\kappa r)}{\kappa r} \simeq (\nu+1)(\kappa r)^\nu \qquad (3.22)$$

so that the expression for $\vec{N}$ by the tip can be approximated as :

$$\vec{N} \simeq (\nu+1)\left[\nu AB\,\hat{r} + \frac{A\dot{B}}{k\sqrt{sn^2\alpha - sn^2\beta}}\,\hat{\beta} + \frac{\dot{A}B}{k\sqrt{sn^2\beta - sn^2\alpha}}\,\hat{\alpha}\right](\kappa r)^{(\nu-1)} \qquad (3.23)$$

which, apart from the multiplicative factor $(\nu+1)\kappa^{(\nu-1)}$, is the static form (2.15).

Furthermore, the dependence of $\vec{N}$ only on the product κr yields the minimum distance from the tip where the dynamic and static solutions are proportional to each other and where the singular behaviour of the static case ap-

proaches, in fact, the true field. Quantitatively speaking, we can say that for any media and frequency, i.e. $\kappa = \frac{2\pi f}{c}$, there exists a maximum radius r_{max} defined by :

$$\kappa r_{max} = \frac{2\pi}{\lambda} r_{max} = \frac{1}{N} \ll 1 \qquad \text{with } N \in [10 \div 100] \qquad (3.24)$$

so that for any $r < r_{max}$ the Bessel function in (3.22) approaches a linear behaviour in κr, and the $\vec{N}$-field becomes proportional to the static field according to (3.23) .

We can also state again the fact that, physically speaking, $\vec{N}$ is originated by the distribution of charge on the conductor, whilst the appearance of $\vec{M}$ is necessarily related to the dynamic effect of moving charges, that is the current, on the conductor .

3.2 The H-field and J-density of current

From the characterization of the E-field spectra just completed we can deduce the spectra relative to the H-field simply remembering Maxwell's equation which link them in the free space surrounding the conductor, i.e :

$$\vec{H} = -\frac{1}{j\omega\mu} \nabla \times \vec{E} \tag{3.25}$$

Using (3.4,5) for the E-field, we obtain for H :

$$\vec{H}_M = \frac{j}{\eta} \left\{ \frac{\nu(\nu+1)}{\kappa r} \Psi_1 \hat{r} + \frac{G}{\kappa r} \left[j \frac{\partial}{\partial \beta} \left(\frac{\partial(\Psi_1 r)}{\partial r} \right) \hat{\beta} + \frac{\partial}{\partial \alpha} \left(\frac{\partial(\Psi_1 r)}{\partial r} \right) \hat{\alpha} \right] \right\} \tag{3.26}$$

$$\vec{H}_N = \frac{j}{\eta} \left\{ -jG \left(j \frac{\partial \Psi_2}{\partial \alpha} \hat{\beta} + \frac{\partial \Psi_2}{\partial \beta} \hat{\alpha} \right) \right\} \tag{3.27}$$

where $\eta = \sqrt{\frac{\mu}{\epsilon}}$ is the impedance of the medium .

The above show immediately that the $\vec{H}_M$-spectrum is that of $\vec{M}$ and consequently of Ψ_1, while the $\vec{H}_N$-spectra is that of $\vec{N}$ and of Ψ_2 .

Naturally the $\vec{H}$-solutions so identified satisfy the b.c. for the magnetic field, which are explicitly :

$$\hat{n} \cdot \vec{H} = 0 \qquad \text{i.e.} \qquad H_n = 0 \tag{3.28}$$

where $\hat{n}$ is the usual normal unit vector to the conducting surface . The tangential component instead generates on the conductor the density of current :

$$\vec{J} = \hat{n} \times \vec{H} \qquad \text{i.e.} \qquad |J| = |H_t| \tag{3.29}$$

Because of the (3.28-29) we will speak indifferently of density of current or magnetic field on the conductor surface .

Finally, looking at (3.4,5,26,27) we point out that the fields $\vec{N}, \vec{H}_N$ constitute an E-mode while $\vec{M}, \vec{H}_M$ constitute an H-mode in respect to the radial direction .

All these properties allow us to complete the similitude between propagation around a sector and in a closed waveguide introduced in 2.3 .

We can also attempt to draw an equivalent rectangular waveguide in the space r, β, α or more suitably in the space r, θ, ϕ as shown in Fig. 3.1 where some walls are effective conductors while others may be thought of as electric or magnetic walls, in accordance to which components of $\vec{E}$ or $\vec{H}$ vanish there .

The so called E and H modes are completely similar to the TM_{i_1,i_2} and TE_{i_1,i_2} respectively in any transverse section where they present i_1, i_2 zeros apart from those possibly present on the conductors along the two dimensions θ, ϕ .

The situation differs in the longitudinal direction and by the termination $r = 0$ of the guide where the r-dependence is that of j_ν or $\frac{j_\nu}{\kappa r}$. The usual pure propagation term, however, is recovered far away from the origin .

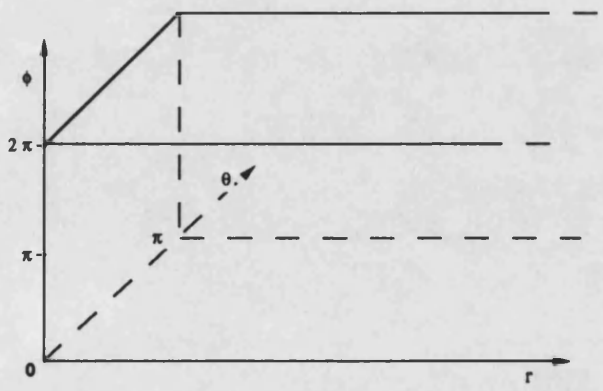

Fig. 3.1 : equivalent rectangular guide in the r,θ,ϕ domain

3.3 The H-field fundamental mode and its main behaviour by the tip

A simple inspection of (3.26,27), taking also in account (3.22), indicates that by the tip $\vec{H}_M$ goes like $(\kappa r)^{\nu-1}$ whilst $\vec{H}_N$ goes like $(\kappa r)^{\nu}$, thus the singular behaviour is due to just $\vec{H}_M$ generated by the Ψ_1 satisfying Neumann b.c. with minimum $\nu \in [0,1]$.

The eigenfunctions $B(\beta), A(\alpha)$, (or $\Theta(\theta), \Phi(\phi)$), pertaining to the fundamental mode are then characterized by the followings parities and periodicities:

$$\text{acute sector} \left\{ \begin{array}{ll} \beta \text{ period } 8K', & \theta \text{ period } 4\pi \text{ (odd)} \\ \alpha \text{ period } 4K \text{ (even)}, & \phi \text{ period } 2\pi \text{ (odd)} \end{array} \right\} \tag{3.30}$$

$$\text{obtuse sector} \left\{ \begin{array}{ll} \beta \text{ period } 8K', & \theta \text{ period } 4\pi \text{ (even)} \\ \alpha \text{ period } 2K \text{ (even)}, & \phi \text{ period } \pi \text{ (even)} \end{array} \right\} \tag{3.31}$$

$$\text{double-sector} \left\{ \begin{array}{ll} \beta \text{ period } 2K' \text{ (even)}, & \theta \text{ period } \pi \text{ (even)} \\ \alpha \text{ period } 4K \text{ (even)}, & \phi \text{ period } 2\pi \text{ (odd)} \end{array} \right\} \tag{3.32}$$

The function $R(r)$ is characterized instead by the curve $\nu(\sigma)$ or better by the degree of magnetic singularity $\tau_h(\sigma) = \nu(\sigma) - 1$.

Because of the discussed 'tie-up' between the spectra relative to the Dirichlet and Neumann problems, that is to say as a consequence of the Babinet's principle [18], we can state the simple and very remarkable relation between the electric and magnetic degrees of singularity for plane sectors and double-sectors :

$$\tau_h(\sigma) = \tau_e(2\pi - \sigma) \qquad \text{for the sector} \tag{3.33}$$

$$\tau_h(\sigma) = \tau_e(\pi - \sigma) \quad \text{for the double-sector} \tag{3.34}$$

For its practical importance we draw the curves relative to the sector in Fig. 3.2 and we report an approximate expression around the particular points $\sigma = 0, \pi, 2\pi$ respectively associated with the semi-indefinite wire, the half-plane and the plane conductor . Only at these points, in fact, ν can be computed in an exact way as $0, \frac{1}{2}, 1$ respectively, whereas techniques are available which permit the determination of approximate analytical expression around these points .

We have :

$$\tau_e(\sigma) = -\tfrac{1}{4}(\tfrac{2\pi-\sigma}{2})^2 + \tfrac{1}{8}(\tfrac{2\pi-\sigma}{2})^4 log(\tfrac{2\pi-\sigma}{2}) + \tfrac{1}{12}(3log\tfrac{1}{2} + 1)(\tfrac{2\pi-\sigma}{2})^4 +$$
$$O[(\tfrac{2\pi-\sigma}{2})^6 \left(log(\tfrac{2\pi-\sigma}{2})\right)^2] \qquad \text{around } \sigma = 2\pi \tag{3.35}$$

$$\tau_e(\sigma) = -\tfrac{1}{2} - \tfrac{1}{\pi}cos(\tfrac{\sigma}{2}) + \tfrac{1}{\pi^2}cos^2(\tfrac{\sigma}{2}) - \left(\tfrac{1}{\pi^3} + \tfrac{1}{6\pi}\right) cos^3(\tfrac{\sigma}{2}) +$$
$$O\left(cos^4(\tfrac{\sigma}{2})\right) \qquad \text{around } \sigma = \pi \tag{3.36}$$

$$\tau_e(\sigma) = -1 + \frac{1}{ln(4(\frac{2}{\sigma}))} \qquad \text{around } \sigma = 0 \tag{3.37}$$

(3.35) had been first determined using perturbation techniques but, in the attempt to extend indefinitely the number of terms in the series, Brown (see [20]) expressed ν and h asymptotically about $k = 1$ that is $\sigma = 2\pi$; the first four terms are just those reported and analogous relation were recovered for h .

(3.36) had been approached instead firstly by Legendre who gives three

terms . Brown succesfully extended to 4 in the above work [20], also providing analogous expression for h .

The accuracy of these two espressions versus the angular distance from the points $\sigma = \pi, 2\pi$ respectively is indicated in [20] .

Relation (3.37) has been, among the others Authors, deduced by De Smedt [16] as the limit case of a sharp corner of arbitrary section . He implemented a static analysis in spherical c.s. turning the problem of applying the b.c. into one of solving integrals of some normal derivatives of the potential along an arbitrary irregular boundary . (3.37) results the particular case of a sector in the more general formula describing the degree of electric singularity for a solid conducting tip .

The complementarity of behaviour for the electric and magnetic singularities can be graphically explained if we think in terms of E-field lines on the plane facing the conductor and, for what said in 3.2, of the density of current lines on the conductor itself as shown in Fig. 3.3 . Precisely, the more reentrant is the sector, the more the E-field lines thicken on the tip while the current bends before it . Conversely, the more protruding is the sector, the more the lines of current thicken on the very tip while the E-field lines rarefy there .

The situation is different for all the other five composite wedges because the above defined fundamental $\vec{H}_M$-mode does not belong to the excitable spectrum.

This can be proved in an alternative, more physical way by requiring that the EM fields around the conducting sectors and the charge and currents on them must satisfy the image principle with respect to the conductor plane(s) of symmetry .

For this purpose, Fig. 3.4a shows the typical behaviour of an H-mode

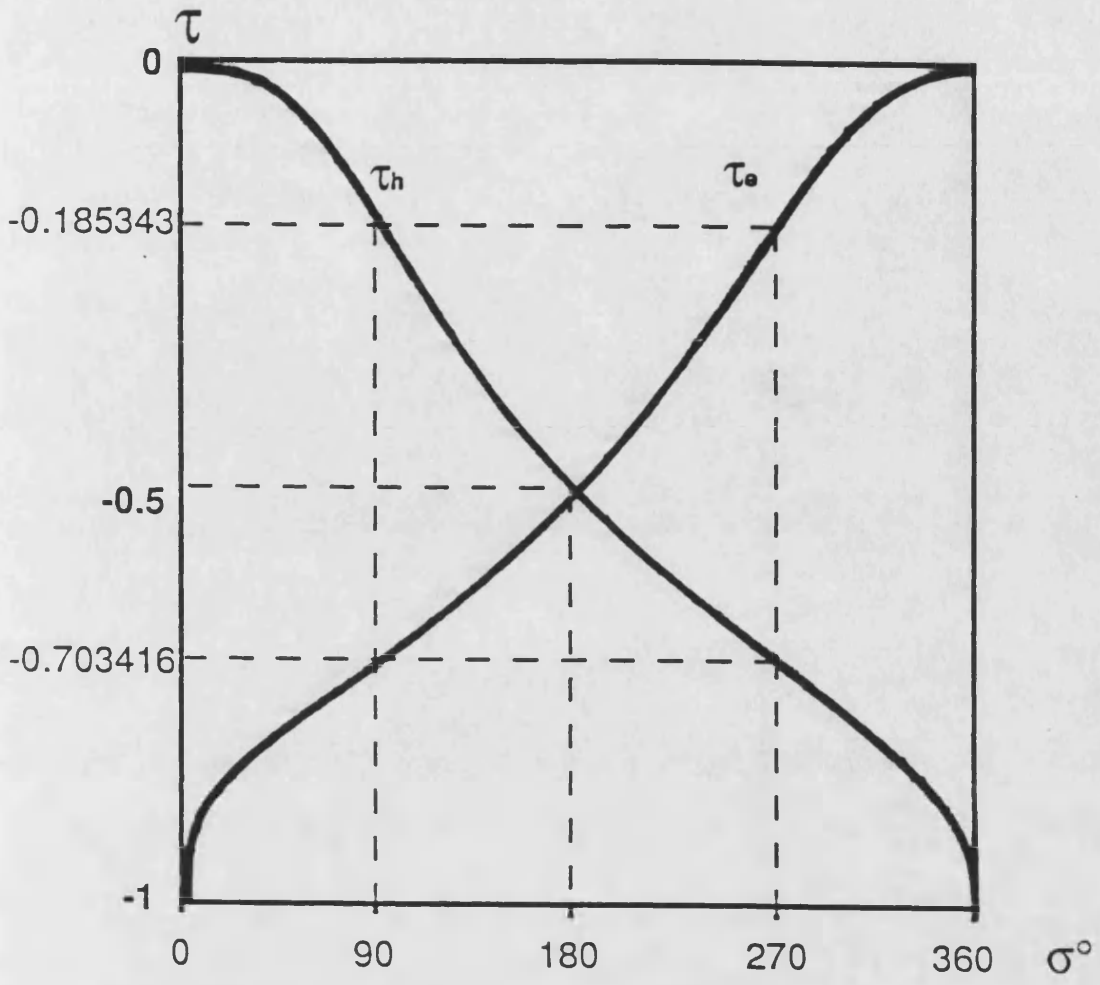

Fig. 3.2 : EM fields degrees of singularity for the plane sector

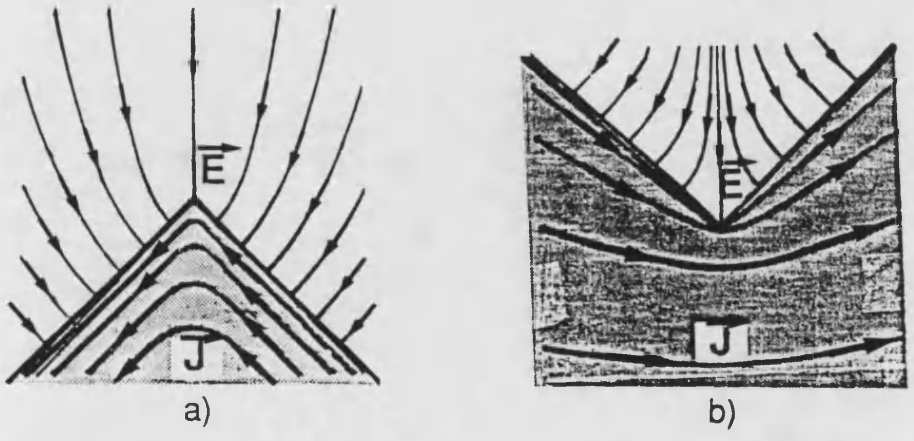

Fig. 3.3 : lines of $\vec{E}$ and $\vec{J}$ for an acute a) and obtuse b) sector

current while Fig. 3.4b shows the typical behaviour of an E-mode current. Only the latter would satisfy the image principle with respect to the median plane, like for the structure in Fig. 2.8, and presents necessarily a zero on the tip.

Similar arguments are valid for all the other four composite wedges .

Thus, for all them, the fundamental H-mode is just the $\vec{H}_N$ associated to the fundamental N-field so that the minimum degree of magnetic zeros τ_h in the origin is related to the degree of electric singularity τ_e by means of :

$$\tau_h(\sigma) = \tau_e(\sigma) + 1 \tag{3.38}$$

We can summarize all these considerations simply by saying that:
for the sector and double-sector the main $\vec{H}$ and $\vec{E}$ behaviours are those of the fundamental H-mode and E-mode respectively, while for any other case, the main behaviour is that of the fundamental E-mode .

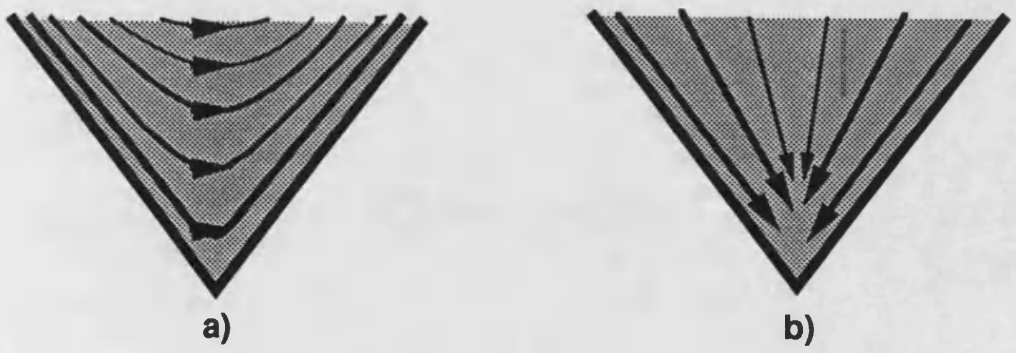

Fig. 3.4 : J-current lines relative to a) an H-mode and b) an E-mode

3.4 The EM fields in trigonometric coordinates

At this stage, all the general properties of the solutions have been pointed out so that we are better placed to give them the familiar aspect of trigonometric forms, expliciting also the Ψ components R, Θ, Φ :

$$\text{H-mode} \begin{cases} \vec{M} = \frac{P}{S}(R_1\Theta_1\dot{\Phi}_1)\,\hat{\theta} - \frac{T}{S}(R_1\dot{\Theta}_1\Phi_1)\,\hat{\phi} \\ \vec{H}_M = \frac{j}{\eta}\frac{1}{\kappa r}[\nu(\nu+1)R_1\Theta_1\Phi_1\,\hat{r} + \frac{T}{S}(r\dot{R}_1)\dot{\Theta}_1\Phi_1\,\hat{\theta} + \frac{P}{S}(r\dot{R}_1)\Theta_1\dot{\Phi}_1\,\hat{\phi}] \end{cases} \tag{3.39}$$

$$\text{E-mode} \begin{cases} \vec{N} = \frac{1}{\kappa r}[\nu(\nu+1)R_2\Theta_2\Phi_2\,\hat{r} + \frac{T}{S}(r\dot{R}_2)\dot{\Theta}_2\Phi_2\,\hat{\theta} + \frac{P}{S}(r\dot{R}_2)\Theta_2\dot{\Phi}_2\,\hat{\phi}] \\ \vec{H}_N = \frac{j}{\eta}[\frac{P}{S}(R_2\Theta_2\dot{\Phi}_2)\,\hat{\theta} - \frac{T}{S}(R_2\dot{\Theta}_2\Phi_2)\,\hat{\phi}] \end{cases} \tag{3.40}$$

where T,P,S are the functionals defined in (D.1,2,3) .

Following the lines of Chapter 2, we give a complete characterization just for the fundamental H-mode relative to the main sectors, i.e. $k^2 = \frac{1}{2}$, reporting in Table 3.1 the ν-values and the most significant series coefficients for the functions $\Theta(\theta)$ and $\Phi(\phi)$.

In particular, those relative to the composite structure are the same as reported in Table 2.1 .

Observations about the dominance of the term with fundamental period in the series, which is also the only one to be used in the analysis of the main behaviour by the conductor, are completely similar to those argued in 2.4 because of the stated relations between the static Ψ and the actual Ψ_1 or Ψ_2 .

Finally, we collect in Table 3.2 the numerical values of τ_h for the eight configurations versus the sector angular aperture . The accuracy of the evaluations is at best of 7 decimal figures obtainable without further computation from the data in Table 2.2 simply by applying (3.33,34,38) .

CHARACTERISTIC COEFFICIENTS OF THE FUNCTIONS R(r),Θ(θ),Φ(φ) Fundamental mode - $k^2 = 0.5$				
	Fig. 2.1a	ν=0.814655	Fig. 2.8a	ν =1.131248
i	θ-per 4π odd	φ-per 2π odd	θ-per 4π even	φ-per 2π even
-5	-0.000002		-0.000003	
-4	-0.000014		-0.000025	
-3	-0.000122		-0.000229	
-2	-0.001289		-0.002524	
-1	-0.020708		-0.046684	
0	1.000000	1.000000	1.000000	1.000000
1	-0.146171	0.010835	-0.218468	-0.009271
2	-0.004733	0.000806	-0.004143	-0.000646
3	-0.000386	0.000082	-0.000315	-0.000064
4	-0.000040	0.000010	-0.000032	-0.000007
5	-0.000005	0.000001	-0.000003	-0.000001
	Fig. 2.1b	ν=0.296584	Fig. 2.8b	ν=1.955326
i	θ-per π even	φ-per 4π even	θ-per π odd	φ-per 4π odd
-5		0.000001		-0.000003
-4		0.000009		-0.000025
-3		0.000075		-0.000249
-2		0.000752		-0.003264
-1		0.010468		-0.131919
0	1.000000	1.000000		1.000000
1	-0.033084	-0.054644	1.000000	-0.417261
2	-0.001994	-0.002632	0.003154	0.011547
3	-0.000186	-0.000231	0.000240	0.000645
4	-0.000021	-0.000025	-0.000025	0.000059
5	-0.000003	-0.000003	0.000003	0.000006
	Fig. 2.2	ν =0.704321	Fig. 2.9	ν =1.311863
i	θ-per π even	φ-per 2π odd	θ-per 2π odd	φ-per 2π even
0	1.000000	1.000000	1.000000	1.000000
1	-0.102762	0.016714	-0.023588	-0.023588
2	-0.005284	0.001279	-0.001543	-0.001543
3	-0.000473	0.000131	-0.000150	-0.000150
4	-0.000052	0.000015	-0.000017	-0.000017
5	-0.000006	0.000002	-0.000002	-0.000002
	Fig. 2.10	ν = 1.918023	Fig. 2.11	ν = 2.688000
i	θ-per π odd	φ-per π even	θ-per π odd	φ-per 2π even
0		1.000000		1.000000
1	1.000000	-0.438126	1.000000	-0.200660
2	0.005747	-0.001841	-0.053492	-0.003350
3	0.000443	-0.000125	-0.002912	-0.000248
4	0.000046	-0.000012	-0.000267	-0.000025
5	0.000005	-0.000001	-0.000030	-0.000003

Table 3.1: characterization of the eigenfunctions $R(r), \Theta(\theta), \Phi(\phi)$ for the acute sector, half acute sector, obtuse sector, half obtuse sector, double sector, half double sector, sector on a plane and half sector on a plane respectively indicated by their Fig. number .

3D-WEDGES Degree of magnetic singularity τ_h							
$\frac{\sigma^\circ}{2}$	Fig.2.1a,b	Fig.2.8a,b	$\frac{\sigma^\circ}{2}$	Fig. 2.2	Fig. 2.9	Fig. 2.10	Fig. 2.11
0.00	0.0000000	1.0000000	0.00	0.0000000	1.0000000	1.0000000	2.0000000
5.00	-0.0019269	1.1665873	2.50	-0.0009547	1.0069497	1.2789616	2.0028342
10.00	-0.0079077	1.2118317	5.00	-0.0038427	1.0037824	1.3434077	2.0111690
15.00	-0.0183830	1.2499530	7.50	-0.0087142	1.0084681	1.3960998	2.0246795
20.00	-0.0338525	1.2847419	10.00	-0.0156253	1.0149799	1.4435835	2.0430298
25.00	-0.0546955	1.3173220	12.50	-0.0246241	1.0233004	1.4881265	2.0659169
30.00	-0.0809612	1.3479878	15.00	-0.0357391	1.0334242	1.5307534	2.0930816
35.00	-0.1121971	1.3766409	17.50	-0.0489683	1.0453591	1.5719618	2.1243052
40.00	-0.1474300	1.4029603	20.00	-0.0642704	1.0591268	1.6119693	2.1594002
45.00	-0.1853447	1.4265126	22.50	-0.0815593	1.0747630	1.6508186	2.1981970
50.00	-0.2245699	1.4468623	25.00	-0.1007028	1.0923175	1.6884303	2.2405277
55.00	-0.2639208	1.4636870	27.50	-0.1215263	1.1118536	1.7246354	2.2862073
60.00	-0.3025154	1.4768731	30.00	-0.1438215	1.1334477	1.7592010	2.3350107
65.00	-0.3397789	1.4865615	32.50	-0.1673581	1.1571889	1.7918567	2.3866444
70.00	-0.3753875	1.4931272	35.00	-0.1918973	1.1831778	1.8223226	2.4407145
75.00	-0.4092000	1.4971126	37.50	-0.2172050	1.2115239	1.8503404	2.4966899
80.00	-0.4411957	1.4991488	40.00	-0.2430628	1.2423432	1.8757026	2.5538665
85.00	-0.4714297	1.4998941	42.50	-0.2692759	1.2757527	1.8982774	2.6113393
90.00	-0.5000000	1.5000000	45.00	-0.2956786	1.3118631	1.9180227	2.6680001
95.00	-0.5270279	1.5001060	47.50	-0.3221360	1.3507670	1.9349886	2.7225767
100.00	-0.5526446	1.5008538	50.00	-0.3485447	1.3925218	1.9493082	2.7737333
105.00	-0.5769839	1.5022990	52.50	-0.3748310	1.4371258	1.9611799	2.8202266
110.00	-0.6001782	1.5070497	55.00	-0.4009492	1.4844843	1.9708463	2.8610865
115.00	-0.6223566	1.5141281	57.50	-0.4268797	1.5343655	1.9785726	2.8957597
120.00	-0.6436452	1.5252239	60.00	-0.4526276	1.5863474	1.9846294	2.9241631
125.00	-0.6641679	1.5416577	62.50	-0.4782217	1.6397625	1.9892784	2.9466328
130.00	-0.6840488	1.5650273	65.00	-0.5037155	1.6936545	1.9927634	2.9638027
135.00	-0.7034156	1.5971311	67.50	-0.5291900	1.7467763	1.9953053	2.9764651
140.00	-0.7224051	1.6396502	70.00	-0.5547600	1.7976561	1.9970996	2.9854520
145.00	-0.7411714	1.6933803	72.50	-0.5805848	1.8447508	1.9983159	2.9915554
150.00	-0.7598998	1.7568773	75.00	-0.6068899	1.8866607	1.9990985	2.9954829
155.00	-0.7788320	1.8249698	77.50	-0.6340066	1.9223365	1.9995683	2.9978387
160.00	-0.7983164	1.8889505	80.00	-0.6624549	1.9511953	1.9998242	2.9991204
165.00	-0.8189236	1.9402857	82.50	-0.6931375	1.9731090	1.9999446	2.9997231
170.00	-0.8417794	1.9750598	85.00	-0.7278994	1.9882884	1.9999891	2.9999455
175.00	-0.8699635	1.9941148	87.50	-0.7719023	1.9971206	1.9999993	2.9999966
180.00	-1.0000000	2.0000000	90.00	-1.0000000	2.0000000	2.0000000	3.0000000

Table 3.2: degree of magnetic singularity or zero versus the angular aperture σ for the sector, half sector, double sector, half double sector, sector on a plane and half sector on a plane respectively indicated by their Fig. number .

3.5 The H-field singularity vector for the main sectors

Considering the main behaviour by the tip of the wedge proper to the fundamental H-mode, we achieve a first general simplification for R if we note that by the tip, i.e. $\kappa r \to 0$, (see also (3.22) and E.6) we have :

$$\lim_{\kappa r \to 0} R(\kappa r) = (\kappa r)^{\nu} \qquad \lim_{\kappa r \to 0} \varrho(\kappa r) = (\nu+1)(\kappa r)^{(\nu-1)} \tag{3.41}$$

consequently, the S functions defined in Appendix D,E become related to each other as :

$$S_{\phi_N} = (\nu+1)\frac{S_{\phi_M}}{\kappa r} = (\nu+1)\kappa^{(\nu-1)} S_{\phi} \tag{3.42}$$

$$S_{\theta_N} = (\nu+1)\frac{S_{\theta_M}}{\kappa r} = (\nu+1)\kappa^{(\nu-1)} S_{\theta} \tag{3.43}$$

so that their explicit forms in x, y, z and X, Y, Z can be obtained directly from the (D.23,24) respectively .

Furthermore, for what will follow, we may neglect the multiplicative dependence on ν and κ, possibly reintroducing it at right time .

We can now apply again the simplifying procedure presented in Chapter 2 so as to recover the singularity functions for the H-field in a complete three-dimensional trigonometric space and its projections on the main rectangular planes .

The quarter plane

Starting then with the quarter plane in the geometry indicated in Fig. 3.5 and the derived structures of the half quarter plane, from (3.30) and (2.43) we can use the approximate eigenfunctions :

$$\Theta_2(\theta) \simeq sin\frac{\theta}{2} \qquad \Phi_2(\phi) \simeq sin\phi \tag{3.44}$$

$$\Theta_1(\theta) \simeq cos\frac{\theta}{2} \qquad \Phi_1(\phi) \simeq cos\phi \tag{3.45}$$

Consequently, the H-field singularity vector components can be written as :

$$s_{H_X} = (1 - cos\theta cos\phi) S_{\phi_N} sin\frac{\theta}{2} \tag{3.46}$$

$$s_{H_Y} = sin\frac{\theta}{2} S_{\theta_N} + cos\frac{\theta}{2} S_{\phi_N} \tag{3.47}$$

$$s_{H_Z} = (1 + cos\theta cos\phi) S_{\phi_N} sin\frac{\theta}{2} \tag{3.48}$$

These assume forms helplessly complicated if rectangular coordinates are explicited, however, following the motivations given for the E-field, we will report explicitly in Table 3.3 only their projections on the main planes .

The resulting forms are obviously just of the six kinds (2.59) already met for $\vec{s}_E$, even though differently distributed in space .

In order to give more physical interpretation to the contents of the Table, we draw in Fig. 3.6 the magnitude $|H|$ on the conductor, where it is also proportional to $|J|$, according to (3.28,29), while Fig. 3.7 shows $|H|$ on the plane normal to the conductor and tangential to its edge .

The eminent features of this behaviour is the transition between the singularity of degree $-\frac{1}{2}$ along the edges to that of degree -0.186345 on the tip . Very

remarkably, we note another advantage of the original choice of orientation for the acute and obtuse sectors of Fig. 2.1 . It consists in the fact that

Table 3.3 results identical to Table 2.4, relative to the E-field singularity vector for the three-quarter plane .

Some care has to be taken while dealing with $\vec{s}_H$ for the sector cut by its median plane as its eigenfunctions are relative to the Dirichlet b.c. so that (3.46,47,48) have to be corrected according to the substitutions:

$$S_{\phi_N} \rightarrow S_{\phi_M}, \quad S_{\theta_N} \rightarrow S_{\theta_M}, \quad \nu - 1 \rightarrow \nu \tag{3.49}$$

Nevertheless, the projection of the singularity functions on the main planes assumes the same forms as in Table 3.3 with just $\nu - 1$ replaced by ν .

The three-quarter plane

When we deal instead with the three-quarter plane of Fig. 3.8 and the half three-quarter plane we can approximate the eigenfunctions and the components of $\vec{s}_H$ in trigonometric form respectively as :

$$\Theta_2(\theta) \simeq cos\tfrac{\theta}{2} \qquad \Phi_2(\phi) \simeq cos2\phi \tag{3.50}$$

$$\Theta_1(\theta) \simeq sin\tfrac{\theta}{2} \qquad \Phi_1(\phi) \simeq sin2\phi \tag{3.51}$$

$$s_{H_X} = r^{\nu-1}cos\tfrac{\theta}{2} + (1 - cos\theta cos\phi)S_{\theta_N}sin\tfrac{\theta}{2} \tag{3.52}$$

$$s_{H_Y} = S_{\phi_N}sin\tfrac{\theta}{2} \tag{3.53}$$

$$s_{H_Z} = r^{\nu-1}cos\tfrac{\theta}{2} + (1 + cos\theta cos\phi)S_{\theta_N}sin\tfrac{\theta}{2} \tag{3.54}$$

Their explicit forms on the main planes are those reported in Table 3.4 whilst the magnitude $|H|$, $|J|$ on the conductor plane and the $|H|$ on the plane orthogonal to it by its edge are shown in Figs. 3.9,10 respectively . The latter highlight the sharper singularity of degree $\simeq -0.703416$ on the tip as compared to that of degree $-\frac{1}{2}$ along the confluent edges . Obviously, as observed for the quarter plane, *Table 3.4 is identical to Table 2.3 relative to the E-field singularity vector for the quarter plane* .

The formulae relative to the half-three-quarter plane can be recovered from (3.52,53,54) by operating the substitutions :

$$S_{\theta_N} \rightarrow S_{\theta_M}, \quad S_{\phi_N} \rightarrow S_{\phi_M}, \quad r^{\nu-1} \rightarrow S_{\phi_M} \tag{3.55}$$

hence, their projection on the main planes are still those reported in Table 3.4 with just $\nu - 1$ replaced by $\nu \simeq 1.955326$, that is a very strong zero on the tip .

The double-quarter plane

Even simpler are the forms relative to the double-quarter plane and derived geometries of Figs. 2.9,10,11 for which the approximate eigenfunctions are, in the order, recovered from Table 2.2 as :

$$\Theta_2(\theta) \simeq 1 \qquad \Phi_2(\phi) \simeq sin\phi \tag{3.56}$$

$$\Theta_1(\theta) \simeq sin\theta \qquad \Phi_1(\phi) \simeq cos\phi \tag{3.57}$$

$$\Theta_1(\theta) \simeq sin2\theta \qquad \Phi_1(\phi) \simeq 1 \tag{3.58}$$

$$\Theta_1(\theta) \simeq sin2\theta \qquad \Phi_1(\phi) \simeq cos\phi \tag{3.59}$$

which using (E.3) provide the $\vec{s}_H$ components for the double-quarter plane:

$$s_{H_X} = (1 - cos\theta cos\phi) S_{\phi_N} \tag{3.60}$$

$$s_{H_Y} = S_{\theta_N} \tag{3.61}$$

$$s_{H_Z} = (1 + cos\theta cos\phi) S_{\phi_N} \tag{3.62}$$

In particular the 2^{nd} equation reveals the physical meaning of S_θ (or S_ϕ) as being the s_{H_Y} singularity vector component for the double-sector with conductor on $\theta = 0, \pi$ (or $\phi = 0, \pi$) .

By projecting these formulas on the main planes, we get in explicit rectangular coordinates the forms of which in Table 3.5 and their interpretation is shown graphically in Figs. 3.12,13, representing respectively the plane of the conductor and the plane orthogonal to the conductor passing through its edge. The order of the Sectors in the Table has been changed in such a way as to put in evidence the fact that *Table 3.5 is identical to Table 2.5 relative to the complementary double sector once x, θ are interchanged with z, ϕ respectively* .

Analogously to the previous cases, the singular vector components for the derived wedges are obtainable from (3.60,61,62) by operating the substitutions:

$$S_{\phi_N} \rightarrow S_{\phi_M} \Theta \dot{\Phi}, \qquad S_{\theta_N} \rightarrow S_{\theta_M} \dot{\Theta} \Phi, \qquad \nu - 1 \rightarrow \nu \tag{3.63}$$

where Θ, Φ are as in (3.57,58,59) . The forms on the main planes are again those reported in Table 3.5 with just $\nu - 1$ replaced into ν whose value, case for case, is recoverable from Table 3.2 .

H-field singularity vector components for a quarter plane			
s_{H_X} (and J_Z)	s_{H_Y}	s_{H_Z} (and $-J_X$)	Sector
on the plane $Y = 0$			
0	$\frac{r^\nu}{\sqrt{\lvert XZ\rvert}}$	0	$z < 0; \phi = 0$
0	$r^{\nu-1}$	0	$z \geq 0; \phi = 0, \pi, \theta = 0$
0	$\frac{r^\nu}{\sqrt{\lvert XZ\rvert}}$	0	$z < 0; \phi = \pi$
$\frac{r^\nu}{\sqrt{\lvert XZ\rvert}}$	0	$\sqrt{\lvert XZ\rvert} r^{\nu-2}$	$x \geq 0; \theta = \pi$
$\sqrt{\lvert XZ\rvert} r^{\nu-2}$	0	$\frac{r^\nu}{\sqrt{\lvert XZ\rvert}}$	$x < 0; \theta = \pi$
on the plane $X = 0$ *(or* $Z = 0$*)*			
$\frac{r^{\nu-\frac{1}{2}}}{\sqrt{\lvert Y\rvert}}$ $(\sqrt{\lvert Y\rvert} r^{\nu-\frac{3}{2}})$	$\frac{r^{\nu-\frac{1}{2}}}{\sqrt{\lvert Y\rvert}}$	$\sqrt{\lvert Y\rvert} r^{\nu-\frac{3}{2}}$ $(\frac{r^{\nu-\frac{1}{2}}}{\sqrt{\lvert Y\rvert}})$	$Z > 0$ (or $X > 0$)
$\lvert Y\rvert r^{\nu-2}$	$r^{\nu-1}$	$\lvert Y\rvert r^{\nu-2}$	$Z \leq 0$ (or $X \leq 0$)

Table 3.3: H-field singularity vector projections on the main planes relative to the conductor and geometry indicated in Fig. 3.5; $\nu \simeq 0.814655$ for the quarter plane and $\nu \simeq 1.131248$ for the half quarter plane .

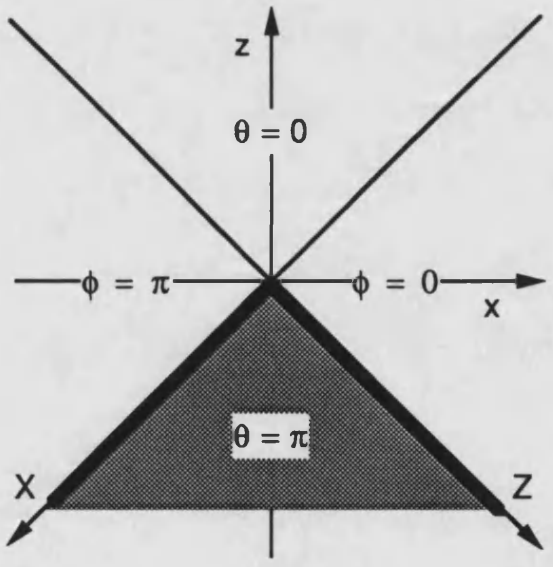

Fig. 3.5 : quarter plane

H-field singularity vector components for a three-quarter plane			
s_{H_X} (and J_Z)	s_{H_Y}	s_{H_Z} (and $-J_X$)	Sector
on the plane $Y = 0$			
$\frac{r^\nu}{\sqrt{\lvert XZ\rvert}}$	0	$\sqrt{\lvert XZ\rvert}r^{\nu-2}$	$z < 0; \phi = 0$
$r^{\nu-1}$	0	$r^{\nu-1}$	$z \geq 0; \phi = 0, \pi, \theta = 0$
$\sqrt{\lvert XZ\rvert}r^{\nu-2}$	0	$\frac{r^\nu}{\sqrt{\lvert XZ\rvert}}$	$z < 0; \phi = \pi$
0	$\frac{r^\nu}{\sqrt{\lvert XZ\rvert}}$	0	$z < 0; \theta = \pi$
on the plane $X = 0$ *(or* $Z = 0$*)*			
$\frac{r^{\nu-\frac{1}{2}}}{\sqrt{\lvert Y\rvert}}$ $(\sqrt{\lvert Y\rvert}r^{\nu-\frac{3}{2}})$	$\frac{r^{\nu-\frac{1}{2}}}{\sqrt{\lvert Y\rvert}}$	$\sqrt{\lvert Y\rvert}r^{\nu-\frac{3}{2}}$ $(\frac{r^{\nu-\frac{1}{2}}}{\sqrt{\lvert Y\rvert}})$	$Z > 0$ (or $X > 0$)
$r^{\nu-1}$	$r^{\nu-1}$	$r^{\nu-1}$	$Z \leq 0$ (or $X \leq 0$)

Table 3.4: H-field singularity vector projections on the main planes relative to the conductor and geometry indicated in Fig. 3.8; $\nu \simeq 0.296584$ for the three-quarter plane and $\nu \simeq 1.955326$ for the half three-quarter plane .

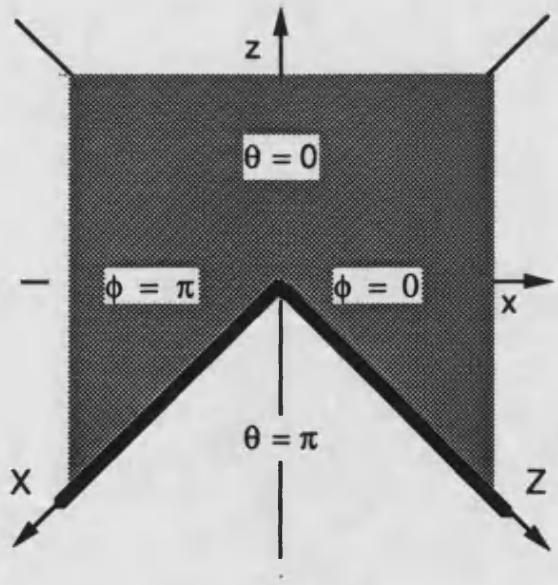

Fig. 3.8 : three-quarter plane

H-field singularity vector components for a double-quarter plane			
s_{H_X} (and J_Z)	s_{H_Y}	s_{H_Z} (and $-J_X$)	Sector
on the plane $Y = 0$			
$\frac{r^\nu}{\sqrt{\lvert XZ\rvert}}$	0	$\sqrt{\lvert XZ\rvert}r^{\nu-2}$	$x < 0; \theta = 0$
$\sqrt{\lvert XZ\rvert}r^{\nu-2}$	0	$\frac{r^\nu}{\sqrt{\lvert XZ\rvert}}$	$x \geq 0; \theta = \pi$
0	$\frac{r^\nu}{\sqrt{\lvert XZ\rvert}}$	0	$\phi = 0$
$\frac{r^\nu}{\sqrt{\lvert XZ\rvert}}$	0	$\sqrt{\lvert XZ\rvert}r^{\nu-2}$	$x \geq 0; \theta = \pi$
$\sqrt{\lvert XZ\rvert}r^{\nu-2}$	0	$\frac{r^\nu}{\sqrt{\lvert XZ\rvert}}$	$x < 0; \theta = \pi$
0	$\frac{r^\nu}{\sqrt{\lvert XZ\rvert}}$	0	$\phi = \pi$
on the plane $X = 0$ *(or* $Z = 0$*)*			
$\frac{r^{\nu-\frac{1}{2}}}{\sqrt{\lvert Y\rvert}}$ $(\sqrt{\lvert Y\rvert}r^{\nu-\frac{3}{2}})$	$\frac{r^{\nu-\frac{1}{2}}}{\sqrt{\lvert Y\rvert}}$	$\sqrt{\lvert Y\rvert}r^{\nu-\frac{3}{2}}$ $(\frac{r^{\nu-\frac{1}{2}}}{\sqrt{\lvert Y\rvert}})$	any Z (or X)

Table 3.5: H-field singularity vector projections on the main planes relative to the conductor and geometry indicated in Fig. 3.11; $\nu \simeq 0.704321$ for the double-quarter plane, $\nu \simeq 1.311863$ for the half double-quarter plane, $\nu \simeq 1.918023$ for the quarter plane on a plane and $\nu \simeq 2.68800$ for its half .

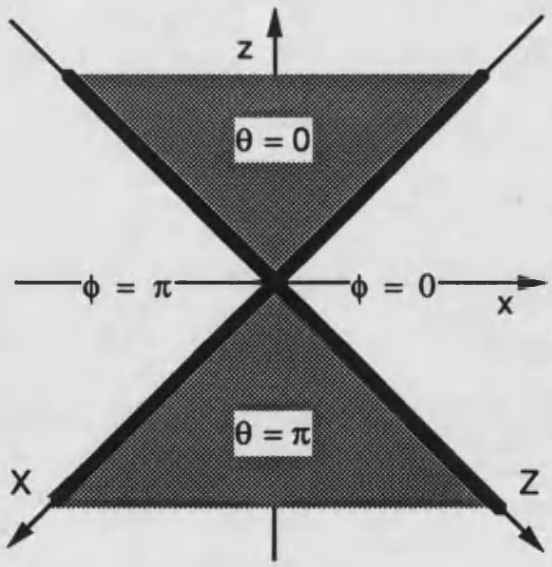

Fig. 3.11: double quarter plane

Magnitude of the magnetic field on the planes

Y = 0	Z = 0
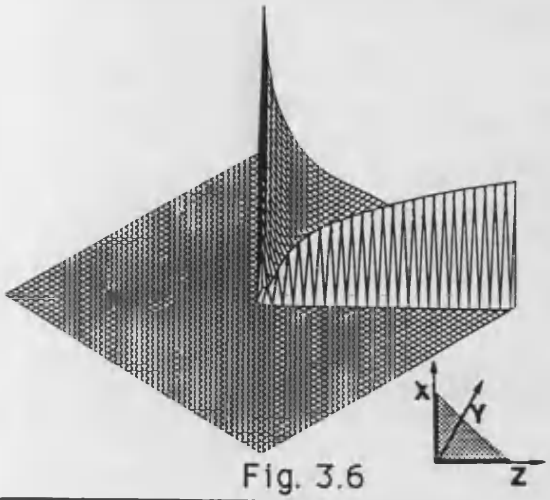 Fig. 3.6	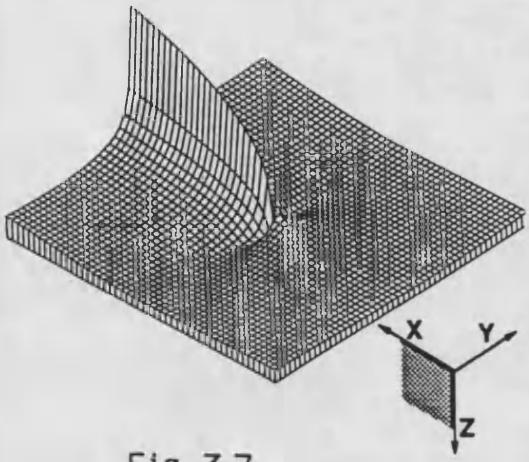 Fig. 3.7
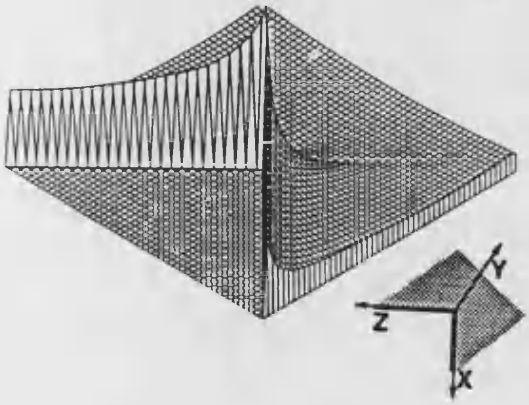 Fig. 3.9	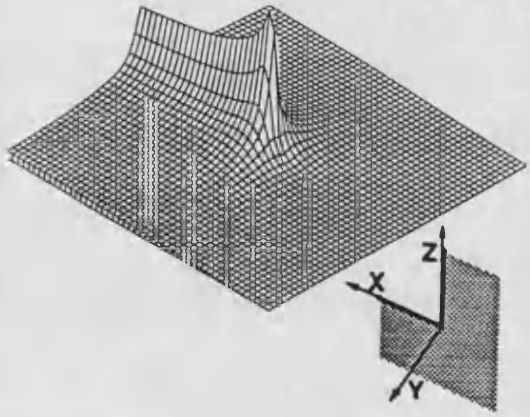 Fig. 3.10
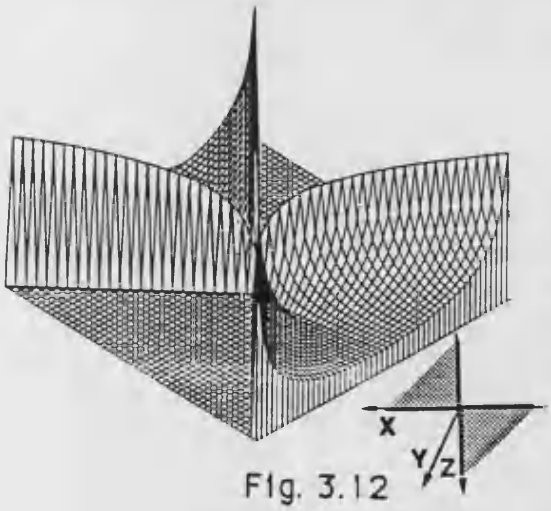 Fig. 3.12	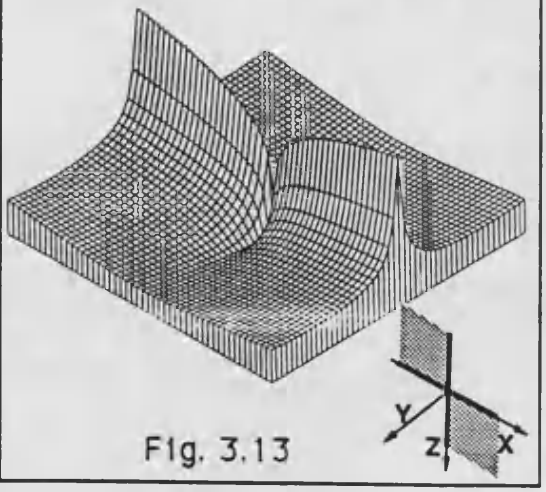 Fig. 3.13

3.6 EM singularity vectors for arbitrary wedges

From equations (3.39,40) it follows a similitude between the espressions of $\vec{N}$ and $\vec{H_M}$ (or $\vec{M}$ and $\vec{H_N}$) .

This similitude becomes a true identity, apart for the multiplicative factor $\frac{i}{\eta}$, if we consider the N-spectrum associated to an acute sector (Fig. 2.1) and the H-spectrum associated to its complementar obtuse sector (Fig. 2.1b) .

In fact the functions R_1, Θ_1, Φ_1 of the first geometry and R_2, Θ_2, Φ_2 of the second geometry are identical because they satisfy Dirichlet and Neumann b.c. pertaining to complementar sectors, that is to say exactly the same b.c. . The same properties are demonstrable in a similar way for $\vec{M}$ and $\vec{H_N}$ and can be extended to the case of the double sector .

In particular, the fundamental N-mode of an acute sector and the fundamental H_M-mode of its complementary are proportional so that the associated singularity vectors are identical as observed, in particular, by comparing Tables 2.3,4,5 with Tables 3.3,4,5 .

Also remembering that the E-fiels singularity vector can be recovered from a simple static analysis we can summarize by postulating that :

In a full dynamical analysis, the EM-field spectra pertaining to any plane sector are recoverable from those pertaining to the sole acute sectors .

Likewise, the EM-fields spectra pertaining to any plane sector are recoverable from those of the sole E-field spectra or H-field spectra pertaining to any plane sector .

In particular, the H-field singularity vectors pertaining to any sector are

recoverable from the E-field singularity vectors pertaining to the complementary sector and then from the static analysis only .

The first postulate is a consequence of the Babinet's principle while the second is a consequence of the first and of the fact the static and dynamical E-fields present the same main behaviour by the conductor .

The two postulates are important also for their possible extension to arbitrarily shaped complementary plane conductors such as, for instance, the degenerate surfaces of the ellipsoidal c.s. for which a static analysis is already available in separable form while the dynamical one is not .

The limit cases $k^2 = 0, 1$ are again postponed to Chapter 4 .

What instead now matters more to us is to attempt the determination of $\vec{s}_E, \vec{s}_H$ for a plane conductor with arbitrary boundary C whose tangent varies continuously everywhere except at a cusp-point O .

Fixing in O the origin of a conical c.s. with the plane conductor lying on the plane $Y = 0$, we can depict the situation as in Fig. 3.14 .

In this situation, the right and left branches of C with respect to O can be expressed by the continuous functions with continuous derivatives $z = f_1(x)$, $z = f_2(x)$. The right and left tangents to C at O are related to the angular coefficients of the curves there as $tg\sigma_1 = \dot{f}_1(0)$, $tg\sigma_2 = \dot{f}_2(0)$.

The values σ_1, σ_2 permit the unique orientation of the main system X, Y, Z making the Z-axis fit the right tangent of C in O .

Naturally, is always possible to single out a small neighbourhood of the tip where the wedge is well enough approximated by the sector of angular aperture

$\sigma = \pi - (\sigma_1 + \sigma_2)$ and for which $\vec{s}_E$ and $\vec{s}_H$ are computed as seen previously .

Obviously, we cannot extend these singularity vectors to the whole of the conductor but the generalization used to pass from the main sectors to arbitrary sectors on the main planes, suggests possible forms, at least, on particular surfaces. For instance, the formulae collected in Tables 3.3,4,5 of Chapter 2,3 on the plane $Y = 0$ can be generalized by substituting :

$$X \rightarrow f_{11}(X, Z) \qquad Z \rightarrow f_{22}(X, Z) \tag{3.64}$$

where f_{11} and f_{22} are the implicit forms of the right and left branches of C, in similitude to the implicit straight line equations (2.72) of the sector edge .

The forms relative to the plane $X = 0, Z = 0$ instead now hold respectively on the planes :

$$f_{11}(X, Z) = 0 \qquad f_{22}(X, Z) = 0 \tag{3.65}$$

whose traces on the plane $Y = 0$ are exactly the right and left branches of C . The ν-value used in each case is that relative to a sector of angular aperture σ .

The complete three-dimensional singularity vectors can be eventually fully determined for just the special cases in which they fit one or more degenerate surfaces of the more general Ellipsoidal c.s. reported in Figs. 1.3,4 .

The investigation of these geometries constitutes one of the main future aims of the work, also motivated by future applications to microwave techniques.

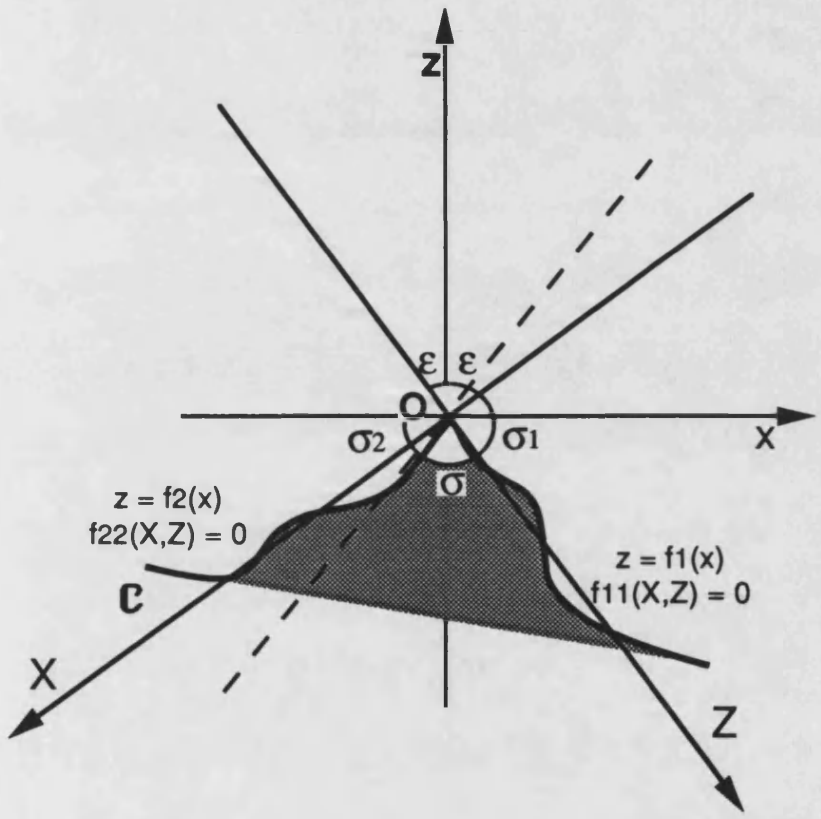

Fig. 3.14 : sector of generic boundary shape C but with a cusp in O

3.7 Uniqueness of the fundamental solution

We observed while imposing the b.c. (3.2,28) that, because of the non uniqueness of the definition of the normal $\hat{n}$ to the conductor on the edges and on the tip, the fundamental solution might not be unique .

This problem was posed first by Rayleigh at the beginning of the century and approached by several authors in different ways . Their conclusions have been satisfactorily summarized by Jones (see [24] and bibliography quoted there) . Of all this analytical effort, we will only report the outstanding physical results .

If we suppose to illuminate with an incident field $\vec{E}_0, \vec{H}_0$ a wedge conductor of arbitrary shape as that of Fig. 3.14, a current $\vec{J}$, a surface charge ρ_s and, possibly, a line of charge ρ_1 on C are induced, which generate the diffracted fields $\vec{E}_1, \vec{H}_1$. Finiteness and continuity of $\vec{J}$ and ρ_s might only fail on C while those of ρ_1 only at O .

Nevertheless, $\vec{J}, \rho_s$ and ρ_1 must always be integrable on the conductor surface S and on C respectively because the complete charge and current on the conductor must remain finite . Under these hypotheses, the application of the regular b.c. on S implies $\rho_1 = 0$, i.e. neither a line of charge is present on C nor an isolated charge is present at O . Consequently, the EM fields components tangential to C vanish there .

Under these conditions, it is possible to satisfy the physical principle that no energy is radiated by the edge, from which the uniqueness of the solution is derived.

A consequence of this result is that there is one only solution, for which $\vec{J}$ and ρ_s are singular at C with degree > -1 and the same happens of the

perpendicular components of E_1 and H_1 to C but external to the conductor .

Similar observations apply to the neighborhood of O where the components E_1 and H_1 radial to O are singular of degree > -1, but become finite on the conductor and on the two straight lines tangent to C at O and arbitrarily close to it .

From the Tables 3,4,5 of Chapters 2,3 it appears immediately how the density of current $\vec{J}$ and charge ρ_s as well as the EM fields relative to the fundamental mode satisfy all these properties .

We can thus conclude by saying that :

just the sole regular b.c. (3.2,28) pertaining to the conductor surface S are sufficient to ensure uniqueness of the fundamental solution . In spite of a singularity of $\vec{J}, \rho_s, \vec{E}_1, \vec{H}_1$ along C this ensure finiteness of charge and current on the conductor and of the diffracted EM energy .

The latter singular b.c. will be denoted as *" singular edge and vertex conditions on C "* as complementary to the *" regular boundary conditions on S ".*

3.8 General remarks

Before closing this Chapter we would like to make some other applicative and general remarks :

i) From the point of view of the applications, it is important to establish how large is the region around the tip where the effect of the spherical singularity may be considered dominant with respect to that along the edges . Analytically speaking, the effect of the tip singularity is originated by $\frac{j_\nu(\kappa r)}{\kappa r}$ and can be considered terminated where the Bessel function j_ν assumes the first maximum ; dependently on ν, this is located where $\kappa r \simeq 1$ (see [11] pg 187) .

Physically speaking, and in order to determine a distance independent of the sector aperture, i.e. of ν, we consider the effect limited to $\kappa r \ll 1$, likewise quantified as in 3.24 .

In the spherical region centered at O and within the above radius, we assume the tip singularity as significant .

ii) The singularity vectors forms reported in Tables 3,4,5 of the last two Chapters can be further simplified .

For instance, when dealing with s_{H_X} for the quarter sector we may consider the single form :

$$\sqrt{\frac{|Z|}{|X|}} r^{\nu-1} \tag{3.66}$$

This no longer represents the actual way in which zeros and singularities along the edges match those on the tip, as obtainable from the exact solution,

but still shows the right degrees of zeros and singularities along the conductor contour.

This might suffice in an application where a single form for the whole surface of integration is of help .

While this simplification is obviously applicable to all the other components and for all the other wedge geometries on the plane $Y = 0$, other forms better suited to the particular problem in question may also be produced .

iii) As a third point, we note the possibility that in particular and quite unusual situations of excitation, the above fundamental modes might not be excited, thus leaving the main behaviour on the tip to be described by a higher mode .

It could be shown in a way similar to that used by Satterwhite [10], that the fundamental mode is not excited when an elementary dipole source of current is placed and oriented respectively as (see also Figs. 3.5,8,11) :

for E-field
- on the median plane $z = 0$, orthogonally to it
- on the sector plane $y = 0$ out of the conductor, orthogonally to it
- on the sector conductor, in radial direction

for H-field
- on the median plane $z = 0$, parallel to it
- on the sector plane $y = 0$ out of the conductor, orthogonally to it
- on the sector conductor, for every direction
- everywhere for a radial direction

It is also possible to show that the next mode to be excited is of the Dirichlet

type for both the EM fields .

iv) The more rigorous analyst can also observe that the scalar wave equation admits for $\nu = h = 0$ the separate solutions :

$$R = c_0 + \frac{c_1}{r} \qquad B = d_0 + d_1\beta \qquad A = e_0 + e_1\alpha \tag{3.67}$$

However, the corresponding fields are the trivial null solution .

v) Last, we would like to note that the structure of Fig. 2.11 can be virtually substituted by the double-sector but with asymmetric excitation as it has satisfied the image principle in respect to the plane conductor itself . As observed, this excitation that may be met in applications never produces a singularity at the tip .

Chapter 4

WEDGES

IN SPHERICAL GEOMETRY

4.1 Introduction

This Chapter shows how classical results dealing with the bidimensional and cone-wedges are analyzable in the framework of a unified theory of the plane sectors and draws some general conclusions about the EM fields singularities on perfectly conducting wedges .

The Chapter can therefore be missed by those who are strictly interested in Microwave applications which are instead presented in the next Chapters .

Proceeding in accordance with the "coordinate matching procedure" presented in Chapter 1, we now analyse those perfectly conducting geometries which are fitting one or more equi-coordinate surfaces of the spherical c.s. .

Studies relative to bidimensional and conical wedges can by now be considered classic ones even though some do resort to approximate or numerical

algorithms (see [25] p. 18,[14, 17]) .

Other composite geometries originated by the similitude with the composite plane wedges studied in the Chapters 2,3 are now introduced for the first time with the main purpose to help us state general properties of the singularity of charge and current at tips of arbitrary shape .

Finally, some limit geometries directly obtained by the degeneracy $k = sin\epsilon \rightarrow 0$ of the planar sectors are analytically better characterized in spherical coordinates as already observed in the Chapters 2,3 .

Actually, there is much more to be obtained from an appropriate use of the named degeneracy process, as not only the spherical geometry, but also the differential equations, the general properties of the solutions and the solutions themselves can be obtained in this way from those pertaining to the conical geometry .

This permits a rigorous, simple and unified analysis of all the above mentioned wedges as well as of those considered in conical geometry and even more.

At this stage, the most important difference is constituted by the degeneration of the two Lamé's equations along α and β into Harmonic and Legendre equations respectively . Consequently a "tie up" between the solutions along θ and ϕ is no longer possible .

Nevertheless, these solutions can be obtained from those formulated in Chapter 1 by submitting them to a degeneracy procedure, even though some of them may behave badly by "blowing up" at $\theta = 0, \pi$ where the Legendre's equation presents its two singular points .

In this context, the most important example is represented by the two

Lamé's solutions, odd and even, of period 4π along θ relative to the acute sector. When $k^2 \to 0$ the series solutions for both cases lose convergence so that the odd one, which in $\theta = 0, \pi$ is 0, now assumes the finite values ± 1 pertaining to the Legendre associated functions $P_m^n(\pm 1)$, while the even one, which in $\theta = 0, \pi$ is finite, now diverges to the 2^{nd} kind of Legendre associated functions $Q_m^n(\pm 1)$.

It is just this "bad degeneracy" which prevents satisfaction of the physical b.c. for the EM fields associated with limit structures like the semi-infinite wire fitting the degenerate surface $\theta = 0$ for which a proper degenerate eigenfunction is $P_0^0 \equiv 1$. This problem leads us to make a distinction between this "physically unrealizable wire" and the wire with finite cross section usually met in applications and for which a possible eigenfunction may be $sin\frac{\theta}{2}$, presenting a 0 on the conductor . This, incidentally, is just the main term in the original Lamé's solution already used for acute sectors of any aperture .

This example, and a few others, justify the study of all the named wedges according to a rigorous and unified dynamic theory so as to single out explicitly or implicitly the whole spectrum of solutions from which we separate, as required, the fundamental mode or a simplified singularity vector .

The procedure aiming to the progressive characterization of the solution will follow the lines of the case of conical geometry, while the static analysis will be left for the sake of brevity .

Finally, from an application point of view, we can remember that the classical bidimensional and conical wedges are more usually met in boxed waveguide and antennas respectively, but, they also occur in the more widespread applications of low frequency and high power engineering .

4.2 Characterization of the solutions

We follow the path of progressive specialization of " the solution " already taken for the conical c.s. . The analytical formulation for this geometry is illustrated in 1.2.1, where the sole trigonometric formalism is used which, since a long time, has been recognized to be by far the most useful one in stating theoretical, computational and applicative results .

Thus, we retrace, one by one, the steps of 1.3 .

The geometrical properties of the spherical coordinate system

We can make again reference to Fig. 1.13 but the two arcs $\mathcal{C}^+, \mathcal{C}^-$ on the sphere of radius r_0 now degenerate into the two points $\mathcal{P}^+, \mathcal{P}^-$ of intersection of this sphere with the positive and negative z semi-axes, namely the degenerate cones $\theta = 0, \pi$ respectively (see Fig. 1.3) .

Any regular cone $\theta = \bar{\theta}$ intersects the sphere on a circle surrounding $\mathcal{P}^+$ if $\bar{\theta} < \frac{\pi}{2}$ or $\mathcal{P}^-$ if $\bar{\theta} > \frac{\pi}{2}$ while ϕ varies from 0 to 2π .

Conversely, the half planes $\phi = \bar{\phi}$ intersect the sphere on a half circle joining $\mathcal{P}^+$ with $\mathcal{P}^-$, while θ varies from 0 to π .

Consequently, any physically meaningful solution F in this geometry has to be 2π-periodic in ϕ, i.e. :

$$F(r, \theta, \phi) = F(r, \theta, \phi + 2\pi) \tag{4.1}$$

The smoothness properties of the solution

Further conditions must be verified on the singular points $\mathcal{P}^+, \mathcal{P}^-$, at the origin and on the sphere of infinite radius whenever they are part of the homogeneous space .

Precisely, in order to ensure smoothness in the way indicated in 1.3.2, at $\mathcal{P}^+$ and $\mathcal{P}^-$ we must have :

$$\lim_{\theta \to 0,\pi} R(r)\Theta(\theta)\Phi(\phi) \quad \text{independent on } \phi \tag{4.2}$$

while in $r = 0, \infty$ the same conditions (1.24,25) have to be satisfied .

The mathematical properties of the Helmholtz equation

In third instance, the solution must also satisfy the scalar wave equation (1.26) for the scalar potential Ψ which, in spherical c.s., separates into the ordinary differential equations directly obtainable from (2.6,1.51,1.44) by setting $k^2 = 0$, i.e. :

$$\ddot{R} + \tfrac{2}{r}\dot{R} + \left(\kappa^2 - \tfrac{\nu(\nu+1)}{r^2}\right) R = 0 \tag{4.3}$$

$$\ddot{\Theta} + \tfrac{cos\theta}{sin\theta}\dot{\Theta} + \left(\nu(\nu+1) - \tfrac{\mu^2}{sin^2\theta}\right) \Theta = 0 \tag{4.4}$$

$$\ddot{\Phi} + \mu^2 \Phi = 0 \tag{4.5}$$

(4.3) is the Bessel's equation analysed in conical c.s., (4.5) is the common Harmonic equation while (4.6) is the Legendre's equation, more commonly known,

as a function of the variable $t = cos\theta$:

$$(1-t^2)\ddot{\Theta} - 2t\dot{\Theta} + \left(\nu(\nu+1) - \frac{\mu^2}{1-t^2}\right)\Theta = 0 \tag{4.6}$$

where the derivatives are now with respect to $cos\theta$.

In summary, the general solutions along the three dimensions can be written as :

$$R(\kappa r) = \mathcal{C} j_\nu^{(1)}(\kappa r) + \mathcal{D} h_\nu^{(2)}(\kappa r) \tag{4.7}$$

$$\Theta(\theta) = \mathcal{E} P_\nu^\mu(cos\theta) + \mathcal{F} Q_\nu^\mu(cos\theta) \tag{4.8}$$

$$\Phi(\phi) = \mathcal{G} cos(\mu\phi) + \mathcal{H} sin(\mu\phi) \tag{4.9}$$

where P_ν^μ and Q_ν^μ are the Legendre functions of 1^{st} and 2^{nd} kind whose general properties are by now well known and to be found for instance in [11, 7]; $\mathcal{C}, \mathcal{D}, \mathcal{E}, \mathcal{F}, \mathcal{G}, \mathcal{H}$ are the linear combination constants .

The smoothness conditions at $r = 0, \infty$ are satisfied by (4.7) as already shown in 3.1.1 while those at $\theta = 0, \pi$ can be satisfied if
$\Theta(\pm 1) = \mathcal{E} P_\nu^\mu(\pm 1) + \mathcal{F} Q_\nu^\mu(\pm 1) = 0$ there.

Actually, at these points P_ν^μ, Q_ν^μ present, in general, a singularity so that the previous equation is written using their asymptotic expression there, as available for instance in [7] .

This way, the conditions can be reduced to the simpler relations :

$$\mathcal{E} = -\mathcal{F}\tfrac{\pi}{2} ctg(\mu\pi) \qquad \text{in } \theta = 0 \tag{4.10}$$

$$\mathcal{E} = -\mathcal{F}\tfrac{\pi}{2} ctg(\nu\pi) \qquad \text{in } \theta = \pi \tag{4.11}$$

In the more important situation where $\mu = 0, 1, 2, ...$, in order to ensure finiteness of Θ, from (4.10) follows $\mathcal{F} = 0$ and from (4.8) follows $\Theta(\theta) = P_\nu^m(cos\theta)$ which, in particular, for $m = 0$ assumes the finite value 1 at $\theta = 0$ but, then, it is also $\Phi(\phi) \equiv 1$ so to satisfy in any case the condition (4.2) .

It is interesting to note that just applying the periodicity condition (4.1) the general solution 4.9 implies :

$$\mu = m = 0, 1, 2, ... \tag{4.12}$$

4.3 The physical boundary conditions and the spectra of eigenvalues and eigenfunctions

In the present geometry the EM fields can be derived from two potential functions Ψ_1, Ψ_2 satisfying the scalar wave equation, according to the same formulation as for the conical case (see [12]) .

Furthemore, since we are going to analyse conductor geometries only fitting one or more equi-coordinate surfaces $\bar{\theta} = const, \bar{\phi} = const$, the b.c. they establish on the EM fields can be straightforwardly reduced to either the Dirichlet or the Neumann type on the eigenfunctions $\Theta(\theta), \Phi(\phi)$ in which Ψ_1, Ψ_2 are separated .

Omitting the explicit treatment of the static case, we identify from now on by the suffixes D,N the two kinds of b.c. respectively .

Moreover, we group the b.c. in two main categories : those pertaining to one or more half planes $\phi = \bar{\phi}$ and those pertaining to one or more cones $\theta = \bar{\theta}$.

We start with the bidimensional wedges (2D-wedges) delimited by planes $\bar{\phi} = const$.

In particular, we will study the half plane and the plane by considering them as limit cases of the acute and obtuse sector respectively .

This is why these two geometries represent the main meeting point between 2D and 3D-wedge analysis .

4.3.1 2D-wedges

These wedges are the easiest to be analysed because the spectrum of eigenvalues ν, μ is determinable in a complete analytical way and the Θ-eigenfunctions are the same for the Dirichlet and Neumann problems .

The half plane

If we consider the half plane conductor fitting, without loss of generality, the surface $\bar{\phi} = 0$, the spectrum of eigenvalues established there by the Dirichlet $\Phi(0) = 0$ b.c. can be obtained, apart from an unessential rotation of axes, from the limit cases $k^2 \rightarrow 1$ of the acute sector . In this way, from the same Fig. 2.3 we can recover the eigenvalues spectrum like :

$$\begin{aligned} &\mu = m - \tfrac{1}{2} && \text{with } m = 1,2,3... \\ &\nu = \mu, \mu+1, \mu+2, ... = \tfrac{n}{2} && \text{with } n = 1,2,3... \end{aligned} \tag{4.13}$$

For this special case, the Neumann b.c. establish in fact exactly the same spectrum since the complementary conductor is the half plane itself . Consequently, for both situations on the conductor wedges $\bar{\theta} = 0, \pi$ (4.10,11) imply $\mathcal{E} = 0$, i.e. :

$$\Theta_{D,N}(\theta) = Q^{\frac{m}{2}}_{\frac{n}{2}}(cos\theta) \tag{4.14}$$

It is perhaps appropriate to note how the above are the only Legendre functions of 2^{nd} kind to be everywhere finite .

The eigenfunctions along ϕ satisfying the two kinds of b.c. are instead

respectively :

$$\Phi_D(\phi) = sin(\frac{m}{2}\phi) \qquad \Phi_N(\phi) = cos(\frac{m}{2}\phi) \tag{4.15}$$

The plane

The situation of a complete plane conductor, without loss of generality fitting the surfaces $\bar{\phi} = 0, \pi$, can be seen as the limit case $k^2 \to 0$ of the double sector . From the same Fig. 2.4 the eigenvalue spectrum can be recovered as :

$$\begin{aligned} &\mu = m && \text{with } m = 1, 2, 3, ... \\ &\nu = \mu, \mu + 1, \mu + 2, ... = n && \text{with } m = 1, 2, 3, ... \end{aligned} \tag{4.16}$$

Consequently, with the same considerations as for the half plane, the eigenfunctions spectrum is given by :

$$\Theta_{D,N}(\theta) = P_n^m(cos\theta) \tag{4.17}$$

$$\Phi_D(\phi) = sin(m\phi) \qquad \Phi_N(\phi) = cos(m\phi) \tag{4.18}$$

We remark that this is the only case where the Legendre functions of 1^{st} kind are polynomials finite everywhere .

The 2D-sector (Fig. 4.1)

The generalization of the two previous cases is represented by a conductor delimited by an arbitrary plane $\phi = \bar{\phi} = \in (0, 2\pi)$ and, without loss of generality $\bar{\phi} = 0$ (see Fig. 4.1) . Satisfaction there of the Newmann and Dirichlet b.c. imply from (4.9,10,11) :

$$\mu = \frac{\pi}{2\pi - \bar{\phi}} m \qquad \text{with } m = 1, 2, 3...$$
$$\nu = \mu, \mu + 1, \mu + 2, ... \tag{4.19}$$

For these eigenvalues, the eigenfunction spectrum (4.8,9) reduces to :

$$\Theta_{D,N}(\theta) = P^{\mu}_{\nu}(cos\theta) - \tfrac{2}{\pi} tg(\mu\pi) Q^{\mu}_{\nu}(cos\theta) \tag{4.20}$$

$$\Phi_D(\phi) = sin(\mu(2\pi - \phi)) \qquad \Phi_N(\phi) = cos(\mu(2\pi - \phi)) \tag{4.21}$$

where the values of the constants $\mathcal{E}, \mathcal{F}$ in (4.20) are such that (4.10,11) are satified keeping $\Theta_{D,N}(\theta)$ everywhere finite .

The 2D-sector on a plane conductor (Fig. 4.2)

This is a useful conductor configuration, especially in its particular cases of infinite and semiinfinite plane conductors as met in boxed waveguides .

The cutting plane is likely to fit just the equi-coordinate $\bar{\theta} = \frac{\pi}{2}$, where P_ν^μ, Q_ν^μ and their first derivatives assume an easy expression (see [7] p. 145) so that the new conditions $\Theta(\frac{\pi}{2}) = 0$ or $\dot{\Theta}(\frac{\pi}{2}) = 0$ mean respectively :

$$\mathcal{E} = -\mathcal{F}\tfrac{\pi}{2} ctg\left((\nu + \mu + 1)\tfrac{\pi}{2}\right) \tag{4.22}$$

$$\mathcal{E} = -\mathcal{F}\tfrac{\pi}{2} ctg\left((\nu + \mu)\tfrac{\pi}{2}\right) \tag{4.23}$$

Naturally, the μ-spectrum is given by (4.19) itself, since no further b.c. are introduced on $\bar{\phi}$-surfaces while the ν-spectrum is a selection of (4.19) so as to satisfy also (4.10), i.e. :

$$\nu_D = \mu + 2n + 1 \tag{4.24}$$

$$\nu_N = \mu + 2n \qquad \text{with } n = 0, 1, 2, ... \tag{4.25}$$

As a consequence, the eigenfunctions Θ, Φ are selections of (4.20,21) according to the ν-values (4.24,25) .

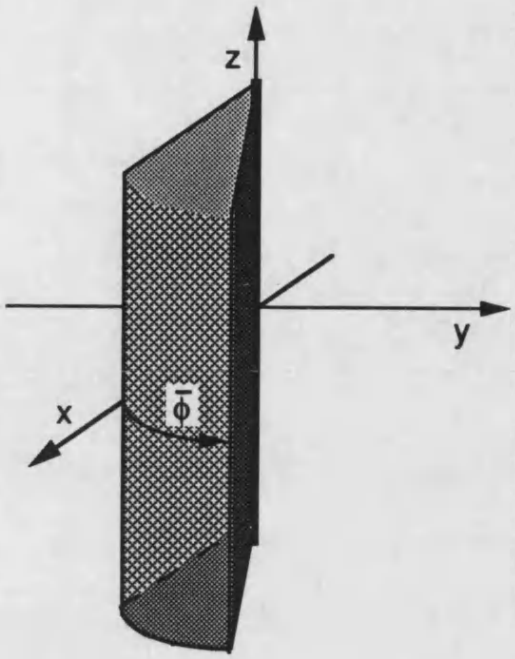

Fig. 4.1 : bidimensional sector

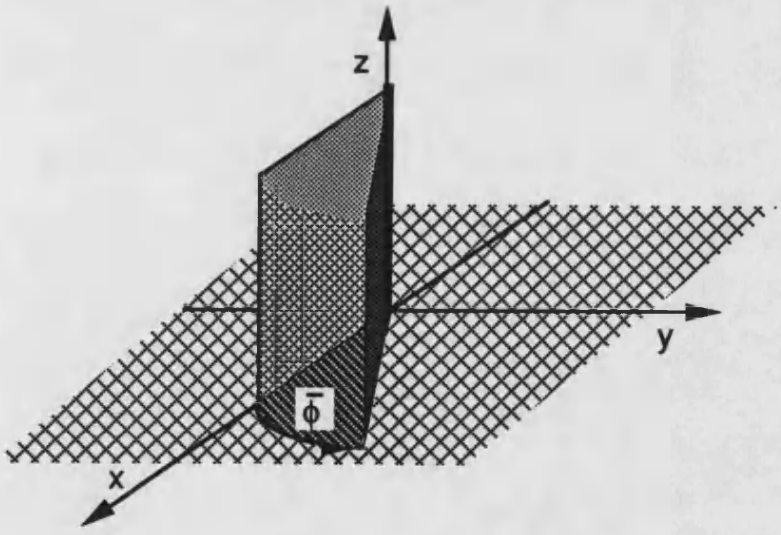

Fig. 4.2 : half bidimensional sector

4.3.2 Cone wedges

When no conductor is present on a plane $\phi = \bar{\phi}$, the periodic condition (4.1) implies the μ and ϕ-spectra to be given respectively by :

$$\mu = m = 0, 1, 2, ... \quad \Phi(\phi) = \mathcal{G}cos(m\phi) + \mathcal{H}sin(m\phi) \tag{4.26}$$

The spectra for ν and Θ are now completely independent of the latter and, case for case, can be determined as follows .

The cone (Fig. 4.3)

The cone $\theta = \bar{\theta}$ divides the whole space into region 1 containing the positive semi-axis (that is the degenerate cone $\theta = 0$) and region 2 containing the negative semi-axis (that is the degenerate cone $\theta = \pi$) as indicated in Fig. 4.3 .

Thus, if the free space is region 1, taking into account (4.10) and the μ-values (4.26), the Dirichlet b.c. $\Theta(\bar{\theta}) = 0$ implies that the ν-spectrum is represented by the zeros of just the 1^{st} kind of the Legendre's functions . We express this by writing :

$$\nu_D : P^m_{\nu_D}(cos\bar{\theta}) = 0 \qquad \text{for } m = 0, 1, 2, ... \tag{4.27}$$

so that the related eigenfunctions are :

$$\Theta(\theta) = P^m_{\nu_D}(cos\theta) \tag{4.28}$$

Instead, in region 2 from (4.11) and the μ-values (4.26), the same Dirichlet b.c. are satisfied when (see (14) p. 144 [7]) :

$$\Theta(\bar{\theta}) = P^\mu_\nu(cos\bar{\theta}) - \frac{2}{\pi} tg(\nu\pi) Q^\mu_\nu(cos\bar{\theta}) = \frac{P^m_\nu(-cos\bar{\theta})}{cos(\nu + m)\pi} = 0 \tag{4.29}$$

So that, as physically obvious, in region 2 the ν and Θ-spectra , within a multiplicative constant are, given by :

$$\nu_D : P^m_{\nu_D}(cos(\pi - \bar{\theta})) = 0 \qquad \text{for } m = 0, 1, 2, ... \tag{4.30}$$

$$\Theta(\theta) = P^m_{\nu_D}(cos(\pi - \theta)) \tag{4.31}$$

For what concerns the Neumann problem in the two regions, the eigenfunctions Θ assumes the same form since the conditions (4.10,11) are still valid while the ν-spectra are now generated by :

$$\text{in region 1} \qquad \nu_N : \dot{P}^m_{\nu_N}(cos\bar{\theta}) = 0 \qquad \text{for } m = 0,1,2... \quad (4.32)$$

$$\text{in region 2} \qquad \nu_N : \dot{P}^m_{\nu_N}(cos(\pi - \bar{\theta})) = 0 \qquad \text{for } m = 0,1,2... \quad (4.33)$$

If a plane conductor is placed at $\bar{\phi} = 0, \pi$ (see Fig. 4.4) the equations for the ν and Θ-spectra remain valid, but the value $\mu = 0$ must be excluded, obtainig finally the spectra :

$$\mu = m = 1,2,3,... \quad (4.34)$$

$$\Phi_D(\phi) = sin(m\phi) \qquad \Phi_N(\phi) = cos(m\phi) \quad (4.35)$$

Analogous considerations can be done for the double cone and related geometries as reported in Appendix F .

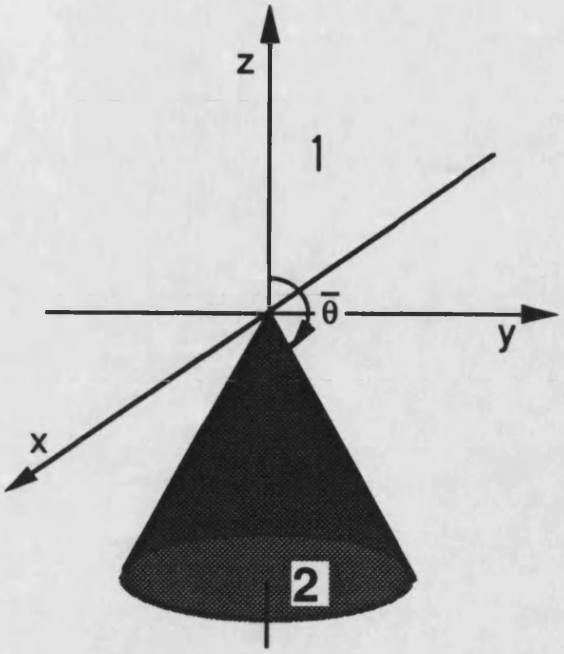

Fig. 4.3 : cone

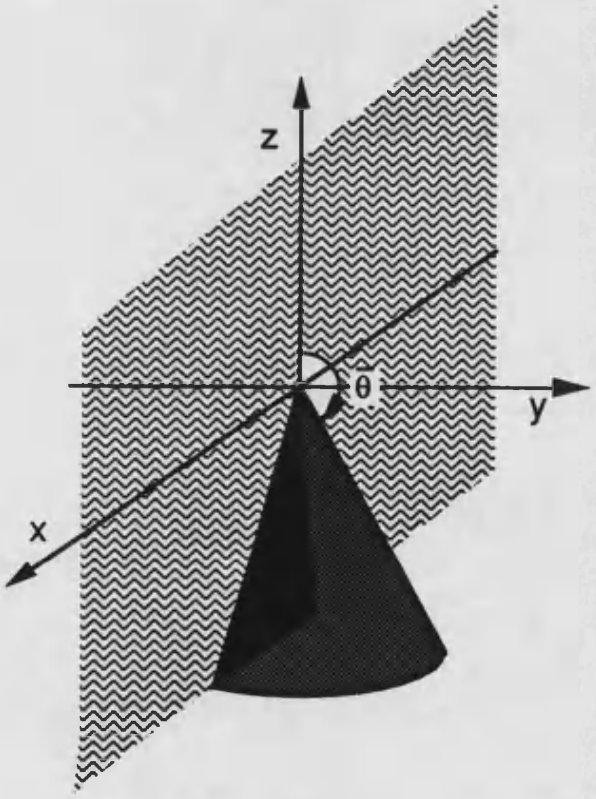

Fig. 4.4 : half cone

4.4 EM fields in spherical coordinate system

Moving along the lines of the procedure presented for the conical geometry, the complete modal spectra for the EM fields relative to a given conductor can be now derived from the spectra of the two scalar potentials Ψ_1, Ψ_2 obtainable from the eigenvalues ν, μ and eigenfunctions $\Theta_\nu^\mu, \Phi_\nu^\mu$ just presented in the previous section.

The explicit EM field expressions can be obtained directly from (3.39,40) passing to the limit $k^2 \to 0$ in the functions P,T,S :

$$\text{E-mode} \begin{cases} \vec{N} = \frac{1}{\kappa r}\left[\nu(\nu+1)R_D\Theta_D\Phi_D\hat{r} + (r\dot{R}_D)\dot{\Theta}_D\Phi_D\hat{\theta} + \frac{1}{\sin\theta}(r\dot{R}_D)\Theta_D\dot{\Phi}_D\hat{\phi}\right] \\ \vec{H}_N = \frac{i}{\eta}\left[\frac{1}{\sin\theta}R_D\Theta_D\dot{\Phi}_D\hat{\theta} - R_D\dot{\Theta}_D\Phi_D\hat{\phi}\right] \end{cases} \tag{4.36}$$

$$\text{H-mode} \begin{cases} \vec{M} = \frac{1}{\sin\theta}R_N\Theta_N\dot{\Phi}_N\hat{\theta} - R_N\dot{\Theta}_N\Phi_N\hat{\phi} \\ \vec{H}_M = \frac{i}{\eta}\frac{1}{\kappa r}\left[\nu(\nu+1)R_N\Theta_N\Phi_N\hat{r} + (r\dot{R}_N)\dot{\Theta}_N\Phi_N\hat{\theta} + \frac{1}{\sin\theta}(r\dot{R}_N)\Theta_N\dot{\Phi}_N\hat{\phi}\right] \end{cases} \tag{4.37}$$

These forms present naturally the same behaviour for $r \to 0, \infty$ and the same distinction in E and H-modes with respect to the radial direction as in the conical geometry (see 3.4) .

We now have at hand all the formulation necessary to identify the fundamental mode as well as the main and the, sometimes, singular behaviour of the EM fields by the tip . Its simplified expression, e.g. a singularity vector representation, will be expressed in the more convenient rectangular coordinates according to the application of the conductor geometry .

4.4.1 Fundamental mode and singularity vectors for 2D-wedges

Considering firstly 2D-wedges as shown in Fig. 4.1 the minimum eigenvalues are:

$$\nu = \mu = \frac{\pi}{2\pi - \bar{\phi}} \tag{4.38}$$

which are ≤ 1 only for $\bar{\phi} \in [0, \pi]$. The correspondent Θ-eigenfunction can be written, using the 3.4(17),3.6.1(15) in [7], as :

$$\Theta_{D,N}(\theta) = P_\nu^\nu(cos\theta) - \frac{2}{\pi} tg(\nu\pi) Q_\nu^\nu(cos\theta) = \frac{2^{-\nu}\Gamma(2\nu+1)}{\Gamma(\nu+1)}(sin\theta)^\nu \tag{4.39}$$

so that, leaving aside an unessential multiplicative constant, the fundamental eigenfunctions satisfying Neumann and Dirichlet b.c. are respectively :

$$\Theta_{D,N}(\theta) = (sin\theta)^\nu \tag{4.40}$$

$$\Phi_D(\phi) = sin(\nu(2\pi - \phi)) \qquad \Phi_N(\phi) = cos(\nu(2\pi - \phi)) \tag{4.41}$$

The main behaviour by the conductor tip can then be recovered by passing to the limit $\kappa r \to 0$ and simplifying in consequence the R-function, as done in (3.22) .

The simplified expression for the fields is then :

$$\vec{N} \propto (\kappa r sin\theta)^{\nu-1}$$
$$\cdot \left[\nu sin\theta sin(\nu(2\pi-\phi))\hat{r} + cos\theta sin(\nu(2\pi-\phi))\hat{\theta} + \nu cos(\nu(2\pi-\phi))\hat{\phi}\right] \quad (4.42)$$
$$\vec{H_M} \propto (\kappa r sin\theta)^{\nu-1}$$
$$\cdot \left[\nu sin\theta cos(\nu(2\pi-\phi))\hat{r} + cos\theta cos(\nu(2\pi-\phi))\hat{\theta} - \nu sin(\nu(2\pi-\phi))\hat{\phi}\right] \quad (4.43)$$

These expressions can be considered as the singularity vectors $\vec{s_E}, \vec{s_H}$ for 2D-wedges .

Remarkably, the possible singularity is controlled by just the term :

$$(r sin\theta)^{\nu-1} = (x^2+y^2)^{\frac{\nu-1}{2}} \quad (4.44)$$

which expresses the fact that :

the cylindrical singularity, if $\nu - 1 < 0$, or zero, if $\nu - 1 > 0$, is uniformly distribuited along the conducting edge which fits the z axis .

The degree of singularity is nowaday generally indicated by :

$$\tau = \frac{\pi}{2\pi - \phi} - 1 \quad (4.45)$$

We note now that, conversely to what happens for 3D-wedges and for the great part of wedges, τ is the same for both the E and H fields .

The complete expression of (4.42,43) in rectangular coordinates is simply obtained by using the inversion formulae :

$$sin\theta = \frac{\Delta}{r} \qquad sin\phi = \frac{y}{\Delta} \qquad sin\frac{\phi}{2} = \frac{1}{\sqrt{2}}\sqrt{1-\frac{x}{\Delta}} \tag{4.46}$$

$$cos\theta = \frac{r}{\Delta} \qquad cos\phi = \frac{x}{\Delta} \qquad cos\frac{\phi}{2} = \pm\frac{1}{\sqrt{2}}\sqrt{1+\frac{x}{\Delta}} \tag{4.47}$$

where we use the signs $\pm$ according to $y \gtrless 0$ respectively while $\Delta = |\sqrt{x^2+y^2}|$.

For their applicative importance, we limit the attention to the half plane ($\nu = \mu = \frac{1}{2}$) and the plane ($\nu = \mu = 1$) conductor, whose minimum eigenfunctions are respectively given by :

$$\Theta_{D,N}(\theta) = \sqrt{sin\theta} \qquad \Phi_D(\phi) = sin(\frac{\phi}{2}) \qquad \Phi_N(\phi) = cos(\frac{\phi}{2}) \tag{4.48}$$

$$\Theta_{D,N}(\theta) = \quad sin\theta \qquad \Phi_D(\phi) = sin(\phi) \qquad \Phi_N(\phi) = cos(\phi) \tag{4.49}$$

The plane conductor introduces the well known zero of degree 1 in the tangential E-field and in the normal H-field . The half plane instead introduce a singularity of degree $-\frac{1}{2}$ in the E and H components normal to the edge and a zero of the same degree on those tangential to it, as known since Sommerfeld's studies .

Quite interesting is also the 2D-wedge cut by the plane conductor $\bar{\theta} = \frac{\pi}{2}$ of Fig. 4.2 because of its occurence in boxed resonators, short circuits or discontinuities in waveguides . Nevertheless, the literature does not treat this case probably because the fields are never singular on the tip .

If, in fact, we look at the (4.24,25), we see that in the origin the fields

present a zero of degree :

$$\tau = \frac{\pi}{2\pi - \bar{\phi}} = \nu - 1 = \mu \tag{4.50}$$

so that the minimum eigenfunction is (see 3.4(17) in [7]) :

$$\Theta_D(\theta) = P_\nu^{\nu-1}(cos\theta) - \frac{2}{\pi} tg((\nu-1)\pi) Q_\nu^{\nu-1}(cos\theta) = \frac{\Gamma(2\nu)}{2cos((1-\nu)\pi)} P_\nu^{1-\nu}(cos\theta) \tag{4.51}$$

while those along Φ remain of the forms (4.41) .

Surprisingly, (4.43) already satisfies the b.c. $H_\theta(\frac{\pi}{2}) = 0$, so this is also a solution for the actual geometry .

This shows that :

the degree of singularity for H remains as in (4.45), that is negative for $\bar{\phi} \in [0, \pi]$, *the only difference being a physical one and consisting in the flow of current from the top half wedge to the plane conductor instead of the lower half one .*

With a view to application, we give an explicit formulation of the main E-field only for the half plane cut by a plane conductor, for which the minimum eigenvalues are $\mu = \nu_D - 1 = \frac{1}{2}$ while the associated eigenfunctions and field expressions are :

$$\Theta_D = cos\theta\sqrt{sin\theta} \qquad \Phi_D(\phi) = sin(\tfrac{3}{2}\phi) \tag{4.52}$$

$$\vec{N} \propto (\tfrac{\kappa r}{sin\theta})^{\frac{1}{2}} \left[3sin\theta cos\theta sin(\tfrac{3}{2}\phi)\hat{r} + (1 - 3sin^2\theta) sin(\tfrac{3}{2}\phi)\hat{\theta} + 3cos\theta cos(\tfrac{3}{2}\phi)\hat{\phi}\right] \tag{4.53}$$

This last singularity vector, together with (4.43) relative to the H-field, can

be explicited, using the (D.16,17,18) for $k^2 = 0$, in terms of the main rectangular coordinates X, Y, Z oriented as in Fig. 4.5 . The projections on the three main planes assume the simpler forms reported in Table 4.1 and they are proportional to the charge and current on the conductor according to the conventions used in 2.4.1,3.2 respectively .

EM fields singularity vectors for a half plane cut by a plane						
s_{E_X}	s_{H_X}	s_{E_Y}	s_{H_Y}	s_{E_Z}	s_{H_Z}	Sector
on the plane $Y = 0$						
0	$\frac{X\sqrt{\lvert Z\rvert}}{r^2}$	$\frac{X}{\sqrt{\lvert Z\rvert}}$	0	0	$\frac{1}{\sqrt{\lvert Z\rvert}}$	$\phi = 0$
$\sqrt{\lvert Z\rvert}$	0	0	$\frac{1}{\sqrt{\lvert Z\rvert}}$	$\frac{X}{\sqrt{\lvert Z\rvert}}$	0	$\phi = \pi$
on the plane $X = 0$						
$\sqrt{r+Z}$	0	0	$\frac{1}{\sqrt{r}}$	0	$\frac{1}{\sqrt{r}}$	$\theta = \frac{\pi}{2}$
on the plane $Z = 0$						
$\sqrt{\lvert Y\rvert}$	$\frac{X\sqrt{\lvert Y\rvert}}{r^2}$	$\frac{X}{\sqrt{\lvert Y\rvert}}$	$\frac{1}{\sqrt{\lvert Y\rvert}}$	$\frac{X}{\sqrt{\lvert Y\rvert}}$	$\frac{1}{\sqrt{\lvert Y\rvert}}$	$\phi = \frac{\pi}{2}, \frac{3\pi}{2}$

Table 4.1: EM fields singularity vectors projections on the main planes for the conductor and geometry of Fig. 4.5 .

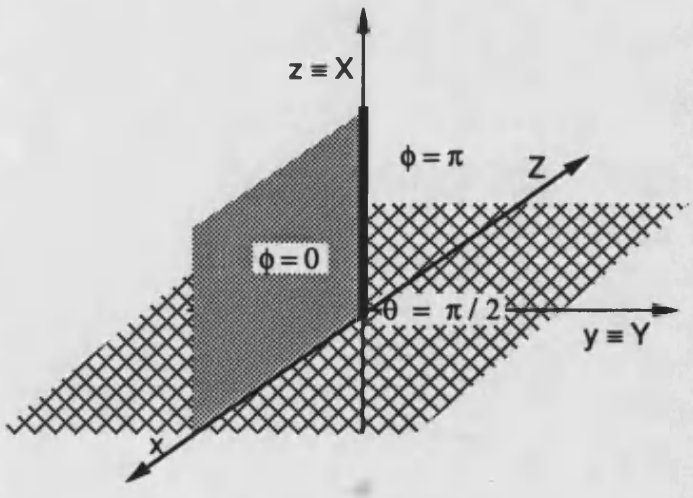

Fig. 4.5 : half plane on a plane conductor

4.4.2 Fundamental mode and singularity vectors for Cone-wedges

From the point of view of determining the spectra of eigenvalues and eigenfunctions, Cone-wedges are located between 2D and 3D-wedges . In fact, while for the former the eigenvalues are determined analytically and for the latter both numerically, for the Cone-wedge, μ is already determined analytically but $\nu_{D,N}$ has to be computed as one of the zeros or zero derivatives of the Legendre's functions.

The accuracy with which the spectrum can be determined is then controlled by the accuracy of this zero-finding procedure so that, from the experience in using conical c.s., we use Hypergeometric series espressions for $Q^{\mu}_{\nu}, P^{\mu}_{\nu}$
(see [7] p. 144) :

$$Q^{\mu}_{\nu}(cos\theta) = -\frac{\pi}{4}V^{\mu}(\theta)\left[tg((\nu+\mu)\frac{\pi}{2})T^{\mu}_{\nu}(cos^2\theta) - ctg((\nu+\mu)\frac{\pi}{2})2cos\theta U^{\mu}_{\nu}(cos^2\theta)\right]$$
$$P^{\mu}_{\nu}(cos\theta) = V^{\mu}(\theta)\left[T^{\mu}_{\nu}(cos^2\theta) - 2cos\theta U^{\mu}_{\nu}(cos^2\theta)\right] \qquad (4.54)$$

where $V^{\mu}(\theta) = \sqrt{\pi}(\frac{2}{sin\theta})^{\mu}$ while :

$$T^{\mu}_{\nu}(cos^2\theta) = \frac{F(\frac{-\nu-\mu}{2},\frac{\nu-\mu+1}{2};\frac{1}{2};cos^2\theta)}{\Gamma(\frac{1-\nu-\mu}{2})\Gamma(1+\frac{\nu-\mu}{2})}, \quad U^{\mu}_{\nu}(cos^2\theta) = \frac{F(\frac{1-\nu-\mu}{2},1+\frac{\nu-\mu}{2};\frac{3}{2};cos^2\theta)}{\Gamma(\frac{1+\nu-\mu}{2})\Gamma(\frac{-\nu-\mu}{2})} \qquad (4.55)$$

are related to the hypergeometric function F and expressible in power series of $cos^2\theta$ (see [7] p. 144) whose coefficients obey a two-terms recursive relation . The dependence on $cos^2\theta$ ensures rapid convergence which is of vital importance when we require high accuracy in the evaluation of the ν-value for a given μ .

By the way of example, when we require an accuracy of, say, 7 decimal figures, the maximum index of the series goes from a few tens when $\theta \simeq \frac{\pi}{2}$ to almost one thousand when $\theta \simeq 0, \pi$.

Among other things, the literature reports various approximate analytical expressions for the zeros of our interest around the integer values of ν, μ since then the series degenerates into terminating polynomials . This permits the use of perturbative techniques for determining approximate series expansions .

Instead, if we look for an easy-to-apply expression for the Legendre functions, we need the Fourier representation :

$$P_\nu^\mu = \sum_{i=0}^{\infty} O_i(\theta;\nu,\mu) sin((\nu+\mu+2i+1)\theta) \tag{4.56}$$

$$Q_\nu^\mu = \frac{\pi}{2} \sum_{i=0}^{\infty} O_i(\theta;\nu,\mu) cos((\nu+\mu+2i+1)\theta) \tag{4.57}$$

where :

$$O_i(\theta;\nu,\mu) = \frac{2}{\sqrt{\pi}} (2sin\theta)^\mu \frac{\Gamma(\nu+\mu+1)}{\Gamma(\nu+\frac{3}{2})} \frac{(\mu+\frac{1}{2})_i (\nu+\mu+1)_i}{i!(\nu+\frac{3}{2})_i} \tag{4.58}$$

The latter also produces a two-terms recursive relation for the coefficients in the series .

The last remark deals with the determination of a simple function which represents just the correct b.c. on the conductor, so as required in a singularity vector for the fields .

This time, things go differently than for the 2D case where the Legendre

functions involved degenerated advantageously into powers of Trigonometric functions, and than for the 3D case where all the terms of the Fourier series for the Lamé' periodic functions present the same behaviour on the conductor, so that the first term is representative of the whole function there . Now, the zeros of P, Q and of their derivatives occur for arbitrary values of $\bar{\theta}$ so that, in general, just the term of fundamental period does not represent correctly the zero on the conductor . For the sake of simplicity, we leave indicated the exact eigenfunction $\Theta(\theta)$ leaving to the user interested in a simplified expression of the EM field the choice of its most appropriate approximations in the specific context .

Thus, let us discuss the main EM field behaviour for Cone-wedges .

The cone (Fig. 4.3)

Thanks to (4.29), only the space region 1 in Fig. 4.3 need to be considered . From (4.26,29) it follows that the fundamental eigenvalue and eigenfunction for the Dirichlet problem are respectively :

$$\mu = 0 \qquad \nu_D(\bar{\theta}) : P_{\nu_D}(cos\bar{\theta}) = 0 \qquad \text{for } \bar{\theta} \in [0, \pi] \tag{4.59}$$

$$\Theta_D = P_{\nu_D}(cos\theta) \qquad \Phi_D(\phi) = 1 \tag{4.60}$$

In fact, from the properties of P_ν follows that ν_D is its smallest zero and the one which tends to 0 as $\bar{\theta} \to \pi$, that is the case of the half wire, which tends to 1 as $\bar{\theta} \to \frac{\pi}{2}$, that is the case of the plane, and which goes to ∞ as $\bar{\theta} \to 0$, that is the space filled by a conductor .

The numerical values of τ_e accurate up to 7 decimal figures versus $\bar{\theta}$ in steps

of 5^o, are collected in Table 4.2 .

A useful asymptotic formula is available around the limit $\bar{\theta} \to \pi, \nu_D = 0$ which, if θ is expressed in radiants, yields (see [16]) :

$$\tau_e \simeq \frac{1}{2ln(\frac{2}{\pi-\theta})} - 1 \qquad \text{around } \theta = \pi \tag{4.61}$$

This formula can be interestingly compared with (3.37), relative to the sector wedge approaching the same wire .

Moreover, the analogous quantities for the Neumann problem are (see 3.8(19) in [7]) :

$$\mu = 1 \qquad \nu_N(\bar{\theta}) : \dot{P}^1_{\nu_N}(cos\bar{\theta}) = \tag{4.62}$$

$$= \frac{1}{sin^2\theta}[cos\bar{\theta}P^1_{\nu_N}(cos\bar{\theta}) + \nu_N(\nu_N+1)sin(\bar{\theta})P_{\nu_D}(cos\bar{\theta})] = 0 \quad \text{for } \bar{\theta} \in [0,\pi] \tag{4.63}$$

$$\Theta_N(\theta) = P^1_{\nu_N}(cos\theta) \qquad \Phi_N(\phi) = cos\phi \tag{4.64}$$

Without loss of generality and for simplicity, from now on we consider the orientation of the axes such that the Φ-eigenfunction with $\mu = m = 1$ (see (4.9)) equals $sin\phi$ for the Dirichlet and $cos\phi$ for the Neumann case . The ν_N in question is the smallest positive zero of $\dot{P}^1_\nu$ and precisely the one which approaches unity as $\bar{\theta} \to \pi$, that is the case of the semi-indefinite wire, to decrease down to $\simeq 0.85$ when $\bar{\theta} \simeq 130^0$, which again approaches unity as $\bar{\theta} \to \frac{\pi}{2}$, that is, the case of the plane conductor, and which diverges as $\bar{\theta} \to 0$, that is the space filled by a conductor .

The evident loss of monotony of the curve $\nu_N(\bar{\theta})$ can be physically so ex-

complete oscillation along any circumference of revolution on the cone surface, that is to say the current flows down from one half cone surface, converging on the acute tip, where it becomes singular, returning on the opposite half surface of the cone (see also Fig. 4.14) . Nevertheless, when the cone degenerates into a wire, the infinitely thin conductor does not permit fluxes in opposite directions at the same points . On the other hand, for the plane conductor there is no longer a tip for the current to converge into, corresponding again to unit value of the ν_N-curve .

The explicit accurate computation of this behaviour is left as further work . However, it has been determined in [14, 17] by mens of a different, more numerical oriented approach .

Finally, the main behaviour of the EM fields by the cone tip can be approximated as :

$$\vec{N} \propto (\kappa r)^{\nu_D - 1}[\nu_D P_{\nu_D}(cos\theta)\hat{r} + P^1_{\nu_D}(cos\theta)\hat{\theta}] \tag{4.65}$$

$$\vec{H}_M \propto \frac{j}{\eta}(\kappa r)^{\nu_N - 1}[\nu_N P^1_{\nu_N}(cos\theta)cos\phi\hat{r} + \dot{P}^1_{\nu_N}(cos\theta)cos\phi\hat{\theta} - P^1_{\nu_N}(cos\theta)sin\phi\hat{\phi}] \tag{4.66}$$

The half cone (Fig. 4.4)

By the arguments relative to the previous case and using the spectra determined in the previous paragraph, it is possible to state that the fundamental eigenvalues and eigenfunctions for the Dirichlet and Neumann problem are now :

$$\mu = 1 \qquad \nu_D(\bar{\theta}) : P^1_{\nu_D}(cos\bar{\theta}) = 0 \quad \text{for } \bar{\theta} \in [0, \pi] \tag{4.67}$$

$$\Theta_D(\theta) = P^1_{\nu_D}(cos\theta) \qquad \Phi_D(\phi) = sin\phi \tag{4.68}$$

$$\mu = 1 \qquad \nu_N(\bar{\theta}) : \dot{P}^1_{\nu_N}(cos\bar{\theta}) = 0 \quad \text{for } \bar{\theta} \in [0, \pi] \tag{4.69}$$

$$\Theta_N(\theta) = P^1_{\nu_N}(cos\theta) \qquad \Phi_N(\phi) = cos\phi \tag{4.70}$$

so that the main behaviour of the fields by the tip is :

$$\vec{N} \propto (\kappa r)^{\nu_D - 1} \left[\nu_D P^1_{\nu_D}(cos\theta) sin\phi \hat{r} + \dot{P}^1_{\nu_D}(cos\theta) sin\phi \hat{\theta}] + \tfrac{1}{\sin\theta} P^1_{\nu_D}(cos\theta) cos\phi \hat{\phi} \right] \tag{4.71}$$

$$\vec{H}_M \propto \tfrac{j}{\eta} (\kappa r)^{\nu_N - 1} \left[\nu_N P^1_{\nu_N}(cos\theta) cos\phi \hat{r} + \dot{P}^1_{\nu_N}(cos\theta) cos\phi \hat{\theta} - P^1_{\nu_N}(cos\theta) sin\phi \hat{\phi} \right] \tag{4.72}$$

Since $\tau_e \geq 0$ (see Table 4.2), the E-field is never singular, while τ_h is exactly that of the cone because the current distribution on the cone surface is unaltered, the only difference being a back-flux on the plane conductor on the location of the missing half cone surface .

The electric singularity relative to the double cone and related geometries are treated in Appendix F and the values obtained are collected in Table 4.2 .

In the same Appendix we outline the procedure to identify the magnetic singularity . As a whole, these result are summarized in [43] .

CONE-WEDGES Degree of electric singularity τ_e							
θ°	Fig. 4.3	Fig. 4.4	θ°	Fig. F.3	Fig. F.4	Fig. F.1	Fig. F.2
-	-	-	0.00	0.0000000	1.0000000	-1.0000000	0.0000000
40.00	1.9322760	4.0120050	2.50	0.3435246	1.0056380	-0.2781341	0.5035213
45.00	1.5478992	3.4053292	5.00	0.4444840	1.0220296	-0.2378589	0.5136593
50.00	1.2400370	2.9207043	7.50	0.5340253	1.0482850	-0.2071357	0.5294822
55.00	0.9878077	2.5248790	10.00	0.6206242	1.0836456	-0.1810110	0.5499078
60.00	0.7772883	2.1956912	12.50	0.7075521	1.1275821	-0.1576552	0.5738756
65.00	0.5988374	1.9178032	15.00	0.7966360	1.1797961	-0.1361582	0.6004249
70.00	0.4455662	1.6802657	17.50	0.8891581	1.2401994	-0.1159804	0.6287209
75.00	0.3124203	1.4750556	20.00	0.9861767	1.3088946	-0.0967612	0.6580578
80.00	0.1956063	1.2961622	22.50	1.0886723	1.3861618	-0.0782365	0.6878540
85.00	0.0922201	1.1389971	25.00	1.1976296	1.4724542	-0.0601974	0.7176482
90.00	0.0000000	1.0000000	27.50	1.3140930	1.5684030	-0.0424675	0.7470943
95.00	-0.0828438	0.8763697	30.00	1.4392119	1.6748298	-0.0248880	0.7759557
100.00	-0.1577473	0.7658762	32.50	1.5742858	1.7927696	-0.0073078	0.8040962
105.00	-0.2258785	0.6667270	35.00	1.7208126	1.9235041	0.0104240	0.8314683
110.00	-0.2881988	0.5774703	37.50	1.8805464	2.0686081	0.0284664	0.8581004
115.00	-0.3455104	0.4969239	40.00	2.0555687	2.2300135	0.0469934	0.8840839
120.00	-0.3984907	0.4241233	42.50	2.2483804	2.4100946	0.0662042	0.9095631
125.00	-0.4477207	0.3582830	45.00	2.4620226	2.6117846	0.0863348	0.9347276
130.00	-0.4937070	0.2987687	47.50	2.7002385	2.8387344	0.1076761	0.9598112
135.00	-0.5369014	0.2450771	50.00	2.9676964	3.0955318	0.1305997	0.9850952
140.00	-0.5777187	0.1968230	52.50	3.2702992	3.3880097	0.1555999	1.0109200
145.00	-0.6165558	0.1537332	55.00	3.6156277	3.7236879	0.1833649	1.0377074
150.00	-0.6538161	0.1156457	57.50	4.0135879	4.1124176	0.2149097	1.0659992
155.00	-0.6899452	0.0825161	60.00	4.4773804	4.5673511	0.2518492	1.0965250
160.00	-0.7254978	0.0544315	62.50	5.0249993	5.1064393	0.2970661	1.1303263
165.00	-0.7612835	0.0316313	65.00	5.6816305	5.7548288	0.3568468	1.1690026
170.00	-0.7987796	0.0145328	67.50	6.4836476	6.5488576	0.4537021	1.2152717
175.00	-0.8418562	0.0037440	70.00	7.4856050	7.5430475	-	1.2745362
180.00	-1.0000000	0.0000000	-	-	-	-	-

Table 4.2: degree of electric singularity versus the angular aperture θ for the cone, half cone, double cone, half double cone, cone on a plane conductor and half cone on a plane conductor respectively indicated by their Fig. number .

4.4.3 The terminating wire and the wire crossing a plane conductor

In microwave techniques one occasionally meets a conductor represented by a segment of wire, sometimes crossing a plane conductor, used as reflecting (fence guide) or radiating (wire antenna) element (see Fig. 4.6) .

One may suppose that the analysis of the main behaviour of the EM fields diffracted by these geometries may possibly be approached by studing the limit case of a cone with $\bar{\theta} \rightarrow 0$, for the region by the tip of the wire, and of a cone with $\bar{\theta} \rightarrow 0$ on the plane conductor $\bar{\theta} = \frac{\pi}{2}$.

It is straighforward to show, however, that we cannot accept the solution relative to these two limit cases because it physically represents absence of wire conductor. In fact the limit Dirichlet solution are respectively :

$$\Theta_D(\theta) = P_0^0(cos\theta) \equiv 1 \qquad \Theta_D(\theta) = P_1^0(cos\theta) = cos\theta \tag{4.73}$$

which satisfy the b.c. pertaining to the free space and the plane conductor $\bar{\theta} = \frac{\pi}{2}$ respectively .

Thus, for a " physical wire conductor " that is a wire conductor with non-vanishing cross section of radius negligible with respect to the wavelength, we have to determine an approximate solution, for instance, by extracting the limit $k^2 \rightarrow 0$ of the singularity vector relative to the acute sector and sector on a plane conductor respectively . This way, we establish the eigenvalues, eigenfunctions and singularity vectors :

i) for the terminating wire (Fig. 4.7) :

$$\nu_D = 0 \qquad \mu_D = 0 \qquad \Theta_D(\theta) = cos\tfrac{\theta}{2} \qquad \Phi_D(\phi) = 1 \tag{4.74}$$

$$\nu_N = 1 \qquad \mu_N = 1 \qquad \Theta_N(\theta) = sin\tfrac{\theta}{2} \qquad \Phi_D(\phi) = cos\phi \tag{4.75}$$

$$\vec{N} \propto (\kappa r)^{-1}[cos\tfrac{\theta}{2}\hat{r} - \tfrac{1}{2}sin\tfrac{\theta}{2}\hat{\theta}] \tag{4.76}$$

$$\vec{H}_M \propto (\kappa r)^{0}[sin\tfrac{\theta}{2}cos\phi\hat{r} + \tfrac{1}{2}cos\tfrac{\theta}{2}cos\phi\hat{\theta} - sin\tfrac{\theta}{2}sin\phi\hat{\phi}] \tag{4.77}$$

ii) for the wire crossing a plane conductor (Fig. 4.8) :

$$\nu_D = 0 \qquad \mu_D = 1 \qquad \Theta_D(\theta) = cos(2\theta) \qquad \Phi_D(\phi) = sin\phi \tag{4.78}$$

$$\nu_N = 0 \qquad \mu_N = 0 \qquad \Theta_N(\theta) = cos(2\theta) \qquad \Phi_N(\phi) = cos\phi \tag{4.79}$$

$$\vec{N} \propto (\kappa r)^{0}[sin2\theta sin\phi\hat{r} - cos2\theta sin\phi\hat{\theta} - sin2\theta cos\phi\hat{\phi}] \tag{4.80}$$

$$\vec{H}_M \propto (\kappa r)^{0}[cos2\theta cos\phi\hat{r} - 2cos2\theta cos\phi\hat{\theta} - cos2\theta sin\phi\hat{\phi}] \tag{4.81}$$

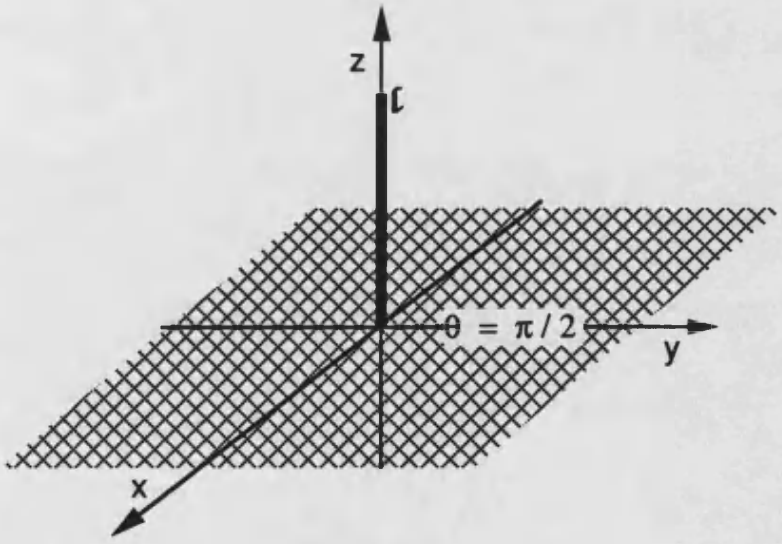

Fig. 4.6 : segment of wire crossing a plane conductor

The presence of a variation along ϕ ensure $H_\phi \neq 0$ and is necessary in order to allow the flow of longitudinal current along the wire .

Furthemore, for all those applications in which just an easy formulation in rectangular coordinate is sufficient, we report in Table 4.3 the projections of the (4.76,77,80,81) on the main planes .

EM fields singularity vectors for the terminated wire					
s_{E_X}	s_{H_X}	s_{E_Y}	s_{H_Y}	s_{E_Z}	s_{H_Z}
$\frac{1}{r}\sqrt{1-\frac{z}{r}}$	$\sqrt{1+\frac{z}{r}}$	$\frac{1}{r}\sqrt{1-\frac{z}{r}}$	$\sqrt{1+\frac{z}{r}}$	$\frac{1}{r}\sqrt{1+\frac{z}{r}}$	$\sqrt{1-\frac{z}{r}}$
EM fields singularity vectors for the wire crossing a plane conductor					
$\frac{z}{r}$	$\frac{\sqrt{x^2+y^2}}{r}$	$\frac{z}{r}$	$\frac{\sqrt{x^2+y^2}}{r}$	$\frac{\sqrt{x^2+y^2}}{r}$	$\frac{z}{r}$

Table 4.3: EM field singularity vectors for the conductors and geometry shown in Figs. 4.7,8 .

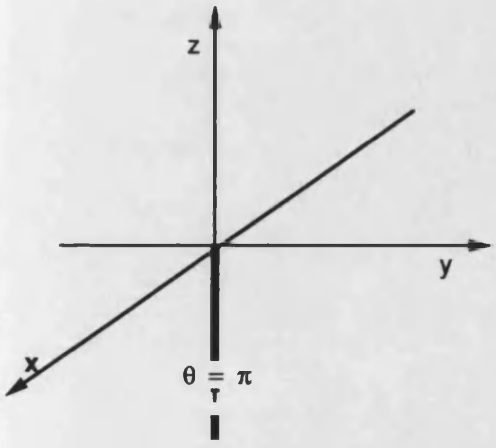

Fig. 4.7 : terminating wire

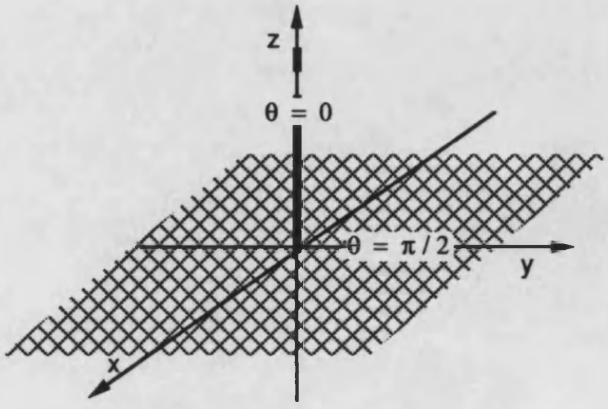

Fig. 4.8: wire crossing a plane conductor

4.5 General features of the charge and current singularities

Having developed the mathematical aspect of the EM singularities involved in the 2D,3D and Cone-wedges, we are now in a position to draw some physical conclusions about the singularities of charge and current with the main aim to find out some features suitable for generalization to any wedge geometry .

The electric singularity is easier to treat than the magnetic one essentially thanks to the fact it is physically originated by the *scalar static* distribution of charge on the tip .

To state this, we can compare τ_e for the six Cones and 3D-wedges drawn in Fig. 4.9 . We note a monotonic behaviour everywhere, starting from the same point when the conical and plane sector degenerate into the same conductor and departing from each other as the solid angle of the cone increases given the same angular aperture as the sector, i.e. $\theta = \sigma$.

Moreover, any cone with elliptic section but with maximum aperture angle $\theta_m = \theta = \sigma$ presents a τ_e-curve located between the two above, named as stated for instance in [14, 17] .

This feature, also approximatively formulated by De Smedt in [16], let us postulate that:

every wedge with conducting surface always contained between an inscribing 3D-wedge and a circumscribing Cone-wedge, but otherwise arbitrarily irregular, presents a value of τ_e between those relative to the latter two ideal limit structures.

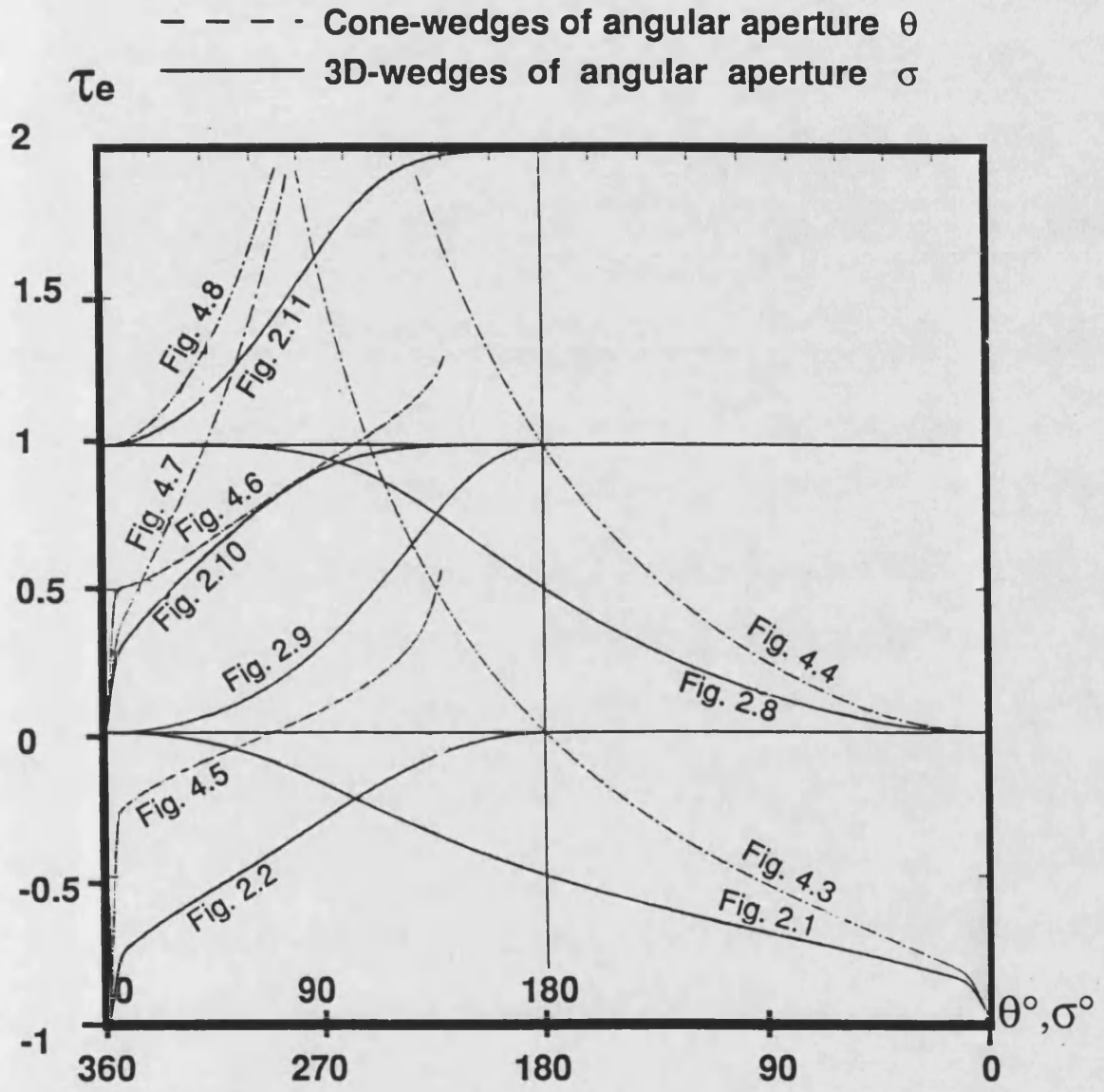

Fig. 4.9 : degree of electric singularity relative to the conductor geometries individuated by the Fig . number indicated

The situation is quite different for the magnetic singularity because it is physically originated by the density of current which, being a vector, is dependent not only on the conducting solid angle, but also on its shape as potential path for the current flux .

In this contex, in Figs. 4.10,11,12,14,15 are drawn the main lines of current associated to the fundamental H-mode and E-mode diffracted by the 2D, 3D and Cone-wedges considered . Also indicated is the analytical formulation of the main terms using the radial distance r from the tip, the 2π-periodic Lamé's functions $\mathcal{L}$ and trigonometric functions Φ .

Comparison of the H-singularities for 2D and 3D-wedges is illuminating in showing the importance of the path . For a 2D-wedge the singularity of the current is always located along the straight wedge and its order increases with decreasing conductor angles . The charge behaves exactly in the same way and the minimum degree of singularity is $-\frac{1}{2}$ for both .

For a 3D-wedge the singular current bends around the tip along smaller and smaller circles as the conductor angle increases, reaching the absolute minimum of degree -1 . This is a complementary behaviour with respect to that of the charge.

For a Cone-wedge, as the path of the current is completely three-dimensional, it is allowed to flow around and on the tip, so that the minimum degree of singularity is just $\simeq -0.15$.

In this situation, it appears difficult to gauge the degree of magnetic singularity for more irregular structures, conversely to the electrical case .

If, in fact, we look at the results for the elliptic cone treated in the above mentioned works [14, 17], we note the existence of two magnetic singularities .

If we look at the cone along the minor axis of its elliptic section, i.e. at its flatter surface, we see the current related to the first singularity flowing down onto the tip to return on the opposite half-cone surface .

In a similar way, the current related to the second singularity flows onto the tip from the half-cone surface one sees looking at the cone along the major axis of its elliptic section, i.e. at its rounder surface .

As intuitive, the named works show that the 2^{nd} singularity is dominant on the first one, the two being identical only for the circular cone .

On the other hand, when the minor axis of the elliptic section vanishes, i.e. 3D-wedges occur, the first singularity vanishes because the flux of current to it related presents opposit signs at the same point of the conductor .The 2^{nd} singularity becomes instead that of the 3D-wedge studied in Chapter 3 .

Another important fact to note is that τ_h for the generic elliptic cone is no longer monotonic with the maximum angular aperture of the conductor, even though the deeper degree of singularity is always comprised between those relative to the Cone-wedge and 3D-wedge with the same maximum angular aperture (see [14]) .

In this context, in similitude to what said for the electric singularity, we postulate that :

every wedge with conducting surface always contained between an inscribing 3D-wedge and a circumscribing Cone-wedge, but otherwise arbitrarily irregular, presents a value of τ_h between those relative to the limit ideal structures . However, no monotonicity holds in general with respect to the maximum angular aperture of the solid angle of the conductor and other weaker singularities may appears as the irregularity of the conductor shape increases .

CURRENT LINES BEHAVIOR ON THE WEDGES

H-modes	E-modes
2D-WEDGES	
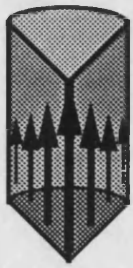	
Fig. 4.10 : like $(r \sin\theta)^{\nu-1}$	Fig. 4.11 : like $r^{\nu}(\sin\theta)^{\nu-1}$
3D-WEDGES	
	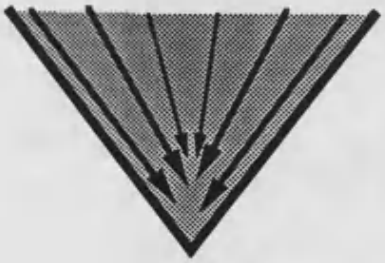
Fig. 4.12 : like $r^{\nu-1}\,\mathcal{L}(\phi)$	Fig. 4.13 : like $r^{\nu}\,\mathcal{L}(\phi)$
CONE-WEDGES	
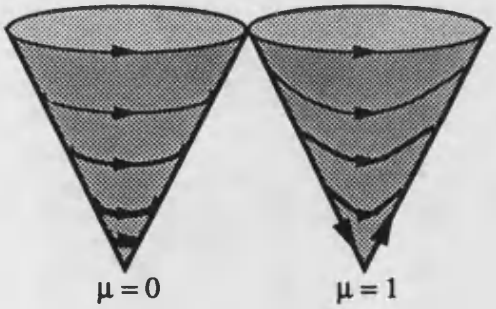	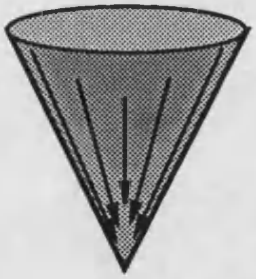
Fig. 4.14 : like $r^{\nu-1}\,\Phi(\phi)$	Fig. 4.15 : like $r^{\nu}\,\Phi(\phi)$

Chapter 5

TAPERS ANALYSIS AND SYNTHESIS OF AN OPTIMUM SMOOTH PROFILE

5.1 Introduction

To the complete mathematical characterization of wedge singularities we have to add a circuital one . In other words, workers in microwave and millimetric integrated circuits (MIC) need to know how much the presence of a 3D-wedge influences the parameters characterizing the circuit of which the wedge is part .

Unfortunately, from this point of view, is not possible to characterize in absolute the wedge behaviour because its effects are strongly dependent on the geometry of the Printed Conductor in its vicinity and from the EM phenomenon

in consideration .

This means that application for application, component for component, the same 3D-wedge produces effects that are qualitatively and quantitatively different.

Printed Conductors involved in planar circuits are often shaped as polygonals, that are a chain of straight edges forming 3D-wedges of arbitrary aperture.

Producing sectors of more arbitrary shape as, for instance, curves of 2^{nd} degree, increases degrees of freedom thus allowing satisfaction of further specifications .

For example, the optimization of the shape of the transition between fin-line and rectangular waveguide has been the object of many studies as we are going to discuss .

In all these situations, it is still possible to apply the singularity vectors forms at least on the plane of the conductor or on the surface normal to it as specified in 3.6 . For a conductor shaped as of segment of hyperbola or parabola, singularity vector forms valid all over space could be determined by solving Laplace's equation in Ellipsoidal or Paraboloidal c.s. (see [1]) .

Moreover, we note that the knowledge of the singularities permits to evaluate the risks of electric breakdowns .

This Chapter starts by remarking that the " elementary brick " of a passive microwave integrated circuits is a thin conductor printed or imbedded in a dielectric support . Hence, it is important to be able to tell whether the latter influences the singularities or not .

Then, we will proceed to analyse extensively a specific application of wedges with arbitrary aperture, like those used in the transition between fin-line and waveguide . We will make an attempt to evaluate the reflection produced by sharp corners and, consequently, suggest a new algorithm to determine the " optimum smooth profile " with respect to the reflection coefficient itself .

The process of optimization of a smooth profile gone on during these last 40 years (see [26, 39, 38, 36, 35] and many others) will be reconsidered pointing out the role of the distribuited singularities . This will permit us to make another step in this direction by ascertaining that the best smooth profile is a product between an exponential and a cosinusoidal function .

5.2 The coexistence of metallic and dielectric wedges

To the hypothesis already formulated in Chapters 2,3 about the independence of the solution of frequency near the conductor, its convergence to that relative to a wedge by the tip and its satisfaction of the edge and vertex conditions, we have to add a new one about the influence of the dielectric usually supporting the printed conductor (see Fig. 5.1) .

Moreover, dielectric wedges may well exist on their own .

The matter has been treated by De Smedt in [15] and others quoted there. The b.c. involved are now more general than the simple Dirichlet or Neumann ones and the determination of the degree of singularity is obtained numerically, so that simple analytic singularity vector forms are not available .

For what concerns our purposes, we have already noted that the normal E and tangential H-components of the singular mode diffracted by the plane conductor vanish, for symmetry, on the portion of plane adjacent and complementary to the conductor itself, that is, the interface air-dielectric in Fig. 5.1,2 .

Moreover the b.c. pertaining to this interface are :

$$\epsilon_0 E_{n_{air}} = \epsilon_d E_{n_{dielectric}} \qquad H_{t_{air}} = H_{t_{dielectric}} \tag{5.1}$$

but these are automatically satisfied by the fields of the fundamental mode diffracted by the printed conductor because all their components involved in (5.1) vanish .

In other words, the singularity vectors remain unaltered in presence of the supporting dielectric .

From the classic point of view of waveguide discontinuities [28], we can say that the geometry of the substrate does not destroy the radial symmetry of the metallization, at least at the air-dielectric interface, so that the radially-directed E an H-modes fitting the conductor can be determined in each medium as if all the space were plenty of it .

The situation is different for the 2D-wedge (see [15]) because the air-dielectric interface is equiplanar to one conductor surface but not to the other, so that the above symmetry is destroyed and ν decreases with consequent higher singularity at the edge .

In some circumstances, the dielectric is cut at the edge of the conductor, so that the two types of edges coexist .

In other cases, the dielectric is cut to a shape of its own, as for the quarter wavelength transformer reported in [31] p.283 .

All these situations have been analysed sufficiently in [15] which reports at least an approximate value of ν .

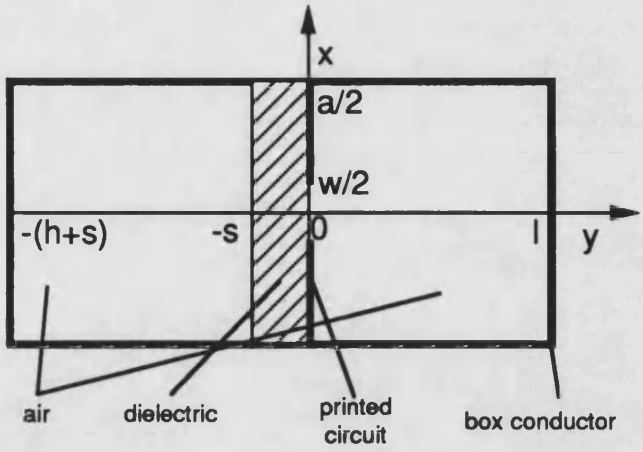

Fig. 5.1 : unilateral fin-line cross section

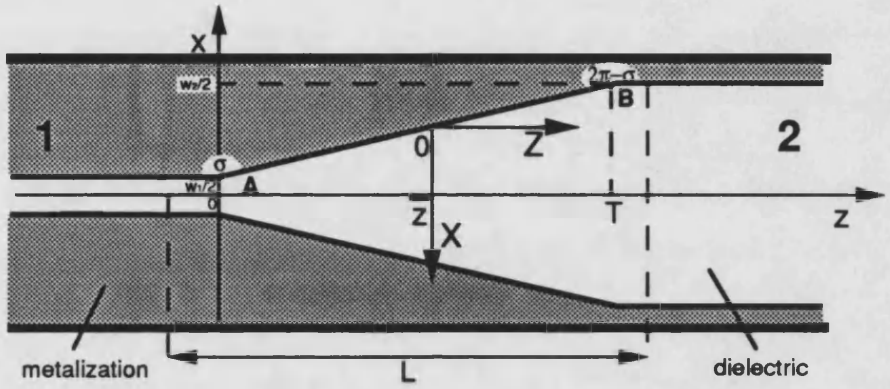

Fig. 5.2 : longitudinal linear taper

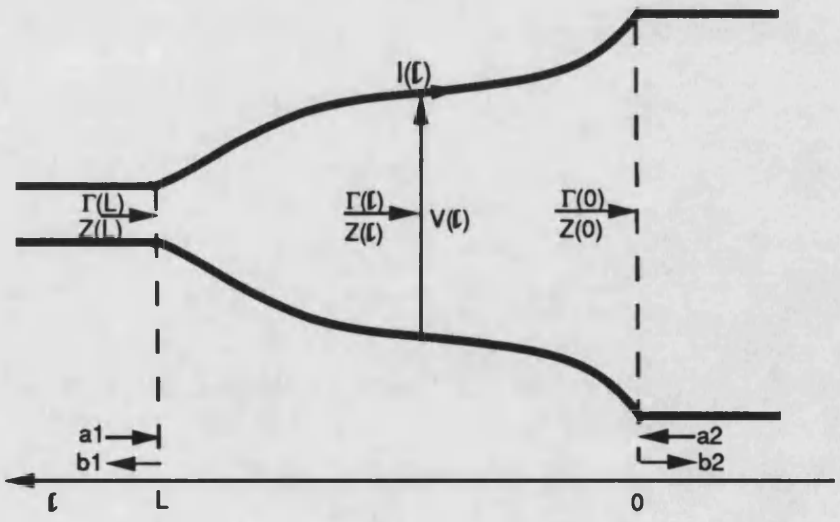

Fig. 5.3 : schematic nonuniform equivalent line

5.3 Non-uniform unilateral fin-line

Given recent improvements in the manufacturing of planar circuits, it would be possible, in principle, to increase design freedom by making use of printed conductors with gradually changing profiles, instead of the abrupt ones that we will consider in Chapter 6 .

For instance, the step impedance in unilateral fin-line shown in Fig. 6.1 could be replaced by a taper of moderate physical length with minimum reflection over a broad band .

Several authors have been working at this problem for the last 40 years, looking for a compromise between specifications and optimum synthesis .

To this effort, we now contribute the exact knowledge of the distributed singularity, which permits us to formulate a new algorithm of analysis with the double purpose of quantifying diffraction by a sharp corner while helping towards a novel synthesis approach .

For this purpose, we start by demonstrating the method for the linear taper profile drawn in Fig. 5.2, that acts as an impedance transformer between two uniform lines of different impedances .

The discontinuity diffracts propagating modes from a uniform section to a non-uniform section, were higher order modes must be excited in order to satisfy the nonuniform b.c., and in particular those at the tips A and B .

Apart from several approximate methods of analysis which involve (see [31]), in fact, optimization by empirical means, up to date, two main complete methods of analysis have been developed .

The first one is the "Equivalent Line Approach", which associates an equiv-

alent line to each guide mode appreciably involved in the phenomenon (see [35]), so that at least a few lines and their mutual couplings need to be involved .

Alternatively, complete multi-mode models require the generation of the complete modal spectrum and the determinations of the coupling between at least the first few modes, which is increasingly difficult as frequency increases . In fact, only the fundamental has been employed in [36] .

These works let us realize that the main analytic difficulty is due to the coupling between several lines or modes along the taper where, singularly, they do not satisfy the b.c. .

In the attempt to avoid this difficulty, we present a " Transverse Resonance Diffraction Method " for non-uniform lines, able to generates modes coincident with those of the uniform guide in regions 1 and 2 of Fig. 5.2 (see also [33]), varying continuously along the non-uniform section in such a way as to satisfy exactly the b.c. the printed conductor actually imposes there .

This way, all the equivalent line modes will be decoupled and, in particular, the progressive and regressive waves of the same mode also result decoupled. An incident mode non propagating in the following uniform section vanishes along the taper, i.e. its energy remains stored along the taper and/or is reflected back.

The only approximation consists in the fact that Maxwell's equations are not exactly satisfied far from the boundaries . The accuracy, however, improves as the taper length increases, that is to say, when the impedance profile of the line we associate to each mode does not change too fast per wavelength along z.

Nevertheless, this is exactly the validity hypothesis for the application of the line theory we are going to use and the optimum taper length will be shown to be at least $\frac{\lambda}{2}$, so that the approximation is not restrictive .

5.4 Theoretical development

The analysis developed in order to identify the modes just defined has been thought of as a generalization of the "Transverse Resonance Diffraction Method", applied since 1986 (see [33]) to the unilateral fin-line with the purpose of determining its complete modal spectrum .

For this reason and that of brevity, we will use the terminology of [33], with the motivations reported there and in the literature quoted there, while pointing out the main steps involved in the generalization .

We start analysing any distinct $z = \bar{z} = const$ section . There we can note that the field can be described completely as a superposition of the LSE and LSM-to-$\hat{z}$ modes which can be derived from two $\hat{y}$-directed Hertzian vector potentials as follows :

$$\vec{E} = -j\omega\mu\nabla \mathrm{x}\vec{\Pi}_h + \kappa^2\vec{\Pi}_e + \nabla\nabla\cdot\vec{\Pi}_e \tag{5.2}$$

$$\vec{H} = \kappa^2\vec{\Pi}_h + \nabla\nabla\cdot\vec{\Pi}_h + j\omega\epsilon\nabla \mathrm{x}\vec{\Pi}_e \tag{5.3}$$

Diffraction on the printed conductor is responsible for coupling between LSE and LSM modes, even though the dominant are LSE and become pure when the fin width reduces to zero .

In the three homogeneous regions of the guide these potentials satisfy the usual scalar wave equation (2.1), but, in order to satisfy the non uniform b.c. along the taper, a more general z-dependence has to be assumed, i.e. :

$$\vec{\Pi}_{e,h}(x,y,z) = \Psi_{e,h}(x,y;z) f(z) e^{-\gamma(z)z} \hat{y} \tag{5.4}$$

In order for (5.4) to satisfy the wave equation, the correction function f can be shown to satisfy the ordinary differential equation :

$$\ddot{f} - 2\dot{f}(\dot{\gamma}z + \gamma) - f[\ddot{\gamma}z + 2\dot{\gamma}z - (\dot{\gamma} + \gamma)^2 + \gamma^2] = 0 \tag{5.5}$$

under the only hypotesis of negligible derivatives of Ψ with respect to z.

In order to ensure decoupling between different modes and between progressive and regressive waves of the same mode it can be shown that (5.5) must be supplied with the b.c. :

$$\frac{df}{dz} = 0 \qquad \text{on the uniform section} \tag{5.6}$$

The analogous regressive wave quantities are recoverable from (5.4,5) by replacing γ by $-\gamma$.

In order to satisfy the b.c. on the metallic walls $x = \pm\frac{a}{2}$ we can further decompose Ψ as :

$$\Psi_e(x,y;z) = \sum_{n=2,4,\ldots} U_{e_n}(z) \chi_{e_n}(y;z) \phi_{e_n}(x) \tag{5.7}$$

$$\Psi_h(x,y;z) = \sum_{n=0,2,\ldots} U_{h_n}(z) \chi_{h_n}(y;z) \phi_{h_n}(x) \tag{5.8}$$

with :

$$\phi_{e_n}(x) = \sqrt{\frac{2}{a}} sin(\frac{n\pi}{a}x) \quad n = 2,4,... \qquad \phi_{h_n}(x) = \begin{cases} \frac{1}{\sqrt{a}} & n = 0 \\ \sqrt{\frac{2}{a}} cos(\frac{n\pi}{a}x) & n = 2,4,... \end{cases} \tag{5.9}$$

where the wavenumber in the $\hat{x}$ direction $\frac{n\pi}{a}$, is related to that γ along $\hat{z}$, to k_{mn} along $\hat{y}$ and to the wavenumber in the medium κ according to the relation :

$$\gamma_m^2(z) + \kappa^2(y) = (\frac{n\pi}{a})^2 + k_{mn}^2(y,z) \tag{5.10}$$

where m is the index of the mode along $\hat{z}$.

(5.10) shows the dependence of k_{mn} on z which, together with the z-dependence of the coefficients U in (5.7,8), constitutes the Ψ dependence on z . In other words, the accuracy of the (5.5) increases, in particular, as $\frac{\partial \Psi}{\partial k_{mn}} \frac{\partial k_{mn}}{\partial z}$ decreases . Naturally, this happens as the profile changes more gradually .

Finally, the b.c. on the surfaces $y = const$ are systematically introduced in the spectral domain so it remains to impose the b.c. pertaining to the fins directly on the fields, whose explicit espressions can be recovered from (5.2,3,4) as :

$$\vec{E} = \left[\left(\frac{\partial^2 \Psi_e}{\partial x \partial y} - j\omega\mu\gamma_{eff}\Psi_h \right) \hat{x} + \left(\kappa^2 \Psi_e + \frac{\partial^2 \Psi_e}{\partial y^2} \right) \hat{y} - \left(j\omega\mu \frac{\partial \Psi_h}{\partial x} + \gamma_{eff} \frac{\partial \Psi_e}{\partial y} \right) \hat{z} \right] \cdot |f| e^{-j\beta_{eff} z} \tag{5.11}$$

$$\vec{H} = \left[\left(\frac{\partial^2 \Psi_h}{\partial x \partial y} + j\omega\mu\gamma_{eff}\Psi_e \right) \hat{x} + \left(\kappa^2 \Psi_h + \frac{\partial^2 \Psi_h}{\partial y^2} \right) \hat{y} - \left(j\omega\epsilon \frac{\partial \Psi_e}{\partial x} - \gamma_{eff} \frac{\partial \Psi_h}{\partial y} \right) \hat{z} \right] \cdot |f| e^{-j\beta_{eff} z} \tag{5.12}$$

where :

$$\gamma_{eff}(z) = \frac{d}{dz}\left[\gamma(z)z - ln(f(z))\right] \tag{5.13}$$

$$\beta_{eff}(z) = \beta(z) - \frac{\angle f(z)}{z} \tag{5.14}$$

In particular, leaving aside the common terms $|f|e^{-j\beta_{eff}z}$, the fields on the plane of the fins $y = 0$ can be synthetically written as :

$$E_x(x,0,z) = \sum_{n=0,2,\ldots} E_{x_n}(z)\phi_{h_n}(x), \quad H_x(x,0,z) = \sum_{n=2,4\ldots} H_{x_n}(z)\phi_{e_n}(x) \tag{5.15}$$

$$E_z(x,0,z) = \sum_{n=2,4,\ldots} E_{z_n}(z)\phi_{e_n}(x), \quad H_z(x,0,z) = \sum_{n=2,4\ldots} H_{z_n}(x)\phi_{h_n}(x) \tag{5.16}$$

There are linked by some integral relations expressible in terms of the Green's admittances on the right and left side of the fins as in [33] . The kernels of these integral equations are expressible in useful series form which, however, are all properly convergent after appropriate integration by parts . Differently to what happens in a uniform section, both E_x and E_z present a singularity of degree $-\frac{1}{2}$ along the taper which becomes deeper in the corner A and weaker in B .

Consequently, the derivatives of the E-field components are no longer integrable and the only remaining possibility is the use of integrals of the H-field . Then, if we leave aside the z dependence, we can write for instance :

$$\begin{bmatrix} -\frac{a}{\pi}\int^x H_z^R(x')dx' \\ (\frac{a}{\pi})^2\int^x\int^{x'} H_x^R(x'')dx''dx' \end{bmatrix} = \begin{bmatrix} \hat{Y}_{11}^R(x,x') & \hat{Y}_{12}^R(x,x') \\ \hat{Y}_{21}^R(x,x') & \hat{Y}_{22}^R(x,x') \end{bmatrix} \begin{bmatrix} E_x^R(x') \\ E_z^R(x') \end{bmatrix} \quad (5.17)$$

where R indicates that the equation is valid in the right sheet of the surface $y = 0$. The b.c. imposed by the fins can be thought as those of continuity of the H-field on the air-dielectric interface since no current flows there .

Writing the analogous of (5.17) on the left of the fins and substracting term by term we can eliminate H :

$$\begin{bmatrix} \hat{Y}_{11}(x,x') & \hat{Y}_{12}(x,x') \\ \hat{Y}_{21}(x,x') & \hat{Y}_{22}(x,x') \end{bmatrix} \cdot \begin{bmatrix} E_x(x') \\ E_z(x') \end{bmatrix} = 0 \qquad x \in [-\frac{a}{2}, \frac{a}{2}] \quad (5.18)$$

This formula holds all over the guide width a as E_x, E_z vanish on the fins . Explicitly, the convergent series kernels are :

$$\hat{Y}_{11}(x,x') = \sum_{n=0,2,..} y_{11_n}^* \phi_{e_n}^*(x)\phi_{h_n}(x') \quad (5.19)$$

$$\hat{Y}_{12}(x,x') = \sum_{n=0,2,..} y_{12_n}^* \phi_{e_n}^*(x)\phi_{e_n}(x') \quad (5.20)$$

$$\hat{Y}_{21}(x,x') = \sum_{n=2,4,..} \frac{y_{12_n}}{n^2} \phi_{e_n}(x)\phi_{h_n}(x') \quad (5.21)$$

$$\hat{Y}_{22}(x,x') = \sum_{n=2,4,..} \frac{y_{22_n}}{n^2} \phi_{e_n}(x)\phi_{e_n}(x') \quad (5.22)$$

where :

$$y^*_{11_n}(z) = \begin{cases} y_{11_0}(z) & n = 0 \\ \frac{y_{11_n}(z)}{n} & n = 2,4,... \end{cases} \qquad y^*_{12_n}(z) = \begin{cases} 0 & n = 0 \\ \frac{y_{12_n}(z)}{n} & n = 2,4,... \end{cases}$$

$$\phi^*_{e_n}(x) = \begin{cases} \frac{1}{\sqrt{a}}(\frac{\pi}{a}x) & n = 0 \\ \phi_{e_n}(x) & n = 2,4,... \end{cases} \tag{5.23}$$

and $y_{11_n}, y_{12_n}, y_{22_n}$ are those defined in [42, 33] where the z dependence is due to the propagation constants and to the strip width $w(z)$.

In order to solve the integral equation (5.18), we have to reduce it to a matrix equation for a discrete and sufficiently large number of $\bar{z}$- values along the taper length . In first instance, and by the way of example, thanks to the fact that $E_x, E_y = 0$ on the fins and the integrands are always even for symmetry with respect to x, we can reduce the 1^{st} integral equation to :

$$\int_{-\frac{a}{2}}^{\frac{a}{2}} ... = \int_{-\frac{w(z)}{2}}^{\frac{w(z)}{2}} ... = 2\int_0^{\frac{w(z)}{2}} [\hat{Y}_{11}(x,x')E_x(x') + \hat{Y}_{12}(x,x')E_z(x')]dx' = 0 \tag{5.24}$$

In second instance, we operate an useful change of variable which avoids explicit integration of the singularities and permits to complete the discretization of the integral :

$$\int_0^{\frac{\pi}{2}} [\hat{Y}_{11}(x,x'(\theta_1))]E_x(x'(\theta_1))\frac{dx'}{d\theta_1}d\theta_1 + \int_0^{\frac{\pi}{2}} [\hat{Y}_{21}(x,x'(\theta_2))]E_z(x'(\theta_2))\frac{dx'}{d\theta_2}d\theta_2 = 0 \tag{5.25}$$

where the functions $\theta_1(x'), \theta_2(x')$ have to be chosen in such a way that $\frac{dx'}{d\theta_1}, \frac{dx'}{d\theta_2}$ compensate exactly the singularities present in E_x, E_z respectively so that the functions :

$$\mathcal{E}_x(\theta_1) = E_x(x'(\theta_1))\frac{dx'}{d\theta_1} = \sum_{m=0,2,\ldots} X_m \varphi_m(\theta_1) \tag{5.26}$$

$$\mathcal{E}_z(\theta_2) = E_z(x'(\theta_2))\frac{dx'}{d\theta_2} = \sum_{m=1,3,\ldots} Z_m \varphi_m(\theta_2) \tag{5.27}$$

are everywhere finite functions in $\theta_1, \theta_2 \in [0, \frac{\pi}{2}]$ while $x' \in [\frac{w}{2}, 0]$. For this purpose, are expressed in terms of complete and orthogonal functions φ_m with coefficients X_m, Z_m . A suitable set of functions for this purpose is as follows :

$$\varphi_m^*(\theta) = \begin{cases} \frac{1}{\sqrt{\pi}} & m = 0 \\ \frac{2}{\sqrt{\pi}} cos(m\theta) & m = 1, 2, \ldots \end{cases} \qquad \theta \in [0, \pi] \tag{5.28}$$

This is a complete set in the space of the even functions in respect of $\theta = 0$, and then can represent $\mathcal{E}_x(\theta_1), \mathcal{E}_z(\theta_2)$ because they can always be extended even in respect of this point .

Furthemore $\mathcal{E}_x$ is also even while $\mathcal{E}_z$ is also odd with respect to $\theta = \frac{\pi}{2}$ so that only the terms with m even represent completely $\mathcal{E}_x$ and those with m odd represent completely $\mathcal{E}_z$.

These two sub-sets are also orthogonal in $\theta \in [0, \frac{\pi}{2}]$ because the product of any two of them is even in respect of $\theta = \pi$ and $\frac{\pi}{2}$ allowing us to write:

$$\int_0^{\pi} \varphi_m^*(\theta)\varphi_n^*(\theta)d\theta = 2\int_0^{\frac{\pi}{2}} \varphi_m^*(\theta)\varphi_n^*(\theta)d\theta = \delta_{mn} \tag{5.29}$$

where m, n are both even or odd . In conclusion, a set of functions orthonormal over the half aperture is given by :

$$\varphi_m(\theta) = \begin{cases} \frac{1}{\sqrt{2\pi}} & m = 0 \\ \frac{1}{\sqrt{\pi}} cos(m\theta) & m = 1, 2, ... \end{cases} \qquad \theta \in [0, \frac{\pi}{2}] \tag{5.30}$$

Following the same argument, the two sets of functions $\phi_{e_n}(x), \phi_{hn}(x)$ are expressible on the aperture as :

$$\begin{aligned} \phi_{e_n}^*(x) &= \textstyle\sum_{m=1,3,...} Q_{mn}\varphi_m(\theta_2) \\ \phi_{h_n}(x) &= \textstyle\sum_{m=0,2,...} P_{mn}\varphi_m(\theta_1) \end{aligned} \qquad n = 0, 2, 4, ... \tag{5.31}$$

The iterative procedure by which the matrix $\underline{\underline{Q}}$ and $\underline{\underline{P}}$ are determined for any $\bar{z}$ section is vital in reducing computing time and will be presented in Appendix G .

Integral equation (5.18) now can be reduced to the matrix equation :

$$\begin{bmatrix} \underline{\underline{Y}}_{11}(\bar{z}) & \underline{\underline{Y}}_{12}(\bar{z}) \\ \underline{\underline{Y}}_{21}(\bar{z}) & \underline{\underline{Y}}_{22}(\bar{z}) \end{bmatrix} \begin{bmatrix} \underline{X}(\bar{z}) \\ \underline{Z}(\bar{z}) \end{bmatrix} = 0 \tag{5.32}$$

where :

$$\left.\begin{aligned}(Y_{11})_{mi} &= \textstyle\sum_{n=0,2,\ldots} y^*_{11_n} Q_{in} P_{mn} \\ (Y_{21})_{mi} &= \textstyle\sum_{n=2,4,\ldots} \frac{y_{21_n}}{n^2} Q_{in} P_{mn}\end{aligned}\right\} m = 0,2,\ldots, i = 1,3,\ldots \qquad (5.33)$$

$$\left.\begin{aligned}(Y_{12})_{mi} &= \textstyle\sum_{n=0,2,\ldots} y^*_{12_n} Q_{in} Q_{mn} \\ (Y_{22})_{mi} &= \textstyle\sum_{n=2,4,\ldots} \frac{y_{22_n}}{n^2} Q_{in} Q_{mn}\end{aligned}\right\} m = 1,3,\ldots, i = 1,3,\ldots \qquad (5.34)$$

In particular, E_z being odd implies $E_{z_0} = Z_0 = 0$.

The condition for non-trivial solutions of the system (5.32) is expressible as :

$$det[\gamma(\bar{z}, w(\bar{z})), \omega; \text{geometric parameters, EM parameters}] = 0 \qquad (5.35)$$

As a way of example, we analyse the following fin-line geometry :

geometric par.: $l = 11.43mm$, $h = 11.186mm$, $s = 0.254mm$, $a = 10.16mm$

EM parameters : $\mu_0 = 4\pi \cdot 10^{-7} \frac{Hn}{m}$, $\epsilon_0 = 8.854 \cdot 10^{-12} \frac{F}{m}$, $\epsilon_r = 2.20$

$\bar{\omega}$: $2\pi f$ at the central X band f = 10GHz .

For any $\bar{z}, \bar{\omega}$ the roots of (5.35) identify the propagation constants $\gamma_m(\bar{z}, \bar{\omega})$ and the EM fields in the same section . The working frequency is such that only the fundamental mode is in propagation for every possible fin aperture w .

The determination of the whole curve $\gamma(z, \omega)$ in the frequency band and of the complete mode spectra is left to further applications .

5.4.1 The map $x - \theta$

The mapping of the variable x into θ, with a view to translate our analysis to a orthonormed space of functions finite everywhere, has been devised by Schwinger [28] for the study of irises in waveguides .

We will now deal with an extension to singularities of arbitrary degree . At the intersection of a line $z = \bar{z}$ with the edge conductor we fix the origin for a new c.s. X, Y, Z as indicated in Fig. 5.1, i.e. related to the waveguide ones according to :

$$X = \frac{w(\bar{z})}{2} - x \qquad Y = y \qquad Z = z - \bar{z} \tag{5.36}$$

The particular situation is shown in Fig. 5.4, where the variable θ is also indicated . The required map can be taken in the general form :

$$\theta^2 = F(\bar{z})X \tag{5.37}$$

Since the electric field is transformed by this map like :

$$\mathcal{E}(\theta) = E(x(\theta))\frac{dx}{d\theta}$$

$$\text{where :} \qquad \frac{d\theta}{dX} = -\frac{d\theta}{dx} = \frac{1}{2}\sqrt{\frac{F(\bar{z})}{\frac{w(\bar{z})}{2} - x}} \tag{5.38}$$

(5.38) must be chosen in such a way that $\frac{d\theta}{dx}$ satisfies the right edges conditions at $x = \frac{w(z)}{2}, \theta = 0$ which, for any $\bar{z}$, can be determined from those obtained

in Chapter 2 .

Precisely, relatively to E_x and around A, for $z = 0^+$, we can write :

$$\theta_{E_x} = \bar{z}^{(\nu_A - \frac{1}{2})}\sqrt{X cos\sigma} \qquad i.e. \qquad F_{E_x} = \bar{z}^{(2\nu_A - 1)} cos\sigma \tag{5.39}$$

where σ is the angular aperture and $\nu_A - 1$ is the electric singularity pertaining to the wedge in A . With this choice, (5.38) shows exactly the degree of singularity $-\frac{1}{2}$ along the edge $X = 0$ and of degree $\nu_A - 1$ on the tip, where also $\bar{z} \rightarrow 0$. The factor $cos\sigma$ takes into account also the limit cases $\sigma = \frac{\pi}{2}, \pi$.

E_z shows exactly the same singularities with the sole exeption of the above limit cases which can be accounted simply by changing $cos\sigma$ with $sin\sigma$, i.e. :

$$\theta_{E_z} = \bar{z}^{(\nu_A - \frac{1}{2})}\sqrt{X sin\sigma} \qquad i.e. \qquad F_{E_z} = \bar{z}^{(2\nu_A - 1)} sin\sigma \tag{5.40}$$

If we indicate with T the taper length (see Fig. 5.2) the expressions around B are the same but with the substitutions $\nu_A \rightarrow \nu_B, \bar{z} \rightarrow \bar{z} - T$.

In order to be useful in determining some recursive relations shown in Appendix G, the previous mapping has to be put in the following form :

$$dsin^4\theta + bsin^2\theta = F(z)cos(\frac{\pi}{a}x) + c \tag{5.41}$$

where b, c, d are constants to be determined so as to satisfy the following mapping conditions :

i) when $\theta = 0$, we must have $x = \frac{w}{2}$, i.e. :

$$c = F[2sin^2(\frac{\pi w}{4a}) - 1] \tag{5.42}$$

ii) when $\theta = \frac{\pi}{2}$, we must have $X = 0$, i.e. :

$$d = 2Fsin^2(\frac{\pi w}{4a}) - b \tag{5.43}$$

iii) in the open interval $\theta \in (0, \frac{\pi}{2})$ the curve $\theta(X)$ must be monotonic in order to ensure a one-to-one correspondence between θ and x values .

$$0 < b < 4F_{min}sin^2(\frac{\pi w}{4a}) \tag{5.44}$$

where F_{min} is the absolute minimum that F assumes in the z-interval under consideration (see Fig. 5.5) .

With these coefficients, we can make the map explicit in the form :

$$cos\frac{\pi}{a}x = \alpha_1 + \alpha_2 cos2\theta + \alpha_3 cos4\theta \tag{5.45}$$

where $\alpha_1 - \alpha_2 + \alpha_3 = 1$ and, moreover, we have :

$$\alpha_1 = 1 - [\frac{5}{2} + \frac{F_{min}}{F}]\frac{Si}{2} \qquad \alpha_2 = -Si \qquad \alpha_3 = [\frac{1}{2} - \frac{F_{min}}{F}]\frac{Si}{2} \tag{5.46}$$

where $Si = sin^2(\frac{\pi w}{4a})$.

Remarkably, $\frac{F_{min}}{F}$ are the same for E_x and E_z (see Fig. 5.6), so that the form (5.45) also presents the advantage of defining a single map :

$$\theta_1(x) = \theta_2(x) = \theta(x) \tag{5.47}$$

It is interesting to note as in A is $(2\nu_A - 1) < 0$ while in B is $(2\nu_B - 1) > 0$, so that $F(z)$ diverges in A and vanishes in B as shown in Fig. 5.5 . For what concerns the zone of influence of the 3D-wedges, in accordance to what said for (3.24), we can consider it to extend to a distance from the tips of the order of :

$$r_{max} \in [0.5 \div 5]mm \qquad \text{when } f = 10GHz \tag{5.48}$$

Consequently, the whole taper can be divided into 3 intervals where different mapping of the forms (5.45) are used . The F profile for the three intervals are indicated in Fig. 5.6: by A, F_{min_A} can be given the F value at $z = r_{max}$ while in the interval around B, F_{min_B} is chosen as the value at a point arbitrarily near to $z = T$ and in the intermediate intervals F_{min} is chosen $\frac{1}{2}F$.

This results in the behaviour of $\frac{F_{min}}{F}$ shown in Fig. 5.6 where, in particular, the value $\frac{1}{2}$ far from the tips ensures $\alpha_3 = 0$ so that there (5.45) reduces to a two term relation as for the classic Schwinger map along the uniform sections .

Because of the necessity to decompose $\phi_{e_n}(x)$ also, we need the following form of the map :

$$sin\frac{\pi}{a}x = \beta_1 cos\theta + \beta_2 cos3\theta + \beta_3 cos5\theta \tag{5.49}$$

where $\beta_1, \beta_2, \beta_3$ are constants determined in such a way that the curves $\theta(x)$ (5.45,49) are as similar as possible . This goal is achieved, for instance, by making the two curves to coincide at the end points $\theta = \frac{\pi}{2}, 0$, (i.e. $x = 0, \frac{w}{2}$) at a point

$\theta_1 = \theta(x_1)$ very close to the conductor wedge $\theta = 0$, so as to assume the same derivatives there, and at an intermediate point $\theta_2 = \theta(x_2)$ such as to minimize the mean distance between the two curves at all other points .

From the explicit relations (5.45,49), it is possible to recover the physical meaning of the map by drawing a typical $\frac{d\theta}{dx}$ behaviour in the three regions as shown in Fig. 5.7 .

One could observe that analogous maps would be required at the tips on the uniform section of the fin-line, however, it will be shown that the value of the propagation constant $\gamma(z)$ closer point to the tip, as computed by the previous map, is quantitatively very close to that obtainable in the uniform section by using the Schwinger map .

In fact, the analytical effort of generating a new map is avoided simply by connecting the curve $\gamma(z)$ in the oblique side and in the uniform section .

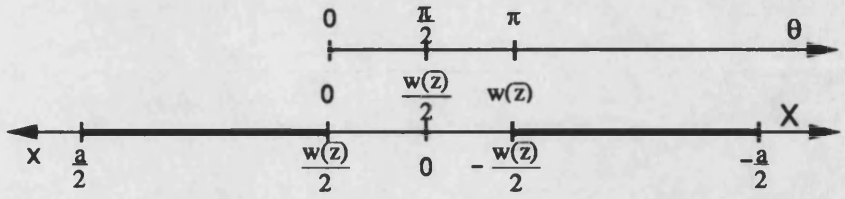

Fig. 5.4 : position of the coordinates x,X,θ with respect of the conductor

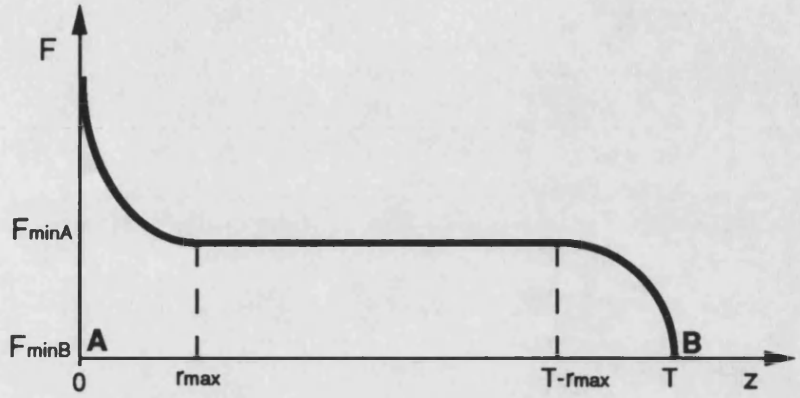

Fig. 5.5

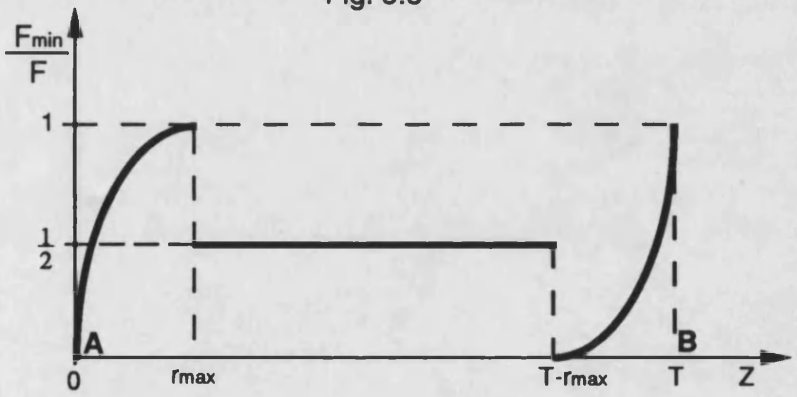

Fig 5.6

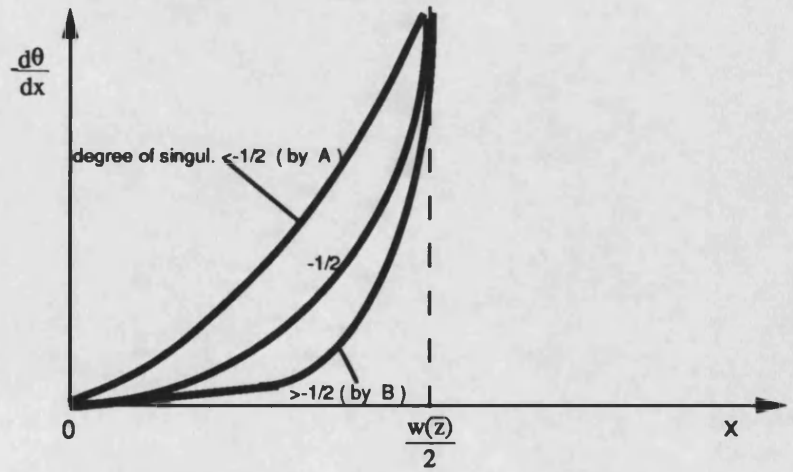

Fig. 5.7

5.5 Computational and theoretical results

For a better physical undestanding, the whole procedure starting with the determination of the propagation constant $\beta(z)$ and ending with the determination of the reflection coefficient at the input of the line, can be usefully divided into three well defined steps :

5.5.1 The determination of $\beta(z)$ and fields for the fundamental mode

The first program is centered on the implementation of the matrix equation (5.32) and related characteristic equation (5.35) . In order to put in evidence the effect of the 3D-wedges on the curve $\beta(z)$, the dimensions of matrix (5.32) were increased up to 20x20 . We have noted that in X-band the propagation constant is in the range $\beta \in [100 - 200]\ rad/m$ and the right singularities at the tips have an influence on the β-value within 1% if compared with the case of $-\frac{1}{2}$ singularity .

Nevertheless, their inclusion is essential for obtaining a monotonic $\beta(z)$, according to the monotonicity of the conductor profile . Also, it ensures continuity of the derivative of β so as required for any physically meaningful quantity . The latter are essential conditions in order to evaluate correctly $\dot{\beta}(z)$ and $\ddot{\beta}(z)$ at the tips, whose importance is shown in the next paragraph .

It has also been noted a small difference between the values of $\beta(z)$ on the uniform side and those at a point just beyond the tip A . This requires interpolating the curve $\beta(z)$ between a point on the uniform side of A and enough distant from it to be considered to be beyond the 3D-wedge effect, and the above point beyond A so as to also satisfy continuity of the first and second derivatives.

The length of the uniform line segment still influenced by the 3D-wedges at A and B, may be taken as r_{max} evaluated in (5.48), so that the electrical length of the taper may be assumed as $L \simeq T + 2r_{max}$ as indicated in Fig. 5.2 .

The evaluation of the set of transverse modal amplitudes $E_{x_n}(z), E_{z_n}(z)$ in (5.15,16) is more critical because, increasing the matrix dimension in (5.32), their values decrease so rapidly that error propagation creeps in . In order to keep the error moderate, two alternative driving equations, expressing the b.c. on the fins in alternative ways, have been substituted in the system (see (5.51,52) below). This is why, the optimum matrix size n goes from 8 for very narrow aperture w down to just 1 when $w \rightarrow a$, that is when only E_{x_0} is different from 0 . In any case, E_{z_n} is about 2 orders of magnitude smaller than E_{x_n} . This confirms for the nonuniform section the same property observed for the uniform ones : LSE and LSM modes are weakly coupled .

5.5.2 The determination of the correction function

The second program deals with the solution of the ordinary complex second order differential equation (5.5) subject to the b.c. (5.6) .

An exact solution obviously does not exist, but an expansion of $f(z)$ by means of a series of Chebyschev polynomials T_n seems quite suitable because both its real and imaginary parts have resulted almost linear, i.e. T_1 dominant.

The critical point is now constituted by the correct reproduction of the first derivative and, even more, of the second derivative of $\beta(z)$ at the two tips where they take on their absolute maxima . As a consequence both γ_{eff} and β_{eff} in (5.11,12) present a step particularly evident in correspondence of the acute tip A (see Fig. 5.8) . However, no cusps are present there . Furthemore, because of

the real part of f, γ_{eff} presents a real part which is almost an order of magnitude smaller than its imaginary part, as shown in the same Fig. 5.8 .

5.5.3 The solution of the equivalent transmission line

To a third program is entrusted the determination of the characteristic impedance $Z(z)$ with consequent translation of the problem into non-uniform line theory. A common definition for the fin-line impedance is :

$$Z(z) = \frac{V^2(z)}{2P_{eff}(z)} \tag{5.50}$$

where V is the voltage difference between the fins expressed within a multiplicative constant as, either :

$$V(z) = \int_{-\frac{w(z)}{2}}^{\frac{w(z)}{2}} E_x(x,0,z)dx = \frac{w}{\sqrt{a}}E_{x_0}(z) + w\sqrt{\frac{2}{a}}\sum_{n=2,4,..} E_{x_n}(z)\frac{sin(n\frac{\pi w(z)}{2a})}{n\frac{\pi w(z)}{2a}} \tag{5.51}$$

$$\text{or} \quad V = \int_{-\frac{a}{2}}^{\frac{a}{2}} E_x(x,0,z)dx = \sqrt{a}E_{x_0}(z) \tag{5.52}$$

Hence, we obtain one of the driving equations mentioned above as :

$$\sum_{n=0,2,...} \delta_n E_{x_n}\frac{sin(n\frac{\pi}{2}\frac{w}{a})}{n\frac{\pi}{2}\frac{w}{a}} = 0 \qquad \text{with : } \delta_n = \begin{cases} \frac{w-a}{\sqrt{a}} & n = 0 \\ w\sqrt{\frac{2}{a}} & n = 2,4,... \end{cases} \tag{5.53}$$

the other being the analogous one for E_z .

The arbitrary multiplicative constant may be fixed in such a way that $E_{x_0} = 1$ or $V = 1$ so as to simplify (5.50) .

The average power flowing across an arbitrary guide cross-section S is :

$$P_{eff} = \frac{1}{2} \int \int_S (E_x H_y^* - E_y H_x^*) dx dy \tag{5.54}$$

where * indicates the complex conjugate . This expression can also be reduced to simple summations since the fields components are expressible in easily integrable Circular and Hyperbolic functions along $\hat{x}$ and $\hat{y}$ respectively (see (5.7,8,9),[42]).

According to these definitions, for the transition from a very narrow fin-line with $w \simeq 0.08a, Z \simeq 50\Omega$ to a rectangular waveguide with $w = a, Z \simeq 450\Omega$, we have obtained the Z profile given in Fig. 5.9 .

It shows an almost linear behaviour for the real part of Z except near the tips and an imaginary part about one order of magnitude lower than the real one. The imaginary part is positive by the acute tip and negative by the obtuse one, so that there always exists an intermediate point where the taper mode impedance is almost real: it is used sometimes to introduce matching elements .

To this profile of impedance we can associate the non-uniform line shown earlier in Fig. 5.3 . In accordance with lines convention, we introduce the coordinate ℓ with origin on the load corresponding to the 2^{nd} uniform fin-line.

The reflection coefficient Γ relative to an incident wave proceeding from section 1 satisfies along the line the well known Riccati's equation :

$$\frac{d\Gamma}{d\ell} + 2\gamma\Gamma + \frac{1}{2}(1 - \Gamma^2)\frac{d(lnZ)}{d\ell} = 0 \tag{5.55}$$

with the only b.c. $\Gamma(0) = 0$ pertaining to a matched termination .

The problem has been solved numerically according to the procedure indicated in [37] that expresses all the functions involved in Chebyschev series so as to reduce all integrations to finite sums . The difficulty is presented by the

interpolation of $Z(\ell)$ or rather of $\frac{\dot{Z}}{Z} = \frac{d(ln(Z))}{d\ell}$ because of the large values of the derivatives of both the imaginary and real parts near the tips (see Fig. 5.9) .

$|\Gamma|$ is reported in Fig. 5.9 where the usual oscillating behaviour with increasing maxima is recovered . The novelty is represented by the fact the minima are no longer 0 due to the presence of the imaginary part of Z.

In order to obtain the taper length that realizes the minimum input reflection coefficient, we compute the scattering parameter $S_{11} = \Gamma$ for discrete values of the physical length T of the taper as reported in Fig. 5.10 .

In accordance to previous works (see [31] for an overview), the length which realises minimum reflection is $T \simeq 18mm$, that is $\simeq 0.57\lambda_0 \simeq \frac{\lambda}{2}$. In fact, the wavelength in guide λ is not too different from that in vacuo λ_0, which at the midband frequency considered is $30mm$. The successive minima in the curve of [31] are located at about multiples of half a wavelength due to the analytical properties of the Riccati's equation itself and to the given impedance profile, as rigourously shown in [26] .

For comparison, analogous curves are obtained for a smaller impedance step of ratio 3:1 . Here we pass from a fin-line width $w \simeq 0.16a$ with $Z \simeq 100\Omega$ to $w \simeq 0.66a$, $Z \simeq 300\Omega$. The situation is reported in Fig. 5.11, that shows how the first minimum of reflection is below 0.1 as generally required in applications . By comparison, a similar attenuation in the previous case of ratio 9:1 is reached at the second or third minimum, that is to say, with a taper length at least double.

Finally we observe that the two Fig. 5.10,11 are not reliable for very short tapers . Roughly speaking, they are those with aperture at A $\sigma < 100^0$
(see Fig. 5.2) but, as said before, these values are enough removed from the first minimum which is the shortest length of practical interest .

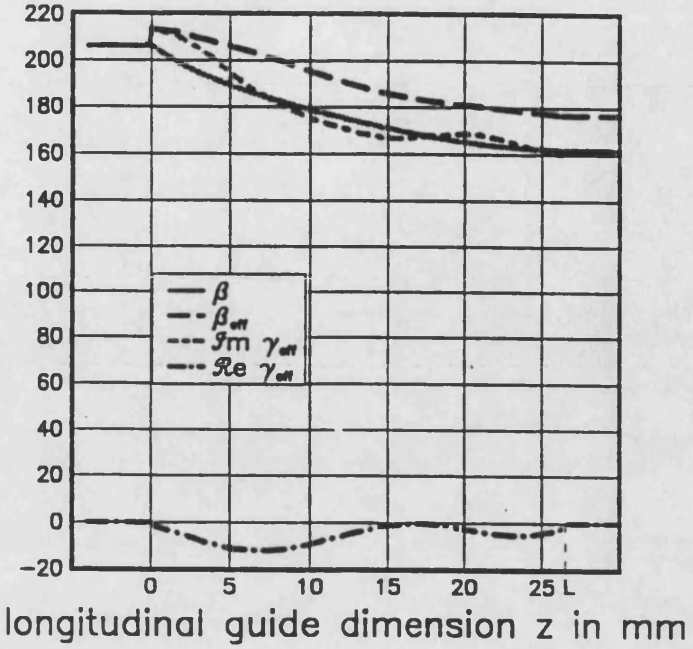

Fig. 5. 8 : β_{err} and γ_{err} compared with β

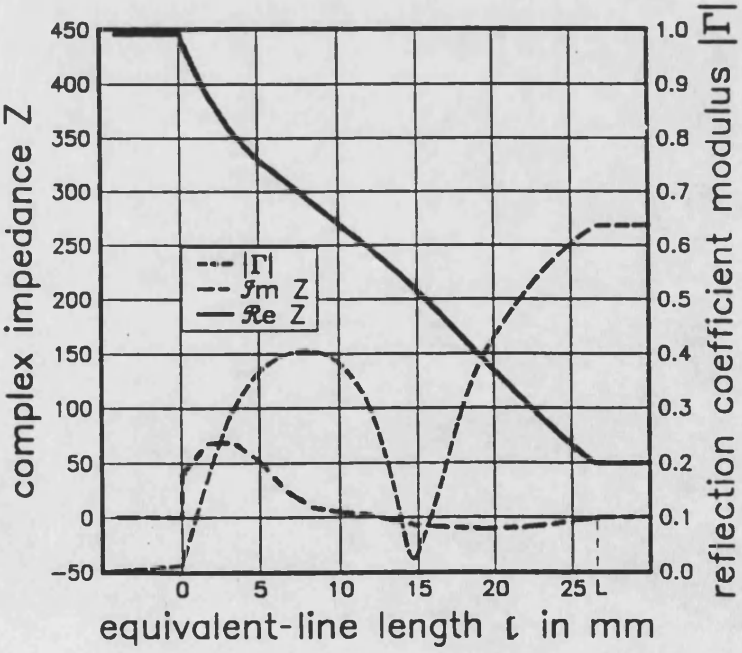

Fig. 5. 9 : Z and |Γ| profiles along the line

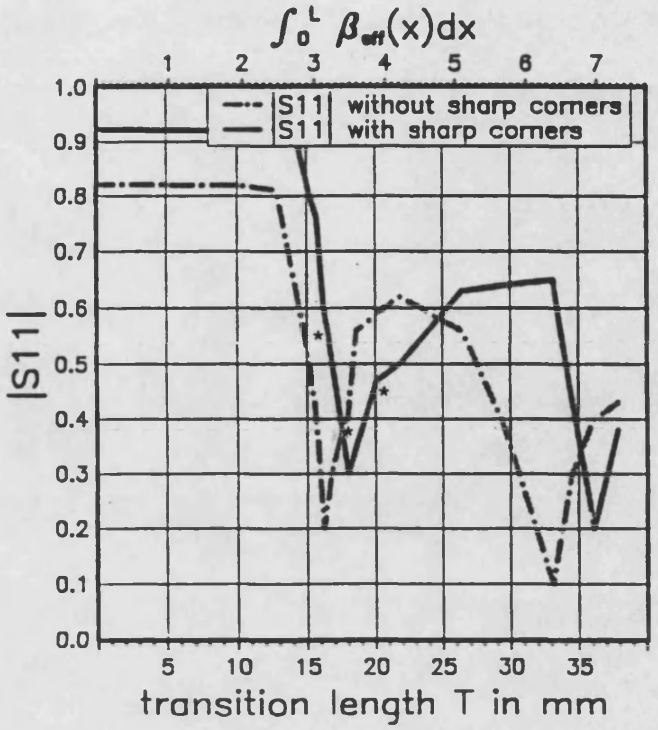

Fig. 5.10 : $|S_{11}|$ at an impedance ratio 9:1

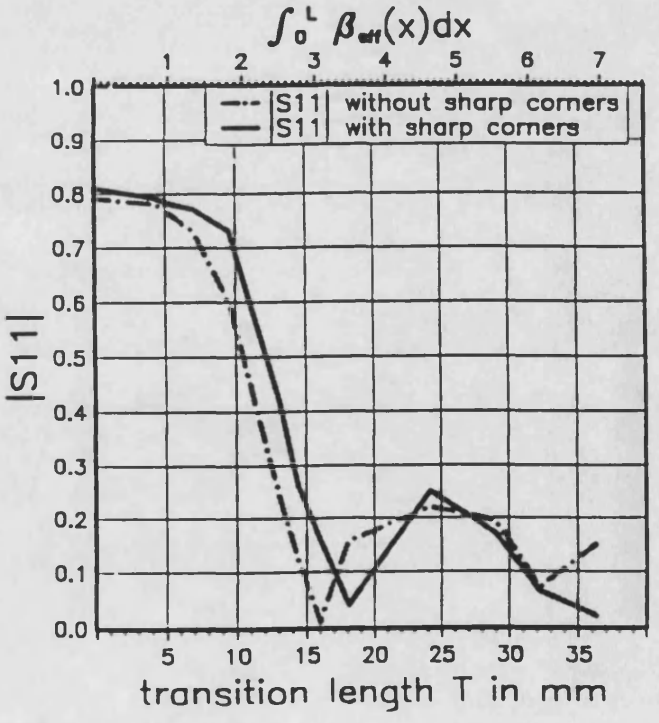

Fig. 5.11 : $|S_{11}|$ at an impedance ratio 3:1

5.6 Experimental results

Differences among authors arise not only about the best analysis technique but also about measurement techniques .

Generically speaking, there are two main ways to proceed .

i) The measurement equipment is calibrated in the medium of the device and then the standards (open, short, offset, match) have to be constructed, and which task presents difficulties when, as in our case, dealing with non standard transmission media .

ii) The measurement equipment is calibrated in the standard X-band rectangular waveguide and the transition to the fin-line medium is characterized in such a way as to perform de-embedding calculations .

Because of the less than perfect fin-line structure that can be manufactured in our laboratory, we follow the 2^{nd} way and carry out the measurement with the help of a HP8510 Network Analyser .

Recently, this matter has been treated in [41], where it is suggested to characterize the device under test by making use of two sets of back-to-back transitions separated by different, known, electrical lengths .

The printed conductor involved in the measurements in question is drawn in Fig. 5.12 where the two identical back-to-back transitions between narrow fin-line and rectangular waveguide are separated by a uniform line of length ℓ .

The " serrated choke " configuration shown in Fig. 5.12 realizes a virtual open circuit exactly at the plane where the box-wall is located : this avoids losses due to a parasitic TEM-mode propagating between the printed conductor and the casing itself because of the imperfect contact .

The analysis of the double transition may be made easier by making use of their transmission matrices and, the transitions being identical, the scattering matrix of the transition itself can be uniquely de-embedded by two measurements of the global S-matrix with different line lengths .

The dimensions of the two circuits and relative measurements of S_{11}, S_{12} for the complete circuit are reported in the Fig. 5.13,14 .

The two line lengths have been chosen so that the lines resonate at a frequency enough removed from 10GHz so as not to affect appreciately the global S-matrix parameters there .

To be precise, the electrical line lengths are about λ at the resonant frequency for S_{11} and their difference is about $\frac{\lambda}{4}$ at the frequency of 10GHz of our interest . This (see [41]) permits to minimize errors due to inaccurate electrical length datas, since in the formulae we need just their difference expressible in terms of the resonant frequencies .

If, in fact, we were considering the line length to be equal to ℓ, we would be wrong both because of measurement errors and because the uniform line is effectively shorter than the uniform segment due to 3D-wedge effects around the tips A, as observed in 5.5 .

The S_{12} values of the global S-matrix at 10GHz are then all we need in order to completely recover $S_{11} = \Gamma$ of the transition .

This procedure has been repeated for the three different taper lengths T= 16 mm, 18 mm, 21 mm so as to characterize well enough the more interesting region around the first minimum . The values obtained, indicated in Fig. 5.10 with an asterix, are in good agreement with the theoretical data .

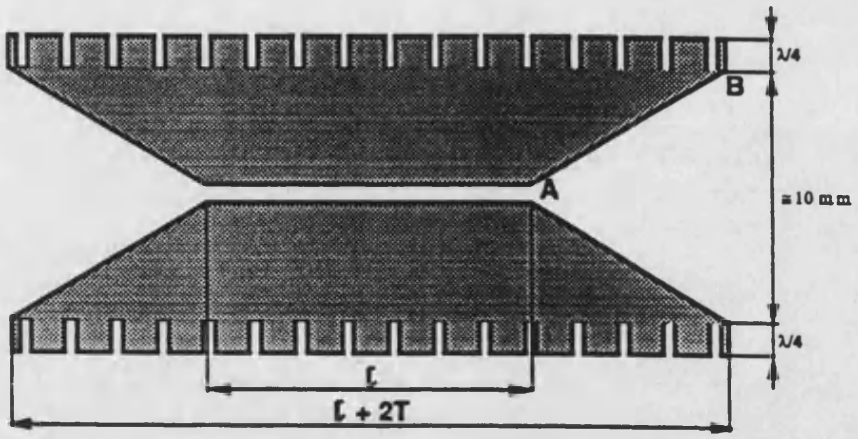

Fig. 5.12 : printed conductor for a linear transition between fin-line and rectangular waveguide

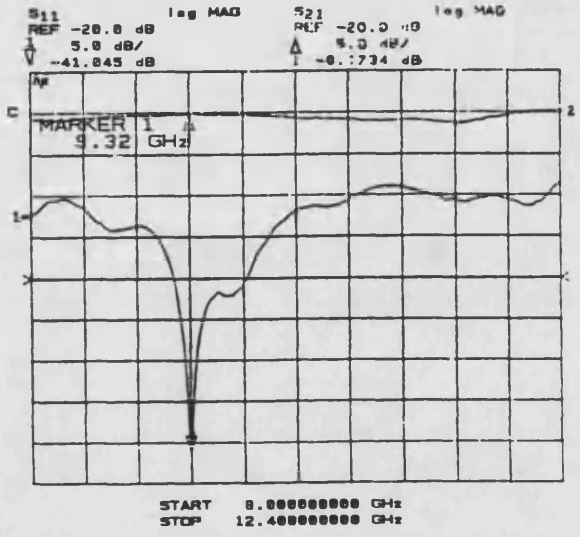

Fig. 5.13 : printed conductor dimensions ℓ = 25 mm, T = 21 mm

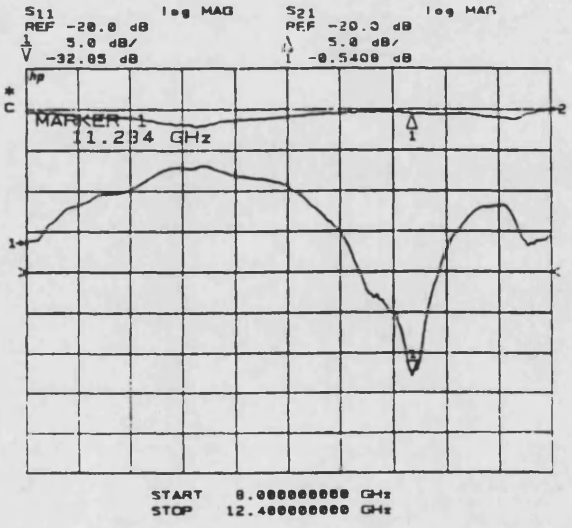

Fig. 5.14 : printed conductor dimensions ℓ = 32 mm, T = 21 mm

5.7 Physical considerations and optimization of a smooth profile

The analysis just concluded permits to look back at the effort gone on during these last 40 years on the synthesis of the " optimum smooth profile " giving a further physical explanation of the reflection in terms of concentrated and distribuited singularities .

This will allow us to devise new means in order to improve performance, i.e. decresing $|S_{11}|$ over a wider band and with a shorter taper length, that is to say, to approach the " optimum taper " .

It is noted that several workers in the field prefer to use shapes with abrupt steps, for instance the quarter wavelength taper, where the reduction of $|S11|$ in the broadband is obtained by introducing matching elements whose position and shape are determined in a quasi-empirical way .

In this work, we only consider a continuous changing profile on the basis of the results obtained from the analysis of the linear taper .

Commenting firstly on Fig. 5.8, we note a faster propagation of the taper mode with respect to the fundamental fin-line mode since $\beta_{eff} > \beta$. This implies a slight decrease of the physical length T necessary to obtain a given electric length indicated by $\int_0^L \beta_{eff}(x)dx$ in Fig. 5.10,11 .

More significant is the presence of a real part of γ_{eff}, representing the reactive attenuation associated to the higher order modes excited and decaying in any section of the non uniform guide so as required for the EM fields in order to satisfy the b.c. there . This effect is responsible for the imaginary part of the equivalent impedance shown in Fig. 5.9 : it shows a dominant capacitive

behaviour at the acute tip and around it and an inductive behaviour at the obtuse tip and around it . From the point of view of the fields, and, in particular, of their distributed singularities, this can be understood noting that there is an increment of charge density in A and of current density in B, as stated in Chapters 2,3 .

Commenting instead Fig. 5.10, we may argue that the steepness of the curve of $|S_{11}|$ around the first minimum indicates that reflection changes fast with frequency, so that the linear taper is only suitable for a narrow band .

Using this information in the context of the general problem of optimization of the profile, we consider two main ways to improve taper performance .

5.7.1 Compensation of the reactance of the two tips

A first attempt to estimate the reflection due to the tips consists in imposing a vanishing derivative in the algorithm interpolating the curve $Z(z)$ at the tips . This yelds the 2^{nd} curves in Fig. 5.10,11, showing appreciably lower minima of $|S_{11}|$ and of taper length than the accurate values .

All profiles without cusps in A and B present vanishing derivatives of the curve $Z(z)$ there but the exact $|S_{11}|$ for the whole taper is dependent on the specific shape of the conductor replacing the tips . For this reason, we do not synthesize any particular conductor profile and we assume that a quantitative approximation of the reflection due to the 3D-wedges A and B is given by the difference between the two minima in Fig. 5.10,11 .

A first practical form of compensation consists in inserting an inductive step in correspondence of the acute corner and a capacitive one at the obtuse one . Unfortunately, their forms and positions have to be optimized empirically

because of the just observed problem of quantifying and localizing the reflection due to the tips .

To this method is perhaps preferable just to cut the sharp edges off by replacing each of them with two corners of angular aperture closer to 180^0, which, as seen in Chapters 2,3, present the same electric and magnetic singularities and intrinsic self-compensating properties .

5.7.2 Design of more general taper profiles

Perhaps the more serious limitation to compensation techniques is due to bandwidth . For this reason Klopfestein in [39] presented an extension of the theory by Collin [27] dealing with optimum cascaded step transformers . He noted that, by allowing the number of sections to increase indefinitely for a fixed over-all length, Collin's result can be extended to the case of a continuous transmission line taper, possibly maintaining small abrupt steps at each end .

This way, the Dolph-Chebyschev profile, with possibly a small impedance step at the ends, produces the minimum reflection coefficient magnitude in the pass band for a specific length of the taper, and likewise, for a given maximum reflection in the pass band, it has minimum length .

The small impedance steps at the ends consist of small steps in the conductor profile, each containing a pair of corners of about 90^0 and 270^0, so that the two complementary effects are localised in a small region producing in fact self-compensation .

Unfortunately, when we actually synthesize these steps, performance decays because higher order mode are excited there which do not allow realization of a pure real impedance step .

In order to avoid this problem, Hecken [38] suggested to substitute the two small steps by two small arcs of exponential lines . This change produces a small but definite increase in the taper length for a given bandwidth and does not completely solve the problem of synthesis .

For all these reasons, in more recent years, workers directed their efforts towards the analysis and synthesis of continuously changing profiles like the exponential, cosine square, circular and others . Renouncing to the optimum performance stated by Klopfestein, they find, more or less empirically, that the best profile is the one that follows a law similar to that of the impedance (see [31] p. 279) .

The exponential line presents the best performance (see [31] p. 274) even though it is somewhat reduced by too abrupt an end at the final section, so that other devices such as quarter wave transformer using notches or protusions in the dielectric need to be employed (see [31] pp. 283) . Other solutions are the double exponential and the double circular taper where two arcs of the same curve but with opposite concavities are connected in order to avoid altogether a discontinuity of the tangent of the curve .

In this search for the best profile, our analysis aims to give analytic justification of the profiles above discussed suggesting, at the same time, an additional shape .

5.8 A new approach to synthesis

Recent developments in CAD programmes allow us the freedom to design any required profile given either analytically or by interpolation between points of a given set .

From the foregoing analysis, we may argue that the profile with minimum reflection is the one with the smoothest f and the smoothest and minima real part of γ_{eff} and imaginary part of Z .

Similarly to what happens along uniform sections, i.e. where γ is constant, this condition can be expressed by saying that γ_{eff} ought to assume a constant complex value :

$$C = a + jb \tag{5.56}$$

Unfortunately, this is too strong a requirement because under the hypothesis of validity of (5.5) and because of the (5.5) itself, (5.56) can be shown to imply $\gamma = C$, which is against the hypothesis of nonuniform line .

For the same reasons, but under weaker conditions, we may require in (5.13):

$$\frac{d}{dz} ln(f(z)) = \frac{\dot{f}}{f} = C \tag{5.57}$$

On the other hand, (5.5) can be reduced to a non-linear differential equation in just $\frac{\dot{f}}{f}$ as :

$$\frac{d}{dz}(\frac{\dot{f}}{f}) + (\frac{\dot{f}}{f})^2 - 2(\frac{\dot{f}}{f})(\dot{\gamma}z + \gamma) - [\ddot{\gamma}z + 2\dot{\gamma} + \gamma^2 - (\dot{\gamma}z + \gamma)^2] = 0 \tag{5.58}$$

which, using (5.57), can be turned into a 2^{nd} degree ordinary differential equation in γ and relative b.c. :

$$\ddot{\gamma} + (\dot{\gamma}z)^2 + 2\dot{\gamma}(\gamma z + Cz - 1) + 2\gamma C = C^2 \tag{5.59}$$

$$\gamma = \gamma_1 \text{ when } z < 0 \qquad \gamma = \gamma_2 \text{ when } z > T \tag{5.60}$$

An approximate numerical solution to this problem is always possible and it provides a function of z with parameters T,C :

$$\gamma = \gamma(z; T, C) \tag{5.61}$$

Nevertheless, the dispersion characteristics :

$$\gamma = \gamma[w(z)] \tag{5.62}$$

can be found independently from (5.35), so that from the system (5.61,62) we can synthesize, at least numerically, the profile :

$$w(z; T, C) \tag{5.63}$$

The length T and the constant C are determined so as to satisfy the given attenuation requirement in the band with minimum T .

Remarkably, the family of curves (5.63) is determinable without using Riccati's equation, having been deduced from just the waveguide properties .

An approximate analytical form of (5.63) is possible in the reasonable hypothesis, already observed for the linear profile, that the imaginary part of f

presents a behaviour almost equal to that of the conductor profile .

In fact, in this hypothesis, noting that the solution of (5.57) is of the form :

$$f \propto e^{Cz} \tag{5.64}$$

we set :

$$w(z') = \mathcal{D}e^{az'}cos(bz') + \frac{\mathcal{E}}{2} \qquad \text{or } (\mathcal{F}e^{az'}sin(bz') + \frac{\mathcal{G}}{2}) \tag{5.65}$$

where $z' = z + z_0'$ and $\mathcal{D}, \mathcal{E}, \mathcal{F}, \mathcal{G}, z_0, a, b$ are constant design parameters .

The length T is chosen in such a way that the curve has vanishing derivative at A and B so that no cusps are present in the taper .

The points of vanishing derivative are found to be :

$$\bar{z}' = \frac{1}{b}arctg(\frac{a}{b}) \tag{5.66}$$

Thus they are a numerable infinity because of the indetermination of $n\pi$ of the arctg .

At these extremants, the 2^{nd} derivative of $w(z')$ is shown to be given by :

$$-(a^2 + b^2)cos(b\bar{z}') \tag{5.67}$$

and we may limit attention to the pair contained in each period of the *cos* function, since at the smaller point of the two the concavity is positive whereas at the other is negative, so as required when we pass from an aperture w_1 to one $w_2 > w_1$.

For instance, if we indicate by z_0' the smallest negative solution of (5.66), the two solutions in question are given by :

$$z_0' = \frac{1}{b} arctg(\frac{a}{b}), \qquad z_1' = \frac{1}{b} arctg(\frac{a}{b}) + \frac{\pi}{b} \tag{5.68}$$

Hence the length T is given by :

$$T = z_1' - z_0' = \frac{\pi}{b} \tag{5.69}$$

This shows that the constants T and b are in fact unique .

The constants $\mathcal{D}, \mathcal{E}$ are determined by forcing the curve to fit the points $w(z' - z_0) = w(0) = w_1$ and $w(T) = w_2$ that is to say :

$$\mathcal{E} = -\frac{w_2}{w_1} \frac{1}{e^{\frac{a}{b}\pi}(1 - e^{\frac{a}{b}\pi})} \qquad \mathcal{D} = \frac{w_1 - \mathcal{E}}{2e^{az_0'} cos(bz_0')} \tag{5.70}$$

Hence, just the two parameters T and a remain available for optimization in respect to reflection and bandwidth .

Relaxing the condition (5.69), b also remains free, but then at least at one end there is a cusp with all that is implied by diffraction produced there .

In conclusion, we have derived a novel conductor profile for a " quasi optimum smooth taper " introducing the shape (5.65), that is to say the product of an exponential times a cosinusoidal function which has never been considered in previous works, restricted to the simpler double-exponential or double-circular profiles . This includes the properties of the exponential taper by the tip A and those of the circular one by B while avoiding the presence of cusps along all its length .

The matter has been discussed in [45] . The rigorous implementation of the system (5.61,62) to synthesize pointwise the profile (5.63) is left for further work.

5.9 Conclusions

In this Chapter, we found that the dielectric support of the planar circuit does not influence the singularity vectors .

The exact fitting of the boundary conditions pertaining to non uniform lines has permitted a novel general modal analysis .

We have analysed theoretically and experimentally a linear taper in fin-line and found that the 3D-wedge influences only within 1% the value of β but much more those of $\dot{\beta}$ and $\ddot{\beta}$.

Furthermore, the classical problem of the synthesis of the " optimum smooth profile " has been reconsidered in the light of a novel algorithm and a new smooth profile of higher degree has been suggested .

Chapter 6

APPLICATION TO THE ANALYSIS OF PLANAR CIRCUIT COMPONENTS

6.1 Introduction

This Chapter shows how the EM fields singularity vectors enters the algorithms more usually implemented in the analysis of Microwave Integrated Circuits (MIC).

Algorithms like the " Mode Matching Technique " and the " Moment Method " require an unknown "trial field" at particular surfaces like that normal to the printed conductor or that of the conductor itself.

Until now the "trial field" has been formulated by series of simple functions which, however, suffer from convergence problems when they are asked to represent the singularities at tips or wedges . However, the exact formulation of the latter given in Chapters 2,3, now allow us to know "a priori" the singular

behaviour of the unknown field .

Consequently, we suggest a more physical way to formulate "trial fields" $\vec{\mathcal{E}}$ and $\vec{\mathcal{H}}$, e.g. by multiplying dyadically (i.e. vector component times vector component) the $\vec{s_e}, \vec{s_h}$ singularity vectors pertaining to the printed conductor times the $\vec{E}, \vec{H}$ fields pertaining to the structure without it .

$\vec{E}$ and $\vec{H}$ are often determinable rigorously and easily because they satisfy the b.c. pertaining to an easy geometry of the EM environment (see loaded rectangular waveguide, etc ...) while $\vec{s_e}, \vec{s_h}$ confer to the resulting $\vec{\mathcal{E}}, \vec{\mathcal{H}}$ also exact satisfaction of the b.c. on the printed conductor, thus providing a "trial field" as similar as possible to the true unknown one .

Specifically, following the general purposes of Chapter 5, we consider the use of the above formulated "trial field" in the analysis of some fundamental planar circuit configurations . We will start by considering an abrupt step in strip-line or fin-line by means of the " Variational Approach ", and proceed to study a situation where more than two $90^0, 270^0$ sectors are involved . This requires the introduction of the concept of global singularity function in a case of application of " Transverse Resonance Approach " . The Chapter ends with some remarks on the problem of a rectangular patch antenna where the " Moment Method " is involved .

Particularly important are the main $90^0, 270^0$ sectors and their singularity vector projections on the main planes, including the conductor itself where the nonvanishing fields components become proportionals to the density of charge and current as announced in Chapters 2,3 .

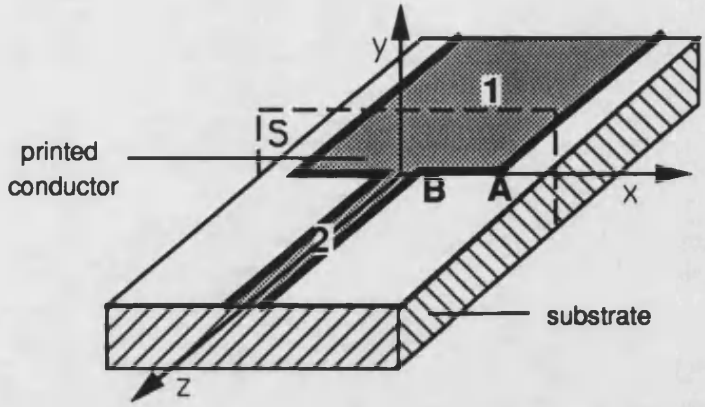

Fig . 6.1 : abrupt step in strip-line

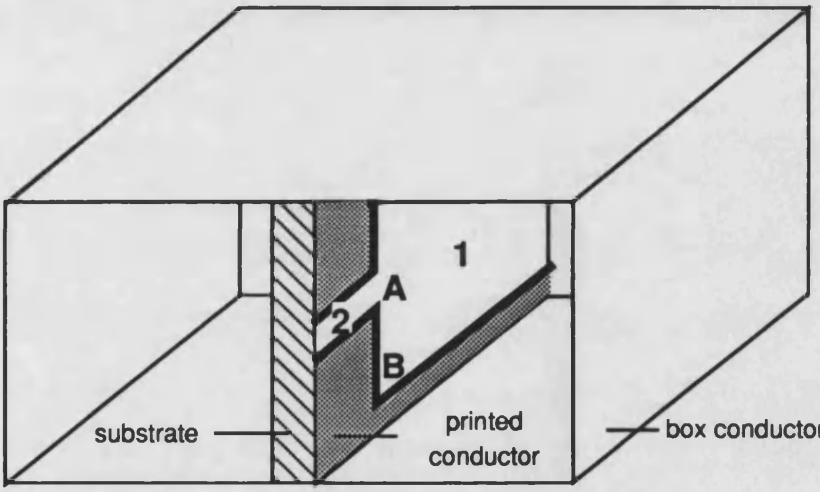

Fig. 6.2 : abrupt step in unilateral fin-line

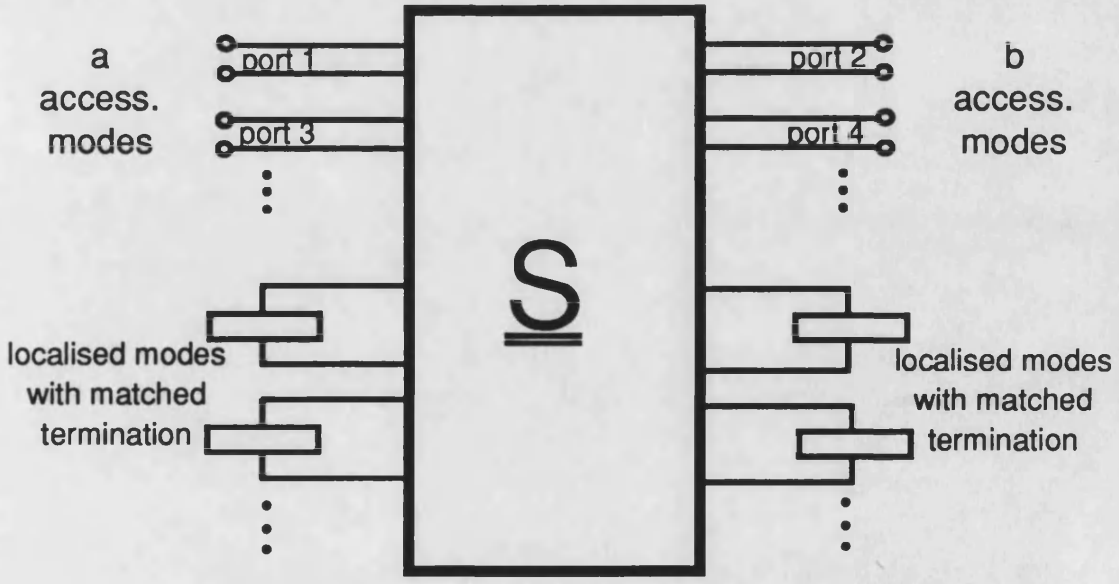

Fig. 6.3 : equivalent network model

6.2 Application of the quarter and three-quarter plane singularity vectors on the plane normal to the conductor

Currently used Microwave Integrated Circuit configurations, such as strip-line and fin-line, make use of abrupt discontinuities as schematically shown in Fig. 6.1,2 where a 90^0-wedge A and a 270^0-wedge B are linked together .

Several passive circuit components such as stepped impedance transformers, filters, mixers, patch antennas etc ..., are manufactured by connections of these two elementary wedges in the form of cascaded transmission lines .

Development and manufacturing costs of these circuit components could be greately reduced if simple and accurate equivalent circuits or network were available for them, as shown for instance in Fig. 6.3 .

Analysis methods such as the simple quasi-static CAD techniques are limited in validity as frequency increases . On the other hand, the numerical efficiency of rigorous, more expensive analyses approaches such as the " Variational Method " (see [32, 33]) may be enhanced by knowing "a priori" the E-field behaviour around the conductor wedges and, in particular, that of its singularity distribuited along the contour .

From a physical point of view, we can think in terms of incident fields constituted by "a" propagating modes in region 1 to the left of the discontinuous cross section S and "b" propagating modes in region 2 to its right . These modes diffract at the discontinuity exciting higher order modes in such a way to satisfy the b.c., in particular, producing on the tips A and B the EM fields singularities

discussed in Chapter 2,3 .

The discontinuity can be represented with the equivalent network model of Fig. 6.3 characterized by its equivalent scattering matrix $\underline{\underline{S}}$.

If we use for the inner product the formalism :

$$< \vec{E}, \vec{H} >= \int\int_S \vec{E} \text{ x } \vec{H} \cdot \hat{z} dS \tag{6.1}$$

the scattering matrix elements S_{ik} can be computed as in [32] .

$$R_{ik} = \frac{< \vec{\mathcal{E}}, \underline{\underline{G}}, \vec{\mathcal{E}} >}{< \vec{\mathcal{E}}, \vec{H}_i^{(1)} >< \vec{\mathcal{E}}, \vec{H}_k^{(1)} >} \tag{6.2}$$

where $\underline{\underline{G}}$ is a dyadic Green operator for scattering depending exclusively on the complete spectrum in the regions 1 and 2, $\vec{H}_i, \vec{H}_k$ are the magnetic fields associated to the i^{th}, k^{th} mode in either regions 1 or 2 and $\vec{\mathcal{E}}$ is the unknown electric field at the cross-section S .

R_{ik} is then related to the scattering matrix elements simply by :

$$R_{ik} = \begin{cases} \frac{1}{S_{ik}-\delta_{ik}} & i \leq a \\ \frac{1}{S_{ik}} & i > a \end{cases} \qquad \text{where : } \delta_{ik} = \begin{cases} 1 & i = k \\ 0 & i \neq k \end{cases} \tag{6.3}$$

A previously used expression for the unknown $\vec{\mathcal{E}}$ is given by :

$$\vec{\mathcal{E}} = \sum_n c_n \vec{e}_n(x, y) \tag{6.4}$$

where $\vec{e}_n$ is the electric field of the n^{th} mode in one of the two uniform sections

or in a virtual uniform section with strip or fin conductor width intermediate between those in the regions 1 and 2 .

In any case, modes of the input and output guides present a singularity of degree $-\frac{1}{2}$ or of a finite value in A and B respectively so that, at least theoretically, we need an infinity of them in order to realize the correct degrees of singularity at the tips .

Thanks to the fact that (6.4) enters the scattering matrix only under the integral sign, in practice, only a few c_n coefficients need to be computed when using variational techniques (see [32]) .

However, the knowledge of the singularity vector $\vec{s}_e$ permits now to express the field on S in a different way, namely :

$$\vec{\mathcal{E}} = (s^G_{e_x}\hat{x}\hat{x} + s^G_{e_y}\hat{y}\hat{y}) \cdot \sum_{n=1}^{\infty} c_n \vec{E}_n(x,y) \tag{6.5}$$

where the $\vec{E}_n$ are the modes of just the slab-loaded waveguide, easier computable than $\vec{e}_n$ as they do not include the printed conductor . $\vec{s}^G_e$ is the global singularity vector on the cross-section S, that can be obtained from those relative to the single wedges A and B by a matching procedure .

We can identify essentially 3 ways of matching the singularity forms relative to the 4 tips involved :

i) the forms relative to A and B determined in Chapter 2 are valid around the tips up to an arbitrary abscissa $\frac{\epsilon}{2}$ as reported in Fig. 6.4,5 and Tables 6.1,2 for the strip-line and fin-line respectively .

ii) With somewhat better physical motivation, the forms in Tables 6.1,2 are valid up to a distance r_{max} from the tips, dependent on the minimum λ involved, as indicated in the general remarks of Chapter 3 . The same forms are then set to a convenient constant value on the remainig part of the surface S .

iii) The two forms are matched along the locus where they assume the same values which, however, is determinable only numerically .

Thus, the global $\vec{s}_e^G$ is everywhere continuous only in the case (iii) while for the other two it is piecewise continuous, the only discontinuity being present in the matching line $x = \frac{c}{2}$.

In specific applications, for instance like in the integration (6.2), we choose between the above matching procedures the one that produces an overall $\vec{s}_e^G$, which contributes to the value of the integral almost exclusively because of its behaviour by the conductor and, in particular, that of its singularities .

Thus, in particular, if the position of the matching section $x = \frac{c}{2}$ or the value of the discontinuity that $\vec{s}_e^G$ presents there in cases (i) and (ii) is important, we must use the more expensive matching procedure (iii) .

Coming back to (6.5), we note that it satisfies exactly all the regular and singular b.c. on the cross section S . Further developments will be directed towards exploring how well $\vec{s}_e^G$ only represents the E-field in S .

A practical difficulty consists now in the integration of forms like :

$$a_i =< \vec{s}_e^G, \vec{H}_i >= \int\int_S (s_x^G H_{iy} - s_y^G H_{ix}) dS \qquad (6.6)$$

In the case of the 90^0-tip, in particular, each integrand shows a singularity of degree :

$$-0.703416 - 0.5 = -1.203416 < -1 \tag{6.7}$$

that is the sum of the electric and magnetic singularities associated to $\vec{s}^G$ and $\vec{H}$ respectively . Nevertheless, the difference of the two integrands is indeed integrable as can be shown by remembering that a_i assumes the physical meaning of excitation coefficient for the modal field component $\vec{H}_i$ by the source $\vec{\mathcal{E}}$-field on S (see also [47]) .

Once the integrability is so ensured, it remains to solve the problem of expressing $\vec{s}_e^G, \vec{H}_i$ in the more appropriate c.s. by the tips in order to investigate the possibility of an analytical solution .

Electric singularity vectors on the plane of an abrupt step in strip-line		
s_{e_x}	s_{e_y}	*range*
$\lvert y\rvert r_A^{\nu_A-2}$	$r_A^{\nu_A-1}$	$0 \leq x \leq \frac{d}{2}$
$\sqrt{\lvert y\rvert} r_A^{\nu_A-\frac{3}{2}}$	$\frac{r_A^{\nu_A-\frac{1}{2}}}{\sqrt{\lvert y\rvert}}$	$\frac{d}{2} < x \leq \frac{c}{2}$
$\sqrt{\lvert y\rvert} r_B^{\nu_B-\frac{3}{2}}$	$\frac{r_B^{\nu_B-\frac{1}{2}}}{\sqrt{\lvert y\rvert}}$	$\frac{c}{2} < x \leq \frac{w}{2}$
$r_B^{\nu_B-1}$	$r_B^{\nu_B-1}$	$\frac{w}{2} < x \leq \frac{a}{2}$

Table 6.1: Referred to the abrupt strip-line of Fig. 6.4

With :

$$\nu_A = 0.296884, \nu_B = 0.814655, r_A = \sqrt{(x-\tfrac{w}{2})^2 + y^2}, r_B = \sqrt{(x-\tfrac{d}{2})^2 + y^2}$$

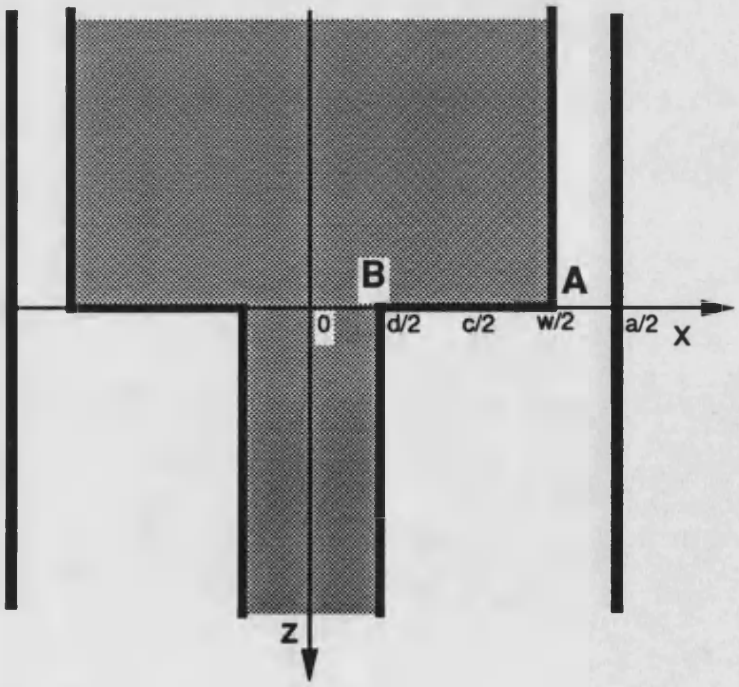

Fig. 6.4 : geometry of the abrupt step in strip-line

Electric singularity vectors on the plane of an abrupt step in fin-line		
s_{e_x}	s_{e_y}	*range*
$r_A^{\nu_A-1}$	$r_A^{\nu_A-1}$	$0 \leq x \leq \frac{d}{2}$
$\sqrt{\lvert y\rvert}r_A^{\nu_A-\frac{3}{2}}$	$\frac{r_A^{\nu_A-\frac{1}{2}}}{\sqrt{\lvert y\rvert}}$	$\frac{d}{2} < x \leq \frac{c}{2}$
$\sqrt{\lvert y\rvert}r_B^{\nu_B-\frac{3}{2}}$	$\frac{r_B^{\nu_B-\frac{1}{2}}}{\sqrt{\lvert y\rvert}}$	$\frac{c}{2} < x \leq \frac{w}{2}$
$\lvert y\rvert r_B^{\nu_B-2}$	$r_B^{\nu_B-1}$	$\frac{w}{2} < x \leq \frac{a}{2}$

Table 6.2: Referred to the abrupt fin-line of Fig. 6.5

With :

$$\nu_A = 0.296884, \nu_B = 0.814655, r_A = \sqrt{(x-\tfrac{d}{2})^2+y^2}, r_B = \sqrt{(x-\tfrac{w}{2})^2+y^2}$$

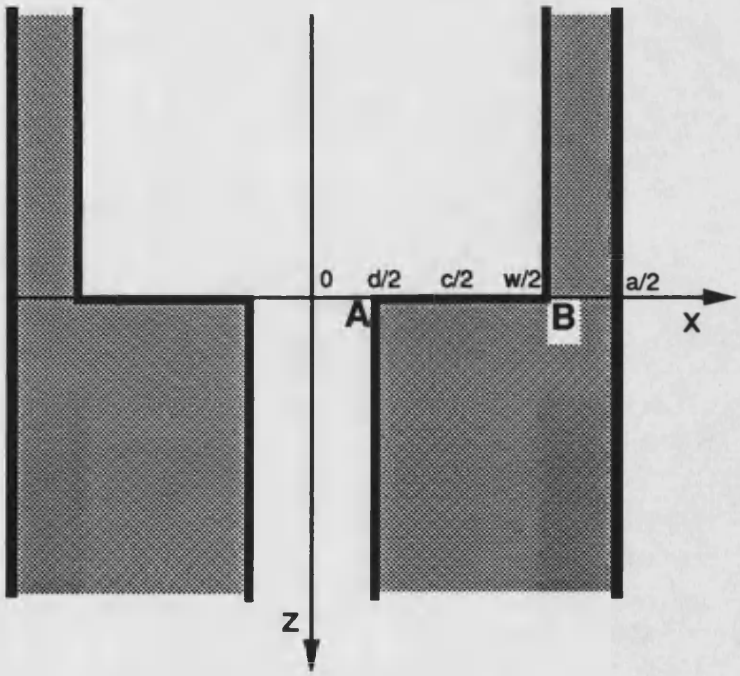

Fig. 6.5 : geometry of the abrupt step in fin-line

6.3 Application of the quarter and three-quarter plane singularity vectors on the plane of the conductor

Moving along the outline of the previous paragraph, we can now consider a situation where the matching surface for the modes incident from the uniform regions is located on the plane of the printed conductor itself .

In order to fix the ideas, we make reference to an inductive notch in bilateral fin-line which cross and longitudinal sections are drawn in Fig. 6.6,7 . Nevertheless, the following can be easily extended to arbitrary conductor shapes as indicated in [34] .

The fin-line is short-circuited at given distances ℓ_1, ℓ_2 away from the abrupt discontinuities so as to realise a resonator of length ℓ .

Looking transversally, the EM fields can be thought as the superposition of the usual TE and TM modes in a loaded rectangular waveguide of inner dimensions ℓ x a , i.e. satisfying the regular b.c. pertaining to the box conductor and the two air-dielectric interfaces .

We suppose that the dominat modes only are propagating along $\hat{y}$, or better resonating, but when the printed conductor is introduced transversally to the propagating direction, they diffract on it exciting higher order modes so as to satisfy the new b.c. and, in particular, the singular ones at the $90^0, 270^0$ tips like A and B respectively .

Circuitally speaking, the discontinuity can be characterized by a two ports of impedance matrix $\underline{\underline{Z}}$ closed on two short-circuited lines with the known char-

acteristic impedance of the two uniform fin-lines to the left and to the right of the discontinuity as depicted in Fig. 6.8 .

For a given resonant frequency ω_r and positioning the short-circuits at the distances ℓ_1, ℓ_2 away from the discontinuity, the resonance condition of the equivalent network is expressible as :

$$(Z_{11} + Z_1)(Z_{22} + Z_2) - Z_{12}^2 = 0 \tag{6.8}$$

where, from line theory, it is simply :

$$Z_i = jZ_{0i}tg(\beta_i \ell_i) \qquad \text{for } i = 1,2 \tag{6.9}$$

and β_i is the modal propagation constant .

The condition for nontrivial solutions for (6.8) can be expressed as :

$$f(\omega_r, \ell_1, \ell_2) = 0 \tag{6.10}$$

The latter permits to determine by means of three successive experiments three pairs of lengths ℓ_1, ℓ_2 which substituted in (6.8,9), yield the three independent parameters Z_{11}, Z_{12}, Z_{22} .

Condition (6.8) is obtained from the application of the b.c. pertaining to the conductor, which in [34] have been chosen of the forms :

$$\mathcal{E}_{t_1} = \mathcal{E}_{t_2} = \mathcal{E}_{t_0} = \sum_i V_i \vec{e}_i \qquad \mathcal{H}_{t_1} = \mathcal{H}_{t_2} = \mathcal{H}_{t_0} = \sum_k I_k \vec{h}_k \tag{6.11}$$

on the aperture surface S_0: $\vec{\mathcal{E}}_{t_{0,1,2}}$ are the tangential components of the electric field on the interface air-dielectric, on its right and on its left respectively and analogously for $\vec{\mathcal{H}}$, while $\vec{e}$ and $\vec{h}$ are defined in the following .

This approach makes use of classical stepped waveguide modes $\vec{e}_i, \vec{h}_k$ orthogonal over S_0 . Their expressions are not easy to handle even for relatively simple geometries of S_0 .

Furthemore, the vectors $\vec{e}_i, \vec{h}_k$ so determined do not satisfy the 3D-wedges singularities on tips like A and B . Consequently, we need to consider quite a few coefficients V_i, I_k in (6.11) and in the non trivial solution (6.10) . Modal couplings are expressed as integrals of the type :

$$\int_{S_0} \vec{E}_{t_{jm}} \cdot \vec{e}_i dS \qquad \int_{S_0} \vec{H}_{t_{jm}} \cdot \vec{h}_k dS \tag{6.12}$$

where $\vec{E}_{t_{jm}}, \vec{H}_{t_{jm}}$ are the components tangential at S_0 of the modal fields of the rectangular waveguide ℓxa .

In this context, we suggest instead to express the b.c. equivalent to (6.11) in the form :

$$\begin{aligned} \mathcal{E}_{t_1} = \mathcal{E}_{t_2} = \mathcal{E}_{t_0} &= (s^G_{e_x}\hat{x}\hat{x} + s^G_{e_z}\hat{z}\hat{z}) \cdot \sum_{i,k} V_{ik}\vec{E}_{t_{ik}} \\ \mathcal{H}_{n_1} = \mathcal{H}_{n_2} = \mathcal{H}_{n_0} &= (s^G_{h_y}\hat{y}\hat{y}) \cdot \sum_{i,k} I_{ik}\vec{H}_{n_{ik}} \end{aligned} \tag{6.13}$$

where $\vec{E}_{t_{ik}}, \vec{H}_{n_{ik}}$ are the tangential electric and normal magnetic components of the waveguide modes respectively .

The first advantage of (6.13) consists in the fact that we can avoid the

determination of the espressions for $\vec{e}_i, \vec{h}_k$ whereas the waveguide modes are easier to handle .

The singularity vector components for the whole conductor are obtainable from the matching procedure indicated in the previous paragraph and the forms for just $s^G_{e_x}, s^G_{e_z}, s^G_{h_y}$ are reported piecewise in Fig. 6.9 for the chain of $90^0, 270^0$ corners (see also [48]) .

Because of the exact satisfaction of the regular and singular b.c. by these functions, further work will aim to exploit the possibility that they alone, possibly multiplied by the fundamental waveguide mode when the aperture is large in respect to the wavelength, need to be considered so as to reduce the non trivial condition (6.10) to finding the roots of just a single equation .

A practical difficulty, also in this case, will be caused by the integration of the forms (6.12) and further effort will be directed in obtaining maximum analyticity of the solution .

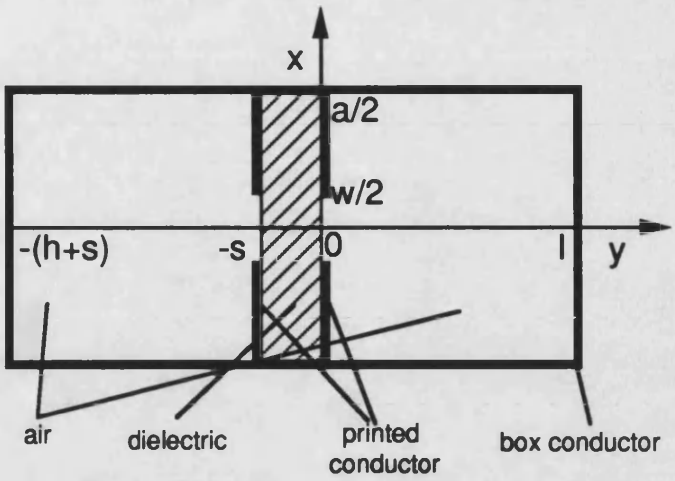

Fig. 6.6 : bilateral fin-line cross section

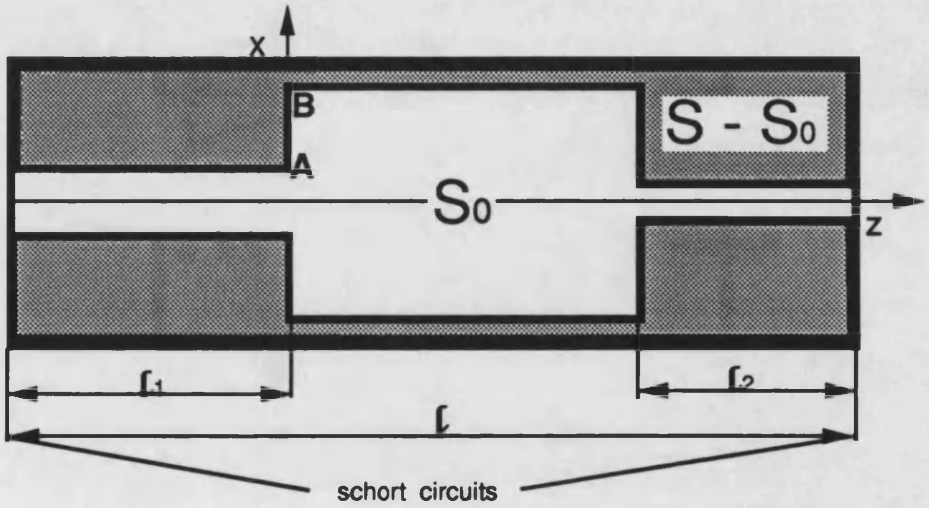

Fig. 6.7 : longitudinal section S on the plane y = 0

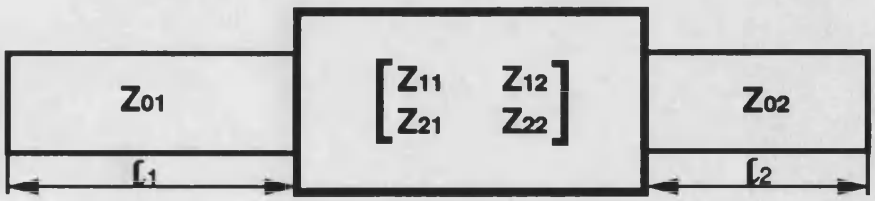

Fig. 6.8 : equivalent network model

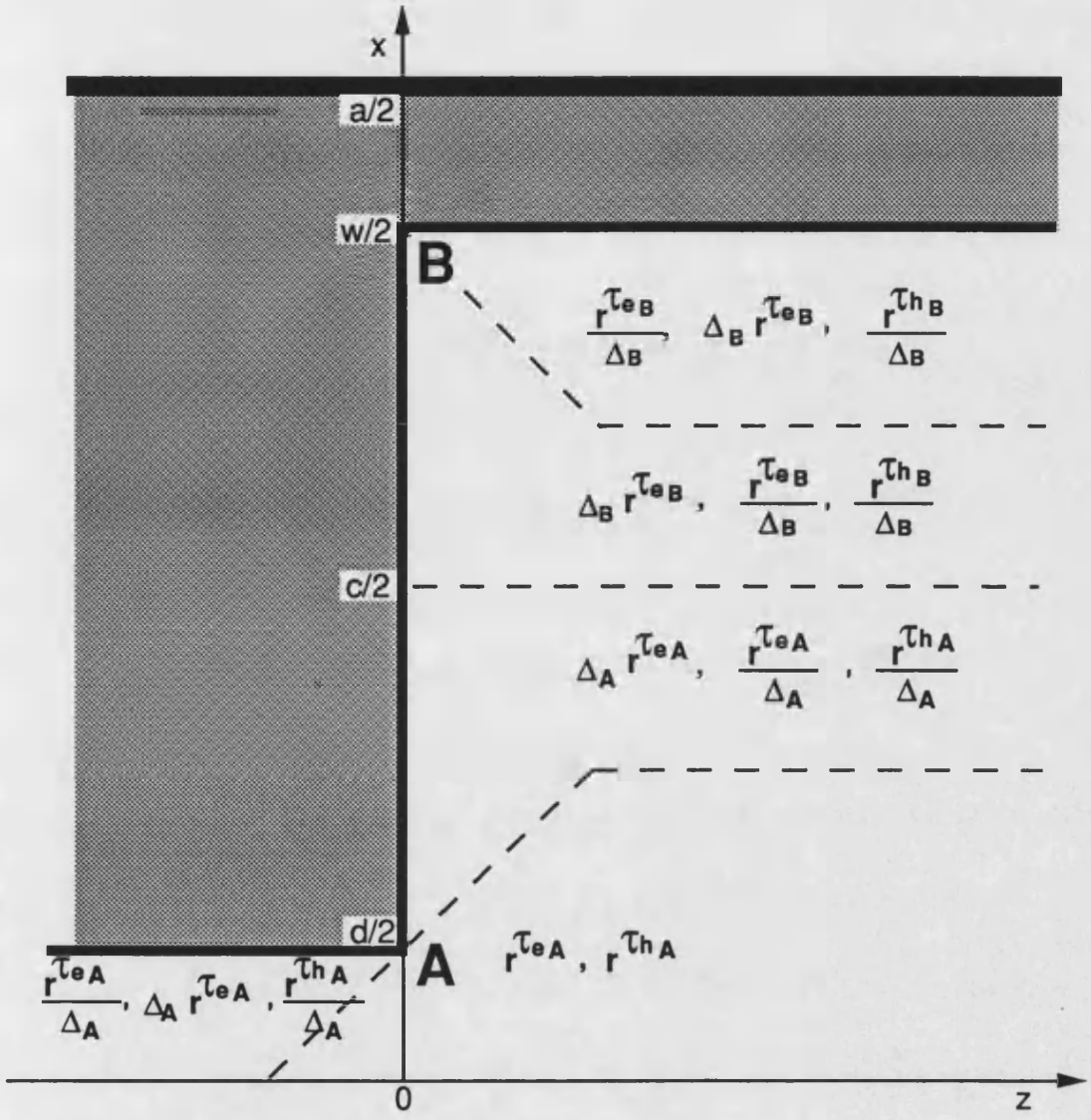

Fig. 6.9 : singularity vectors components on the plane of the conductor

The three expressions indicated in each sector of Fig. 6.9 represent the values of $s^G_{e_x}, s^G_{e_z}, s^G_{h_y}$ respectively and the symbols used there stand for :

$$\begin{array}{llll} \tau_{e_A} & = \nu_e(90^o) - 1 & = -0.703416 & = \tau_{h_B} \\ \tau_{e_B} & = \nu_e(270^o) - 1 & = -0.185343 & = \tau_{h_A} \\ x_A = x - \frac{d}{2} & \Delta_A = \sqrt{\frac{|x_A z|}{x_A^2 + z^2}} & x_B = x - \frac{w}{2} & \Delta_B = \sqrt{\frac{|x_B z|}{x_B^2 + z^2}} \end{array}$$

6.4 Application of the current and charge singularity vectors

A typical antenna problem requires the radiation pattern due to diffraction of a printed conductor which, also depending on the required polarization of the EM fields, may assume the shape of a rectangular patch or of an arbitrary polygonal.

A standard analysis method determines the fields from a scalar V and a vectorial $\vec{A}$ potentials which, in their turn, are expressible in terms of integrals of the corresponding Green's functions G, weighted by the unknown distributions of surface density of electric charge and current (see for instance [40]) as :

$$\vec{A}(\vec{r}) = \int_{S_0} \vec{G}_A(\vec{r}/\vec{r}') \cdot \vec{J}_S(\vec{r}')dS' \tag{6.14}$$

$$V(\vec{r}) = \int_{S_0} G_V(\vec{r}/\vec{r}')\rho_S(\vec{r}')dS' \tag{6.15}$$

These integrals are currently solved by applying the Moments Method . This effects a subdivision of the conductor surface S_0 according to a grate, often rectangular, each cell of which is identified by the vector $\vec{r}'$.

The unknown current $\vec{J}_S(\vec{r}')$ and charge $\rho_S(\vec{r}')$ pertaining to each cell are represented by a set of simple and everywhere continuous functions which satisfy some consistency conditions on the boundaries of contiguous cells .

Even though the number of representing functions is of fact reducible to 1 or 2 for cells belonging to regular conductor areas, things go differently for those belonging to the edges and tips since the singularities there cause serious problems of convergence .

The situation is remedied by decreasing the step size of the cells in proximity of the singular points . We suggest instead to change the representing functions or better to weight them with the projections of the singularity vectors on the conductor where they become proportional to the charge and current as indicated in 2.4.1 and 3.2 respectively .

In particular, the forms pertaining to the fundamental sectors can be recovered directly from Tables 2.3,4,5 and 3.3,4,5 for the charge and current respectively .

No problem of matching between singularity functions of contiguous wedges rise for the rectangular patch antenna, since the wedges are all of 90^0 aperture . Moreover, generalization to any angular aperture follows the lines of 2.6 and 3.6.

This way, the step size of the singular cells can again be equal to that of the regular cells, but the problem of convergence is turned into the integration of (6.14,15) where it appears a multiplicative weight function for $\vec{J}_S$ and ρ_S which is a known, singular but integrable function .

6.5 Conclusions

In this Chapter we have made some comments about the application to three commonly used algorithms in the analysis of planar circuits, of the exact knowledge of the EM fields singularities distributed along the edges or concentrated on the tip of the Printed Conductor .

Actually, a preliminary operation of matching of the singularity vectors relative to contiguous wedges is necessary in order to determine the global singularity vector for the whole Printed Conductor .

A global singularity function pertaining to the whole Printed Conductor permits the choice of a different and more physical formulation of the "trial field" on the aperture or "trial current and charge" on the conductor .

In this approach, the problem of the determination of the coefficients of a series representation, as for instance when using variational techniques, and of their convergence in correspondence of the tips is turned into the integration of the integrable singularity functions times a function finite everywhere .

Further work will be directed towards an analytic solution of this problem .

SUMMARY

The results obtained in this work are of utility in the analysis of circuitry involving Printed Conductors .

Conceptually speaking, we have ideally devided the EM environment of the circuit into the supporting structure and the Printed Conductor .

The EM fields pertaining to the supporting structure are completely and rigorously determinable by classic methods, like those of the Hertzian potentials, for instance .

From the point of view of the analysis, the Printed Conductor introduces, instead, new and somewhere singular vector boundary conditions for the fields in the existing environment .

The first three Chapters have dealt with the reduction of the named boundary conditions pertaining to sectors or double-sectors into singularity vectors of easy analytical form, by studying the solutions of the scalar and vector wave equations in the geometry of a conical coordinate system .

Several analytical simplifications due to the separability of the above equations in the conical geometry and to the special coordinate surfaces the boundary conditions pertain to, has permitted to single out very accurately the complete modal spectra of the wedges .

In particular we formulate exactly the singularity of the fundamental wedge mode distribuited along the edge and concentrated at the tip conductor .

The singularity vector we require is just its simplified form .

As a confirmation of the Babinet's Principle we have found, by an indipendent approach, that the EM-fields spectra pertaining to any plane sector are recoverable from those of just the E-field spectrum or H-field spectrum pertaining to any plane sector .

As a consequence of this, the H-field singularity vector pertaining to any sector is equal to the E-field singularity vector pertaining to the complementary sector, which in turn is just that of the static analysis .

Similar properties are established for the double sector .

The investigation of the EM singularities has been extended in Chapter 4 to 2D and Cone-wedges .

Even though these are analyzable in a spherical coordinate system, a unification of the theory of Chapters 1 to 4 has been possible, which also suggests some general conclusions about the charge and current singularities at the tips of a conductor of arbitrary shape .

A clear relation of inverse proportionality between degree of electric singularity and the maximum angle of aperture of the tip has appeared that affords insight into more irregular tip geometries .

Conversely, the vector density of current is related to the shape of the conductor at the tip rather than to the maximum angular aperture . As a consequence, more than one singularity may occur and a monotonic relation between degree of current singularity and maximum angle of aperture of the conductor is, in general, no longer possible .

Chapter 5 has dealt with the classic problem of tapers .

A more general method of analysis has been suggested by the exact knowledge of the distribuited singularities along the conductor edge and has permitted an estimation of the reflection due to the sharp corners .

A new "optimum" smooth taper profile has been suggested .

Finally, in Chapter 6 we have indicated how to match the singularity vectors pertaining to individual wedges to each other so as to determine a singularity vector for the whole Printed Conductor .

Their introduction in three typical algorithms for circuit component analysis is suggested .

Appendix A

Boundary conditions and periodicity conditions

In 1.3.4 we are asked to investigate the possibility that the boundary conditions (1.32,33,34) for the Lamé's equation (1.27) are reducible to parity and periodicity conditions for the solution $w(z)$. For this purpose, we need to recall the following properties of Hill's equation relatively to an odd and an even solution with respect to the origin :

$$i) \quad w_1(z) \text{ is even , } w_2(z) \text{ is odd} \tag{A.1}$$

$$ii) \quad w_1(0) = \dot{w}_2(0) = 1, \ \dot{w}_1(0) = w_2(0) = 0 \tag{A.2}$$

$$iii) \quad w_1(z \pm 2K) = w_1(2K)w_1(z) \pm \dot{w}_1(2K)w_2(z) \tag{A.3}$$

$$iv) \quad w_2(z \pm 2K) = w_2(2K)w_1(z) \pm \dot{w}_2(2K)w_2(z) \tag{A.4}$$

$$v) \quad w_1(z)\dot{w}_2(z) - w_2(z)\dot{w}_1(z) \equiv 1 \tag{A.5}$$

$$vi) \quad w_1(2K) = \dot{w}_2\ (2K) \tag{A.6}$$

and analogous relations are valid changing $2K$ with $\pm m2K$, m integer.

For reasons of syntheticity, through the demonstrations we will use the symbolism :

: (), ,... which stands for :" from ( ) and, ,and ...it follows that"

and $\overset{()}{=}$ which means that: " from ( ) and , , and ...it is = to "

The general solution and derivative of (1.27) are expressed as :

$$w(z) = aw_1(z) + bw_2(z) \tag{A.7}$$

$$\dot{w}(z) = a\dot{w}_1(z) + b\dot{w}_2(z) \tag{A.8}$$

where a,b are two constants to be determined together with the periodicity properties from the b.c. as in what follows .

The b.c. $w(-K) = 0,\ w(K) = 0$

Under this condition the properties of w can be recovered considering that :

: $(A.7)$ written in $z = 0 \rightarrow w(0) = aw_1(0) + bw_2(0)$: (ii) $a = w(0)$

: $(A.8)$ written in $z = 0 \rightarrow \dot{w}(0) = a\dot{w}_1(0) + b\dot{w}_2(0)$: (ii) $b = \dot{w}(0)$

which together with (A.7) imply :

$$w(z) = w(0)w_1(z) + \dot{w}(0)w_2(z) \tag{A.9}$$

but (A.9) can be reduced to :

$$\begin{aligned}
\text{in } z = K \quad & w(K) = w(0)w_1(K) + \dot{w}(0)w_2(K) \overset{(1.32)}{=} 0 \\
\text{in } z = -K \quad & w(-K) = w(0)w_1(-K) + \dot{w}(0)w_2(-K) \\
& \overset{(i)}{=} \quad w(0)w_1(K) - \dot{w}(0)w_2(K) \overset{(1.32)}{=} 0 \\
\text{i.e. } & \textit{either} \qquad w(0)w_1(K) = \dot{w}(0)w_2(K) \\
& \textit{or} \qquad w(0)w_1(K) = -\dot{w}(0)w_2(K)
\end{aligned}$$

This system admits 4 solutions :

$$\begin{aligned}
w(0) = 0, \dot{w}(0) = 0 \quad & : (A.9) \quad w(z) \equiv 0 \\
w(0) = 0, w_2(K) = 0 \quad & : (A.9) \quad w(z) = \dot{w}(0)w_2(z), w_2(K) = 0 \quad \text{(A.10)} \\
w_1(0) = 0, \dot{w}(0) = 0 \quad & : (A.9) \quad w(z) = w(0)w_1(z), w_2(K) = 0 \quad \text{(A.11)} \\
w_1(K) = 0, w_2(K) = 0 \quad & : (v) \quad \text{with } z = K \text{ is impossible}
\end{aligned}$$

Nevertheless only (A.10,11) are consistent and express the fact that the solution can be only pure even or pure odd . Let us see if periodicity also occurs:

$$\begin{aligned}
& : (iii), z = K \quad w_1(K) = w_1(2K)w_1(K) - \dot{w}_1(2K)w_2(K) \quad : (A.10) \quad w_1(2K) = 1 \\
& : (iv), z = K \quad w_2(K) = w_2(2K)w_1(K) - \dot{w}_2(2K)w_2(K) \quad : (A.10) \quad w_2(2K) = 0
\end{aligned}$$

which together with :

$$\begin{aligned}
& : (v), z = 2K \qquad w_1(2K)\dot{w}_2(2K) - w_2(2K)\dot{w}_1(2K) = 1 \\
& \text{imply :} \qquad \dot{w}_2(2K) = 1 \quad : (iv) \quad w_2(z \pm 2K) = -w_2(z)
\end{aligned}$$

so that : $w_2(z)$ and hence $w(z)$ is odd with period 2K

analogously :

$$: (iii), z = K \quad w_1(K) = w_1(2K)w_1(K) - \dot{w}_1(2K)w_2(K) \quad : (A.11) \quad \dot{w}_1(2K) = 0$$

$$: (iv), z = K \quad w_2(K) = w_2(2K)w_1(K) - \dot{w}_2(2K)w_2(K) \quad : (A.11) \quad \dot{w}_2(2K) = -1$$

which together with :

$$: (v), z = 2K \qquad w_1(2K)\dot{w}_2(2K) - w_2(2K)\dot{w}_1(2K) = 1$$

imply : $\qquad w_1(2K) = -1 \quad : (iv) \quad w_1(z \pm 2K) = -w_1(z)$

hence : $w_1(z)$ has anti-period $2K$

so that w in question is even and periodic with period $4K$.

Summing up, the initial b.c. are translated into :

$$\text{either } w(z) \text{ even with period } 4K \tag{A.12}$$

$$\text{or } w(z) \text{ odd with period } 2K \tag{A.13}$$

The b.c. $\dot{w}(-K) = 0, w(K) = 0$ **or** $w(-K) = 0,\ \dot{w}(K) = 0$

An analogous but more tedious proof can be developed for the above b.c. which yields the periodicity condition :

$$w(z) \text{ has period } 8K \tag{A.14}$$

However, this time w is neither even nor odd but a linear combination of w_1 and w_2 . From the complete proof it is possible to show that the b.c. can only

determine the ratio :

$$\frac{\dot{w}(0)}{w(0)} = \dot{w}_1(2K)$$

Furthermore, it will be proved that between the even w_1 and odd w_2 solutions there exists the relation $w_2(z) = w_1(z+2K)$, which derived and written at $z = 0$ yields $\dot{w}_2(0) = \dot{w}_1(2K) \overset{(ii)}{=} 1$.

This way, $w(0) = \dot{w}(0) = 1$ and the general form (A.9) becomes simply :

$$w(z) = w_1(z) + w_2(z) \tag{A.15}$$

The b.c. $w(-K) = \dot{w}(K) = 0$ give obviously origin to the specular solution $w^s(z) = w(-z)$ i.e. :

$$w^s(z) = w_1(z) - w_2(z) \tag{A.16}$$

Finally we can show using the properties of w_1 and w_2 that $w(z)$ and $w^s(z)$ are odd or even with respect to the points where the b.c. they satisfy vanish or have vanishing derivative respectively .

The b.c. $\dot{w}(-K) = 0, \dot{w}(K) = 0$

These b.c. can be proved to yield a condition of fundamental periodicity in a way similar to that of the first case, in fact they imply :

$$\text{either } w(z) \text{ even with period } 2K \tag{A.17}$$

$$\text{or } w(z) \text{ odd with period } 4K \tag{A.18}$$

Appendix B

Fourier series espression of the solution

In this Appendix we explicitly collect the three-term recursive formulae and associated continued fractions relative to the coefficients of the Fourier series representation of the 6 periodic Lamé's functions presented in 1.4.3 . Precisely, we report the more useful characteristic equation obtained from the continued fraction by making explicit the variable :

$$\eta = 2h - \nu(\nu+1)k^2 \tag{B.1}$$

Also explicitly indicated are the forms that are more suitable for the numerical implementation of the characteristic equation itself . For the 6 cases in question the solutions can be written in the order as follows .

Even solution with period π (i.e. $2K$ or $2K'$)

The Fourier series form for this solution is :

$$E_{c_\nu}^{2m}(v) = \sum_{i=0}^{\infty} A_{2i} cos(2iv) \tag{B.2}$$

The recursivity of the coefficients can be shown to be expressible as (see [6]) :

$$\frac{1}{2}(\nu-1)(\nu+2)k^2 A_2 + \eta A_0 = 0 \quad i=0 \tag{B.3}$$

$$\frac{1}{2}(\nu-3)(\nu+4)k^2 A_4 + [\eta - 4(2-k^2)]A_2 + \nu(\nu+1)k^2 A_0 = 0 \quad i=1 \tag{B.4}$$

$$\frac{1}{2}(\nu-2i-1)(\nu+2i+2)k^2 A_{2i+2} + [\eta - 4i^2(2-k^2)]A_{2i} + \frac{1}{2}(\nu+2i-1)(\nu-2i+2)k^2 A_{2i-2} = 0 \quad i \geq 2 \tag{B.5}$$

The latter generate a continued fraction (see, for instance, [7]) which we report, for reason of space, writing the successive fractions on the same line :

$$\eta = -\frac{(\nu^2-1)\nu(\nu+2)\frac{k^4}{8}}{2-k^2-\frac{\eta}{4}} - \frac{(\nu^2-9)(\nu-2)(\nu+4)\frac{k^4}{16^2}}{2-k^2-\frac{\eta}{16}} - \frac{(\nu^2-25)(\nu-4)(\nu+6)\frac{k^4}{48^2}}{2-k^2-\frac{\eta}{36}} - \cdots \tag{B.6}$$

This espression can also be seen as a transcendental function in ν, h with parameter k^2 and can be usefully implemented using the following espressions :

$$\frac{A_{2I+2}}{A_{2I}} \simeq -\left(\frac{1-k'}{k}\right)^2 \qquad I \gg 1 \tag{B.7}$$

$$\frac{A_{2i}}{A_{2i-2}} = \frac{-\frac{1}{2}(\nu+2i-1)(\nu-2i+2)k^2}{\eta - 4i^2(2-k^2) + \frac{1}{2}(\nu-2i-1)(\nu+2i+2)k^2 \frac{A_{2i+2}}{A_{2i}}} \qquad 2 \leq i < I \tag{B.8}$$

$$\frac{A_2}{A_0} = \frac{-\nu(\nu+1)k^2}{\eta - 4(2-k^2) + \frac{1}{2}(\nu-3)(\nu+4)k^2 \frac{A_4}{A_2}} \qquad i=1 \tag{B.9}$$

$$\eta = -\frac{1}{2}(\nu-1)(\nu+2)k^2 \frac{A_2}{A_0} \qquad i=0 \tag{B.10}$$

The first and last equations correspond to the (1.60) ; in particular the truncation maximum index I depends on the accuracy required for the solution $\{X_i\}$ and decreases with increasing rate of convergence, i.e. with k^2, for :

$$\lim_{k^2\to 0}(\frac{1-k'}{k})^2 = 0 \qquad \lim_{k^2\to 1}(\frac{1-k'}{k})^2 = 1 \tag{B.11}$$

Odd solution with period π (i.e. $2K$ or $2K'$)

The Fourier series form for this solution is :

$$E_{s_\nu}^{2m}(v) = \sum_{i=1}^{\infty} B_{2i} sin(2iv) \tag{B.12}$$

The recursivity relations are now :

$$(\eta - 8 + 4k^2)B_2 + \frac{1}{2}(\nu-3)(\nu+4)k^2 B_4 = 0 \quad i = 0 \tag{B.13}$$

$$\frac{1}{2}(\nu-2i)(\nu+2i+1)k^2 B_{2i} + [\eta - (2i+2)^2(2-k^2)]B_{2i+2} + \frac{1}{2}(\nu-2i-3)(\nu+2i+4)k^2 B_{2i+4} = 0 \quad i \geq 1 \tag{B.14}$$

which generates the characteristic equation :

$$\eta = 4(2-k^2) - \frac{(\nu^2-9)(\nu-2)(\nu+4)\frac{k^4}{8^2}}{2-k^2-\frac{\eta}{16}} - \frac{(\nu^2-25)(\nu-4)(\nu+6)\frac{k^4}{48^2}}{2-k^2-\frac{\eta}{36}} - \ldots \tag{B.15}$$

and which is computationally implemented as :

$$\frac{B_{2I+2}}{B_{2I}} \simeq -(\frac{1-k'}{k})^2 \qquad I \gg 1 \tag{B.16}$$

$$\frac{B_{2i+2}}{B_{2i}} = \frac{-\frac{1}{2}(\nu-2i)(\nu+2i+1)k^2}{\eta-(2i+2)^2(2-k^2)+\frac{1}{2}(\nu-2i-3)(\nu+2i+4)k^2\frac{B_{2i+4}}{B_{2i+2}}} \qquad 1 \leq i < I \tag{B.17}$$

$$\eta = 4(2-k^2) - \tfrac{1}{2}(\nu-3)(\nu+4)k^2\frac{B_4}{B_2} \qquad i = 0 \tag{B.18}$$

Even solution with period 2π (i.e. $4K$ or $4K'$)

In this case the Fourier series form is :

$$E_{c_\nu}^{2m+1}(v) = \sum_{i=0}^{\infty} A_{2i+1} cos(2i+1)v \tag{B.19}$$

The three-term recursivity relations among the coefficients are :

$$\tfrac{1}{2}(\nu-3)(\nu+3)k^2 A_3 + [\eta - (2-k^2) +^{(*)} \tfrac{1}{2}\nu(\nu+1)k^2]A_1 = 0 \quad i=0 \tag{B.20}$$

$$\tfrac{1}{2}(\nu-2i-2)(\nu+2i+3)k^2 A_{2i+3} + [\eta-(2i+1)^2(2-k^2)]A_{2i+1} +$$
$$\tfrac{1}{2}(\nu-2i+1)(\nu+2i)k^2 A_{2i-1} = 0 \quad i \geq 1 \tag{B.21}$$

which generates the characteristic equation :

$$\eta = (2-k^2) -^{(*)} \frac{1}{2}\nu(\nu+1)k^2 - \frac{(\nu^2-4)(\nu-1)(\nu+3)\frac{k^4}{6^2}}{2-k^2-\frac{\eta}{9}} - \frac{(\nu^2-16)(\nu-3)(\nu+5)\frac{k^4}{30^2}}{2-k^2-\frac{\eta}{25}} - \cdots \tag{B.22}$$

and which is computationally implemented as :

$$\frac{A_{2I+3}}{A_{2I+1}} \simeq -(\frac{1-k'}{k})^2 \qquad I \gg 1 \tag{B.23}$$

$$\frac{A_{2i+1}}{A_{2i-1}} = \frac{-\frac{1}{2}(\nu-2i+1)(\nu+2i)k^2}{\eta-(2i+1)^2(2-k^2)+\frac{1}{2}(\nu-2i-2)(\nu+2i+3)k^2\frac{A_{2i+3}}{A_{2i+1}}} \qquad 1 \leq i < I \tag{B.24}$$

$$\eta = (2-k^2) -^{(*)} \tfrac{1}{2}\nu(\nu+1)k^2 - \tfrac{1}{2}(\nu-2)(\nu+3)k^2\frac{A_3}{A_1} \quad i=0 \tag{B.25}$$

Odd solution with period 2π (i.e. $4K$ or $4K'$)

The Fourier series form for this solution is :

$$E_{s_\nu}^{2m+1}(v) = \sum_{i=1}^{\infty} B_{2i+1} sin(2i+1)v \tag{B.26}$$

The relation are completely analogous to those of the even case but with an opposition of the signs indicated with $^{(*)}$ in the (B.20,22,25) .

Even solution with period 4π (i.e. $8K$ or $8K'$)

The Fourier series form for this solution is :

$$E_{c_\nu}^m(v) = \sum_{i=-\infty}^{\infty} A_i cos(2i + \frac{1}{2})v \qquad \text{(B.27)}$$

Now the series is bilateral so that a unique relation expresses the three-term recursivity where the index i assumes all the positive and negative integers :

$$\frac{1}{2}(2\nu + 4i + 3)(2\nu - 4i - 1)k^2 A_{i+1} + [4\eta - (4i-1)^2(2-k^2)]A_i + \frac{1}{2}(2\nu + 4i - 3)(2\nu - 4i + 5)k^2 A_{i-1} = 0 \quad -\infty < i < \infty \qquad \text{(B.28)}$$

Consequently, in general, we can write a continued fraction for i departing from $+\infty$ and another for i departing from $-\infty$ to be made consistent at a common finite i value .

No useful form for the characteristic equation does exist if we except the case in which $\nu = \frac{2n+1}{2}$ is any odd integer, when it becomes an algebraic equation of degree $\nu + \frac{1}{2}$.

In our applications this will not happen so we report only the relations used in the computational implementation :

$$\frac{A_{I_1+1}}{A_{I_1}} \simeq -(\frac{1-k'}{k})^2 \qquad I_1 \gg 1 \qquad \text{(B.29)}$$

$$\frac{A_i}{A_{i-1}} = \frac{-\frac{1}{2}(2\nu+4i-3)(2\nu-4i+5)k^2}{4\eta-(4i-1)^2(2-k^2)+\frac{1}{2}(2\nu+4i+3)(2\nu-4i-1)k^2\frac{A_{i+1}}{A_1}} \qquad 1 \le i < I_1 \qquad \text{(B.30)}$$

$$(\frac{A_1}{A_0})^+ = \frac{1}{(\frac{A_0}{A_1})^-} \qquad \text{consistency condition} \tag{B.31}$$

$$\frac{A_i}{A_{i+1}} = \frac{-\frac{1}{2}(2\nu+4i+3)(2\nu-4i-1)k^2}{4\eta-(4i-1)^2(2-k^2)+\frac{1}{2}(2\nu+4i-3)(2\nu-4i+5)k^2\frac{A_{i-1}}{A_1}} \qquad 0 \geq i > I_2 \tag{B.32}$$

$$\frac{A_{I_2+1}}{A_{I_2+1}} \simeq -(\frac{1-k'}{k})^2 \qquad I_2 \ll -1 \tag{B.33}$$

The consistency condition equates the value $(\frac{A_1}{A0})^+$ obtained when $i = 1$ in (B.30) with $(\frac{A_1}{A_0})^-$ obtained when $i = 0$ in (B.32) .

The 1^{st} equation (1.60) is now substituted by the asymptotic behaviour at $-\infty$ as reported in (B.33) .

Odd solution with period 4π (i.e. $8K$ or $8K'$)

Finally the Fourier form for this solution is :

$$E^m_{s_\nu}(v) = \sum_{i=-\infty}^{\infty} B_i cos(2i - \frac{1}{2})v \tag{B.34}$$

It is immediate to prove that a π shift introduced in the even solution (B.27) provides an odd form of this kind, in fact :

$$E^m_{c_\nu}(v+\pi) = \sum_{i=-\infty}^{\infty} A_i cos(2i + \frac{1}{2})(v+\pi) = cos(\frac{\pi}{2}) \sum_{i=-\infty}^{\infty} A_i cos(2i + \frac{1}{2})v +$$
$$sin(\frac{\pi}{2}) \sum_{i=-\infty}^{\infty} A_i sin(2i + \frac{1}{2})v = \sum_{i=-\infty}^{\infty} A_i sin(2i + \frac{1}{2})v \tag{B.35}$$

Furthermore, the above is still solution of Lamé's equation because it presents periodic coefficients with period π, so that we can use in (B.34) the same coefficients $\{A_i\}$ used for the even solution (B.27) .

Appendix C

Evaluation of the eigenvalues

In this Appendix we report as a way of example the numerical evaluation of the first 15 components of the $\{\nu, h\}$ spectrum of eigenvalues relative to the acute sector .

The individual eigenvalues are identified by the mode label defined in 2.3 .

We compute values with k^2-steps of 0.02 for a total of 50 evaluations in the complete interval $k^2 \in [0, 1]$, inclusive of the limit values $k^2 = 0, 1$ where ν and h are determinable analytically as indicated in 2.3 .

The accuracy is up to 6 decimal places and the evaluations relative to k^2 not present in the Table may be recovered by interpolation; in this case, the accuracy increases where the higher order derivatives decrease .

ACUTE SECTOR
Eigenvalue ν

k^2	(0,0)	(0,1)	(0,2)	(0,3)	(0,4)
0.00	0.000000	1.000000	2.000000	3.000000	4.000000
0.02	0.148618	1.196147	2.232894	3.264692	4.293285
0.04	0.165600	1.224037	2.269993	3.309568	4.344365
0.06	0.177521	1.243971	2.296407	3.340843	4.378596
0.08	0.187133	1.260170	2.317618	3.365212	4.403980
0.10	0.195391	1.274120	2.335578	3.385110	4.423556
0.12	0.202750	1.286539	2.351237	3.401753	4.438931
0.14	0.209467	1.297832	2.365137	3.415862	4.451118
0.16	0.215703	1.308256	2.377621	3.427914	4.460828
0.18	0.221566	1.317980	2.388922	3.438255	4.468586
0.20	0.227134	1.327125	2.399206	3.447149	4.474796
0.22	0.232463	1.335781	2.408599	3.454806	4.479773
0.24	0.237596	1.344014	2.417198	3.461400	4.483767
0.26	0.242568	1.351875	2.425081	3.467078	4.486975
0.28	0.247406	1.359405	2.432313	3.471964	4.489554
0.30	0.252134	1.366636	2.438948	3.476164	4.491628
0.32	0.256770	1.373596	2.445033	3.479773	4.493297
0.34	0.261331	1.380304	2.450611	3.482869	4.494640
0.36	0.265832	1.386779	2.455719	3.485523	4.495721
0.38	0.270284	1.393035	2.460391	3.487795	4.496591
0.40	0.274700	1.399084	2.464659	3.489737	4.497291
0.42	0.279091	1.404935	2.468551	3.491394	4.497853
0.44	0.283465	1.410598	2.472095	3.492807	4.498304
0.46	0.287833	1.416078	2.475316	3.494008	4.498665
0.48	0.292203	1.421382	2.478237	3.495027	4.498954
0.50	0.296584	1.426513	2.480880	3.495890	4.499185
0.52	0.300986	1.431475	2.483268	3.496620	4.499368
0.54	0.305416	1.436271	2.485418	3.497233	4.499513
0.56	0.309883	1.440904	2.487350	3.497749	4.499627
0.58	0.314398	1.445374	2.489080	3.498180	4.499717
0.60	0.318970	1.449683	2.490625	3.498538	4.499787
0.62	0.323610	1.453832	2.492000	3.498835	4.499841
0.64	0.328329	1.457820	2.493219	3.499080	4.499883
0.66	0.333139	1.461648	2.494295	3.499281	4.499915
0.68	0.338056	1.465315	2.495241	3.499444	4.499939
0.70	0.343095	1.468821	2.496067	3.499576	4.499957
0.72	0.348275	1.472165	2.496786	3.499681	4.499970
0.74	0.353616	1.475345	2.497405	3.499764	4.499980
0.76	0.359144	1.478360	2.497936	3.499829	4.499987
0.78	0.364890	1.481208	2.498386	3.499879	4.499991
0.80	0.370890	1.483886	2.498763	3.499917	4.499995
0.82	0.377192	1.486393	2.499076	3.499945	4.499997
0.84	0.383854	1.488725	2.499330	3.499965	4.499998
0.86	0.390957	1.490878	2.499533	3.499979	4.499999
0.88	0.398609	1.492846	2.499691	3.499988	4.500000
0.90	0.406967	1.494624	2.499809	3.499994	4.500000
0.92	0.416272	1.496200	2.499894	3.499997	4.500000
0.94	0.426931	1.497563	2.499950	3.499999	4.500000
0.96	0.439744	1.498691	2.499982	3.500000	4.500000
0.98	0.456779	1.499543	2.499997	3.500000	4.500000
1.00	0.500000	1.500000	2.500000	3.500000	4.500000

ACUTE SECTOR
Eigenvalue h

k^2	(0,0)	(0,1)	(0,2)	(0,3)	(0,4)
0.00	0.000000	0.000000	0.000000	0.000000	0.000000
0.02	0.001711	0.026248	0.071711	0.137134	0.221317
0.04	0.003878	0.054346	0.146405	0.276352	0.439375
0.06	0.006314	0.083487	0.222213	0.414145	0.648482
0.08	0.008968	0.113425	0.298468	0.549138	0.846619
0.10	0.011814	0.144020	0.374745	0.680474	1.032938
0.12	0.014837	0.175177	0.450727	0.807579	1.207306
0.14	0.018026	0.206825	0.526158	0.930075	1.370072
0.16	0.021376	0.238905	0.600823	1.047737	1.521891
0.18	0.024881	0.271368	0.674539	1.160465	1.663592
0.20	0.028541	0.304170	0.747144	1.268260	1.796083
0.22	0.032353	0.337272	0.818503	1.371204	1.920271
0.24	0.036317	0.370635	0.888498	1.469443	2.037029
0.26	0.040434	0.404226	0.957029	1.563166	2.147161
0.28	0.044704	0.438009	1.024016	1.652594	2.251397
0.30	0.049131	0.471952	1.089393	1.737968	2.350386
0.32	0.053715	0.506023	1.153112	1.819536	2.444701
0.34	0.058461	0.540189	1.215136	1.897550	2.534844
0.36	0.063372	0.574418	1.275447	1.972255	2.621255
0.38	0.068452	0.608678	1.334034	2.043889	2.704314
0.40	0.073707	0.642938	1.390902	2.112677	2.784355
0.42	0.079142	0.677164	1.446062	2.178831	2.861666
0.44	0.084762	0.711324	1.499537	2.242552	2.936500
0.46	0.090577	0.745385	1.551356	2.304022	3.009079
0.48	0.096592	0.779315	1.601555	2.363413	3.079593
0.50	0.102817	0.813078	1.650175	2.420880	3.148215
0.52	0.109263	0.846642	1.697262	2.476569	3.215091
0.54	0.115939	0.879973	1.742865	2.530610	3.280354
0.56	0.122859	0.913037	1.787034	2.583124	3.344120
0.58	0.130037	0.945799	1.829824	2.634220	3.406493
0.60	0.137487	0.978224	1.871288	2.683999	3.467564
0.62	0.145229	1.010279	1.911481	2.732552	3.527416
0.64	0.153282	1.041928	1.950458	2.779963	3.586122
0.66	0.161669	1.073138	1.988271	2.826307	3.643749
0.68	0.170418	1.103873	2.024976	2.871654	3.700356
0.70	0.179560	1.134100	2.060624	2.916068	3.755998
0.72	0.189131	1.163784	2.095266	2.959606	3.810722
0.74	0.199174	1.192891	2.128952	3.002320	3.864574
0.76	0.209741	1.221387	2.161731	3.044260	3.917595
0.78	0.220895	1.249237	2.193649	3.085470	3.969821
0.80	0.232713	1.276406	2.224752	3.125989	4.021287
0.82	0.245292	1.302858	2.255084	3.165855	4.072023
0.84	0.258758	1.328557	2.284686	3.205102	4.122060
0.86	0.273275	1.353463	2.313600	3.243760	4.171423
0.88	0.289072	1.377531	2.341866	3.281859	4.220137
0.90	0.306473	1.400714	2.369523	3.319423	4.268226
0.92	0.325979	1.422952	2.396608	3.356478	4.315712
0.94	0.348429	1.444170	2.423159	3.393044	4.362613
0.96	0.375457	1.464260	2.449215	3.429142	4.408950
0.98	0.411272	1.483041	2.474813	3.464788	4.454740
1.00	0.500000	1.500000	2.500000	3.500000	4.500000

ACUTE SECTOR
Eigenvalue ν

k^2	(1,0)	(1,1)	(1,2)	(1,3)	(2,0)
0.00	1.000000	2.000000	3.000000	4.000000	2.000000
0.02	1.004933	2.014267	3.027296	4.043318	2.000038
0.04	1.009799	2.027687	3.051654	4.079951	2.000156
0.06	1.014636	2.040574	3.074245	4.112806	2.000358
0.08	1.019460	2.053071	3.095554	4.142973	2.000650
0.10	1.024286	2.065267	3.115858	4.171031	2.001036
0.12	1.029122	2.077221	3.135333	4.197329	2.001521
0.14	1.033977	2.088979	3.154101	4.222093	2.002113
0.16	1.038857	2.100574	3.172249	4.245472	2.002815
0.18	1.043769	2.112034	3.189839	4.267565	2.003636
0.20	1.048718	2.123380	3.206918	4.288441	2.004581
0.22	1.053710	2.134631	3.223518	4.308141	2.005657
0.24	1.058751	2.145803	3.239663	4.326695	2.006872
0.26	1.063845	2.156908	3.255368	4.344118	2.008234
0.28	1.068998	2.167957	3.270642	4.360422	2.009750
0.30	1.074215	2.178959	3.285489	4.375615	2.011430
0.32	1.079502	2.189922	3.299907	4.389705	2.013283
0.34	1.084864	2.200853	3.313891	4.402703	2.015318
0.36	1.090307	2.211758	3.327433	4.414628	2.017546
0.38	1.095837	2.222639	3.340520	4.425503	2.019977
0.40	1.101462	2.233502	3.353141	4.435358	2.022625
0.42	1.107186	2.244348	3.365278	4.444233	2.025501
0.44	1.113019	2.255178	3.376917	4.452172	2.028618
0.46	1.118968	2.265993	3.388041	4.459230	2.031993
0.48	1.125041	2.276791	3.398633	4.465462	2.035639
0.50	1.131248	2.287571	3.408679	4.470929	2.039575
0.52	1.137600	2.298328	3.418165	4.475693	2.043818
0.54	1.144107	2.309059	3.427080	4.479819	2.048389
0.56	1.150781	2.319757	3.435417	4.483367	2.053308
0.58	1.157637	2.330413	3.443171	4.486399	2.058602
0.60	1.164690	2.341019	3.450342	4.488971	2.064295
0.62	1.171958	2.351561	3.456934	4.491138	2.070419
0.64	1.179459	2.362026	3.462953	4.492949	2.077004
0.66	1.187217	2.372397	3.468414	4.494451	2.084090
0.68	1.195257	2.382655	3.473331	4.495687	2.091719
0.70	1.203608	2.392777	3.477725	4.496692	2.099939
0.72	1.212306	2.402737	3.481618	4.497502	2.108807
0.74	1.221392	2.412506	3.485037	4.498147	2.118389
0.76	1.230916	2.422052	3.488008	4.498654	2.128765
0.78	1.240938	2.431338	3.490562	4.499045	2.140030
0.80	1.251531	2.440323	3.492729	4.499342	2.152301
0.82	1.262790	2.448962	3.494541	4.499562	2.165725
0.84	1.274836	2.457205	3.496028	4.499721	2.180490
0.86	1.287828	2.464998	3.497223	4.499831	2.196848
0.88	1.301987	2.472281	3.498156	4.499905	2.215138
0.90	1.317632	2.478986	3.498860	4.499952	2.235854
0.92	1.335253	2.485039	3.499363	4.499979	2.259750
0.94	1.355675	2.490346	3.499697	4.499993	2.288093
0.96	1.380513	2.494789	3.499893	4.499998	2.323351
0.98	1.413941	2.498176	3.499982	4.500000	2.371873
1.00	1.500000	2.500000	3.500000	4.500000	2.500000

ACUTE SECTOR
Eigenvalue h

k^2	(1,0)	(1,1)	(1,2)	(1,3)	(2,0)
0.00	1.000000	1.000000	1.000000	1.000000	4.000000
0.02	1.020223	1.081072	1.172676	1.295030	4.020305
0.04	1.040886	1.164169	1.350073	1.598168	4.041240
0.06	1.061991	1.249178	1.531595	1.907627	4.062838
0.08	1.083538	1.336030	1.716842	2.222171	4.085131
0.10	1.105532	1.424674	1.905495	2.540773	4.108156
0.12	1.127981	1.515075	2.097281	2.862500	4.131951
0.14	1.150891	1.607203	2.291950	3.186458	4.156556
0.16	1.174271	1.701036	2.489262	3.511761	4.182013
0.18	1.198130	1.796557	2.688983	3.837520	4.208368
0.20	1.222481	1.893751	2.890877	4.162834	4.235668
0.22	1.247335	1.992607	3.094699	4.486787	4.263964
0.24	1.272706	2.093113	3.300196	4.808458	4.293311
0.26	1.298608	2.195259	3.507102	5.126928	4.323764
0.28	1.325057	2.299036	3.715135	5.441294	4.355386
0.30	1.352070	2.404435	3.923997	5.750687	4.388240
0.32	1.379666	2.511445	4.133373	6.054293	4.422394
0.34	1.407865	2.620054	4.342929	6.351374	4.457922
0.36	1.436690	2.730249	4.552312	6.641285	4.494902
0.38	1.466164	2.842013	4.761153	6.923490	4.533416
0.40	1.496313	2.955327	4.969068	7.197577	4.573553
0.42	1.527165	3.070168	5.175660	7.463260	4.615407
0.44	1.558752	3.186507	5.380526	7.720383	4.659079
0.46	1.591107	3.304312	5.583256	7.968909	4.704678
0.48	1.624267	3.423543	5.783445	8.208915	4.752321
0.50	1.658273	3.544150	5.980695	8.440571	4.802134
0.52	1.693170	3.666079	6.174625	8.664130	4.854252
0.54	1.729006	3.789261	6.364878	8.879905	4.908824
0.56	1.765838	3.913618	6.551124	9.088254	4.966009
0.58	1.803725	4.039057	6.733074	9.289565	5.025985
0.60	1.842737	4.165470	6.910477	9.484244	5.088943
0.62	1.882951	4.292732	7.083131	9.672699	5.155097
0.64	1.924454	4.420697	7.250883	9.855336	5.224685
0.66	1.967346	4.549200	7.413630	10.032549	5.297971
0.68	2.011740	4.678048	7.571319	10.204717	5.375256
0.70	2.057769	4.807024	7.723945	10.372197	5.456880
0.72	2.105586	4.935881	7.871548	10.535329	5.543236
0.74	2.155373	5.064343	8.014208	10.694426	5.634779
0.76	2.207347	5.192097	8.152039	10.849780	5.732047
0.78	2.261769	5.318799	8.285189	11.001661	5.835682
0.80	2.318961	5.444068	8.413829	11.150315	5.946467
0.82	2.379326	5.567486	8.538150	11.295968	6.065372
0.84	2.443383	5.688598	8.658359	11.438827	6.193630
0.86	2.511812	5.806911	8.774676	11.579078	6.332858
0.88	2.585546	5.921892	8.887329	11.716889	6.485251
0.90	2.665923	6.032960	8.996554	11.852413	6.653936
0.92	2.754984	6.139476	9.102591	11.985786	6.843661
0.94	2.856148	6.240707	9.205687	12.117130	7.062331
0.96	2.976040	6.335746	9.306098	12.246554	7.325185
0.98	3.131657	6.423265	9.404096	12.374151	7.671059
1.00	3.500000	6.500000	9.500000	12.500000	8.500000

ACUTE SECTOR
Eigenvalue ν

k^2	(2,1)	(2,2)	(3,0)	(3,1)	(4,0)
0.00	3.000000	4.000000	3.000000	4.000000	4.000000
0.02	3.000191	4.000572	3.000000	4.000002	4.000000
0.04	3.000778	4.002319	3.000002	4.000014	4.000000
0.06	3.001780	4.005266	3.000007	4.000049	4.000000
0.08	3.003214	4.009420	3.000017	4.000119	4.000000
0.10	3.005096	4.014769	3.000034	4.000239	4.000001
0.12	3.007439	4.021284	3.000061	4.000426	4.000002
0.14	3.010256	4.028924	3.000100	4.000697	4.000004
0.16	3.013557	4.037634	3.000155	4.001074	4.000008
0.18	3.017351	4.047355	3.000228	4.001577	4.000013
0.20	3.021645	4.058019	3.000323	4.002231	4.000021
0.22	3.026445	4.069555	3.000445	4.003063	4.000032
0.24	3.031753	4.081891	3.000599	4.004102	4.000048
0.26	3.037572	4.094954	3.000790	4.005378	4.000069
0.28	3.043903	4.108672	3.001023	4.006926	4.000098
0.30	3.050744	4.122977	3.001305	4.008782	4.000136
0.32	3.058095	4.137801	3.001644	4.010985	4.000185
0.34	3.065951	4.153078	3.002049	4.013575	4.000249
0.36	3.074309	4.168746	3.002529	4.016596	4.000330
0.38	3.083164	4.184742	3.003093	4.020093	4.000433
0.40	3.092511	4.201007	3.003756	4.024115	4.000562
0.42	3.102344	4.217479	3.004529	4.028708	4.000722
0.44	3.112656	4.234098	3.005428	4.033924	4.000922
0.46	3.123441	4.250802	3.006470	4.039812	4.001169
0.48	3.134692	4.267527	3.007674	4.046423	4.001473
0.50	3.146403	4.284205	3.009062	4.053806	4.001846
0.52	3.158565	4.300767	3.010660	4.062009	4.002301
0.54	3.171173	4.317137	3.012494	4.071079	4.002856
0.56	3.184216	4.333237	3.014597	4.081059	4.003532
0.58	3.197688	4.348985	3.017005	4.091991	4.004354
0.60	3.211578	4.364294	3.019759	4.103912	4.005350
0.62	3.225876	4.379077	3.022907	4.116856	4.006559
0.64	3.240568	4.393245	3.026502	4.130851	4.008024
0.66	3.255639	4.406711	3.030607	4.145922	4.009799
0.68	3.271068	4.419390	3.035293	4.162089	4.011952
0.70	3.286833	4.431209	3.040644	4.179365	4.014564
0.72	3.302903	4.442104	3.046756	4.197757	4.017737
0.74	3.319238	4.452022	3.053741	4.217262	4.021597
0.76	3.335790	4.460932	3.061735	4.237868	4.026302
0.78	3.352495	4.468818	3.070896	4.259546	4.032051
0.80	3.369272	4.475683	3.081416	4.282246	4.039096
0.82	3.386022	4.481550	3.093531	4.305884	4.047760
0.84	3.402616	4.486458	3.107539	4.330335	4.058460
0.86	3.418896	4.490463	3.123819	4.355405	4.071749
0.88	3.434667	4.493632	3.142884	4.380811	4.088368
0.90	3.449692	4.496043	3.165449	4.406138	4.109350
0.92	3.463683	4.497783	3.192590	4.430797	4.136220
0.94	3.476292	4.498944	3.226080	4.453972	4.171418
0.96	3.487086	4.499626	3.269322	4.474546	4.219480
0.98	3.495453	4.499935	3.330966	4.490945	4.291616
1.00	3.500000	4.500000	3.500000	4.500000	4.500000

ACUTE SECTOR
Eigenvalue h

k^2	(2,1)	(2,2)	(3,0)	(3,1)	(4,0)
0.00	4.000000	4.000000	9.000000	9.000000	16.000000
0.02	4.081528	4.164358	9.030191	9.110806	16.040236
0.04	4.166228	4.337786	9.060777	9.223300	16.080953
0.06	4.254272	4.520771	9.091782	9.337606	16.122167
0.08	4.345837	4.713729	9.123229	9.453864	16.163894
0.10	4.441099	4.916996	9.155146	9.572227	16.206153
0.12	4.540232	5.130815	9.187561	9.692865	16.248965
0.14	4.643410	5.355335	9.220506	9.815967	16.292349
0.16	4.750801	5.590609	9.254017	9.941740	16.336329
0.18	4.862568	5.836602	9.288132	10.070416	16.380932
0.20	4.978870	6.093197	9.322893	10.202248	16.426185
0.22	5.099856	6.360210	9.358347	10.337514	16.472119
0.24	5.225668	6.637394	9.394545	10.476522	16.518769
0.26	5.356439	6.924457	9.431545	10.619606	16.566172
0.28	5.492293	7.221062	9.469408	10.767131	16.614371
0.30	5.633344	7.526843	9.508203	10.919496	16.663413
0.32	5.779697	7.841403	9.548009	11.077130	16.713350
0.34	5.931448	8.164317	9.588910	11.240497	16.764243
0.36	6.088685	8.495136	9.631001	11.410094	16.816158
0.38	6.251487	8.833380	9.674388	11.586451	16.869172
0.40	6.419925	9.178536	9.719189	11.770129	16.923370
0.42	6.594066	9.530051	9.765535	11.961717	16.978851
0.44	6.773966	9.887327	9.813574	12.161831	17.035729
0.46	6.959679	10.249710	9.863472	12.371107	17.094133
0.48	7.151250	10.616485	9.915413	12.590199	17.154212
0.50	7.348721	10.986864	9.969606	12.819767	17.216142
0.52	7.552125	11.359977	10.026287	13.060478	17.280124
0.54	7.761488	11.734871	10.085722	13.312994	17.346394
0.56	7.976828	12.110499	10.148209	13.577964	17.415232
0.58	8.198148	12.485726	10.214091	13.856020	17.486963
0.60	8.425441	12.859331	10.283754	14.147769	17.561978
0.62	8.658674	13.230020	10.357638	14.453786	17.640737
0.64	8.897794	13.596447	10.436246	14.774607	17.723795
0.66	9.142709	13.957244	10.520155	15.110722	17.811817
0.68	9.393286	14.311053	10.610027	15.462567	17.905606
0.70	9.649333	14.656577	10.706624	15.830513	18.006142
0.72	9.910584	14.992619	10.810832	16.214847	18.114619
0.74	10.176678	15.318135	10.923682	16.615747	18.232511
0.76	10.447130	15.632270	11.046387	17.033248	18.361638
0.78	10.721306	15.934388	11.180383	17.467177	18.504273
0.80	10.998376	16.224094	11.327393	17.917074	18.663275
0.82	11.277277	16.501233	11.489516	18.382062	18.842269
0.84	11.556658	16.765881	11.669363	18.860665	19.045916
0.86	11.834830	17.018326	11.870270	19.350554	19.280291
0.88	12.109709	17.259036	12.096651	19.848190	19.553504
0.90	12.378769	17.488638	12.354638	20.348369	19.876737
0.92	12.638985	17.707879	12.653326	20.843670	20.266248
0.94	12.886767	17.917616	13.007552	21.323844	20.747767
0.96	13.117769	18.118801	13.445441	21.775124	21.368429
0.98	13.326209	18.312498	14.037681	22.178792	22.243083
1.00	13.500000	18.500000	15.500000	22.500000	24.500000

Appendix D

The E-field expressed in a rectangular coordinate system

In 2.5 we are asked to express the E-field in rectangular coordinates x, y, z for ease of application .

In this Appendix we effect this change of variables and also define a main c.s. which permits easier formulation of the singularity vector .

A first step toward the "rectangularization" of forms like (2.42) implies tedious geometrical transformations that we simplify by making use of the abbreviations :

$$T(\theta; k^2) = \sqrt{1 - k'^2 cos^2\theta} \qquad P(\phi; k^2) = \sqrt{1 - k^2 cos^2\phi} \tag{D.1}$$

$$S(\theta, \phi; k^2) = \sqrt{k^2 sin^2\phi + k'^2 sin^2\theta} \tag{D.2}$$

$$S_\theta(r, \theta, \phi; k^2) = \frac{sin\theta}{S^2} r^{\nu-1} \qquad S_\phi(r, \theta, \phi; k^2) = \frac{sin\phi}{S^2} r^{\nu-1} \tag{D.3}$$

The rectangular $\vec{E}$ components can be recovered by decomposing the unit vectors

$\hat{r},\hat{\theta},\hat{\phi}$ along $\hat{x},\hat{y},\hat{z}$ according to their direction cosines as (see also [12] pg 25) :

$$\hat{r}= T cos\phi\ \hat{x} + sin\theta sin\phi\ \hat{y} + P cos\theta\ \hat{z} \tag{D.4}$$

$$\hat{\theta}= \tfrac{1}{S}[k'^2 sin\theta cos\theta cos\phi\ \hat{x} + T cos\theta sin\phi\ \hat{y} - PT sin\theta\ \hat{z}] \tag{D.5}$$

$$\hat{\phi}= \tfrac{1}{S}[-PT sin\phi\ \hat{x} + P sin\theta cos\phi\ \hat{y} - k^2 cos\theta sin\phi cos\phi\ \hat{z}] \tag{D.6}$$

and then from (2.42) we get :

$$E_x = -T[\nu cos\phi r^{\nu-1}\Theta\Phi + k'^2 cos\theta cos\phi S_\theta \dot{\Theta}\Phi - P^2 S_\phi \Theta\dot{\Phi}] \tag{D.7}$$

$$E_y = -[\nu sin\theta sin\phi r^{\nu-1}\Theta\Phi + T^2 cos\theta S_\phi \dot{\Theta}\Phi + P^2 cos\phi S_\theta \Theta\dot{\Phi}] \tag{D.8}$$

$$E_z = -P[\nu cos\theta r^{\nu-1}\Theta\Phi - T^2 S_\theta \dot{\Theta}\Phi + k^2 cos\theta cos\phi S_\phi \Theta\dot{\Phi}] \tag{D.9}$$

where (D.1,2,3) can be expressed in rectangular coordinates by making use of the useful transformation formulae :

$$r^2 = x^2 + y^2 + z^2 \qquad sin^2\theta = \frac{a_\theta + |\sqrt{\Delta_2}|}{2(k'r)^2} \qquad sin^2\phi = \frac{a_\phi + |\sqrt{\Delta_2}|}{2(kr)^2} \tag{D.10}$$

from which the expression for $sin\theta, cos\theta, sin\phi, cos\phi$ can be straightforwardly obtained by adopting the following signs for the square root :

$$sin\phi \begin{cases} > 0 \text{ for } y > 0 \\ \text{any value} \in [-1,+1] \text{ for } y = 0 \qquad cos\phi \text{ gets the sign of } x \\ < 0 \text{ for } y < 0 \end{cases}$$
$$sin\theta \geq 0 \qquad\qquad cos\theta \text{ gets the sign of } z \tag{D.11}$$

In this way, S_θ, S_ϕ becomes :

$$S_\theta(x,y,z;k^2) = \frac{1}{\sqrt{2}k'}\sqrt{1+\frac{a_\theta}{|\sqrt{\Delta_2}|}}\frac{r^{\nu-1}}{|\sqrt{\Delta_2}|^{\frac{1}{2}}} \qquad \text{with the sign of } sin\theta \quad \text{(D.12)}$$

$$S_\phi(x,y,z;k^2) = \frac{1}{\sqrt{2}k}\sqrt{1+\frac{a_\phi}{|\sqrt{\Delta_2}|}}\frac{r^{\nu-1}}{|\sqrt{\Delta_2}|^{\frac{1}{2}}} \qquad \text{with the sign of } sin\phi \quad \text{(D.13)}$$

The new symbols $a_\theta, a_\phi, \Delta_2$ stand for :

$$a_\theta(x,y,z;k^2) = [(k'x-kz)(k'x+kz)+(k'^2-k^2)y^2] = -a_\phi(x,y,z;k^2) \quad \text{(D.14)}$$

$$\Delta_2 = [(k'x-kz)^2+y^2][(k'x+kz)^2+y^2] \geq 0 \quad \text{(D.15)}$$

the latter present the property to vanish on the two degenerate lines $k'x = \pm kz$ where the sector edges lie . For this reason, it would be very advantageous to rotate the axes x, z of $\pi - \epsilon$ clockwise so that the positive z-axis always fits a conductor edge as shown in Fig. D.1a-b,2 . Obviously, the other edge also fits the positive x axis in the special but important case of sector apertures $\sigma = 90^0, 270^0$. For this reason, we name by *main sector* and *main rectangular c.s.* the conductor with $k^2 = 0.5$ and the c.s. X, Y, Z fitting exactly its edges .

The direct and reverse relations between x, y, z and X, Y, Z can be expressed as :

$$X = -(k'x+kz) \qquad x = -k'X + kZ \quad \text{(D.16)}$$

$$Y \equiv y \qquad y \equiv Y \quad \text{(D.17)}$$

$$Z = kx - k'z \qquad z = -(kX + k'Z) \quad \text{(D.18)}$$

In the main system $a_\theta, a_\phi, \Delta_2$ become simply :

$$a_\phi = [(k^2 - k'^2)(X^2 + Y^2) + 2kk'XZ] = -a_\theta \tag{D.19}$$

$$\Delta_2 = \{[(k^2 - k'^2)X + 2kk'Z]^2 + Y^2\}[X^2 + Y^2] \tag{D.20}$$

But their simplest form is obtained when the main sectors are considered, i.e. $k^2 = k'^2 = 0.5$:

$$a_\phi = XZ = -a_\theta \tag{D.21}$$

$$\Delta_2 = (XZ)^2 + (Yr)^2 \tag{D.22}$$

which substituted in (D.10) not only provides the easiest expressions for $r^2, sin^2\theta, sin^2\phi$ but also sets in evidence an important interpretation of :

$$S_\theta = \sqrt{1 - \frac{XZ}{|\sqrt{(XZ)^2 + (Yr)^2}|}} \frac{r^{\nu-1}}{|\sqrt{(XZ)^2 + (Yr)^2}|^{\frac{1}{2}}} \tag{D.23}$$

$$S_\phi = \sqrt{1 + \frac{XZ}{|\sqrt{(XZ)^2 + (Yr)^2}|}} \frac{r^{\nu-1}}{|\sqrt{(XZ)^2 + (Yr)^2}|^{\frac{1}{2}}} \tag{D.24}$$

The functions S_θ, S_ϕ are continuous everywhere except on the two axes X and Z along which they present a cylindrical singularity like $(Y^2 + Z^2)$ and $(X^2 + Y^2)$ respectively that matches the spherical singularities $r^{\nu-1}$ on the tip .

The terms under the main root represent just the zeros of S_θ in $\theta = 0, \pi$ and of S_ϕ in $\phi = 0, \pi$.

The physical importance of these functions consists in the fact that the matching of the zeros and of the singularities they describe are those of some E-field components, as we prove in 2.5 .

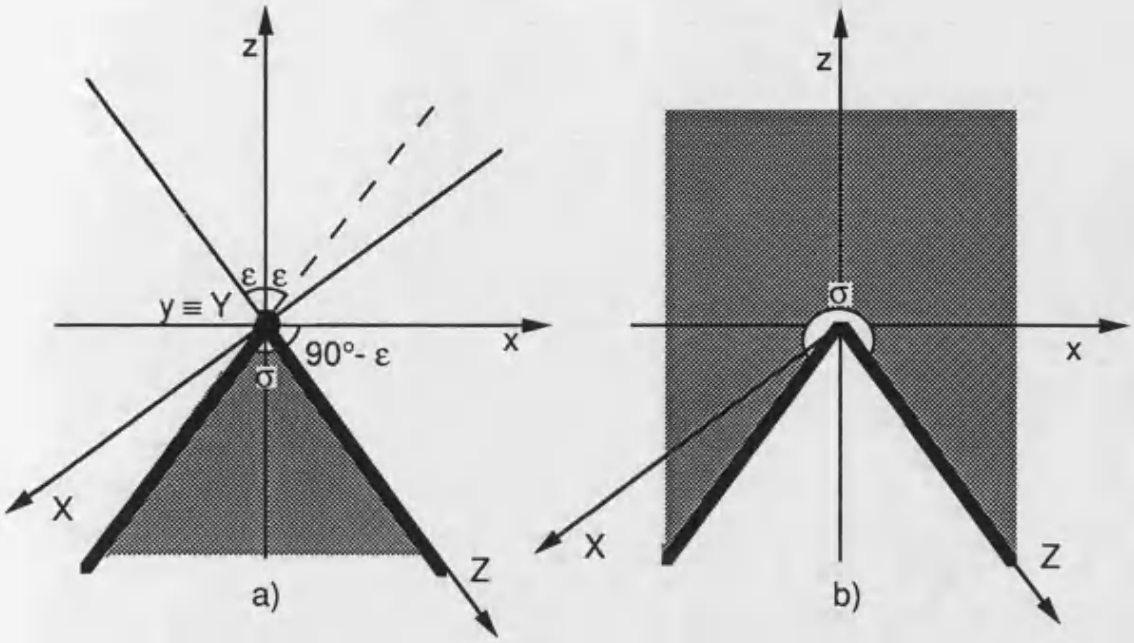

Fig. D.1 : main rectangular system for acute a) and obtuse b) sector

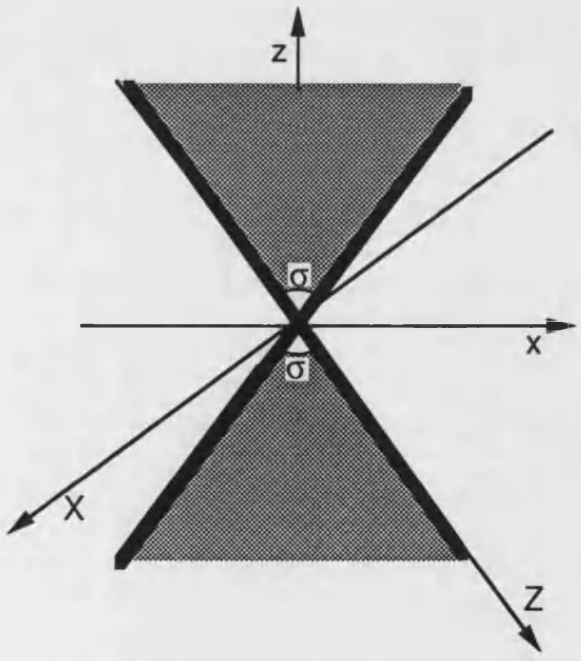

Fig. D.2 : main rectangular system for double sector

Appendix E

The EM fields

in rectangular coordinates

In this Appendix, following the lines of Appendix D, we express the dynamic EM fields $\vec{H}_M, \vec{M}, \vec{H}_N, \vec{N}$ in rectangular coordinates x, y, z or in those X, Y, Z of the main rectangular c.s. defined by means of the (D.16,17,18) .

To start with, it is well to have a look at the (3.39,40) and note that if we indicate by R, Θ, Φ, without distinction, the components of Ψ_1, Ψ_2 we can write the formal identifications :

$$\vec{H}_M \equiv \frac{j}{\eta}\vec{N} \tag{E.1}$$

$$\vec{H}_N \equiv \frac{j}{\eta}\vec{M} \tag{E.2}$$

So that, leaving the distinction to emerge at the due time, we can limit our attention to the expressions for $\vec{N}$ and $\vec{M}$. Their forms in terms of $\hat{x}, \hat{y}, \hat{z}$ can be

obtained from (3.39,40) using the (D.4,5,6) :

$$\begin{aligned}\vec{N} &= T\left[\nu(\nu+1)cos\phi\frac{R}{\kappa r}\Theta\Phi + k'^2 cos\theta cos\phi S_{\theta_N}\dot{\Theta}\Phi - P^2 S_{\phi_N}\Theta\dot{\Phi}\right]\hat{x} \\ &+ \left[\nu(\nu+1)sin\theta sin\phi\frac{R}{\kappa r}\Theta\Phi + T^2 cos\theta S_{\phi_N}\dot{\Theta}\Phi + P^2 cos\phi S_{\theta_N}\Theta\dot{\Phi}\right]\hat{y} \\ &+ P\left[\nu(\nu+1)cos\theta\frac{R}{\kappa r}\Theta\Phi - T^2 S_{\theta_N}\dot{\Theta}\Phi + k^2 cos\theta cos\phi S_{\phi_N}\Theta\dot{\Phi}\right]\hat{z} \qquad \text{(E.3)}\end{aligned}$$

where, using the functions S in (D.2), is :

$$S_{\theta_N}(\kappa r,\theta,\phi) = \tfrac{sin\theta}{S^2}\varrho(\kappa r) \qquad \text{(E.4)}$$

$$S_{\phi_N}(\kappa r,\theta,\phi) = \tfrac{sin\phi}{S^2}\varrho(\kappa r) \qquad \text{(E.5)}$$

$$\varrho(\kappa r) = \tfrac{1}{\kappa r}\tfrac{d(rR)}{dr} = \tfrac{1}{\kappa r}\tfrac{d(\kappa r R(\kappa r))}{d(\kappa r)} \qquad \text{(E.6)}$$

while :

$$\begin{aligned}\vec{M} &= P\left[k'^2 cos\theta cos\phi S_{\theta_M}\Theta\dot{\Phi} + T^2 S_{\phi_M}\dot{\Theta}\Phi\right]\hat{x} \\ &+ PT\left[cos\theta S_{\phi_M}\Theta\dot{\Phi} - cos\phi S_{\theta_M}\dot{\Theta}\Phi\right]\hat{y} \\ &- T\left[P^2 S_{\theta_M}\Theta\dot{\Phi} + k^2 cos\theta cos\phi S_{\phi_M}\dot{\Theta}\Phi\right]\hat{z} \qquad \text{(E.7)}\end{aligned}$$

where :

$$S_{\theta_M}(\kappa r, \theta, \phi) = \frac{sin\theta}{S^2} R(\kappa r) \tag{E.8}$$

$$S_{\phi_M}(\kappa r, \theta, \phi) = \frac{sin\phi}{S^2} R(\kappa r) \tag{E.9}$$

A further decomposition along the main axes X, Y, Z can be recovered using the (D.16,17,18) so as to obtain straightforwardly $N_Y \equiv N_y, M_Y \equiv M_y$ and, respectively :

$$\begin{aligned} N_X &= -\nu(\nu+1)\left[k'Tcos\phi + kPcos\theta\right]\frac{R}{\kappa r}\Theta\Phi + T\left[kPT - k'^3 cos\theta cos\phi\right] S_{\theta_N}\dot{\Theta}\Phi \\ &+ P\left[k'PT - k^3 cos\theta cos\phi\right] S_{\phi_N}\Theta\dot{\Phi} \end{aligned} \tag{E.10}$$

$$\begin{aligned} N_Z &= \nu(\nu+1)\left[kTcos\phi - k'Pcos\theta\right]\frac{R}{\kappa r}\Theta\Phi \\ &+ \left[PT + kk'cos\theta cos\phi\right]\left[k'TS_{\theta_N}\dot{\Theta}\Phi - kPS_{\phi_N}\Theta\dot{\Phi}\right] \end{aligned} \tag{E.11}$$

$$M_X = P\left[kTP - k'^3 cos\theta cos\phi\right] S_{\theta_M}\Theta\dot{\Phi} - T\left[k'TP - k^3 cos\theta cos\phi\right] S_{\phi_M}\dot{\Theta}\Phi \tag{E.12}$$

$$M_Z = \left[PT + kk'cos\theta cos\phi\right]\left[k'PS_{\theta_M}\Theta\dot{\Phi} + kTS_{\phi_M}\dot{\Theta}\Phi\right] \tag{E.13}$$

Appendix F

The double cone wedge and related geometries

F.1 Introduction

In this Appendix we deal with the determination of the complete spectra of eigenvalues, eigenfunctions and associated fields pertaining to the double cone of Fig. F.1, the half double cone of Fig. F.2, the cone on a plane of Fig. F.3 and the half cone on a plane of Fig. F.4 .

The main behaviour of the fields by the tip is also formulated and, in particular, the electric degree of singularity or of zero is computed with an accuracy of 7 decimal figures while that of the magnetic field is estimated .

F.2 The spectra of the double cone structures

If we consider the region between the surfaces $\theta = \bar{\theta}, \pi - \bar{\theta}$ in Fig. F.1, satisfaction of the Dirichlet b.c. imply (see (4.8)) :

$$\mathcal{E} P_\nu^m(cos\bar{\theta}) + \mathcal{F} Q_\nu^m(cos\bar{\theta}) = 0 \tag{F.1}$$

$$\mathcal{E} P_\nu^m(cos(\pi - \bar{\theta})) + \mathcal{F} Q_\nu^m(cos(\pi - \bar{\theta})) = 0 \tag{F.2}$$

which, for the properties (14,15) p.144 of [7], ensure non trivial solutions for $\mathcal{E}$ and $\mathcal{F}$ if and only if :

$$\mathcal{E} = -\mathcal{F} \frac{\pi}{2} ctg((\nu + m)\frac{\pi}{2}) \tag{F.3}$$

Thus the ν and θ-spectra are respectively given by :

$$\nu_D : P_{\nu_D}^m(cos\bar{\theta}) - \tfrac{2}{\pi} tg((\nu_D + m)\tfrac{\pi}{2}) Q_{\nu_D}^m(cos\bar{\theta}) = 0 \quad \text{for } m = 0, 1, 2, ... \tag{F.4}$$

$$\Theta_D(\theta) = P_{\nu_D}^m(cos\theta) - \tfrac{2}{\pi} tg((\nu_D + m)\tfrac{\pi}{2}) Q_{\nu_D}^m(cos\theta) \tag{F.5}$$

Furthermore, because of the same relations in [7], (F.1,2) also hold for the derivatives of P_ν^m, Q_ν^m . Consequently, the ν and Θ-spectra pertaining to the Neumann b.c. are given respectively by :

$$\nu_N : \quad \dot{P}_{\nu_N}^m(cos\bar{\theta}) - \tfrac{2}{\pi} tg((\nu_N + m)\tfrac{\pi}{2}) \dot{Q}_{\nu_N}^m(cos\bar{\theta}) = 0 \quad \text{for } m = 0, 1, 2, ... \tag{F.6}$$

$$\Theta_N(\theta) = P^m_{\nu_N}(cos\theta) - \tfrac{2}{\pi} tg((\nu_N + m)\tfrac{\pi}{2}) Q^m_{\nu_N}(cos\theta) \qquad \text{(F.7)}$$

On this structure we can imagine three different cuts effected by plane conductors fitting the cartesian planes similar to those analysed for the 3D double sector in Chapters 2 .

They can still be analysed in an easy way because the associate spectra can be determined, in the order, as :

i) The half-double cone (see Fig. F.2)

Simple physical considerations about this geometry let us realize that the ν, Θ-spectra are those in (F.4,5,6,7) whilst the μ, Φ-ones are selections from (4.26) according to the (4.34,35) (i.e. excluding the value $m = 0$) .

ii) The cone on a plane conductor (Fig. F.3)

The relations between the constants $\mathcal{E}$,$\mathcal{F}$ introduced by the plane conductor $\bar{\theta} = \frac{\pi}{2}$ are as in (4.22,23) hence, for the Dirichlet and Neumann cases we have :

$$\nu_D : P^m_{\nu_D}(cos\bar{\theta}) - \tfrac{2}{\pi} tg((\nu_D + m + 1)\tfrac{\pi}{2}) Q^m_{\nu_D}(cos\bar{\theta}) = 0 \quad \text{for } m = 0, 1, ... \qquad \text{(F.8)}$$

$$\Theta_D(\theta) = P^m_{\nu_D}(cos\theta) - \tfrac{2}{\pi} tg((\nu_D + m + 1)\tfrac{\pi}{2}) Q^m_{\nu_D}(cos\theta) \qquad \text{(F.9)}$$

$$\nu_N : \dot{P}^m_{\nu_N}(cos\bar{\theta}) - \tfrac{2}{\pi} tg((\nu_N + m)\tfrac{\pi}{2}) \dot{Q}^m_{\nu_N}(cos\bar{\theta}) = 0 \quad \text{for } m = 0, 1, ... \qquad \text{(F.10)}$$

$$\Theta_N(\theta) = P^m_{\nu_N}(cos\theta) - \tfrac{2}{\pi} tg((\nu_N + m)\tfrac{\pi}{2}) Q^m_{\nu_N}(cos\theta) \qquad \text{(F.11)}$$

while the μ, Φ spectra are the general ones (4.26) .

iii) The half-cone on a plane conductor (Fig. F.4)

The new b.c. pertaining the plane $\bar{\phi} = 0, \pi$ in respect to the previous case leave (F.8,9,10,11) unaltered, whereas the μ, Φ spectra are those in (4.34,35).

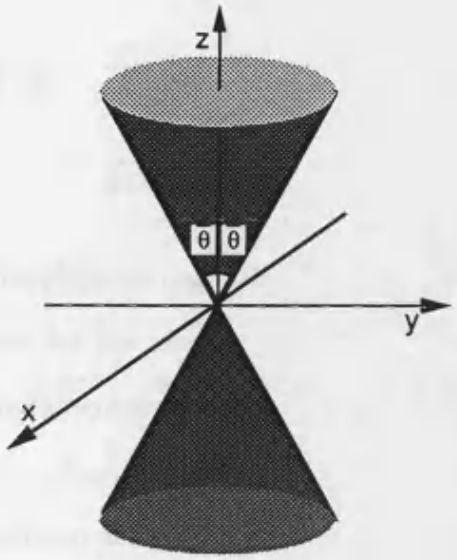

Fig. F.1 : double cone

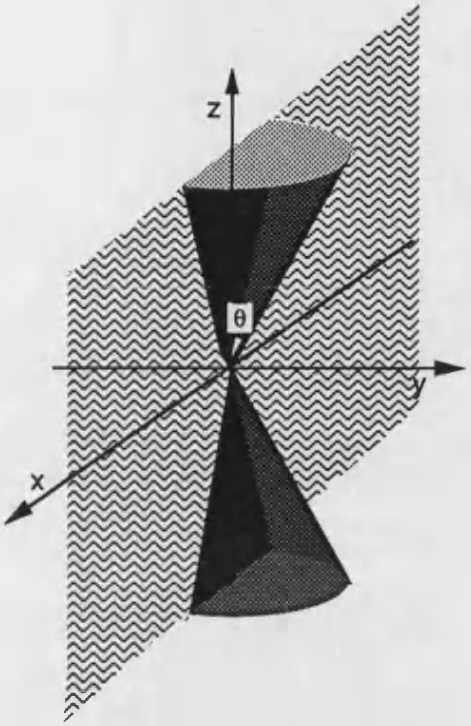

Fig. F.2 : half double cone

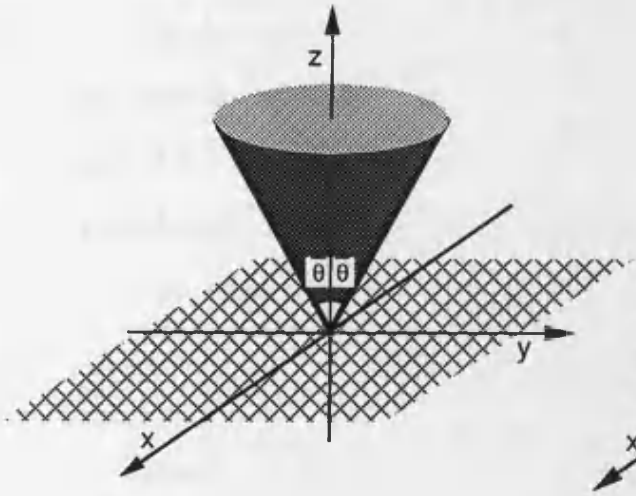

Fig. F.3 : cone on a plane conductor

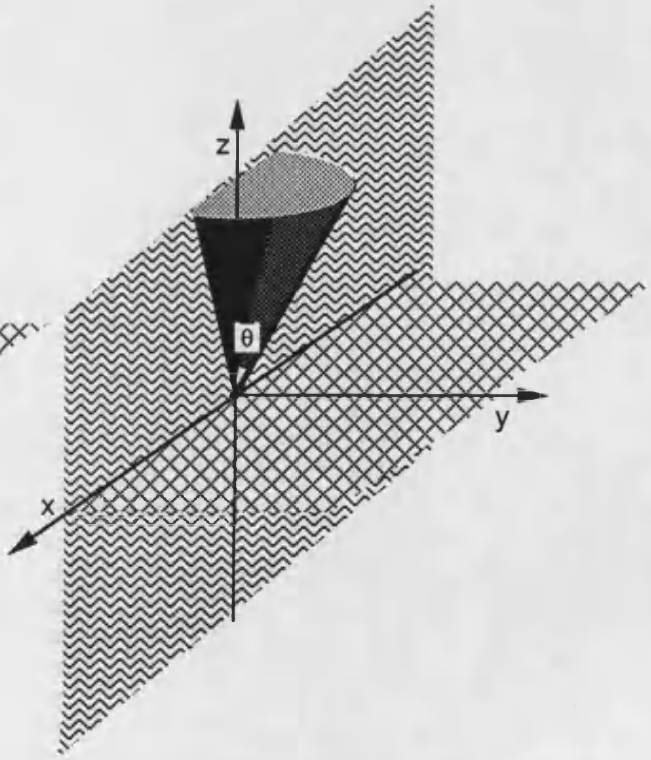

Fig. F.4 : half cone on a plane conductor

F.3 The main field behaviour for double cone structures

The physical considerations about the current flux made for the cone in 4.4.2 still hold for the present geometry permitting a straightforward indentification of the fundamental modes .

Starting with the double cone, the fundamental quantities for the Dirichlet problem are :

$$\mu = 0 \quad \nu_D(\bar{\theta}) : P_{\nu_D}(cos\bar{\theta}) - \tfrac{2}{\pi} tg(\nu_D \tfrac{\pi}{2}) Q_{\nu_D}(cos\bar{\theta}) = 0 \quad \text{for } \bar{\theta} \in [0, \tfrac{\pi}{2}] \quad \text{(F.12)}$$

$$\Theta_D(\theta) = P_{\nu_D}(cos\theta) - \tfrac{2}{\pi} tg(\nu_D \tfrac{\pi}{2}) Q_{\nu_D}(cos\theta) = 0 \qquad \Phi_D(\phi) = 1 \quad \text{(F.13)}$$

In this case too, the determination of the electric degree of singularity does not present difficulty since τ_e grows monotonically from -1 as $\bar{\theta} = 0$, that is the case of the wire, to 0 when $\bar{\theta} \simeq 33^o$ up to ∞ as $\bar{\theta} = \frac{\pi}{2}$ which is the space filled by a conductor . Its values are reported in Table 4.2 with the usual accuracy .

For what concerns instead the Neumann problem, the main quantities are :

$$\mu = 1 \quad \nu_N(\bar{\theta}) : \dot{P}^1_{\nu_N}(cos\bar{\theta}) - \tfrac{2}{\pi} tg(\nu_N \tfrac{\pi}{2}) \dot{Q}^1_{\nu_N}(cos\bar{\theta}) = 0 \quad \text{for } \bar{\theta} \in [0, \tfrac{\pi}{2}] \quad \text{(F.14)}$$

$$\Theta_N(\theta) = P^1_{\nu_N}(cos\theta) - \tfrac{2}{\pi} tg(\nu_N \tfrac{\pi}{2}) Q^1_{\nu_N}(cos\theta) = 0 \qquad \Phi_N(\phi) = cos\phi \quad \text{(F.15)}$$

The τ_h-curve is again nonmonotonic and its evaluation is left to further developments; for our purposes, we restrict attention to the limit solution for

$\bar{\theta} \rightarrow 0$, that is the case of the wire, that can be obtained as a limit case of the double sector :

$$\nu = 1 \qquad \mu = 1 \qquad \Theta_N(\theta) = sin\theta \qquad \Phi_N(\phi) = cos\phi \qquad \text{(F.16)}$$

In any case, the main behaviour of the fields is of the type :

$$\vec{N} \propto (\kappa r)^{\nu_D - 1}[\nu_D \Theta_D(cos\theta)\hat{r} + \dot{\Theta}_D(cos\theta)\hat{\theta}] \qquad \text{(F.17)}$$

$$\vec{H}_M \propto \frac{i}{\eta}(\kappa r)^{\nu_N - 1}[\nu_N \Theta_N(cos\theta)cos\phi\hat{r} + \dot{\Theta}_N(cos\theta)cos\phi\hat{\theta} - \Theta_N(cos\theta)sin\phi\hat{\phi}] \qquad \text{(F.18)}$$

Geometries related to the double-cone

For these three last geometries, the value $\mu = 0$ is excluded for the Neumann problem so that the main H-field behaviour is as for the original double-cone .

Instead, for what concerns the main eigenvalues, eigenfunctions and E-field behaviour related to the Dirichlet problem we can write in the order :

i) for the half double cone (Fig. F.2) :

$$\mu = 1 \quad \nu_D(\bar{\theta}) : P^1_{\nu_D}(cos\bar{\theta}) - \frac{2}{\pi} tg(\nu_D \frac{\pi}{2}) Q^1_{\nu_D}(cos\bar{\theta}) = 0 \quad \text{for } \bar{\theta} \in [0, \tfrac{\pi}{2}] \qquad \text{(F.19)}$$

$$\Theta_D(\theta) = P^1_{\nu_D}(cos\theta) - \frac{2}{\pi} tg(\nu_D \frac{\pi}{2}) Q^1_{\nu_D}(cos\theta) \qquad \Phi_D(\phi) = sin\phi \qquad \text{(F.20)}$$

$$\vec{N} \propto (\kappa r)^{\nu_D - 1}[\nu_D \Theta_D(cos\theta)sin\phi\hat{r} + \dot{\Theta}_D(cos\theta)sin\phi\hat{\theta} + \Theta_D(cos\theta)cos\phi\hat{\phi}] \qquad \text{(F.21)}$$

ii) for the cone on a plane conductor (Fig. F.3) :

$$\mu = 0 \quad \nu_D(\bar{\theta}) : P_{\nu_D}(cos\bar{\theta}) - \tfrac{2}{\pi} tg((\nu_D + 1)\tfrac{\pi}{2}) Q_{\nu_D}(cos\bar{\theta}) = 0 \quad \text{for } \bar{\theta} \in [0, \tfrac{\pi}{2}] \quad \text{(F.22)}$$

$$\Theta_D(\theta) = P_{\nu_D}(cos\theta) - \tfrac{2}{\pi} tg((\nu_D + 1)\tfrac{\pi}{2}) Q_{\nu_D}(cos\theta) = 0 \qquad \Phi_D(\phi) = 1 \quad \text{(F.23)}$$

$$\vec{N} \propto (\kappa r)^{\nu_D - 1} [\Theta_D(cos\theta)\hat{r} + \dot{\Theta}_D(cos\theta)\hat{\theta}] \quad \text{(F.24)}$$

iii) for the half cone on a plane (Fig. F.2) :

$$\mu = 1 \quad \nu_D(\bar{\theta}) : P_{\nu_D}(cos\bar{\theta}) - \tfrac{2}{\pi} tg(\nu_D \tfrac{\pi}{2}) Q_{\nu_D}(cos\bar{\theta}) = 0 \quad \text{for } \bar{\theta} \in [0, \tfrac{\pi}{2}] \quad \text{(F.25)}$$

$$\Theta_D(\theta) = P_{\nu_D}(cos\theta) - \tfrac{2}{\pi} tg(\nu_D \tfrac{\pi}{2}) Q_{\nu_D}(cos\theta) = 0 \qquad \Phi_D(\phi) = sin\phi \quad \text{(F.26)}$$

$$\vec{N} \propto (\kappa r)^{\nu_D - 1} [\Theta_D(cos\theta) sin\phi \hat{r} + \dot{\Theta}_D(cos\theta) sin\phi \hat{\theta} + \Theta_D(cos\theta) cos\phi \hat{\phi}] \quad \text{(F.27)}$$

The values of τ_e for these last three geometries are collected together with those relative to the others Cone-wedges in Table 4.2 versus $\bar{\theta}$ at 2.5^0 intervals .

Appendix G

Changing sets of basis functions

G.1 Recursivity relation for the coefficients P_{mn}

In 5.4 we are asked to determine the coefficients P_{mn} relative to the mapping between the sets of functions ϕ_{h_n}, φ_m :

$$n = 0, 2, ... \qquad \phi_{h_n}(x) = \sum P_{mn}\varphi_m(\theta) \qquad m = 0, 2, ... \qquad \text{(G.1)}$$

according to the map $\theta(x)$ in the form (5.45) .

For this purpose we can start decomposing the generic term of the first base making use of the Chebyschev polinomials of the 1^{st} kind :

$$cos(\frac{n\pi}{a}x) = T_n(cos\frac{\pi x}{a}) = T_n(\alpha_1 + \alpha_2 cos2\theta + \alpha_3 cos4\theta) = \sum_{m=0,2,..}^{4n} p_{mn} cos(m\theta)$$
$$n = 0, 2, ... \qquad \text{(G.2)}$$

Since n is even and the (5.45) contains only even multiple of θ up to 4, m can be

only even with a maximum $4n$.

Furthemore the recursive relation for the Chebyschev polynomials :

$$T_n(cos\frac{\pi x}{a}) = 2cos(\frac{\pi x}{a})T_{n-1}(cos\frac{\pi x}{a}) - T_{n-2}(cos\frac{\pi x}{a}) \qquad \text{(G.3)}$$

yields analogous properties for the expansion coefficients p_{mn} .

In fact substituting the last equation into the previous we obtain :

$$\sum_{m=0}^{4n} p_{mn}cos(m\theta) =$$

$$= 2[\alpha_1 + \alpha_2 cos2\theta + \alpha_3 cos4\theta] \sum_{m=0}^{4(n-1)} p_{mn-1}cos(m\theta) - \sum_{m=0}^{4(n-2)} p_{mn-2}cos(m\theta) \quad \text{(G.4)}$$

and taking in account the following properties of the *cos* function :

$$cos(-i\theta) = cos(i\theta) \qquad cos(i\theta)cos(j\theta) = \frac{1}{2}[cos(i+j)\theta + cos(i-j)\theta] \quad \text{(G.5)}$$

we can establish a recursivity relation among the coefficients :

$$p_{mn} = \delta_1 p_{mn-1} + \delta_2 p_{m+4n-1} + \delta_3 p_{m+2n-1} + \delta_4 p_{m-2n-1} + \delta_5 p_{m-4n-1} + \delta_6 p_{mn-2} \quad \text{(G.6)}$$

where:

$$\delta_1 = \begin{cases} 2\alpha_1 + \alpha_3 & m = 2 \\ 2\alpha_1 & m \neq 2 \end{cases} \qquad \delta_2 = \alpha_3 \ \forall m \qquad \delta_3 = \alpha_2 \ \forall m \quad \text{(G.7)}$$

$$\delta_4 = \begin{cases} 0 & m+0 \\ 2\alpha_2 & m=2 \\ \alpha_2 & m \geq 4 \end{cases} \qquad \delta_5 = \begin{cases} 0 & m=0,2 \\ 2\alpha_3 & m=4 \\ \alpha_3 & m \geq 6 \end{cases} \qquad \delta_6 = -1 \ \forall m \quad \text{(G.8)}$$

with the initial values :

$$p_{00} = 1 \qquad p_{01} = \alpha_1 \qquad p_{21} = \alpha_2 \qquad p_{41} = \alpha_3 \qquad \text{(G.9)}$$

If we further take into account the orthonormalization constants in the two sets of functions $\phi_{h_n}(x), \varphi_m(\theta)$ we obtain the coefficients :

$$P_{mn} = \sqrt{\frac{\delta_n}{\delta_m}}\sqrt{\frac{2\pi}{a}}p_{mn} \qquad \text{where : } \delta_n, \delta_m = \begin{cases} 2 & m,n=0 \\ 1 & m,n \neq 0 \end{cases} \qquad \text{(G.10)}$$

We need just to consider even n and m values of this matrix so that the resulting matrix is always triangular and with a number of non vanishing terms larger than in the uniform sections, especially around the tips where also $\alpha_3 \neq 0$.

The rapidity of convergence to 0 with m of the single column ($n = const$) depends on w and increases as $w \rightarrow a$.

G.2 Recursivity relation for the coefficients Q_{mn}

Together with the previous transformation, we have to consider the following one:

$$n = 0, 2, ... \qquad \phi_{e_n}(x) = \sum Q_{mn}\varphi_m(\theta) \qquad m = 1, 3, ... \qquad \text{(G.11)}$$

Along the previous lines we can make use of the 2^{nd} kind of Chebyschev polynomials and their properties so as to write :

$$n = 0, 2, ... \qquad sin(\frac{n\pi}{a}x) = sin(\frac{\pi}{a}x)U_{n-1}(cos\frac{\pi}{a}x) = \sum_{m=0,2,..}^{4(n-1)} q_{mn}cos(m\theta) \quad (G.12)$$

Since the recursivity relation for U is identical to that for T, the q_{mn} presents exactly the same recursivity relation (G.3), however since $T_1(x) = x$ and $U_1(x) = 2x$ the initial values are :

$$p_{00} = 1 \qquad p_{01} = 2\alpha_1 \qquad p_{21} = 2\alpha_2 \qquad p_{41} = 2\alpha_3 \qquad (G.13)$$

Because of the (5.49), the (G.11) may be written for m odd as :

$$sin\frac{n\pi}{a}x = \sum_{m=1,3,..}^{4n+1} Q'_{mn}cos(m\theta) =$$
$$= [\beta_1 cos\theta + \beta_2 cos3\theta + \beta_3 cos5\theta] \sum_{m=0,2,..}^{4(n-1)} q_{mn-1}cos(m\theta) \qquad (G.14)$$

which, for the same (G.5), leads to the relations valid for $n = 1, 2, ...$:

$$Q'_{1n} = (2q_{0n-1} + q_{2n-1})\frac{\beta_1}{2} + (q_{2n-1} + q_{4n-1})\frac{\beta_2}{2} + (q_{4n-1} + q_{6n-1})\frac{\beta_3}{2} \quad m = 1$$
$$Q'_{3n} = (q_{2n-1} + q_{4n-1})\frac{\beta_1}{2} + (2q_{0n-1} + q_{6n-1})\frac{\beta_2}{2} + (q_{2n-1} + q_{8n-1})\frac{\beta_3}{2} \quad m = 3$$
$$Q'_{5n} = (q_{4n-1} + q_{6n-1})\frac{\beta_1}{2} + (q_{2n-1} + q_{8n-1})\frac{\beta_2}{2} + (2q_{0n-1} + q_{10n-1})\frac{\beta_3}{2} \quad m = 5$$
$$Q'_{mn} = (q_{m-1n-1} + q_{m+1n-1})\frac{\beta_1}{2} + (q_{m-3n-1} + q_{m+3n-1})\frac{\beta_2}{2}$$
$$+(q_{m-5n-1} + q_{m+5n-1})\frac{\beta_3}{2} \qquad m \geq 7 \quad (G.15)$$

where $\beta_1, \beta_2, \beta_3$ are coefficients computed as indicated in 5.4.1 .

Finally, taking in account the orthonormalization constants we obtain :

$$Q_{mn} = \sqrt{\frac{\delta_n}{\delta_m}}\sqrt{\frac{2\pi}{a}}Q'_{mn} \quad \text{where: } \delta_n, \delta_m = \begin{cases} 2 & m,n = 0 \\ 1 & m,n \neq 0 \end{cases} \tag{G.16}$$

At last, we need to map the function :

$$(\frac{\pi}{a})x = \gamma_1 cos\theta + \gamma_2 cos3\theta + \gamma_3 cos5\theta \tag{G.17}$$

where the constants $\gamma_1, \gamma_2, \gamma_3$ can be obtained directly for comparison of (5.49) with (G.17), that is to say, they assume the same expressions for $\beta_1, \beta_2, \beta_3$ respectively but with the substitutions :

$$sin\frac{\pi}{a}X_1 \rightarrow \frac{\pi}{a}X_1 \qquad sin\frac{\pi}{a}X_2 \rightarrow \frac{\pi}{a}X_2 \qquad sin\frac{\pi}{a}X_3 \rightarrow \frac{\pi}{a}X_3 \tag{G.18}$$

Hence, in order to obtain the expansion coefficients of the function $\frac{1}{\sqrt{a}}\frac{\pi}{a}x$, we set :

$$Q_{10} = \frac{1}{\sqrt{a}}\gamma_1 \qquad Q_{30} = \frac{1}{\sqrt{a}}\gamma_2 \qquad Q_{50} = \frac{1}{\sqrt{a}}\gamma_3 \tag{G.19}$$

In conclusion, apart from the first row, the $\underline{\underline{U}}$ matrix presents the same triangular properties as $\underline{\underline{P}}$.

Bibliography

[1] F.M. Arscott and A. Darai, " Curvilinear Co-ordinate Systems in which the Helmholtz Equation Separates ",
IMA Journal of Applied Mathematics, vol. 27, pp. 33-70, 1981 .

[2] F.M. Arscott, " *Periodic Differential Equations* ",
London, Pergamon Press, 1964.

[3] F.M. Arscott, " The land beyond Bessel: a survey of Higher special functions",
Proc. of Ordinary and Partial Diff. Equations, Dundee, pp. 26-45, 1980.

[4] W. Magnus and S. Winkler, " *Hill's Equation* ",
New York, Wiley, 1966 .

[5] E.L. Ince, " The Periodic Lamé' Functions ",
Proc. Royal Society, Edinburg, vol. 60, pp. 47-63, 1940 .

[6] E.L.Ince, " Further Investigations into the Periodic Lamé' Functions ",
Proc. Royal Society, Edinburg, vol. 60, pp. 83-99, 1940 .

[7] A. Erdélyi, W. Magnus, F. Oberhettinger, F.G. Tricomi, (Bateman Manuscript Project), " *Higher Transcendental Functions* ", New York, McGraw Hill, 1955 .

[8] J.K.M. Jansen, " *Simple-Periodic and non-Periodic Lamé' Functions* ", Amsterdam, Mathematical Centre Tracs, no. 72 .

[9] L. Kraus and L.M. Levine, " *Diffraction by An Elliptic Cone* ", Research Report, New York University, no. EM-156, March 1960 .

[10] R.S. Satterwhite, " *Diffraction by a plane angular sector* ", PhD Dissertation, The Ohio State University, 1969 .

[11] P. Moon and D.E. Spencer, " *Field Theory Handbook* ", Berlin, Springer-Verlag, 1971 .

[12] P.M. Morse and H. Feshbach, " *Method of Theoretical Physics* ", New York, McGraw-Hill, 1953 .

[13] J. Van Bladel, " *Electromagnetic Fields* ", New York, McGraw-Hill, 1964, pp. 201-202 .

[14] R. De Smedt and J.G. Van Bladel, " Field Singularities at the Tip of a Metallic Cone of Arbitrary Cross Section ", *IEEE Trans. on A&P*, vol. AP-34, no. 7, pp. 865-870, July 1986 .

[15] R. De Smedt, " Singular field behaviour near the tip of a dielectric-metallic corner ", *Radio Science*, vol. 22, no. 7, pp. 1190-1196, December 1987 .

[16] R. De Smedt, " Electric Singularity Near the tip of a Sharp Cone ",
IEEE Trans. on A&P, vol. 36, no. 1, pp. 152-155, January 1988 .

[17] J. Boersma and J.K.M. Jansen, " *Electromagnetic fields singularities at the tip of an elliptic cone* ",
Res. Report, Eindoven Univ. of Tecnology The Netherlands, December 1990.

[18] J. Boersma, " Singularity exponents for complementary sectors ",
Electronic Letters, vol. 27, no. 16, pp. 1484-1485, August 1991 .

[19] J.N. Sahalos, " Investigation into Nonperiodic Lamé' Functions and Applications to Electromagnetic Problems ",
Journal of Franklin Institute, vol. 315, no. 3, pp. 195-210, March 1983 .

[20] S.N. Brown and K. Stewartson, "Flow near the Apex of a Plane Delta Wing",
JIMA Journal , pp. 206-216, 1969 .

[21] L. Kraus, " *Diffraction by a Plane Angular Sector* ",
New York University, Thesis, 1955 .

[22] J. Radlow, " Diffraction by a Quarter Plane ",
Archive for Mechanics and Analysis, vol. 8, pp. 139-158, 1961 .

[23] D.S. Jones, " *The Theory of electromagnetism* ",
New York, Pergamon Press, 1964 .

[24] D.S. Jones, " Diffraction by an Edge and by a Corner ",
Quart. Journ. Mech. and Applied Math., vol. 5, pt. 3, pp. 363-378, 1952 .

[25] R.E. Collin, " *Field Theory of Guided Waves* ",
New York, McGraw Hill, 1960 .

[26] R.E. Collin, " *Fundation for microwave engineering* ",
McGraw-Hill, Physical and Quantum Electronics Serie, 1966 .

[27] R.E. Collin, " Theory and design of wide-band multisection quarter-wave transformers ",
Proc. IRE, vol. 43, pp. 179-185, February 1955 .

[28] J. Schwinger and D.S. Saxon, "*Discontinuities in waveguides* ",
Doc. on Modern Physics, New York, Gordon and Br. Sc. Publ. inc., 1968.

[29] B.A. Hargrave and B.D. Sleeman, " The Numerical Solution of Two-parameter Eigenvalue Problems in Ordinary Differential Equations with an Application to the Problem of Diffraction by a Plane Angular Sector ",
Journal Inst. Maths Applics, no. 14, pp. 23-30, 1974 .

[30] I.S. Gradshtein and I.M. Ryshik, " *Tables of integral series and products* ",
New York-London, Accademic Press, 1980 .

[31] B. Bhat and S.K. Koul, " *Analysis, Design and Applications of fin line* ",
Norwood, MA, Artech House, 1987 .

[32] C.J. Railton and T. Rozzi, " The Rigorous Analysis of Cascaded Step Discontinuities in Microstrip ",
IEEE Trans. on MTT, vol. 36, no. 7, pp. 1177-1185, July 1988 .

[33] C.A. Olley and T. Rozzi, " An Approximate Variational Solution to the Step Discontinuity in Finline ",
IEEE Trans. on MTT, vol. 37, no. 6, pp. 977-983, June 1989 .

[34] R. Sorrentino and T. Itoh, " Transverse Resonance Analysis of Finline Discontinuities ",
IEEE Trans. on MTT, vol. MTT-32, no. 12, pp. 1633-1638, December 1984.

[35] A. Beyer and I. Wolff, " Calculation of the Transmission Properties of Inhomogeneous Finline ",
Proc. 10^{th} *European Microwave Conference*, pp. 322-326, 1980 .

[36] D. Mirshekar-Syahkal and J.B. Davies, " Accurate Analysis of Tapered Planar Transmission Lines for Microwave Integrated Circuits ",
IEEE Trans. on MTT, pp. 123-128, February 1981 .

[37] A. Bergquist, " Wave Propagation on Nonuniform Transmission Lines ",
IEEE Trans. on MTT, pp. 557-558, August 1978 .

[38] R.P. Hecken, "A Near-Optimum Matching Section Without Discontinuities",
IEEE Trans. on MTT, vol. MTT-20, no. 11, pp. 734-739, November 1972 .

[39] R.W. Klopfstein, " A transmission line taper of improved design ",
Proc. IRE, vol. 44, pp. 31-35, January 1956 .

[40] J.R. Mosig and F.E. Gardiol, " General integral equation formulation for microstrip antennas and scatterers ",
IEE Proceedings vol. 132, pt. H, no. 7, pp. 424-432, December 1985 .

[41] S.R. Pennock, C.M.D. Rycroft, P.R. Shepherd and T. Rozzi, " Transition characterization for de-embedding purposes ",
Proc. 17^{th} *European Microwave Conf.*, pp. 355-360, Rome, September 1987.

[42] S. Marchetti, " *Modal Characterization of Finline Structures for Millimeter Waves* ", Degree Thesis, Ancona University, 1986 .

[43] S. Marchetti and T. Rozzi, "Electric Field Behavior Near Metallic Wedges", *IEEE Trans. on A&P*, vol. 38, no. 9, September 1990 .

[44] S.Marchetti and T. Rozzi, " Electric Field Singularities at Sharp Edges of Planar Conductors ",
IEEE Trans. on A&P, vol. 39, pp. 1312-1320, September 1991 .

[45] S. Marchetti and T. Rozzi, " $\vec{H}$-field and $\vec{J}$-current Singularities at Sharp Edges in Printed Circuits ",
IEEE Trans. on A&P, vol. 39, pp. 1321-1331, September 1991 .

[46] S. Marchetti and T. Rozzi, " Edges Singularities of Discontinuities in Microwave Integrated Circuits (MIC) ",
7^{th} *National Meeting of Applied Electromag.*, pp. 189-192, Sept. 1988, Rome.

[47] S. Marchetti and T. Rozzi, " Electric Field Singularities in Microwave Integrated Circuits (MIC) ",
Proc. 20^{th} *European Microwave Conf.*, pp. 823-828, Sept. 1990, Budapest.

[48] S. Marchetti and T. Rozzi, " EM Field Singularities in Microwave Integrated Circuits (MIC) ",
Proc. International IEEE AP-S, pp. 882-885, June 1991, London, Ontario .

[49] S. Marchetti and T. Rozzi, " Generalized Transverse Resonance Method for Nonuniform Lines in Microwave integrated Circuits (MIC) ",
Proc. 21^{st} *European Microwave Conf.*, pp. 878-883, September 1991, Stuttgart .